

LEIDENFROST FILM BOILING OF INTERMEDIATE  
AND EXTENDED BUBBLY MASSES  
OF LIQUID NITROGEN

By

EDWARD G. KESHOCK

Bachelor of Mechanical Engineering  
University of Detroit  
Detroit, Michigan  
June, 1958

Master of Science  
Oklahoma State University  
Stillwater, Oklahoma  
May, 1966

Submitted to the Faculty of the Graduate College  
of the Oklahoma State University  
in partial fulfillment of the requirements  
for the Degree of  
DOCTOR OF PHILOSOPHY  
May, 1968

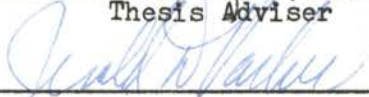
OCT 25 1968


LEIDENFROST FILM BOILING OF INTERMEDIATE  
AND EXTENDED BUBBLY MASSES  
OF LIQUID NITROGEN

Thesis Approved:



Thesis Adviser







Dean of the Graduate College

688436

## ACKNOWLEDGMENTS

I would like to express my deep gratitude to Dr. Kenneth J. Bell, not only for his guidance and exemplary standards of technical excellence during the course of this study, but also for the genuine respect and consideration that was never absent from his teacher-student relationships.

Likewise, I am indebted to Dr. Jerald D. Parker for his respectful counseling and guidance, both in planning a program of graduate study and in providing illuminating observations pertinent to the present research study.

To my parents, I am grateful for their continuous support and encouragement and am hopeful that in some measure I have been able to ease any remembrances of past sacrifices which they have had to undergo in my behalf.

Also, I am very appreciative for the many expressions of encouragement from friends and former associates which seemed to be forthcoming when most needed.

Most especially, I am thankful to my wife, Mary Jo, not only for having shown understanding and patience in undergoing the many sacrifices which often are a part of student life, but also for having provided a warm and hospitable home atmosphere which so often proved to be a source of inner consolation and strength.

The financial support provided by the U. S. Army Research Office for conducting the present research is gratefully acknowledged.

## TABLE OF CONTENTS

Chapter	Page
I. INTRODUCTION . . . . .	1
II. LITERATURE SURVEY . . . . .	8
III. DISCUSSION OF THEORETICAL MODELS . . . . .	18
IV. EXPERIMENTAL APPARATUS . . . . .	36
V. EXPERIMENTAL PROCEDURE . . . . .	50
Calibration of Depositors . . . . .	50
Preparation of Equipment . . . . .	51
Photographic Studies . . . . .	54
VI. RESULTS . . . . .	56
Area-Volume Calibration . . . . .	56
Total Vaporization Times . . . . .	68
Comparison With Theory . . . . .	72
Corrected Total Vaporization Times . . . . .	80
Procedure for Obtaining Corrected Total Vaporization Times . . . . .	81
Dimensionless Total Vaporization Times . . . . .	86
Leidenfrost Temperature . . . . .	93
Heat Transfer Coefficients . . . . .	96
Vapor Breakthrough Dynamics . . . . .	110
VII. ANALYSIS . . . . .	122
VIII. DISCUSSION . . . . .	133
IX. CONCLUSIONS . . . . .	137
X. RECOMMENDATIONS . . . . .	139
BIBLIOGRAPHY . . . . .	141
APPENDIX A - CALIBRATION OF DEPOSITORS . . . . .	145
APPENDIX B - TOTAL VAPORIZATION TIME MEASUREMENTS . . . . .	148
APPENDIX C - PROPERTY VALUES EMPLOYED IN COMPUTER CALCULATIONS . . . . .	155

Chapter	Page
APPENDIX D - COMPUTER PROGRAM . . . . .	158
APPENDIX E - HEAT TRANSFER COEFFICIENTS AS A FUNCTION OF DROP PROJECTED AREA . . . . .	165
APPENDIX F - HEAT TRANSFER COEFFICIENTS AS A FUNCTION OF DROP LIFETIME . . . . .	176
APPENDIX G - MAXIMUM VAPOR-DOME AREA MEASUREMENTS . . . . .	187
APPENDIX H - CELL SPACING MEASUREMENTS . . . . .	189
APPENDIX I - VAPOR FRACTION MEASUREMENTS . . . . .	191

LIST OF TABLES

Table	Page
I. Summary of Measured Total Vaporization Times . . . . .	70
II. Summary of Measured Total Vaporization Times Corrected for Radiation and Free Convection . . . . .	85
III. Plate Temperature at Transition From Nucleate to Film Boiling . . . . .	94
IV. Maximum Vapor Dome Areas (Measured) and Corresponding Diameters (Calculated) . . . . .	120
V. Cell Spacing (Center-to-Center) . . . . .	120

## LIST OF FIGURES

Figure	Page
1. Conventional Boiling Curve Illustrating Metastable Boiling Line . . . . .	2
2. Film Boiling States of Liquid Masses . . . . .	5
3. Heat and Mass Transfer Paths for the Spherical Drop Model . . . . .	19
4. Calculated Evaporation Rates Versus Time for Water . . . . .	23
5. Schematic Model of the Evaporation of a Flat Disk . . . . .	25
6. Universal Average Drop Thickness Curve . . . . .	31
7. Universal Total Vaporization Time Curve . . . . .	34
8. Schematic of Experimental Equipment . . . . .	37
9. Schematic of Aluminum Test Plate . . . . .	39
10. Schematic of Test Surface and Cooling System . . . . .	42
11. Temperature-Time History of Plate Surface During Cooling System Operation . . . . .	44
12. Teflon Depositor . . . . .	47
13. Pyrex Beaker Depositor . . . . .	48
14. Plan Area of Drop Versus Time - $A_0 = 0.0759 \text{ in.}^2$ . . . . .	58
15. Plan Area of Drop Versus Time - $A_0 = 0.247 \text{ in.}^2$ . . . . .	59
16. Plan Area of Drop Versus Time - $A_0 = 0.786 \text{ in.}^2$ . . . . .	60
17. Plan Area of Drop Versus Time - $A_0 = 1.69 \text{ in.}^2$ . . . . .	61
18. Plan Area of Drop Versus Time - $A_0 = 2.35 \text{ in.}^2$ . . . . .	62
19. Plan Area of Drop Versus Time - $A_0 = 3.61 \text{ in.}^2$ . . . . .	63
20. Plan Area of Drop Versus Time - $A_0 = 4.31 \text{ in.}^2$ . . . . .	64

Figure	Page
21. Plan Area of Drop Versus Time - $A_o = 8.55 \text{ in.}^2$ . . . . .	65
22. Comparison of Theoretical and Experimental Values of Drop Plan Area as a Function of Drop Volume . . . . .	67
23. Total Vaporization Time of Drops of Various Initial Volumes as a Function of $\Delta T$ . . . . .	69
24. Plan Area of Drop Throughout Drop Lifetime - $\Delta T = 32.9^\circ \text{ F}$ . . . . .	73
25. Plan Area of Drop Throughout Drop Lifetime - $\Delta T = 32.9^\circ \text{ F}$ . . . . .	74
26. Plan Area of Drop Throughout Drop Lifetime - $\Delta T = 61.4^\circ \text{ F}$ . . . . .	75
27. Plan Area of Drop Throughout Drop Lifetime - $\Delta T = 104.8^\circ \text{ F}$ . . . . .	76
28. Plan Area of Drop Throughout Drop Lifetime - $\Delta T = 293^\circ \text{ F}$ . . . . .	77
29. Corrected Total Vaporization Time Versus $\Delta T$ . . . . .	79
30. Dimensionless Vaporization Time Versus Dimensionless Volume (Uncorrected for Radiation or "Free Convection") . . . . .	88
31. Dimensionless Vaporization Time Versus Dimensionless Volume (Data Corrected for Radiation and "Free Convection") . . . . .	90
32. Heat Transfer Coefficient (Corrected) During Drop Vaporization as a Function of Drop Volume - $\Delta T = 35.2^\circ \text{ F}$ . . . . .	99
33. Heat Transfer Coefficient (Corrected) During Drop Vaporization as a Function of Drop Volume - $\Delta T = 62^\circ \text{ F}$ . . . . .	100
34. Heat Transfer Coefficient (Corrected) During Drop Vaporization as a Function of Drop Volume - $\Delta T = 104^\circ \text{ F}$ . . . . .	101
35. Heat Transfer Coefficient (Corrected) During Drop Vaporization as a Function of Drop Volume - $\Delta T = 304^\circ \text{ F}$ . . . . .	102
36. Heat Transfer Coefficient (Corrected) During Drop Vaporization as a Function of Drop Volume - $\Delta T = 383^\circ \text{ F}$ . . . . .	103



Figure	Page
37. Heat Transfer Coefficient (Corrected) During Drop Vaporization as a Function of Drop Volume - $\Delta T = 35.2^\circ \text{ F}$ . . . . .	104
38. Heat Transfer Coefficient (Corrected) During Drop Vaporization as a Function of Drop Volume - $\Delta T = 62^\circ \text{ F}$ . . . . .	105
39. Heat Transfer Coefficient (Corrected) During Drop Vaporization as a Function of Drop Volume - $\Delta T = 105^\circ \text{ F}$ . . . . .	106
40. Heat Transfer Coefficient (Corrected) During Drop Vaporization as a Function of Drop Volume - $\Delta T = 293^\circ \text{ F}$ . . . . .	107
41. Heat Transfer Coefficient (Corrected) During Drop Vaporization as a Function of Drop Volume - $\Delta T = 383^\circ \text{ F}$ . . . . .	108
42. Corrected Heat Transfer Coefficient Versus $\Delta T$ for Various Drop Volumes . . . . .	109
43. Tracing of Side View of Drop Experiencing Vapor Breakthrough . . . . .	112
44. Simultaneous Top and Side View of Drops Experiencing Vapor Breakthrough . . . . .	113
45. Sequential Top and Side Views of a Drop Experiencing Vapor Breakthrough . . . . .	114
46. Area-Time History of Vapor Breakthrough Region in Two Drops . . . . .	115
47. Vapor Breakthrough Regions at Several Times During Vaporization of $\approx 0.9$ ml Drop . . . . .	116
48. Comparison of Theoretical and Experimental Values of Maximum Vapor Dome Diameters as a Function of $\Delta T$ . . . . .	118
49. Comparison of Theoretical and Experimental Values of Cell Spacing as a Function of $\Delta T$ . . . . .	119
50. Schematic Model of Extended Liquid Drop Experiencing Several Vapor Breakthroughs . . . . .	124
51. Prediction of Number of Vapor Breakthroughs in a Given Volume of Liquid . . . . .	128
52. Thermal Expansion Coefficient for Teflon and Pyrex . . . . .	156

Figure	Page
53. Comparison of Experimental and Theoretical Heat Transfer Coefficients as a Function of Drop Projected Area - $\Delta T = 33^\circ \text{ F}$ . . . . .	166
54. Comparison of Experimental and Theoretical Heat Transfer Coefficients as a Function of Drop Projected Area - $\Delta T = 62^\circ \text{ F}$ . . . . .	167
55. Comparison of Experimental and Theoretical Heat Transfer Coefficients as a Function of Drop Projected Area - $\Delta T = 105^\circ \text{ F}$ . . . . .	168
56. Comparison of Experimental and Theoretical Heat Transfer Coefficients as a Function of Drop Projected Area - $\Delta T = 293^\circ \text{ F}$ . . . . .	169
57. Comparison of Experimental and Theoretical Heat Transfer Coefficients as a Function of Drop Projected Area - $\Delta T = 383^\circ \text{ F}$ . . . . .	170
58. Comparison of Experimental and Theoretical Heat Transfer Coefficients as a Function of Drop Projected Area - $\Delta T = 35^\circ \text{ F}$ . . . . .	171
59. Comparison of Experimental and Theoretical Heat Transfer Coefficients as a Function of Drop Projected Area - $\Delta T = 62^\circ \text{ F}$ . . . . .	172
60. Comparison of Experimental and Theoretical Heat Transfer Coefficients as a Function of Drop Projected Area - $\Delta T = 105^\circ \text{ F}$ . . . . .	173
61. Comparison of Experimental and Theoretical Heat Transfer Coefficients as a Function of Drop Projected Area - $\Delta T = 303^\circ \text{ F}$ . . . . .	174
62. Comparison of Experimental and Theoretical Heat Transfer Coefficients as a Function of Drop Projected Area - $\Delta T = 382^\circ \text{ F}$ . . . . .	175
63. Variation of Heat Transfer Coefficient to Drop During Drop Lifetime - $\Delta T = 35^\circ \text{ F}$ . . . . .	177
64. Variation of Heat Transfer Coefficient to Drop During Drop Lifetime - $\Delta T = 62^\circ \text{ F}$ . . . . .	178
65. Variation of Heat Transfer Coefficient to Drop During Drop Lifetime - $\Delta T = 105^\circ \text{ F}$ . . . . .	179
66. Variation of Heat Transfer Coefficient to Drop During Drop Lifetime - $\Delta T = 303^\circ \text{ F}$ . . . . .	180

Figure	Page
67. Variation of Heat Transfer Coefficient to Drop During Drop Lifetime - $\Delta T = 382^{\circ} \text{ F}$ . . . . .	181
68. Variation of Heat Transfer Coefficient to Drop During Drop Lifetime - $\Delta T = 293^{\circ} \text{ F}$ . . . . .	182
69. Variation of Heat Transfer Coefficient to Drop During Drop Lifetime - $\Delta T = 383^{\circ} \text{ F}$ . . . . .	183
70. Variation of Heat Transfer Coefficient to Drop During Drop Lifetime - $\Delta T = 33^{\circ} \text{ F}$ . . . . .	184
71. Variation of Heat Transfer Coefficient to Drop During Drop Lifetime - $\Delta T = 62^{\circ} \text{ F}$ . . . . .	185
72. Variation of Heat Transfer Coefficient to Drop During Drop Lifetime - $\Delta T = 105^{\circ} \text{ F}$ . . . . .	186

## NOMENCLATURE

### Letter Symbols

A	plan area of drop
A'	modified plan area of drop (liquid region only) due to vapor breakthrough
A <sub>v</sub>	total plan area of vapor breakthrough region in extended drop
A <sub>vd</sub>	plan area of vapor dome (vapor breakthrough region) in an extended drop
A <sub>int</sub>	average integrated drop area during drop lifetime;
	$\frac{\sum_{i=1}^n \frac{A_i + A_{i+1}}{2} \Delta t}{\tau}$
A <sub>2</sub>	area of upper surface of drop
C <sub>p</sub>	specific heat of vapor at constant pressure, BTU/lb-°F
C <sub>s</sub>	concentration of vapor in air at drop surface, gm-mole/cm <sup>3</sup>
C <sub>∞</sub>	concentration of vapor in air at infinite distance from drop, gm-mole/cm <sup>3</sup>
D <sub>c</sub>	diffusion coefficient, cm <sup>2</sup> /sec
D	drop diameter
D <sub>int</sub>	average diameter, calculated from average integrated drop area during drop lifetime
f	radiation correction factor; $f = \frac{\bar{h}_c}{h_T} = \frac{1}{\left[ 1 + \frac{1}{4} \frac{h_r}{\left( 1 + \frac{7}{20} \frac{p}{\lambda} \right) C_p \Delta T} \right]^3}$

$g$	acceleration of gravity, $32.2 \text{ ft/sec}^2$
$g_c$	dimensional conversion factor; $32.2 \text{ ft-lb}_m/\text{lb}_f\text{-sec}^2$
$Gr$	Grashof number
$h_c$	over-all heat transfer coefficient to drop due to combined heat transfer modes of conduction, convection, and radiation, $\text{BTU/hr-ft}^2\text{-}^\circ\text{F}$
$\bar{h}_c$	average value of $h_{c-r-fc}$ during drop lifetime, $\text{BTU/hr-ft}^2\text{-}^\circ\text{F}$
$h_T$	total heat transfer coefficient for heat transfer by conduction and radiation only, $\text{BTU/hr-ft}^2\text{-}^\circ\text{F}$
$h_r$	$\frac{\epsilon_1 \sigma_r (T_w^4 - T_s^4)}{(T_w - T_s)}$ , $\text{BTU/hr-ft}^2\text{-}^\circ\text{F}$
$h_{cr}$	over-all heat transfer coefficient that would exist if no heat had been transferred to the drop by radiation, $\text{BTU/hr-ft}^2\text{-}^\circ\text{F}$
$h_{crfc}$	heat transfer coefficient to drop (lower surface) that would exist if no heat had been transferred to drop by radiation or convection, $\text{BTU/hr-ft}^2\text{-}^\circ\text{F}$
$h_{fc}$	free convection heat transfer coefficient to top surface of drop, $\text{BTU/hr-ft}^2\text{-}^\circ\text{F}$
$h_t$	heat transfer coefficient to liquid drop, $\text{BTU/hr-ft}^2\text{-}^\circ\text{F}$
$i$	time increment index
$j$	approximate number of vapor breakthrough regions in an extended liquid mass
$k$	thermal conductivity, $\text{BTU/hr-ft-}^\circ\text{F}$
$k_c$	mass transfer coefficient based on concentration, $\text{cm/sec}$
$t$	average drop thickness
$t^*$	dimensionless average drop thickness

L	length of horizontal square plate upon which free convection heat transfer coefficient is based
$L_e$	characteristic length of drop
m	time increment index
M	molecular weight of vapor, gm/gm-mole
n	number of vapor domes in an extended liquid mass
P	pressure, lbs/ft <sup>2</sup> , dynes/cm <sup>2</sup>
$P_s$	partial pressure of the diffusing vapor, dynes/cm <sup>2</sup>
$\Delta P$	pressure difference across drop interface, lbs/ft <sup>2</sup>
Pr	Prandtl number
q	rate of heat transfer, BTU/hr
$Q_c$	heat transferred to lower surface of drop by conduction, BTU
$Q_{comb}$	total heat transferred to drop by conduction, convection, and radiation, BTU
$Q_{fc}$	heat transferred to drop by free convection, BTU
$Q_r$	heat transferred to drop by radiation, BTU
$Q_{r1}$	heat transferred to lower surface of drop by radiation from plate, BTU
$Q_{r2}$	heat transferred to upper surface of drop by radiation from plate, BTU
$Q_{rup}$	heat transferred to upper surface of drop by radiation from environment, BTU
r	radial coordinate, radius
$r_o$	initial drop radius
$r_1, r_2$	principal radii of curvature of drop
Re	Reynolds number
Sc	Schmidt number

T	temperature, °F, °R
$\Delta T$	plate (boiling surface) temperature minus liquid saturation temperature, °F
t	time, sec
$\Delta t$	time increment, sec
t*	dimensionless time
$t_{rc}$	(calculated) vaporization time of drop that would exist if no heat transfer to drop had occurred by radiation, sec
u	radial velocity, ft/sec
V	drop volume, ml
V*	dimensionless drop volume
w	axial velocity (normal to plate surface), ft/sec
$W_1$	rate of evaporation from lower surface of drop, gm/sec
$W_2$	rate of evaporation from upper surface of drop, gm/sec
z	axial coordinate

#### Greek Letter Symbols

$\alpha$	thermal diffusivity, ft <sup>2</sup> /hr
$\delta$	distance between lower surface of drop and plate
$\epsilon$	emissivity
$\lambda$	latent heat of vaporization, BTU/lb
$\lambda^*, \lambda^*$	modified latent heat of vaporization, BTU/lb
$\lambda_c$	critical wavelength
$\lambda_d$	most dangerous wavelength
$\mu$	dynamic viscosity, lb <sub>f</sub> -sec/ft <sup>2</sup>
$\nu$	kinematic viscosity, ft <sup>2</sup> /sec
$\rho$	density, lb/ft <sup>3</sup>

$\sigma$	surface tension, lb/ft
$\sigma_r$	Stefan-Boltzmann constant, BTU/hr-ft <sup>2</sup> -°R <sup>4</sup>
$\tau$	total vaporization time of drop
$\Omega$	field force

### Superscript

' modified quantity due to effects of vapor breakthrough

### Subscripts

amb	ambient
act	actual (measured) value or calculated from measured value
avg	average value or calculated from average value
l	liquid
min	minimum
s	saturation temperature
theor	theoretical
v	vapor
w, p	wall (or plate) properties
o	initial value
$l^*$	characteristic length, $\left[ \frac{g_c \sigma}{g(\rho_l - \rho_v)} \right]^{\frac{1}{2}}$



## CHAPTER I

### INTRODUCTION

The Leidentfrost phenomenon may be succinctly defined as the film boiling of small liquid masses on a hot solid surface. This phenomenon is observed in everyday life when water droplets glide over the surface of a very hot iron or skillet. The phenomenon was first studied in 1756 by J. G. Leidenfrost (1), who observed the behavior of small water droplets on a glowing hot iron spoon. He noted the rather long vaporization times of the droplets when the spoon was very hot, contrasting with the very short vaporization times that occurred after the spoon had cooled somewhat.

The foregoing observations of Leidenfrost may be readily explained today with the assistance of Figure 1. Figure 1 is a typical "boiling curve", wherein the heat flux transferred from a heated solid surface to the liquid that covers it is plotted against the difference between the heated surface temperature and the saturation temperature of the liquid (log-log scales). The boiling curve is comprised of four regions, each of which is characterized by a different mechanism of heat transfer. The first region, AB, is the nonboiling convection region, wherein heat is conducted across the heated wall into the liquid; the heat is then transferred throughout the liquid by natural convection and vaporization takes place at the liquid-gas interface. The second region, BC, is the region of stable nucleate boiling. In

# CONVENTIONAL BOILING CURVE ILLUSTRATING METASTABLE BOILING LINE

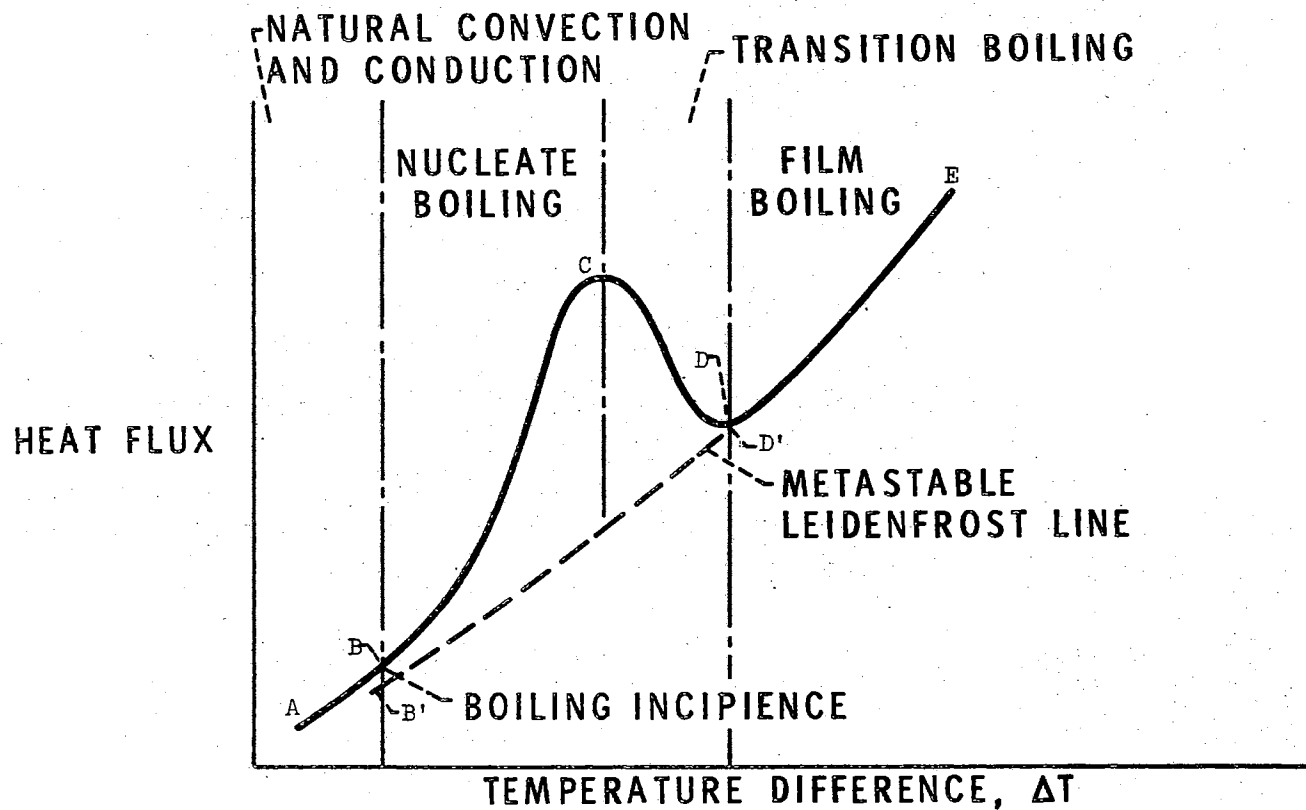


Figure 1. Conventional Boiling Curve Illustrating Metastable Boiling Line

this region, heat removal from the surface is enhanced remarkably by the mechanism of nucleate boiling, in which vapor bubbles are generated at preferred nucleation sites on the solid surface. As indicated in Figure 1, the heat transfer rate increases markedly with only small increases in  $\Delta T$ . As  $\Delta T$  is increased, more and more nucleation sites are activated, with an accompanying increase of heat transfer. Finally, at point C, the heat flux reaches a maximum, since the formation of more vapor at this point tends only to insulate the solid surface from the liquid.

The region CD is termed the transition boiling region. Here, the surface is almost completely blanketed with a vapor layer. The vapor layer is unstable and, consequently, the liquid makes very rapid intermittent contact with the solid surface. As  $\Delta T$  is increased, the heat transfer gradually decreases until it reaches a minimum at point D where the region of stable film boiling has its origin. Point D is also termed the Leidenfrost point; that is, the point of minimum heat flux. At this point, the surface is now blanketed by a relatively stable and quiescent vapor film. Since heat must be transferred to the liquid by conduction across the vapor film, the heat transfer rate is low. With higher temperature differences ( $\Delta T$ 's), the heat transfer rate (by conduction) increases gradually both because of a higher  $\Delta T$  and because of a gradual increase in thermal conductivity of the vapor film. At very high temperatures heat is removed from the solid surface in significant amounts by thermal radiation, also.

It is of more than passing interest to note that recent studies have cast doubt upon the existence of a unique  $\Delta T$  where the onset of stable film boiling occurs; that is, a unique Leidenfrost point. It

has been postulated (2) that for a very smooth, vibration-free solid surface, a small mass of liquid initially undergoing film boiling (Region DE) can be made to traverse the dashed line, B'-D' if the surface temperature is gradually lowered. The line B'-D' has been termed the metastable Leidenfrost line.

Returning to the observations of Leidenfrost, it becomes evident from Figure 1 that when the spoon was at a very high temperature, the liquid drop was never in direct contact with the spoon since it was in the film boiling region. Because of the low heat transfer coefficients characteristic of film boiling the vaporization time was very long. At lower spoon temperatures, the drop was evidently in the nucleate boiling region where, due to the characteristically high heat fluxes (and high heat transfer coefficients), the vaporization time was much shorter.

The Leidenfrost phenomenon is associated with the film boiling of discrete masses of liquid as shown in Figure 2(a) through (3),<sup>1</sup> while pool film boiling is associated with a continuous or essentially infinite amount of fluid (completely covering the heated surface). Hence, the Leidenfrost phenomenon involves the additional variable of initial liquid volume.

The motivating interest in the Leidenfrost phenomenon is twofold. First, the phenomenon is of interest in itself - interesting in its interrelated aspects of heat transfer and fluid dynamics

Secondly, as noted in Reference 3, which is a thorough and the most recent survey of Leidenfrost phenomenon studies, modern technology is moving in the general direction of more extreme temperatures, both

---

<sup>1</sup>Figures 2, 5, 6, and 7 are reproduced from References 14 and 15 with the permission of the author, Dr. K. J. Baumeister.

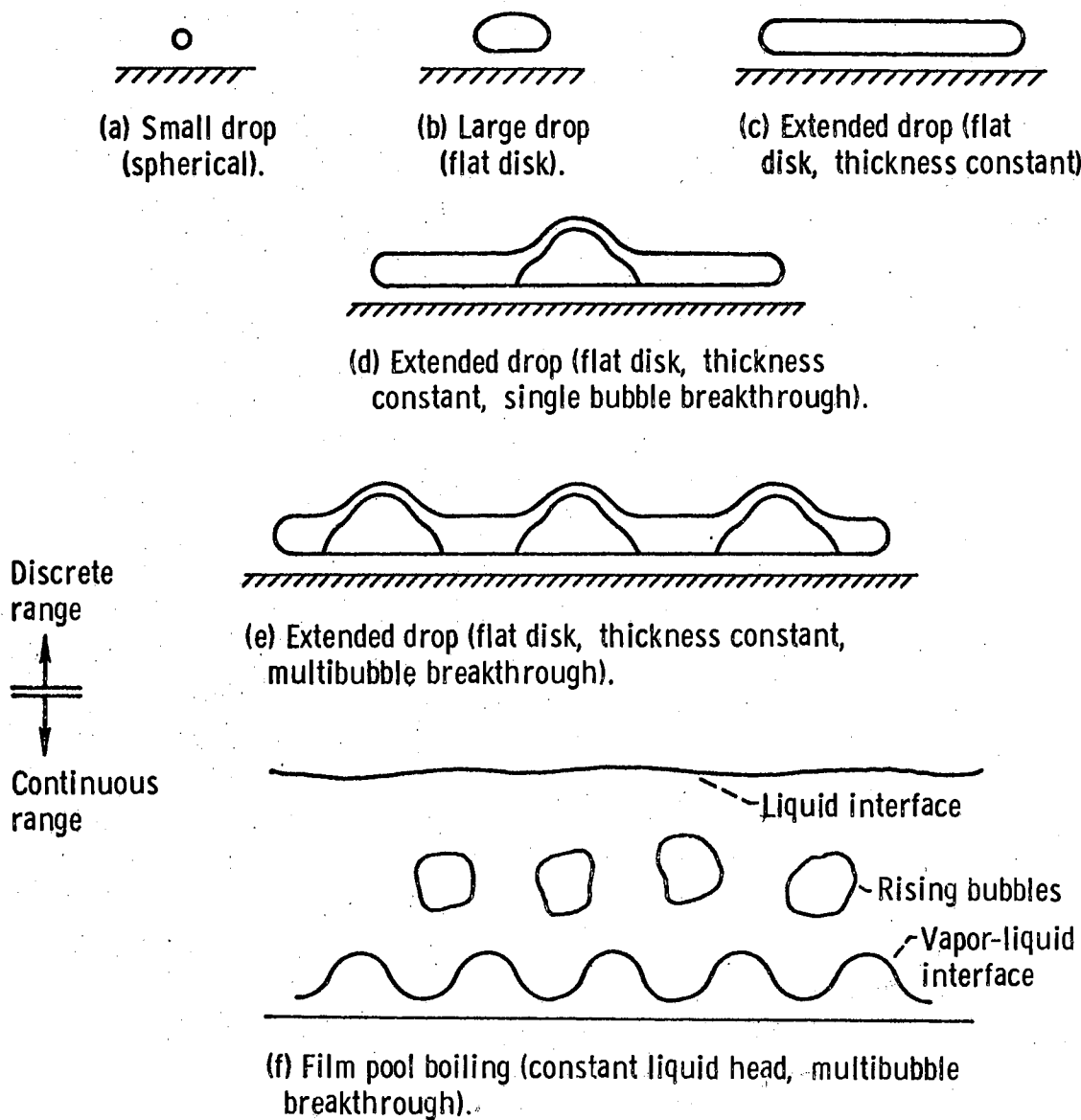


Figure 2. Film Boiling States of Liquid Masses

high and low, and high heat fluxes. Since film boiling frequently exists under these conditions, the phenomenon becomes of practical interest also. In some cases film boiling may be desirable, although more frequently it is undesirable. In either case an understanding of the film boiling phenomenon is obviously required in order to predict practical consequences.

Several instances in which film boiling and the Leidenfrost phenomenon in particular are of interest are (3):

- (1) Spray or fog cooling of nuclear reactors that have accidentally had a coolant loss and, consequently experience a very large rise in wall temperature.
- (2) The use of a water spray to cool steel billets or the rolls in rolling mill operations.
- (3) Water spray during continuous casting.
- (4) The design of quick response steam generators by spraying liquid on a hot surface.
- (5) The stable operation of a steam iron with a changing water inventory.
- (6) Film cooling of a rocket nozzle, either by breakdown of a continuous liquid film or direct spray injection.
- (7) Cool-down of cryogenic liquid storage tanks and transfer lines during filling. An interesting corollary problem is the possibility of minimizing cryogenic liquid loss by deliberate production of a vapor film next to the wall by film boiling.
- (8) Use of air-dropped solutions to control forest fires.
- (9) Fuel vaporization in a diesel engine.

The general goal of the present study is to investigate the Leidenfrost phenomenon for liquid nitrogen masses ranging from large drops to extended drops with vapor breakthrough (Figure 2(a) through (e)). More specific goals will be outlined following the next chapter.

## CHAPTER II

### LITERATURE SURVEY

Among the earlier studies of the Leidenfrost phenomenon are those of Pleteneva and Rebinder (4 and 5) and Borishansky (6 and 7). Pleteneva and Rebinder experimentally determined the Leidenfrost temperatures (the temperature at which the evaporation time of a given droplet size is a maximum) for several fluids (water, benzene, chloroform, methyl alcohol, propyl alcohol, isoamyl alcohol, nitrobenzol, ortho toluidine, and ethylene glycol). They found that the evaporation time of water reached a maximum value at a plate temperature of  $275^{\circ}\text{C}$  in air at one atmosphere. They also found that the maximum evaporation time for organic liquids was proportional to the absolute boiling point of the liquid. Borishansky obtained total vaporization times for several fluids (water, ethanol, carbon tetrachloride, and benzene) over a large range of droplet sizes (0.0465 to 25 ml). He proposed a dimensionless correlation for the vaporization times of small droplets, using only a heat continuity equation at the vapor-liquid interface and a differential heat balance equation on the droplet as a basis for generating the dimensionless correlating groups. Radiation effects were omitted as being negligible. In addition, momentum and mass balances were not made. Hence, the fluid dynamics of the vapor film were neglected as was the effect of mass diffusion from the top of the droplet.

Gottfried (8) took all of the foregoing neglected effects into



account in the most complete analytical approach until that time (described in greater detail in "Discussion of Theoretical Models"). Postulating a physical mechanism based on simultaneous conduction, convection, diffusion, and radiation, and assuming the droplets to be perfectly spherical, he obtained a semi-empirical numerical solution using a digital computer, giving predicted vaporization times that agreed with his experimental results to a maximum error of 25 per cent. His experimental studies consisted of the determination of total vaporization times for drops of water, ethyl alcohol, benzene, and carbon tetrachloride over the size range from 0.0058 to 0.0415 milliliter, and for  $\Delta T$  values from  $50^{\circ}$  to  $500^{\circ}$  C.

Although Gottfried's work was primarily an analytical approach, it was necessary to introduce an experimentally obtained "universal" constant into his analysis. Lee (9) extended and improved Gottfried's analysis, thereby eliminating the need for an experimentally obtained constant. In addition, Lee obtained a simplified expression that permitted calculation of evaporation times without necessitating the use of a digital computer. This was done by using Lee's experimental data and a regression analysis to obtain two constants for a correlational equation. The correlational equation agreed with most of his 72 experimental points to within  $\pm 20$  per cent, with a maximum deviation of  $\pm 30$  per cent. Lee's experiments consisted primarily of the study of vaporization times of water, ethanol, benzene, carbon tetrachloride, and n-octane droplets ranging from 0.001 to 0.03 milliliter in initial volume. The results of the preceding investigations are reported in a later publication by Gottfried, Lee, and Bell (10).

Both Gottfried's and Lee's experiments, described previously, dealt

with small droplet sizes such that the droplets were not far from spherical. Patel and Bell (11) extended their work by investigating the film boiling of extended liquid masses (although Borishansky (7) was the first to study extended masses). As seen in Figure 2(a) to (e), for sufficiently large liquid masses, interfacial instability phenomena eventually appear, resulting in bubble breakthrough. A relatively large amount of literature is available dealing with interfacial instability phenomena and will be discussed later.

The next significant work appearing in the literature was that of Baumeister (12 and 13), who made an analytical and experimental investigation of small droplet evaporation (0.05 to 1.0 ml). Using an analog computer he solved the momentum, energy, static equilibrium, and continuity equations simultaneously and obtained overall heat transfer coefficients in closed form for a flat bottomed drop, with no radiation or diffusion effects considered. The theoretical results agreed with the experimental within  $\pm 20$  per cent.

Baumeister later simplified the foregoing analysis by neglecting inertia terms in the momentum equations before solving the governing system of equations (14). Because of this simplification use of an analog computer was not required. Solutions for heat transfer coefficients were obtained in closed form and were shown to agree with the previously obtained computer solutions.

The preceding investigations (12, 13, and 14) served as the basis for Baumeister's next contribution (15), a generalized correlation for the entire range of initial fluid volumes from small spherical droplets to extended bubbly masses. The correlation is presented as a single curve relating dimensionless vaporization time to dimensionless initial

liquid volume. In all of Baumeister's theoretical analysis, he assumed the liquid mass to be disc-shaped (circular cylinder). Hence, it might be anticipated that errors would arise in the small droplet region, where the drops are nearly spherical, and the extended mass region, where bubble breakthrough occurs (Figure 2). A geometry factor was introduced in order to extend the validity of his correlation to these two configurations. Apparently, however, interfacial instability phenomena resulting in bubble breakthrough were not considered to have any appreciable influence on heat transfer to the fluid. A more detailed discussion of the theoretical models of Gottfried, Lee, Bell, and Baumeister dealing with possible shortcomings, will be presented in the chapter on theory.

Most of the Leidenfrost investigations have been for pure liquid masses. However, studies have also been made of binary mixtures. Godleski (16) and Godleski and Bell (17) have studied total vaporization times and composition changes during vaporization for water-ethanol, ethanol-benzene, and benzene-toluene solutions into air. Their results show that the Leidenfrost point and the total vaporization time for the binary changes in a fairly regular way between the values for the pure components.

In addition, the effect of volatile and nonvolatile surface-active agents in water has been investigated in Reference 5. The chief effect of the surface-active agents was to change the effective heat transfer area, a result of the changing drop shape produced by the decrease in surface tension.

A relatively large amount of literature is available dealing with interfacial instability phenomena in pool film boiling. Hence, a

logical extension of the pool film boiling studies would be to determine the applicability of these results to the phenomena observed in the Leidenfrost phenomenon for extended masses (Figures 2(d) and (e)) and pool film boiling (Figure 2(f)). Several studies exist of interfacial instability phenomena that arise when a dense phase (liquid) is supported by a lighter phase (vapor) in a gravitational field (18, 19, 20 and 21), as occurs in film boiling. Mathematically speaking, it is conceivable that any perturbation on the vapor-liquid interface would disrupt the interface sufficiently to lead to vapor release or bubble formation. Practically, however, surface tension of the liquid tends to damp out perturbations of short wavelengths (19), while very large wavelength perturbations cannot exist unless a linear dimension of the boiling surface is of comparable length. Intermediate to these extremes is a critical wavelength, which has been derived from hydrodynamic considerations only (20) and is given by

$$\lambda_c = 2\pi \left[ \frac{g_c \sigma}{g(\rho_l - \rho_v)} \right]^{\frac{1}{2}} \quad (1)$$

The critical wavelength is the length of the smallest perturbation that can grow in amplitude on a flat, horizontal interface. The assumptions involved in the derivation are (1) both fluids are deep compared with the wavelength of the disturbance of the interface, (2) the fluids are incompressible, (3) there is no shear at the vapor-liquid interface, and (4) the fluid fields are irrotational. Conventionally, instabilities occurring without relative motion of the vapor and liquid phases is termed Taylor instability. When relative velocity is important the instability is termed a Helmholtz instability.

It has also been shown (22) that some perturbations grow more rapidly

than others. The wavelength of the perturbation growing most rapidly is the "most dangerous wavelength" and is given by

$$\lambda_d = \sqrt{3} \lambda_c = 2\sqrt{3} \pi \left[ \frac{g_c \sigma}{g(\rho_l - \rho_v)} \right]^{\frac{1}{2}} . \quad (2)$$

The first attempt to apply instability theory to film boiling was made by Chang (23), who noted that the vapor-liquid interface might exhibit waves of wavelength equal to the critical wavelength (Equation (1)). Using this wave approach, Chang subsequently derived a film boiling heat transfer coefficient as a function of  $\Delta T$  for a flat surface.

Prior to Chang's work, Bromley (24) made one of the first predictions of heat transfer in film boiling from a horizontal tube. Bromley analyzed the problem by employing the film-condensation model of Nusselt and interchanging the liquid and vapor phases. That is, he assumed that the tube is surrounded by a thin vapor film in laminar flow, separating the tube from the liquid. The suggestion of instability effects was made by Chang in 1956.

Zuber (22 and 25) later modified and extended Chang's approach and derived equations predicting the minimum heat flux in film boiling. The results of his analysis showed that the minimum heat flux was governed by a Taylor-type instability, and hence the minimum flux expression is governed by hydrodynamic considerations rather than by thermal transport properties.

Berenson (26) modified and extended the methods suggested by Zuber and succeeded in obtaining the heat transfer coefficient as a function of  $\Delta T$  for pool film boiling on a flat plate. His expression for the heat transfer coefficient was quite similar to that derived by

Bromley (24), which applied only to circular tubes. By analyzing the effect of vapor velocity on the results of the Taylor instability analysis, he concluded that near the minimum film boiling heat flux the Taylor instability model is valid. Also, he derived an expression for the  $\Delta T$  at which the minimum heat flux occurs, which, as mentioned previously is also a definition of the Leidenfrost point.

An experimental study by Hosler and Westwater (27) showed that film boiling from a horizontal flat surface can be treated as a Taylor hydrodynamic instability, as evidenced by measurements of inter-bubble distances, bubble periods, break-off diameters, and geometric arrangement of bubbles.

In view of the previous stability studies and their applications to film boiling heat transfer, it is natural to ask whether these results may also be applied to the Leidenfrost phenomenon for extended masses. This possibility was investigated by Patel (28) and Patel and Bell (11) who studied masses up to 10 milliliters in volume of water, carbon tetrachloride, benzene, and ethanol. Several of their most significant conclusions are:

1. The Leidenfrost phenomenon for extended masses does not differ markedly from that for small droplets except for bubble breakthrough phenomena.
2. Bubbles begin to break through the center of an extended mass when the diameter is about as large as the most dangerous wavelength.
3. Bubble dynamics appear to be governed by a Taylor instability with a characteristic wavelength between the critical and the most dangerous wavelength.

The authors state that these results clearly suggest an analytical treatment of heat transfer to extended masses in film boiling very similar to those for submerged surface film boiling proposed by Zuber and others.

All of the boiling studies cited thus far have dealt with "ordinary" liquids -- liquids with boiling points near ordinary room temperature. In recent years liquefied gases have played an increasingly important part in engineering technology. An obvious instance is the use of liquid propellants in rocketry. Since liquefied gases have very low boiling points, their contact with any surfaces at ordinary ambient temperatures immediately results in film boiling. Hence, when one deals with cryogenic fluids (liquefied gases at low temperatures) one must often deal with nucleate and film boiling heat transfer.

An excellent literature survey has been compiled dealing with boiling heat transfer investigations for oxygen, nitrogen, hydrogen, and helium by Brentari, Giarratano, and Smith (29). An earlier survey by Richards, Stewart, and Jacobs (30) is likewise useful.

Flynn, Draper, and Roos (31) were the first to obtain data for both the nucleate and film boiling regions on the same surface. They investigated the boiling of liquid nitrogen at atmospheric pressure from a 2-inch length of 5/8-inch outside diameter copper tubing. Their  $q/A$  (heat flux) versus  $\Delta T$  data indicated a minimum heat flux (film boiling regime) at a temperature difference of 48° K (86° R). Although their data shows a high degree of internal consistency, some lack of agreement was apparent upon comparison with other data reported in the literature. These discrepancies are attributed to two sources: (1) nature of the surface and (2) selecting the proper temperature for fluid property evaluation.

Frederking and Daniels (32) investigated the kinematics of vapor removal for film boiling of liquid nitrogen from a sphere. In another study, Frederking, et al. (33) investigated effects of interfacial instability on film boiling of saturated liquid helium I above a horizontal surface. A correlation of the data was obtained which was reported to be useful both for helium I and nitrogen.

While several studies have been made for both the nucleate and film boiling of liquid nitrogen from flat surfaces, spheres and cylinders, no investigations have been made of the Leidenfrost phenomenon.

The general purpose of the present study was to investigate the transfer of heat occurring during the vaporization of discrete masses of liquid nitrogen undergoing film boiling into a nitrogen atmosphere at atmospheric pressure. The initial drop sizes ranged in size from large disc-shaped drops (Figure 2(b) to extended pancake-shaped masses in which vapor breakthrough occurs (Figure 2(c)).

Specific goals were as follows:

1. Determination of total vaporization times over the given size range for values of  $\Delta T$  ranging from zero to about  $400^{\circ}$  F.
2. Determination of the Leidenfrost point for the range of drop sizes.
3. Determination of vaporization rates and instantaneous heat transfer coefficients during the lifetime of liquid mass at several  $\Delta T$  values.
4. Investigation of interfacial instability phenomena for extended masses, for example, bubble size, spacing and frequency, and their influence upon heat transfer to the masses.
5. Comparison of the experimental results described in items 1



to 4 preceding with existing theory or results appearing in the literature.

6. Modification, extension, or introduction of correlations as warranted by results.

## CHAPTER III

### DISCUSSION OF THEORETICAL MODELS

Two theoretical models will be discussed here which are the basis of analysis of the heat, mass and **momentum** transfer processes of the Leidenfrost phenomenon. These models are the Gottfried-Lee-Bell model (10), which applies only to spherical or near-spherical droplets, and the Baumeister model (12-15), which is asserted to be valid over the entire range of drop configurations (Figure 2(a) to (e)).

In the analysis of both References 10 and 12, it is assumed that vapor generation from the lower surface of the drops is produced by conduction of heat across the vapor layer supporting the drop and radiation from the plate surface to the drop. (In References 12 and 13, radiation effects are introduced only as a radiation correction factor after the main analysis has been carried out.) In both References 10 and 12, the flow of vapor beneath the drop is assumed laminar and radially symmetric, and at the solid surface and drop surface the radial vapor velocity is assumed to be zero. The liquid drop is assumed to be at its saturation temperature. Properties of the vapor are evaluated at the mean film temperature  $[(T_w + T_{sat})/2]$  and are assumed constant.

The Gottfried-Lee-Bell model (or spherical drop model) for droplet evaporation is shown in Figure 3. The physical processes occurring in the model are (a) heat conduction,  $Q_c$ , through the (moving) vapor film between the hot solid surface and the lower surface of the drop, (b) net

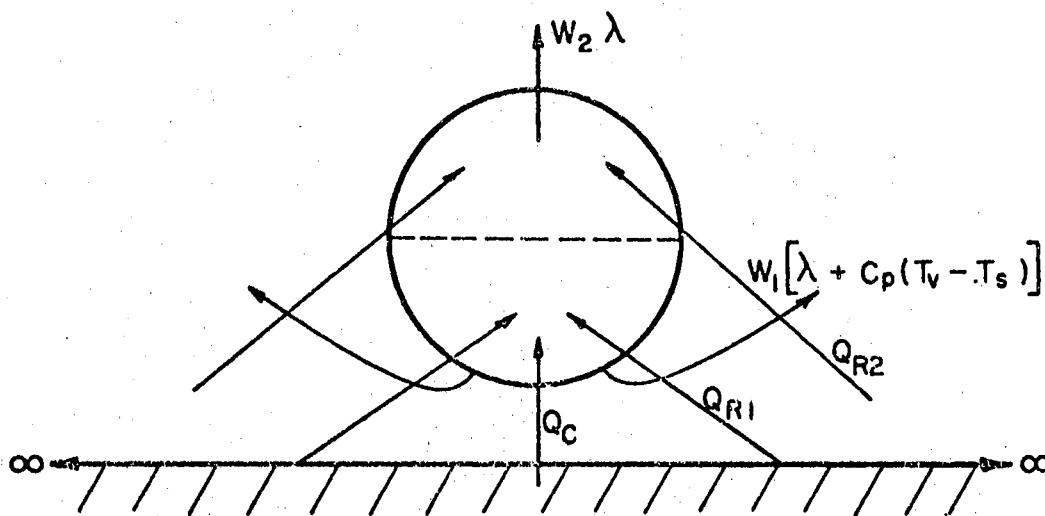


Figure 3. Heat and Mass Transfer Paths for the Spherical Drop Model

heat radiated to the lower and upper surfaces of the drop,  $Q_{R1}$  and  $Q_{R2}$ , respectively, (c) evaporation from the lower surface  $W_1$ , and (d) diffusion controlled evaporation from the upper surface  $W_2$ . The drop is assumed to be a perfect sphere throughout the evaporation process.

The equations written for the mass, heat, and momentum balances are as follows:

Mass balance:

$$\rho \frac{dV}{dt} = - (W_1 + W_2) \quad (3)$$

Heat balance:

$$Q_c + Q_{R1} + Q_{R2} = W_1 [\lambda + C_p (T_p - T_s)] + W_2 \lambda \quad (4)$$

Momentum balance:

$$\frac{\partial u}{\partial t} + u \frac{\partial u}{\partial r} = - \frac{g_c}{\rho v} \frac{\partial P}{\partial r} - \frac{\partial \Omega}{\partial r} + \frac{\mu}{\rho v} \left( \frac{\partial^2 u}{\partial r^2} + \frac{1}{r} \frac{\partial u}{\partial r} + \frac{\partial^2 u}{\partial z^2} \right). \quad (5)$$

In the momentum balance equation it is assumed that the variation of  $u$  with respect to time is small compared to variations with respect to spatial coordinates. Also, assuming inertial terms and field forces to be negligibly small, and assuming  $\delta \ll r$  so that

$$\frac{\partial^2 u}{\partial r^2} + \frac{1}{r} \frac{\partial u}{\partial r} \ll \frac{\partial^2 u}{\partial z^2}.$$

Equation (5) simplifies to

$$g_c \frac{\partial P}{\partial r} = \mu \frac{\partial^2 u}{\partial z^2}. \quad (6)$$

The loss from the upper surface  $W_2$  is assumed to occur by pure molecular diffusion, and is calculated from the expression:

$$W_2 = \frac{k_c M P_s}{RT_s} A_2 = \frac{M D P_s}{r R T_s} A_2. \quad (7)$$

This expression is obtained from a correlation given by Froessling (34) for mass transfer from spheres,

$$\frac{k_c r_o}{D_c} = 1.0 + 0.3 \text{ Re}^{1/2} \text{ Sc}^{1/3} . \quad (8)$$

For the present case, the relative air velocity past the spherical drop is assumed to be zero. Also, from the general theory of mass transfer,

$$W_2 = k_c M(C_s - C_\infty) A_2 . \quad (9)$$

If the diffusing medium is assumed to be an ideal gas, and it is further assumed that the vapor concentration at an infinite distance from the drop surface,  $C_\infty$ , is zero, one may then use Equations (8) and (9) to arrive at Equation (7).

Writing a material balance for the lower half surface of the drop and equating the excess pressure exerted by the vapor film on the drop to the weight of the drop, an expression is obtained for  $W_1$  involving numerical evaluation of complicated integrals. The reader is referred to References 8, 9, and 10 for details of this derivation for  $W_1$ .

Expressions for radiative heat transfer  $Q_{R1}$  and  $Q_{R2}$  were developed by deriving configuration factors from the plate surface to the upper and lower surfaces of the drop.

Solutions to Equations (3), (4), and (6) were obtained numerically and involve a formidable amount of computation. Details of the computational procedures are found in Reference 9 together with a listing of the computer programs used to carry out the computations. Given an initial drop size, the fluid properties and the wall temperature, solutions are obtained for instantaneous drop volume, drop radius, and evaporation rate, from which total evaporation times are obtained.

Several interesting results of the preceding analysis are as follows. For water drops at  $\Delta T = 324^\circ \text{ F}$  and  $\Delta T = 720^\circ \text{ F}$  the radiative heat fluxes are calculated to be 30 and 60 per cent, respectively, of

the conductive-convective heat flux. These results indicate that radiation heat transfer is sufficiently large that it must be taken into consideration.

In addition, the importance of mass diffusion from the upper half of the drop is indicated in one instance by a change in analytical vaporization rate curves of  $\pm 15$  per cent for a change in diffusion coefficient of  $\pm 20$  per cent.

Another illustration of the importance of mass diffusion can be obtained from Figure 4. In Figure 4 the rates of evaporation per unit area from the lower and upper halves of the drop,  $W_1/A_1$  and  $W_2/A_2$  are plotted as a function of time for water drops at  $500^\circ$  and  $900^\circ$  F wall temperature. At higher wall temperatures, the evaporation rate from the lower half of the drop predominates over molecular diffusion from the upper half of the drop. At lower wall temperatures the situation is reversed, with the condition being most pronounced toward the end of the droplet lifetime. Hence, these results indicate that mass transfer resulting from molecular diffusion apparently must be taken into consideration if error is to be avoided.

The complicated numerical calculations necessitated in the previous analysis were greatly reduced by Lee who obtained the following dimensional correlational equation from 79 of his data points using a regression analysis.

$$\frac{\rho_l r_o}{\tau} = 0.0117 \left[ \frac{k_v \Delta T r_o g \rho_v (\rho_l - \rho_v)}{\mu_v \lambda^{**}} \right] + 2.38 \left[ \frac{\sigma_r \epsilon_p (T_p^4 - T_s^4)}{\lambda^{**}} \right] \quad (10)$$

where  $\tau$  is the total droplet vaporization time. The first group of bracketed terms represents the conductive-convective contribution to droplet vaporization, while the second group represents the radiative

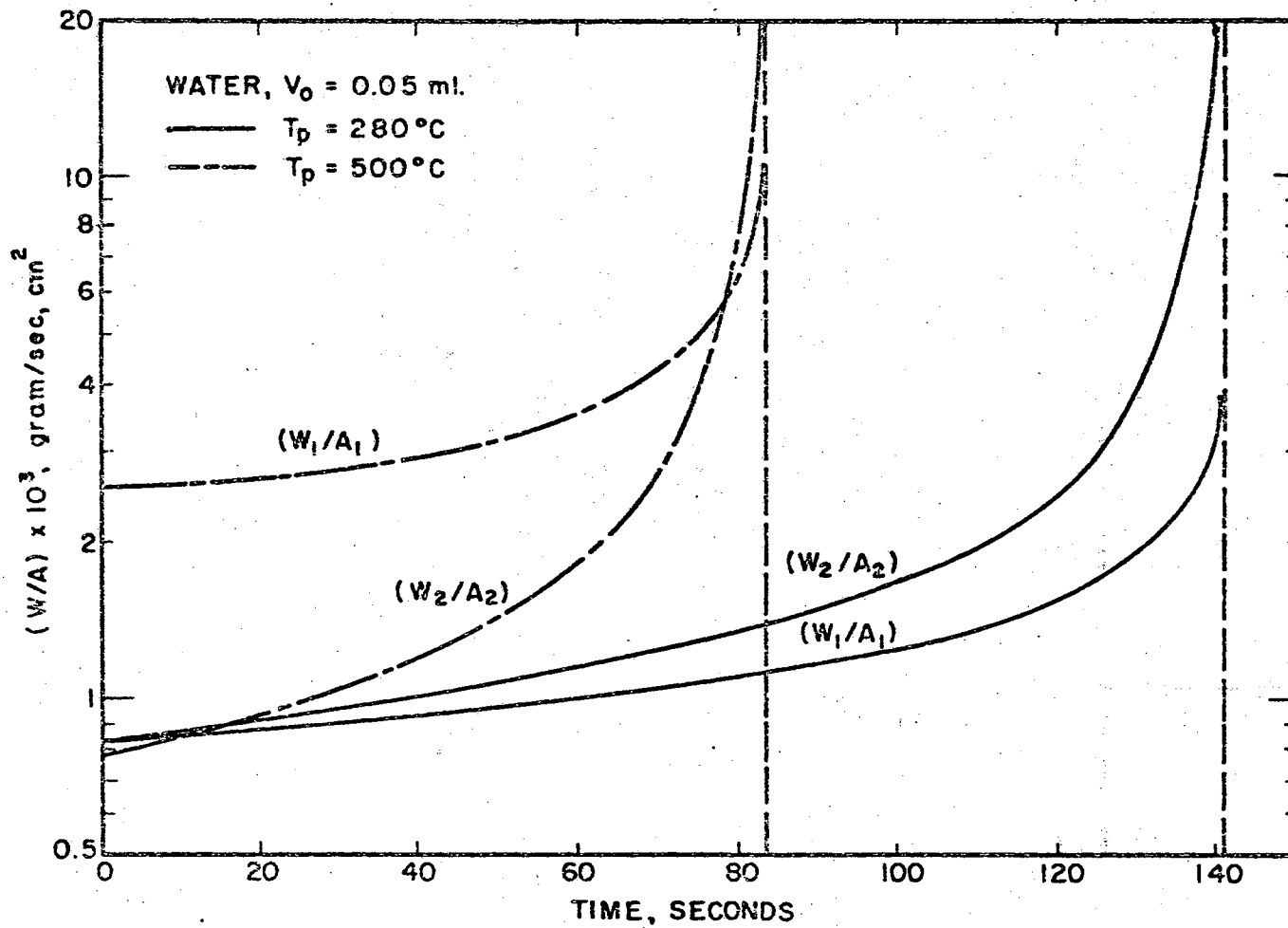


Figure 4. Calculated Evaporation Rates Versus Time for Water

the radiative contribution. Equation (10) thus provides a quick estimate of the overall droplet evaporation time. The average scatter of data about the correlation Equation (10) is about  $\pm 20$  per cent (9).

The model employed by Baumeister in his theoretical investigations (12, 13, 14, and 15) is a cylindrical, circular disc as shown in Figure 5. Baumeister's work differs from the previous investigations chiefly in that he ultimately attempts to predict heat transfer coefficients and vaporization times over the entire range of liquid volumes -- from spherical drops to extended bubbly masses -- with one universal correlation.

For the sake of completeness, it should be pointed out that Borishansky also made the same attempt. However, Borishansky's correlation was derived using only a heat continuity equation at the vapor-liquid interface and a differential heat balance equation on the drop. Momentum and mass balances were not made and hence the fluid dynamics of the vapor film were neglected.

The assumptions unique to Baumeister's model are as follows:

1. Heat transfer to and evaporation from the upper surface are considered negligible compared to that occurring beneath the drop.
2. Radiation is neglected.
3. A uniform gap thickness is assumed.
4. The thickness of the disk approximating a given drop is defined by

$$t = \frac{V}{\pi r_o^2} \quad (11)$$

where the relation between  $V$  and  $r_o$  was obtained (12 and 15) by



# SCHEMATIC MODEL OF THE EVAPORATION OF A FLAT DISK

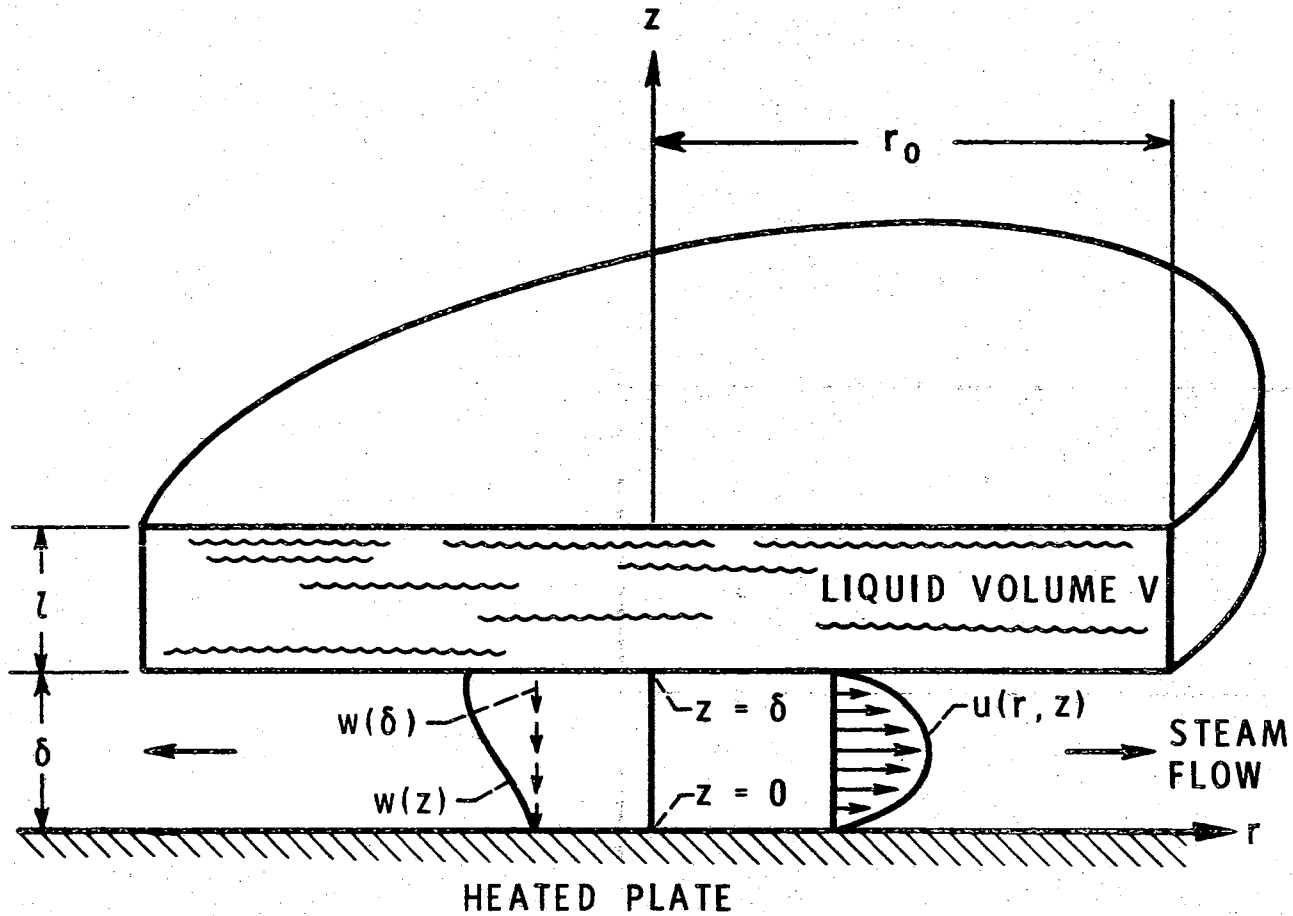


Figure 5. Schematic Model of the Evaporation of A Flat Disk

numerical solution of the Laplace equation,

$$\frac{1}{r_1} + \frac{1}{r_2} = \frac{\Delta P}{\sigma} \quad (12)$$

which results from a balance of the gravitational and surface tension forces acting on the liquid drop.

Immediately it is to be noted that assumptions (1) and (2) are not in accord with the results of the Gottfried-Lee-Bell analysis, although as is seen later, Baumeister developed a radiation correction factor. Regarding the assumption of mass diffusion from the top surface, Baumeister (12) utilized the statement of Kutateladze (35, p. 376) that the external surface of the spheroid is covered by superheated vapor flowing from beneath the spheroid. The mass transport from the upper surface was thus reasoned to be reduced to a near zero value. Furthermore, Baumeister states that even in the absence of a vapor cover, both the free convective and radiant heat transfer, together with the free convective evaporation (estimated from a correlation by Wade (36)), are negligible when compared to that occurring beneath the droplet.

The matter of radiant heat transfer is not really in question. One analysis (10) is very explicit in describing the transfer of heat by radiation and incorporates this term into the energy equation. The second analysis adds on a correction factor for radiation heat transfer after the momentum, continuity, static equilibrium, and energy (less radiant energy) equation have been satisfied. Hence, the difference lies in the form in which radiation effects are introduced. In both cases, of course, the attempt to obtain accurate radiation properties is often a problem in itself.

Regarding mass diffusion from the upper surface, however, a

fundamental difference exists. References 35 and 36 have been used to support the contention that mass diffusion from the drops upper surface is negligible. The results of Wachters, et al. (37) offer evidence that contradicts the foregoing contention, however. In their studies of the film boiling of water drops, it was found that the evaporation rates in dry air were appreciably larger than in a saturated atmosphere. This difference was attributed to the much higher evaporation rate (mass-diffusion) at the sides and top of drop when in dry air. Obviously, additional work investigating mass transfer effects is desirable. In the present study, it was anticipated that mass diffusion perse would not be appreciable since the vaporizing nitrogen drops were located in a pure nitrogen atmosphere.

Examining the mathematical details of Baumeister's analysis (12) in greater detail, momentum equations are written for velocities in both the r- and z-directions. This compares with only a single equation for radial flow in the spherical drop analysis. The assumption is made that flow beneath the drop is laminar and incompressible with negligible energy dissipation. This assumption is based upon low values of Reynolds number calculated by Lee (9) and Baumeister (12). For a 0.5-cubic centimeter water drop on a flat plate the analysis of Reference 14 indicates a gap thickness of 0.00475 inch, an average radial vapor velocity at the edge of the drop of 5.25 feet per second, and a Reynolds number of 10.6. The results of Lee indicate that the Reynolds number never exceeds 16 for all liquids and conditions studied. Hence, this assumption is well justified. Also the body force of the vapor in the momentum equation is neglected.

Another assumption is that the inertia terms in the Navier-Stokes

equations are negligible. Detailed justification for this assumption is given in Appendix A of Reference 14, where a comparison of acceleration terms are compared with viscous terms. For radial flow under a one-cubic centimeter water drop on a plate at 600° F, the viscous terms always dominate the inertia terms, going from a minimum value of 18 at the lower surface of the drop to an infinite value at the solid surface. In the z-direction, however, the basis for justification is not quite so strong. The maximum ratio of inertial to viscous terms is about 20, but in a region near the center of the gap the computed inertia times are larger than the viscous terms (at  $z = \delta/2$  the viscous term is identically zero). However, it is reasoned that inertia terms affect the velocity, pressure, and temperature profiles only slightly near the wall or vapor-liquid interface. Since the heat transfer coefficient is dependent mostly on the gap thickness, which is determined by the pressure distribution at the vapor-liquid interface, the heat transfer coefficient was felt to be unaffected by the inertia terms.

The equations to be solved are:

Momentum:

$$0 = -\frac{g_c}{\rho} \frac{\partial P}{\partial r} + \nu \left( \frac{\partial^2 u}{\partial r^2} + \frac{1}{r} \frac{\partial u}{\partial r} - \frac{u}{r^2} + \frac{\partial^2 u}{\partial z^2} \right) \quad (13)$$

$$0 = -\frac{g_c}{\rho} \frac{\partial P}{\partial z} + \nu \left( \frac{\partial^2 w}{\partial r^2} + \frac{1}{r} \frac{\partial w}{\partial r} + \frac{\partial^2 w}{\partial z^2} \right) \quad (14)$$

Continuity:

$$\frac{\partial u}{\partial r} + \frac{u}{r} + \frac{\partial w}{\partial z} = 0 \quad (15)$$

Energy:

$$u \frac{\partial T}{\partial r} + w \frac{\partial T}{\partial z} = \alpha \nabla^2 T \quad (16)$$

where it is assumed that

$$u \frac{\partial T}{\partial r} \ll w \frac{\partial T}{\partial z}$$

and

$$\frac{1}{r} \frac{\partial}{\partial r} \left( r \frac{\partial T}{\partial r} \right) \ll \frac{\partial^2 T}{\partial z^2} .$$

The boundary conditions for Equations (13) to (16) are:

$$z = 0, u = 0, w = 0, T = T_p$$

$$z = \delta, u = 0, w = w(\delta), T = T_{\text{sat}}$$

$$r = 0, u = 0$$

Static equilibrium:

$$\int_0^{r_0} P(r, \delta) 2\pi r dr = V\rho \frac{g}{g_c} \quad (17)$$

with boundary conditions at  $r = r_0$ , and  $z = 0$ ,  $P = P_0$

Interfacial energy balance:

$$-\rho_v \lambda w(\delta) = -k \left. \frac{\partial T}{\partial z} \right|_{z=\delta} . \quad (18)$$

The solution of Equations (13) to (18) are obtained with the aid of a similarity transform that reduces the partial differential Equations (13) to (15) to a set of ordinary differential equations. Since constant fluid properties were assumed, the equations of motion are not interrelated with the energy equation, that is, the velocity field is not dependent upon the temperature distribution. The reader is referred to References 12, 13, and 14 for details of the solution of the preceding equations. It is sufficient to say here that the following expression for a heat transfer coefficient to the drop is derived:

$$h_t = 0.68 \left[ \frac{k_v^3 \rho_v \rho_l g \lambda^*}{\mu_v \Delta T L_e} \right]^{1/4} \quad (19)$$

where  $\lambda^*$  is a modified latent heat of vaporization,

$$\lambda^* = \frac{\lambda}{\left(1 + \frac{7}{20} \frac{C_p \Delta T}{\lambda}\right)^3} \quad (20)$$

and  $L_e$  is a geometry factor, defined as

$$L_e = \frac{r_o^4}{V} = \frac{V}{\pi t^2} \quad (21)$$

where  $t$  is an average drop thickness simply related to the volume by

$$V = A_t .$$

It is apparent that for a given drop volume, one must know the average drop thickness  $t$  or the maximum drop radius  $r_o$  in order to calculate the geometry factor  $L_e$  to be used in Equation (19). This problem amounts to obtaining the drop shape as a function of liquid volume. This has been done in References 12 and 15 by numerical solution of the Laplace capillary equation (or Gibbs-Kelvin equation),

$$\frac{1}{r_1} + \frac{1}{r_2} = \frac{\Delta P}{\sigma_t} . \quad (22)$$

Defining the dimensionless drop volume as

$$V^* = \frac{V}{\left(\frac{\sigma_c g_c}{\rho_t g}\right)^{3/2}} \quad (23)$$

and the dimensionless average drop thickness as

$$t^* = \frac{t}{V^{1/3}} \quad (24)$$

one can represent the solutions to Equation (22), over the complete range of drop sizes, by the dashed line shown in Figure 6 (reproduced from Reference 15).

Before proceeding further, it should be pointed out that

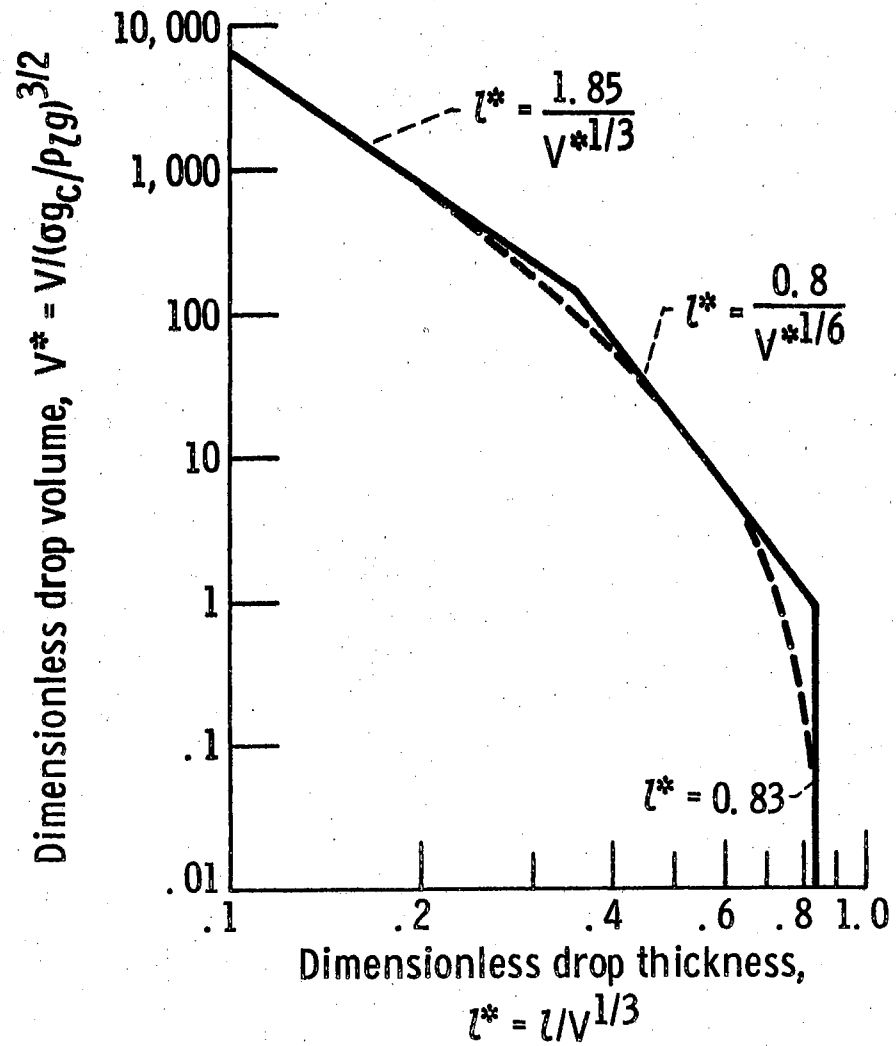


Figure 6. Universal Average Drop Thickness Curve

Equation (19) is very similar to Bromley's (24) expression for the heat transfer coefficient for a horizontal tube in film boiling,

$$h = 0.62 \left[ \frac{k_v^3 \lambda \rho_v g(\rho_l - \rho_v)}{\mu_v \Delta T D} \right]^{\frac{1}{4}} . \quad (25)$$

Equation (19) differs from Equation (25) only in its prefactor constant, the modified latent heat of vaporization (Equation (20)), and the geometry factor  $L_e$  in place of the tube diameter  $D$ . Although  $L_e$  is termed a geometry factor, it is a less-than-satisfying description since little physical significance can be ascribed to it other than that obtained from Equation (21). Furthermore, and perhaps of greater significance, for extended masses, no provision is made for the effect of bubble breakthrough on the physical configuration predicted by the Laplace capillary equation results. The likelihood that  $L_e$  may indeed be a function of interfacial instability phenomena will be investigated in a later section of this thesis.

Returning to Figure 6, Baumeister and Hamill attempt to obtain a universally applicable heat transfer coefficient by incorporating the universal drop shape curve results. This universal heat transfer coefficient can then be used to calculate total vaporization times from the following interfacial energy balance:

$$\lambda \rho_l \frac{dV}{dt} = h(V) A(V) \Delta T . \quad (26)$$

From the universal drop shape curve, one can obtain the heat transfer area  $A(V)$  and  $L_e$ , which is substituted into the heat transfer coefficient expression, Equation (19). Substituting the resulting expressions into Equation (26), and integrating, one can obtain the total vaporization time for a given initial drop volume. In order to simplify calculations,



the universal shape curve in Figure 6 is approximated by three straight lines corresponding to three ranges of drop size, which are (1) the extended drop region,  $V^* > 155$ , (2) the intermediate drop range,  $0.8 < V^* < 155$ , and (3) the small, spherical drop range,  $V^* < 0.8$ .

Defining a dimensionless vaporization time as

$$t^* = \frac{t}{f \left( \frac{\rho_l^{1/2} \mu_v \lambda^4 \sigma^{5/2} g_c^{5/2}}{k_v^3 g^{7/2} \lambda^* \rho_v \Delta T^3} \right)^{1/4}} \quad (27)$$

Baumeister and Hamill present as their final result, a plot of  $t^*$  against  $V^*$ , as shown in Figure 7.

Since the model upon which the preceding analysis is based is a cylindrical disc, one tends to question the validity of the universal curve in the spherical drop region,  $V^* < 0.8$  for two reasons. First, a uniform gap does not exist beneath the drop as assumed, and secondly, the heat transfer area is greater than the projected area of the sphere. Compensation is made for the latter by taking the effective heat transfer area as the average of the projected area of the sphere and the surface area of the lower half of the sphere. In addition, mass diffusion from the top surface of the drop is entirely neglected and is in contradiction with the results shown in Figure 4 and also those reported in Reference 37. In the extended drop region, the most likely source of error is that no provision has been made for changes of configuration due to bubble breakthrough.

In spite of the foregoing differences with reality, however, the generalized curve of Figure 6 is seen to be a reasonable agreement with a sizeable body of data. Indeed, this agreement is offered as substantiation (15) of the validity of the assumptions made in the

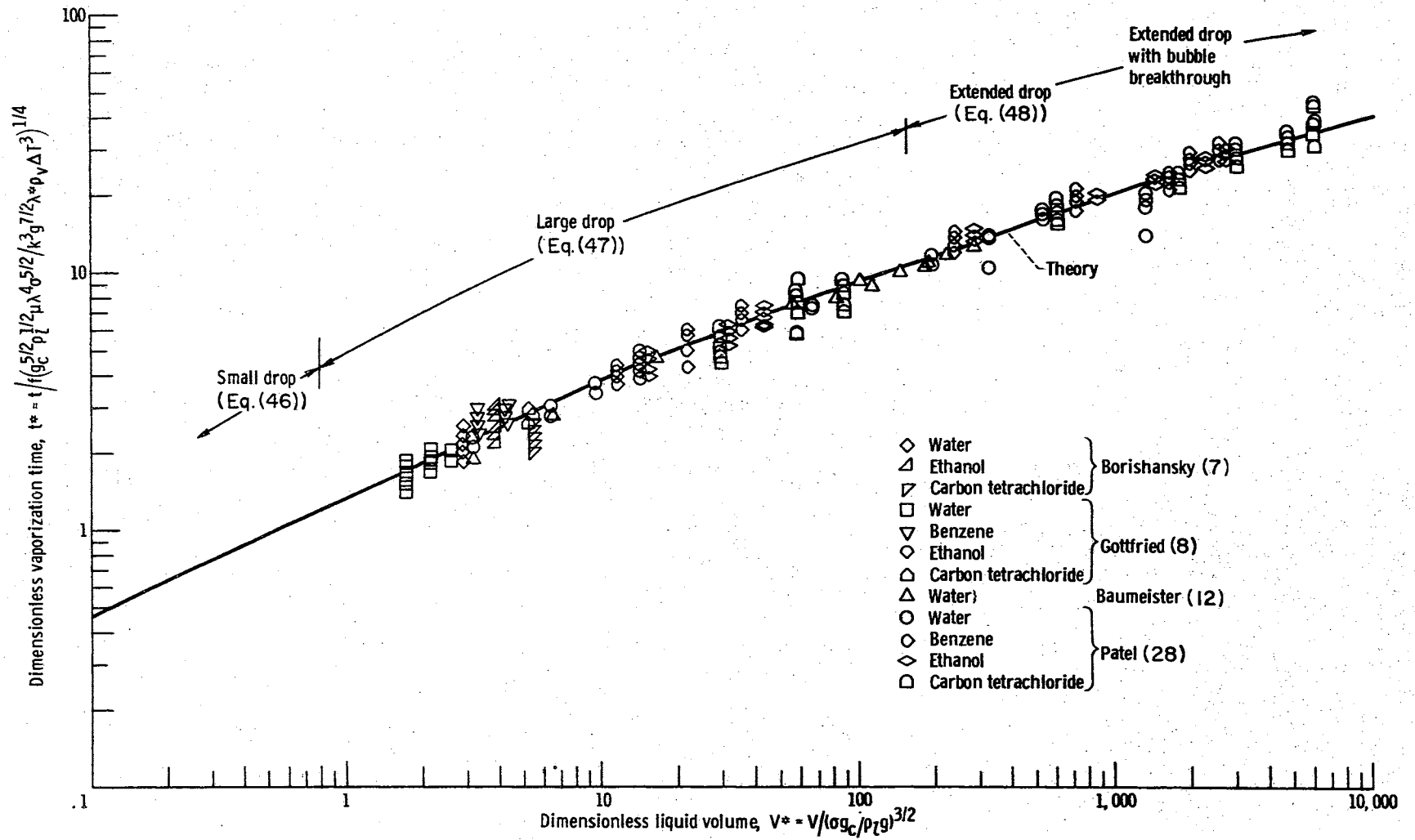


Figure 7. Universal Total Vaporization Time Curve

analysis.

In the present investigation, the low surface tension of liquid nitrogen may result in a more rigorous test of the universality of the curve for large values of  $V^*$ . Because of the low surface tension of liquid nitrogen, a given volume should experience many more vapor breakthroughs than, for example, the same volume of water. Hence, the influence of vapor breakthrough on overall heat transfer may be more readily discernible.

## CHAPTER IV

### EXPERIMENTAL APPARATUS

With liquids, such as water, alcohol, benzene, etc., the boiling point is rather high and consequently the heated surface must typically be maintained at temperatures on the order of hundreds of degrees Fahrenheit in order to study the film boiling region. In contrast, cryogenic fluids, or those fluids having very low boiling points, are far into the film boiling region when the solid surface temperature is at room temperature. Therefore, if quantities such as the Leidenfrost point are to be determined, the problem becomes one of cooling the heated surface to temperatures where the onset of stable film boiling occurs. With liquid nitrogen, this is predicted to occur at a  $\Delta T$  of about  $85^{\circ}$  F, (26), or at wall temperatures of  $-235^{\circ}$  F.

In addition to the necessity of a coolant system to control the boiling surface temperature, it is also necessary to conduct such vaporization tests of cryogenic fluids in a moisture-free atmosphere. This is necessary not only to prevent frost formation on the plate surface, but also to prevent condensation and freezing of water vapor within the vaporizing nitrogen drop itself. Consequently, the present experiments were conducted within a controlled atmosphere enclosure, a Fisher Scientific Isolatorlab, as shown in the schematic diagram of Figure 8. A pure nitrogen atmosphere was also desired in order to eliminate mass transfer from the drops by molecular diffusion. As shown

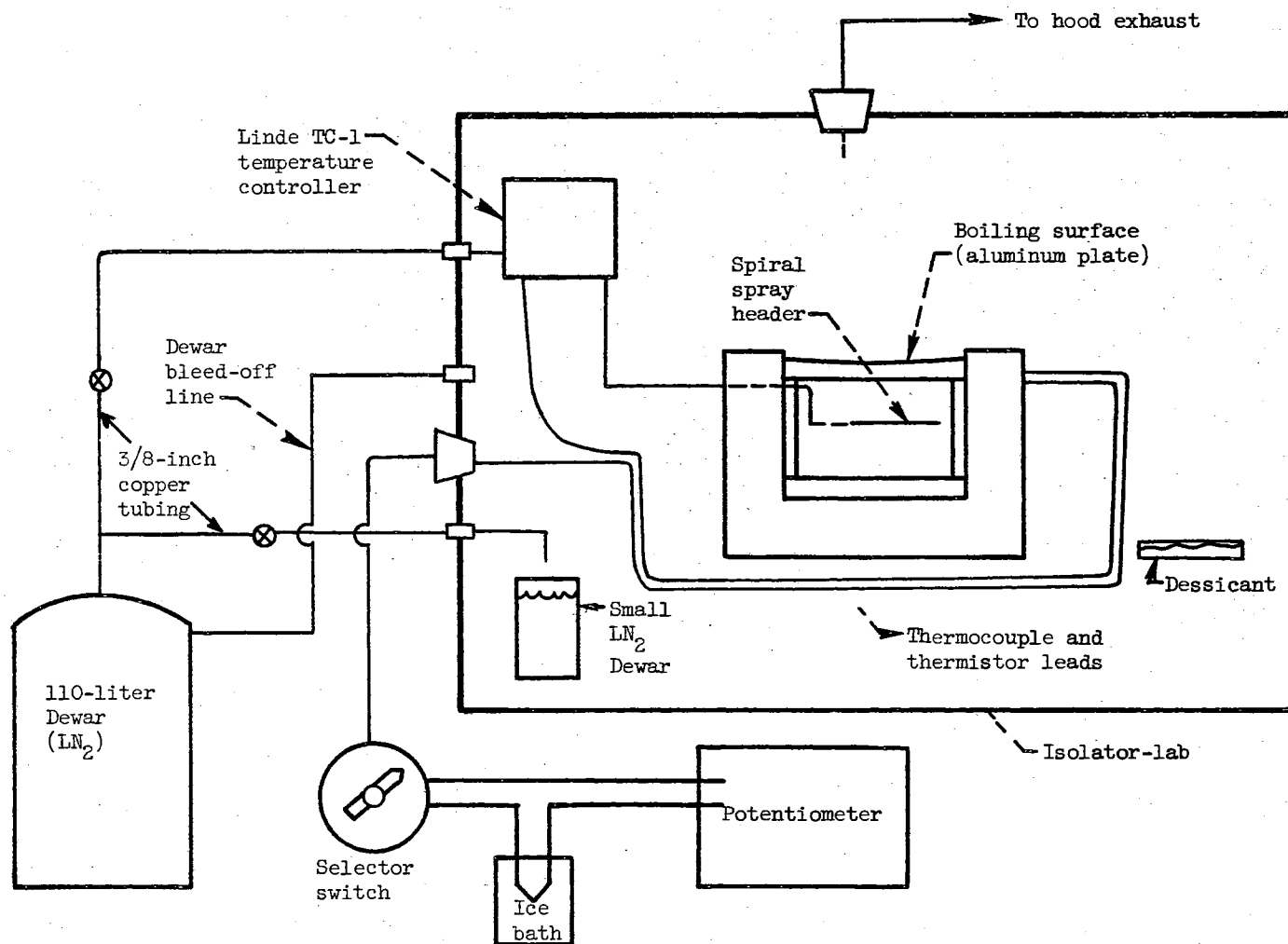


Figure 8. Schematic of Experimental Equipment

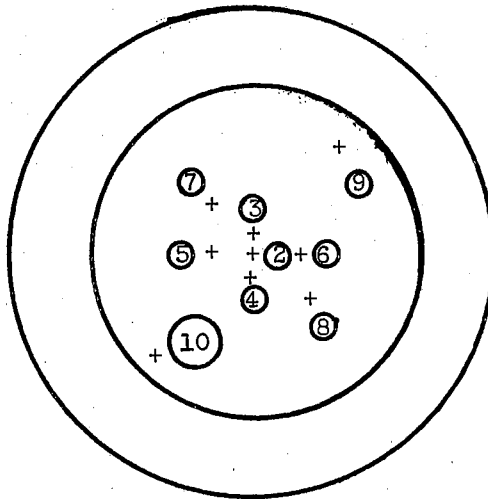
in Figure 8, the nitrogen atmosphere was maintained by introducing vaporized nitrogen from a 110-liter dewar of liquid nitrogen and from the coolant system (described later).

The surface on which the Leidenfrost phenomenon tests were made is shown in Figure 9. The plate is of high purity (99 per cent minimum) aluminum (temper designation 1100), is nominally of 3/4-inch thickness, and is six inches in overall diameter. The plate design is in accord with the results of Batten (38) who investigated the effect of surface temperature transients upon determination of the Leidenfrost point. His conclusion is that a large diameter, thick plate of high thermal conductivity should be used to minimize temperature transients. Such transients are of particular concern with extended masses, where, for example, Patel (28) noted temperature depressions of as much as 59° F upon depositing a 10-millimeter mass of water on a stainless steel plate at film boiling conditions.

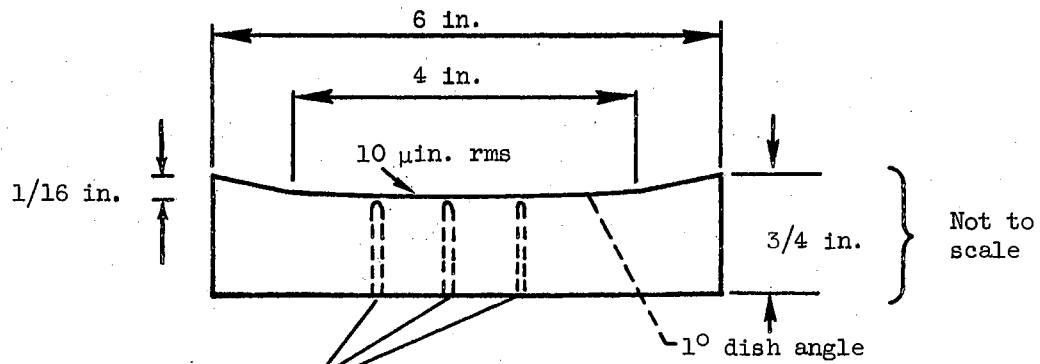
Nine-copper-constantan thermocouples were imbedded 1/16 inch from the top surface as shown. The thermocouples, which were B and S 26-gauge, sheathed in polyvinyl insulation, were placed in the 0.084-inch diameter holes drilled in the bottom surface of the plate. Saureisen P-1 cement was used to fill the space between the sheathing and the aluminum, securing the thermocouples and also restoring the solid composition of the plate. The thermocouples were connected to a selector switch and the output was read by a L and N Model 8687 potentiometer readable to 0.001 millivolt.

The thermocouples were calibrated over the temperature range from -320.4° F to 32° F. The three calibration points were the boiling point of liquid nitrogen, -320.4° F, the sublimation point of CO<sub>2</sub>, -109.3° F,

T.C. No.	Dist. from center, in.
3,4	0.25
5,6	0.50
7,8	0.90
9,10	1.50



(Thermocouples located  
45° apart)



0.080 in. diameter  
thermocouple holes  
drilled to 1/16 in.  
of surface

Figure 9. Schematic of Aluminum Test Plate

and the ice fusion temperature. The  $\text{CO}_2$  point was established by arranging a well packed wet mixture of dry ice and pure reagent quality ethyl alcohol, with excess alcohol on top, in a partially insulated 500-millimeter beaker. The amount of insulation was adjusted until a gentle bubbling was observed at the surface of the alcohol. The foregoing procedure was similar to that recommended by Kannuluik and Law (39). The emf-temperature data obtained in this calibration were virtually indistinguishable from the values tabulated in the NBS circular 561 (40). Consequently, table values of emf-temperature were used thereafter.

The top surface of the plate was dished at a  $1^\circ$  angle over a 4-inch diameter circular area in order to position the drops at the plate center, and also facilitate photographic studies. A dished plate is also of use in preventing large liquid masses from separating into numerous smaller drops upon deposition. A  $1^\circ$  dished surface has been found to have no noticeable effect on total vaporization times (12).

Due to the purity ( $> 99$  per cent) of the aluminum, it was difficult to obtain an extremely smooth surface finish (2 to 4  $\mu\text{in. rms}$ ) as reported in a few previous studies. Because of the "softness" of the metal there was a tendency for tiny pits to develop during the machining process at widely spaced points on the surface. Consequently, the surface was finally prepared by hand polishing using silicon carbide powder (grit numbers 240 to 1000), grinding compound ranging from 800 to 3200 mesh size, and micropolish compound down to 0.3 micron particle size. Using this procedure, a surface roughness of about 10 microinches rms was finally obtained.

Cooling of the plate was accomplished by means of a liquid nitrogen spray directed into the space beneath the plate (referred to hereafter



as the spray chamber) as shown in Figure 10. The walls of the spray chamber were formed by a  $2\frac{1}{2}$ -inch length of  $\frac{1}{4}$ -inch wall by 6-inch outside diameter lucite cylinder. The bottom of the chamber consisted of a  $\frac{3}{4}$ -inch thick aluminum plate similar to that used for the boiling surface. The aluminum plates were positioned on the lucite cylinder by means of a 0.30-inch by 0.024-inch deep shoulder along their periphery.

The spray header consisted of a single turn coil of  $\frac{3}{8}$ -inch copper tubing closed at its end. Nine 0.043-inch holes were spaced equally around the coil. One header was made in which the spray holes were directed upward. A second header had the spray holes directed sideways toward the cylinder walls. At higher plate temperatures both coils proved satisfactory. At lower plate temperatures an upward spray of nitrogen impinging directly upon the bottom of the plate (and thermocouples leading therefrom) resulted in severe temperature fluctuations in temperature indications. Hence, the sideward spray was employed.

Instrumentation leads and the spray header were introduced into the spray chamber through suitably sized passages at the top of the lucite cylinder. No effort was made to minimize the clearances between the spray header and its passages since the excess clearance served as an exhaust pathway for the vaporized nitrogen. Four additional semi-circular exhaust passages of 0.125-inch diameter were spaced equally at the top of the cylinder also. The spray chamber and boiling surface were placed within a  $10\frac{3}{4}$ -inch diameter by  $5\frac{3}{4}$ -inch length of expanded polystyrene insulation (see Figure 10). This arrangement provided about two inches of insulation at the bottom of the chamber and  $2\frac{3}{8}$  inches around the sides. The insulation extended slightly above the aluminum plate, in an effort to minimize free convection currents across the

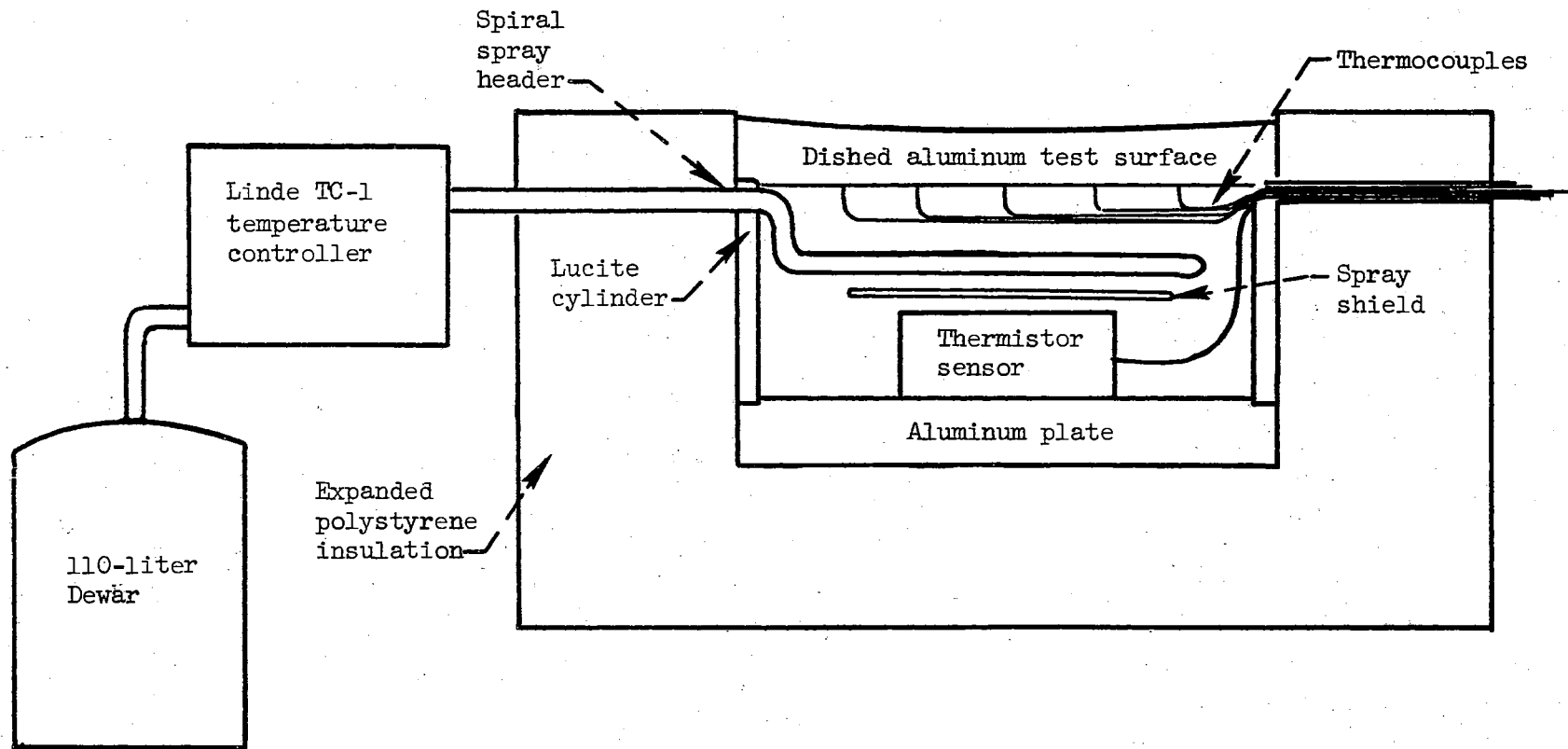


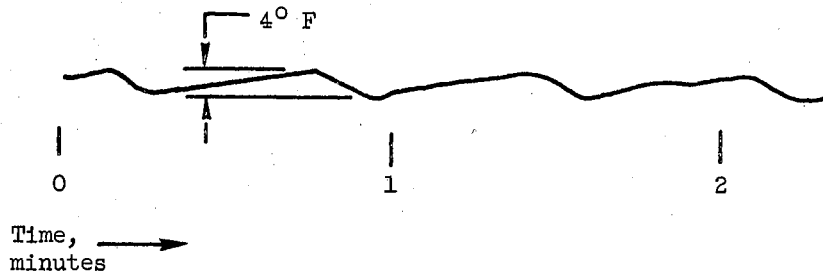
Figure 10. Schematic of Test Surface and Cooling System

boiling surface.

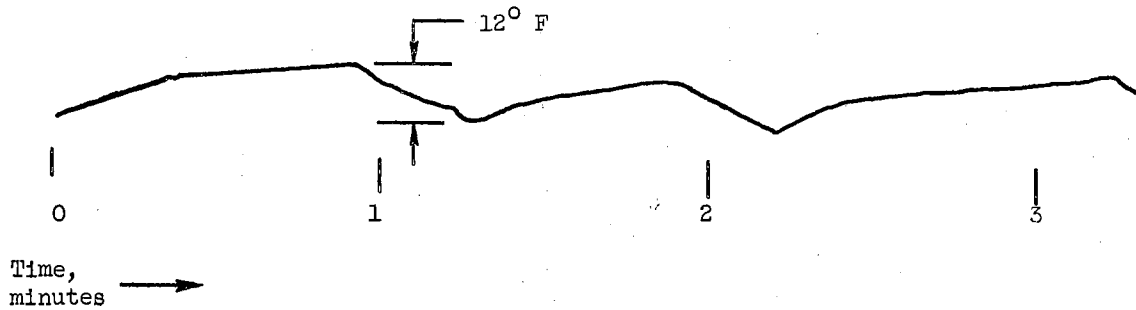
The method of controlling the plate temperature may be explained with the assistance of the schematic diagram of Figure 8. Two thermistors were located at the base of the spray chamber (Figure 10), and were shielded so as to avoid direct contact with a spray or jet of liquid nitrogen from the spray header. Two ranges of temperature control were possible, ranging from about  $-200^{\circ}$  to  $70^{\circ}$  F, and from  $-320^{\circ}$  to  $-150^{\circ}$  F, each range requiring a separate thermistor with characteristics compatible to that range. A Linde temperature controller, Model TC-1, received a temperature signal from one of the thermistors, depending upon whether the high- or low-range scale was operative. Thus, depending upon the temperature within the spray chamber, a solenoid valve within the temperature controller controlled the nitrogen flow from a 110-liter supply dewar.

When operating on the high-range scale (from room temperature to about  $-150^{\circ}$  F) the plate surface temperature variation indicated by the thermocouples was on the order of only a few degrees. No temperature measurements within the spray chamber were recorded since only the plate surface temperature was of importance. At lower plate temperatures the surface temperature variations became increasingly larger such that temperature control of the plate surface was maintained within closer limits by manual control of the dewar valve. Manual control was made possible by setting the TC-1 controller at its lowest point, thus maintaining its solenoid control valve in the open position. Typical traces of the temperature variation are shown in Figure 11.

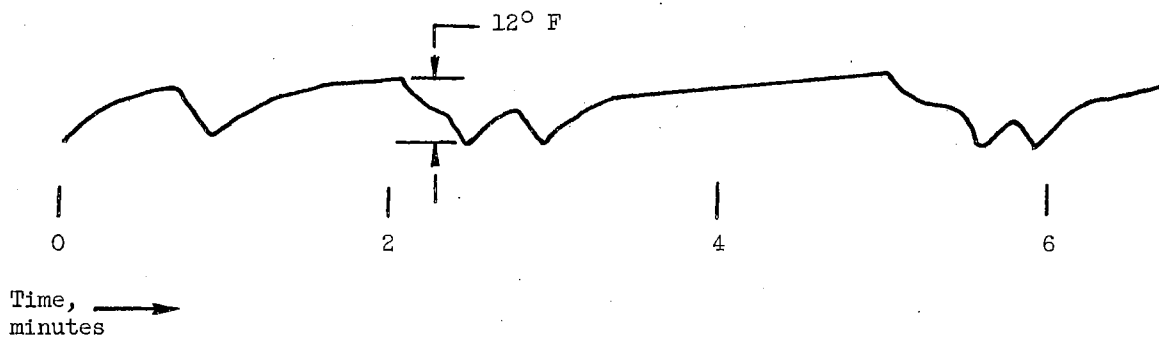
Referring again to Figure 8, handling of equipment within the Isolatorlab was accomplished through rubber gloves that were an integral



(a) Average temperature,  $59^{\circ}$  F.



(b) Average temperature,  $-162^{\circ}$  F. High range on temperature controller.



(c) Average temperature,  $-162^{\circ}$  F. Low range on temperature controller.

Figure 11. Temperature-Time History of Plate Surface During Cooling System Operation

part of the unit. Electrical power was introduced into the Isolatorlab by means of a service inlet panel having four 110-volt ac, three-wire grounded receptacles. The copper tubing wall penetrations were accomplished by using standard bulkhead fittings with neoprene gaskets placed between the fittings and the wall. The thermocouple wires leading from the selection switch to the reference junction outside the Isolatorlab penetrated the wall through a rubber stopper, which was sprayed with a protective vinyl coating to prevent any leakage. The thermocouple selector switch was placed within the Isolatorlab, as was the temperature controller, and a mercury-in-glass thermometer for measuring the atmosphere temperature. A small electrical fan, producing an air movement of a few CFM was also placed within in order to assist in removing water vapor from the enclosure atmosphere.

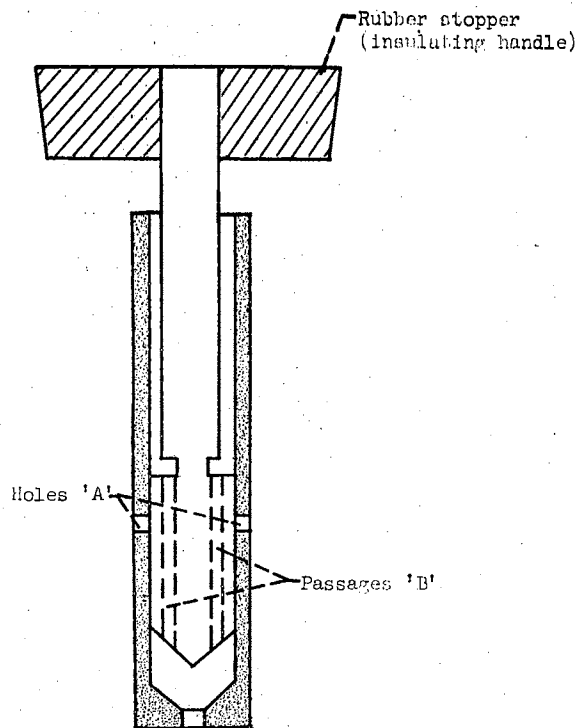
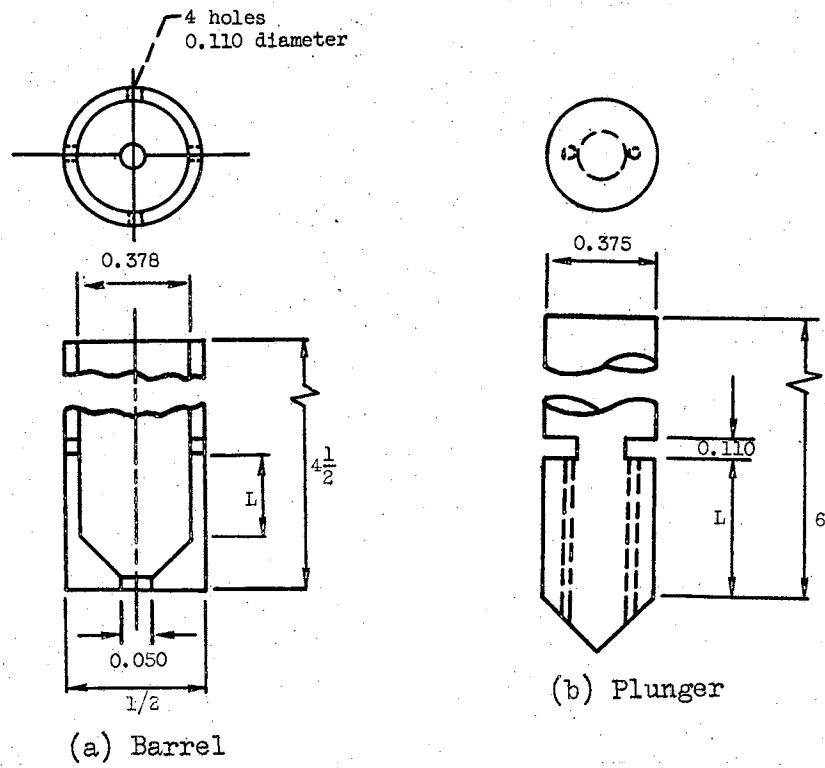
Excess pressure caused by vaporizing nitrogen within the Isolatorlab was relieved by two exhaust lines of  $\frac{1}{2}$ -inch tygon tubing which were vented into a hood exhaust. A slight overpressure of a few inches of water was always maintained in the Isolatorlab by adjustment of pinch clamps on the tubing.

Deposition of nitrogen drops of known volume onto the boiling surface proved to be a formidable problem. Previous studies with ordinary liquids employed hypodermic syringes successfully. With cryogenic fluids, however, this technique is entirely unsatisfactory. If a volume of liquid is drawn up into a syringe, film boiling occurs almost immediately at the syringe walls and the fluid is expelled. Modified syringes were made in which the syringe chamber walls and almost all of the tip were cooled and insulated by a surrounding volume of liquid nitrogen. The result was the same -- surface tension forces were not

operative in holding the liquid nitrogen in the syringe. Consequently, it was necessary to devise a device with some positive means of preventing liquid ejection. This was accomplished with the device shown in Figure 12.

The device is made of teflon, a good insulating material, in order to prevent vaporization of the liquid nitrogen while still in the depositor. The operating procedure was: (1) immerse the cylinder and plunger into a depth of liquid higher than the holes 'A', (2) remove the depositor, allowing excess fluid to drain off through the holes 'A', and (3) place the depositor over the boiling surface and lift the plunger, allowing fluid held within the passages 'B' to be deposited. By varying the length, diameter and number of the passages, three depositors of 0.161, 0.357, and 0.990 milliliter volume were developed.

It was found that for volumes greater than one milliliter, such a depositor led to another problem. At larger fluid volumes the exit velocity from the depositor was sufficiently high to break the liquid mass into numerous small drops that often skirted off the edge of the plate. Hence, a second type of depositor design was warranted. The second type of depositor (Figure 13) was made simply by modification of various sizes of pyrex beakers. A long pyrex rod was fused to a given beaker as shown and was a sufficiently poor heat conductor to serve as a handle. A second, small diameter, glass rod was fused to the pouring lip of the beaker. This tip was necessary in order to guide the liquid gently onto the plate surface, thereby avoiding the initial experiences of having the liquid impact from a height of about an inch and break into small droplets. Three beaker-type depositors were made from 2-, 5-, and 10-milliliter capacity beakers.



(c) Assembly

Figure 12. Teflon Depositor

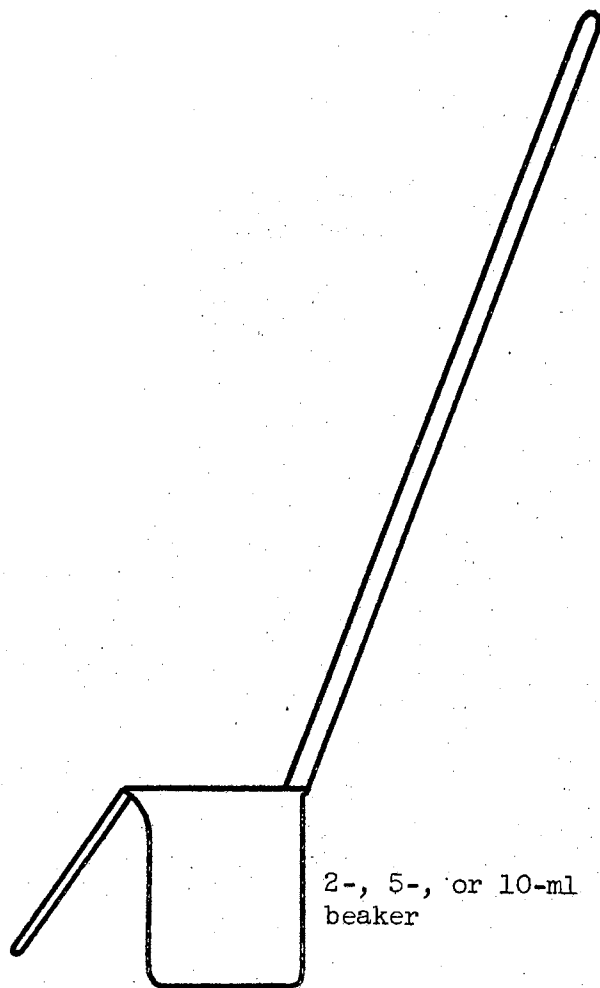


Figure 13. Pyrex Beaker Depositor



Photographic data were obtained (primarily) by a 16-millimeter Bolex H-16 Rex movie camera. Filming speeds from 12 to 64 frames per second, in addition to single frame exposures, were possible. A Switar 25-millimeter lens and a Macro-50-millimeter lens were used. A set of extension tubes (5, 10, 20, and 40 mm) were also available. An electrically driven (ac) motor drive (Bolex Unimotor) was used to film long sequences without stopping and also to insure a constant film speed. Speeds of 12, 16, 18, 24, and 32 frames per second were attainable with the Unimotor drive. Sixteen-millimeter Kodak Double-X negative film was used. In some photographs, a 4-inch long,  $45^\circ$  half-silvered prism was used to obtain both top and side views of droplet vaporization simultaneously.

Total vaporization times were measured with a stop watch readable to a tenth of a second.

## CHAPTER V

### EXPERIMENTAL PROCEDURE

#### Calibration of Depositors

In previous studies the procedure for calibrating depositors has been to weigh several drops of a test fluid individually on a precision balance scale. From such information, an average drop size was calculated together with average deviations, etc. Due to the fact that nitrogen evaporates at room temperature, this information was obtained using other fluids. The teflon depositors were calibrated using ethyl alcohol, since the small passageways of the depositors dictated use of a low surface tension fluid. The beaker-type depositors were calibrated using water.

With each depositor, ten individual samples were weighed. The results are presented in Appendix A, and give the average drop size and its uncertainty at the 95 per cent confidence level for each depositor.

A correction factor that is of some significance arises from thermal expansion (contraction) effects on depositor volume. For teflon, the mean linear thermal expansion is about  $2410(10^{-5})$  inch per inch over the temperature range from  $140^{\circ}$  to  $540^{\circ}$  R, while for pyrex it is about  $57(10^{-5})$  inch per inch over the same range (see Figure 52, Appendix C). Assuming the volumetric coefficient is three times the linear coefficient, the volume changes due to calibration at room temperature, rather than at the liquid nitrogen temperature, have been calculated,

and are also shown in Appendix A. The per cent error (where the error is assumed to be twice the fractional standard deviation) is seen to become larger in the direction of decreasing depositor size, and is a maximum of 15.9 per cent for the 0.357-milliliter depositor. The uncertainty of a measurement is taken as twice the standard deviation (95 per cent confidence limits), calculated from the values of the ten measurements.

#### Preparation of Equipment

Water-vapor removal from the Isolatorlab enclosure was accomplished primarily by silica-gel and phosphorous pentoxide dessicants placed in shallow containers at two levels within the enclosure. The small fan produced air movement over the surface of the dessicants in order to speed the vapor-removal process.

Since no access to the enclosure was possible during a test, all necessary equipment for a run was placed within the enclosure before the water-vapor removal process had begun. The equipment necessary was:

- (1) Three teflon depositors
- (2) Three beaker-type depositors
- (3) Level indicator
- (4) Levelling shims
- (5) Two 500-milliliter insulated containers for liquid nitrogen
- (6) Kimwipe optical tissues
- (7) Squeeze-bulb for cleaning of test surface
- (8) Scale for photographic studies.

After the dessicant and necessary equipment had been placed within the enclosure, the system was purged of the resident air by operating

the plate cooling system and thus introducing vaporized nitrogen gas. This was done for several minutes in order to rapidly reduce the water vapor content of the enclosure atmosphere by simple displacement. A continuous purging process was also introduced by connecting the bleed-off line from the 110-liter dewar to a penetration in the enclosure. Drying of the enclosure atmosphere continued for at least a full day before any tests were conducted, with two days being the rule for tests at low plate temperatures. In addition to these measures, the copper tubing in the cooling system was left uninsulated. Hence, once tests had begun the coolant line served as a "cold trap" by condensing traces of water vapor still present. All these measures were still not entirely successful at low plate temperatures (lower than about  $-150^{\circ}$  F). Resort was had to optical tissues to wipe off any thin traces of frost that formed on the plate surfaces at low temperatures.

In beginning a test, the temperature controller setting was adjusted to the desired point and the flow through the exhaust lines adjusted to permit the removal of the excess nitrogen gas generated in the cooling process. The liquid nitrogen containers were filled by opening valve 2, Figure 8.

After the plate temperature had reached an equilibrium value (or more correctly, cycled about the desired equilibrium value) a depositor was placed into a liquid nitrogen container for a few minutes until both the barrel and plunger (Figure 10) had undergone the same thermal contraction. The fan was then turned off so that drop evaporation occurred with a minimum of convective mass diffusion.

In depositing drops onto the test surface the time required to transfer the depositor from the nitrogen supply to a position just above

the plate and deposit the drop was about three seconds. The brief transit time together with the insulating qualities of the teflon was necessary to minimize vaporization of the nitrogen mass while it was still in the depositor. At the instant of drop impact, a stopwatch was started to measure the total vaporization time of the drop. Due to the low surface tension of liquid nitrogen, gentle deposition of the drops was required to prevent fragmentation.

Close checks on the plate temperature were maintained between vaporization of drops, and also during vaporization when time permitted. At low temperatures, where drop vaporization times were long and manual control of the cooling system was necessary, the temperature indications were monitored almost continuously throughout the drop lifetime.

At a given plate temperature, about ten vaporization lifetimes for a particular depositor were generally measured. This was believed necessary because of the relative imprecision (relative to that obtainable by using syringe deposition with ordinary fluids) in repeatedly obtaining equal liquid masses from a given depositor. This relative imprecision was especially evident for the beaker-type depositors. Hence, to improve the statistically-based confidence limits, the number of samples was increased to ten in most cases. This compares with three trials sufficient in most previous studies.

For every vaporization time measurement, an average temperature was recorded based upon the potentiometer observation during the drop lifetime. The average of the ten temperatures was used as the plate temperature.

### Photographic Studies

The 16-millimeter Bolex movie camera was used primarily to obtain vaporization rate data and vapor breakthrough dynamics information. The camera was positioned vertically above the plate just above the inclined viewing window of the Isolatorlab. The combination of 25- and 50-millimeter lenses and a set of extension tubes permitted closeup views of the vaporizing masses. Two 500-watt photo flood lamps were also located outside of the Isolatorlab and directed onto the plate surface to provide the necessary illumination.

Camera speeds of 32 and 64 frames per second were used to study vapor breakthrough phenomena. For vaporization rate studies over the drop lifetime single frame exposures were taken every five seconds. The long lifetime of drops at low plate temperatures made continuous filming, even at the lowest camera speeds, impossible, in addition to providing large excesses of information.

Several photographic studies were also made with the plate at room temperature and located outside the Isolatorlab. This permitted very close photographs of breakthrough dynamics and made possible top and side views (using a right-angle silvered prism) simultaneously. These results were qualitative in nature, since exposure of nitrogen drops to a water-vapor-laden air atmosphere, rather than a dry nitrogen atmosphere, makes quantitative comparisons questionable.

Quantitative studies of the films were made by projecting single frames onto a screen using a movie projector. The images were traced onto  $8\frac{1}{2}$ -by 11-inch sheets of paper and the desired measurements then made from the tracings. Measurements of the projected drop area (plan view) and vapor breakthrough areas were made using a planimeter. Due

to the low surface tension of liquid nitrogen the shapes of the masses were often quite irregular. Hence, measurements of maximum and minimum diameters could not be used to calculate areas, as has been the standard procedure in past boiling studies. For this reason also, projection of the photographs on a Recordak viewer or Vanguard Motion Analyzer was not done because of the impracticality of making planimeter measurements on such viewers.

## CHAPTER VI

### RESULTS

#### Area-Volume Calibration

One of the goals of the present study was to determine heat transfer coefficients throughout a drop lifetime, thus requiring the determination of the instantaneous rate of change of volume (mass). It is possible to obtain this information photographically provided one is able to determine the relationship between liquid volume and the projected area of a given mass.

Theoretical predictions of drop shapes without vapor breakthrough have been calculated from the Laplace capillary equation (Equation (12)). But for extended masses where vapor breakthrough occurs, no theory exists to account for the resulting distortions of the fluid mass. Hence, an experimentally derived relationship, or calibration curve, is required.

In the present case, data for the calibration curve were obtained photographically. At plate temperatures lower than  $-230^{\circ}$  F, where the vaporization rate was low, motion pictures were taken of the various sized nitrogen masses as they were deposited on the plate surface. Knowing the volume of liquid held by each of the six depositors, and measuring the initial projected area,  $A_0$  of each of the drops, a calibration curve was constructed. The areas were measured with a planimeter traced around the perimeter of the liquid mass. In instances where vapor breakthrough occurred, the vapor area was not subtracted



from the total area within the periphery.

In some cases the initial area  $A_0$  was also determined by another technique. Single frame exposures were taken every five seconds, generally starting at  $t = 5$  seconds. By measuring and plotting the area as a function of time, a curve could be extrapolated backwards to  $t = 0$ , thus indicating  $A_0$ . The measurements from both the initial frame films and the extrapolated curves were averaged together to yield the  $A_0$  data used in the calibration curve.

For beaker-type depositors, the initial area was more difficult to obtain because while the nitrogen was being deposited onto the surface, requiring from four seconds for the 2-milliliter beaker to 11 seconds for the 10-milliliter beaker on the average, it was also vaporizing. Hence, the first pictures of the whole, pancake-shape extended mass does not correspond to the volume of the beaker depositor. To correct for this error pictures were taken for several seconds after the mass had been deposited and the correct area was determined by extrapolation back to zero time after deposition. The zero time location was approximated as one-half the deposition time, since shortly after deposition only a small mass is vaporizing on the hot solid surface, while the remainder is in the beaker where essentially no vaporization is occurring.

The curves from which  $A_0$  was determined are shown in Figures 14 through 21. It is evident that some variation in the  $A_0$  values arises just by the choice of the curve "best" fitting the data. Scatter in the area measurements may also arise from distortions in the liquid mass due to vapor breakthrough, particularly for the smaller mass sizes. For a mass only large enough to sustain a single vapor dome cell the area within the perimeter of the drop will differ, depending upon whether the

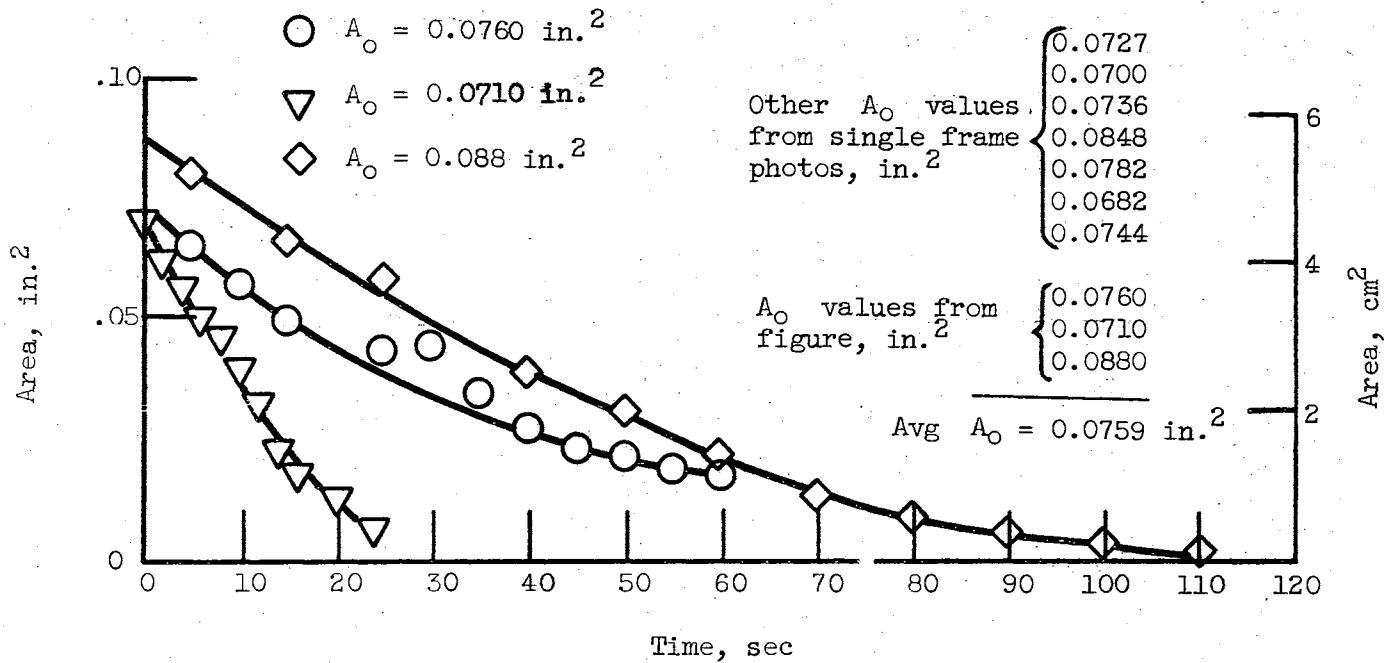


Figure 14. Plan Area of Drop Versus Time -  $A_0 = 0.0759 \text{ in.}^2$

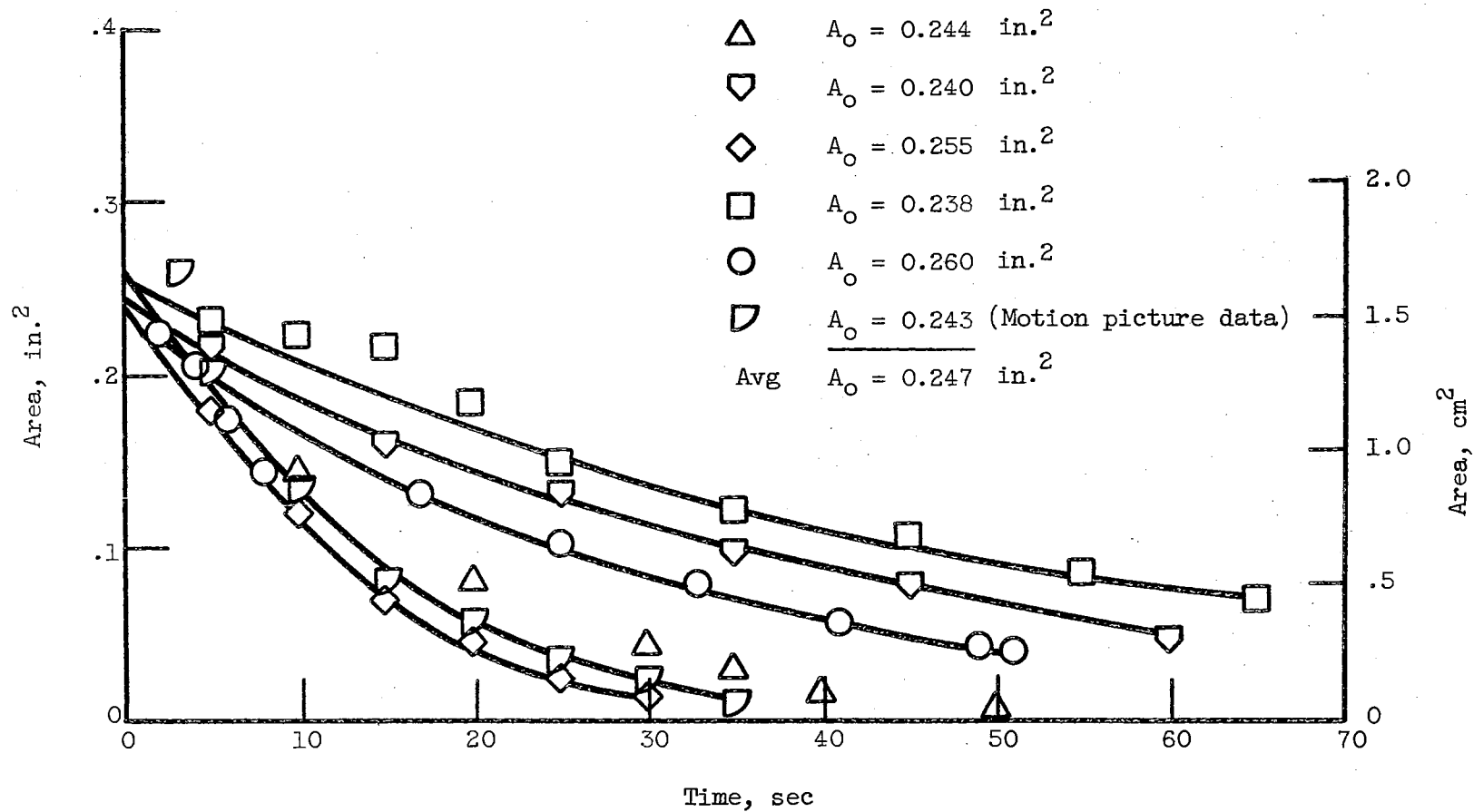


Figure 15. Plan Area of Drop Versus Time -  $A_0 = 0.247 \text{ in.}^2$

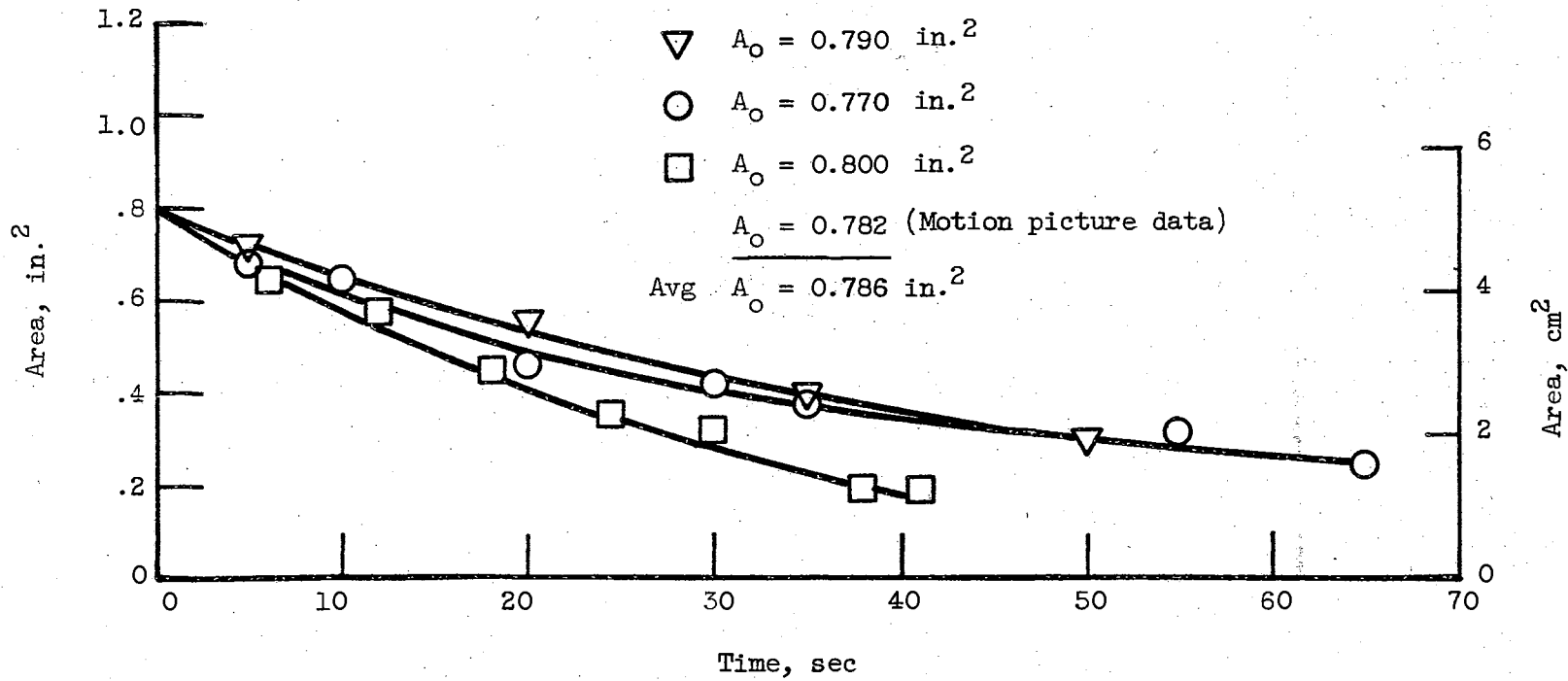


Figure 16. Plan Area of Drop Versus Time -  
 $A_o = 0.786 \text{ in.}^2$

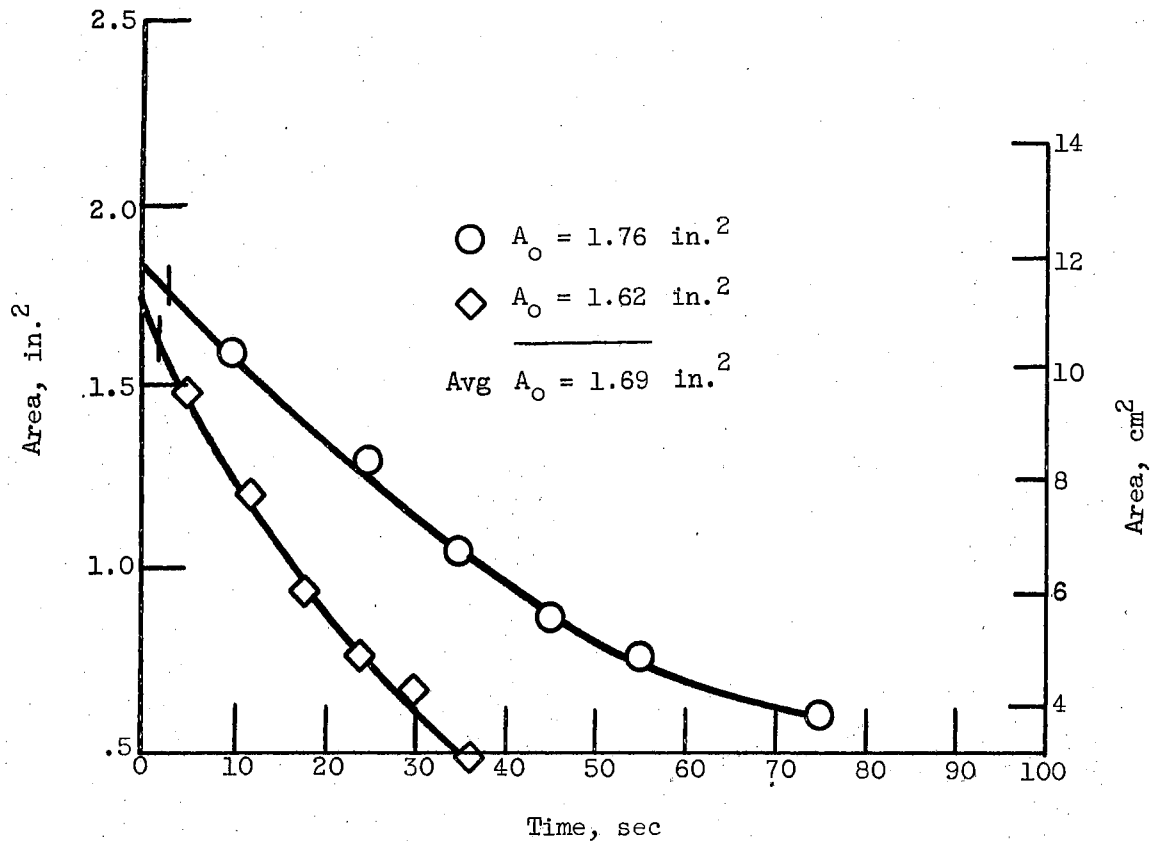


Figure 17. Plan Area of Drop Versus Time -  
 $A_o = 1.69 \text{ in.}^2$

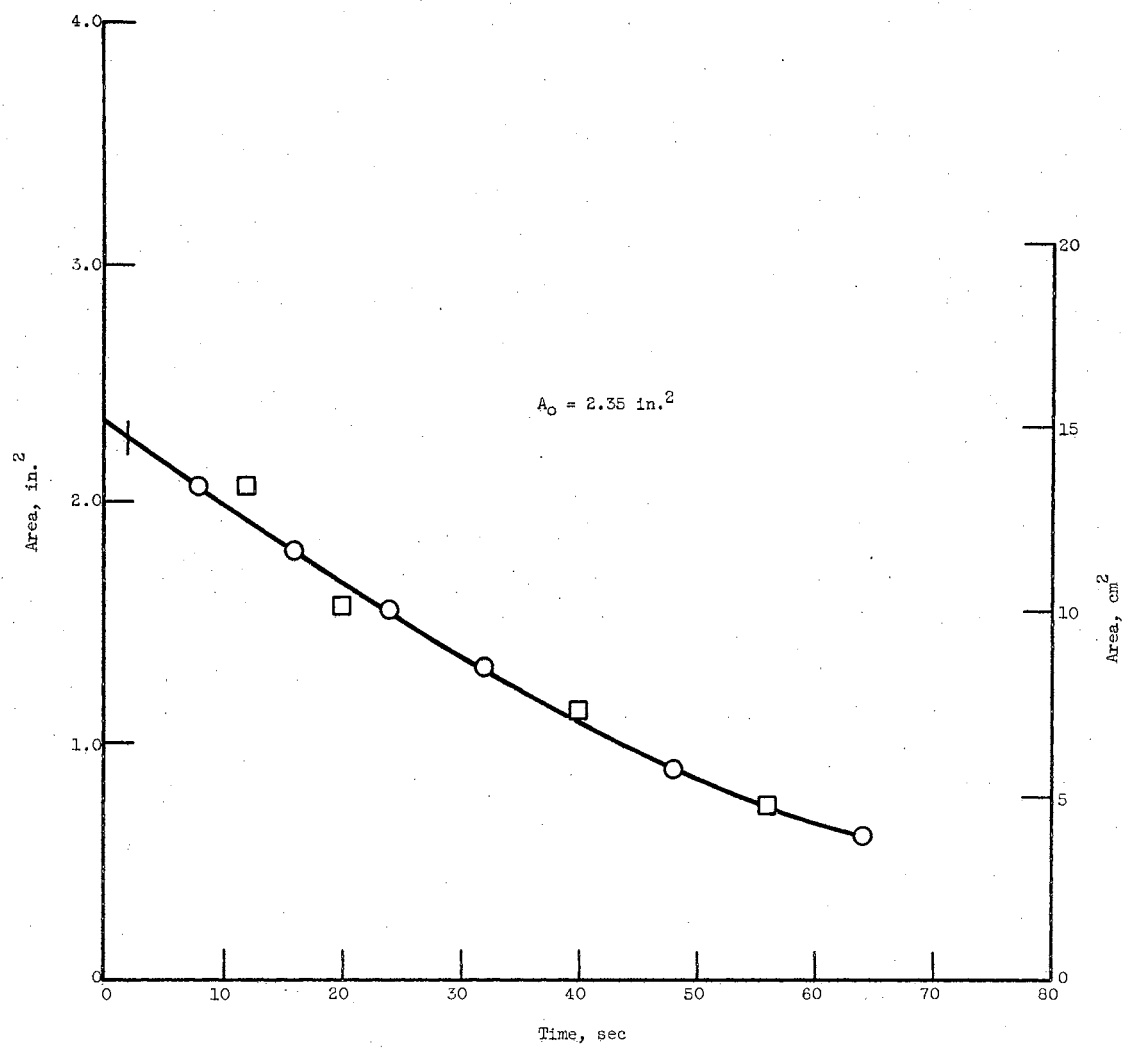


Figure 18. Plan Area of Drop Versus Time -  
 $A_0 = 2.35 \text{ in.}^2$

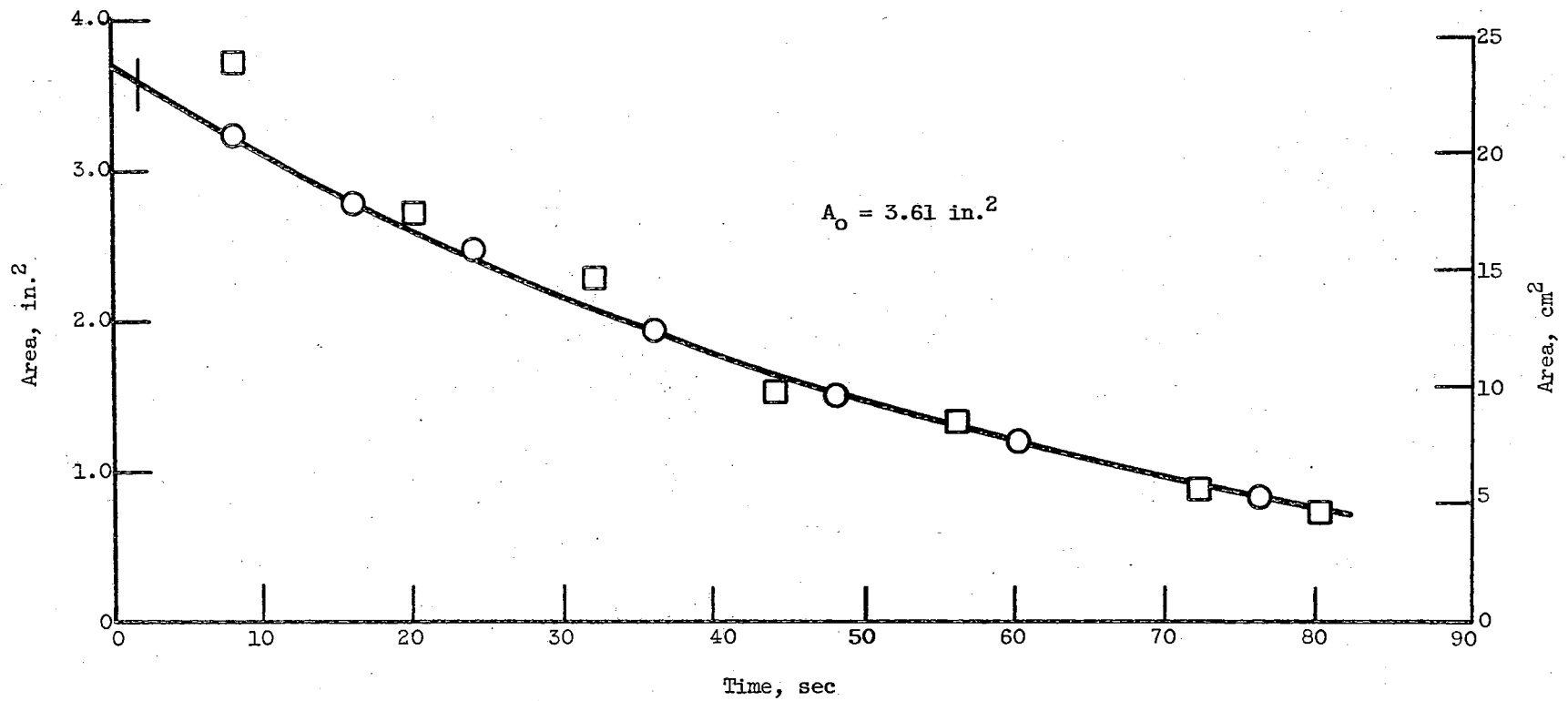


Figure 19. Plan Area of Drop Versus Time -  $A_0 = 3.61 \text{ in.}^2$

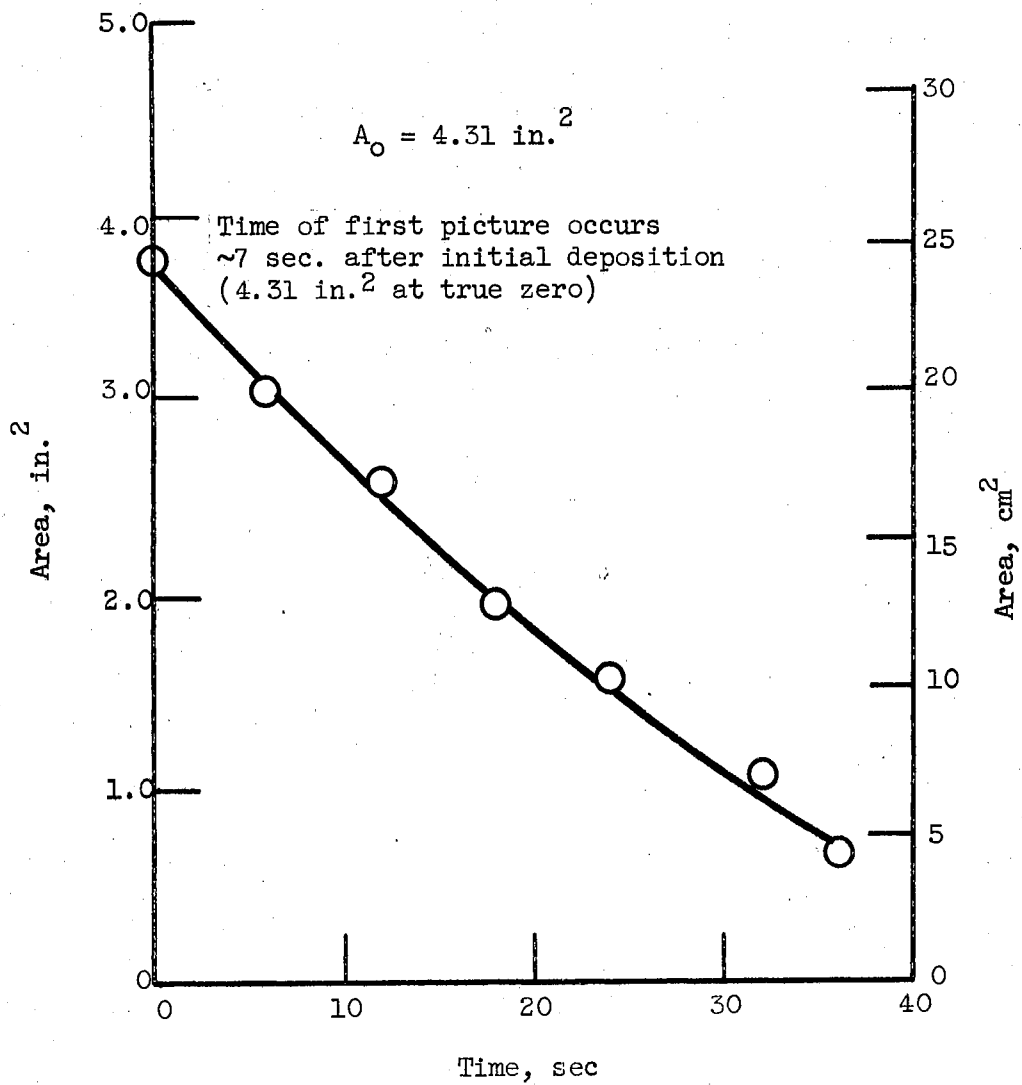


Figure 20. Plan Area of Drop Versus Time -  
 $A_0 = 4.31 \text{ in.}^2$



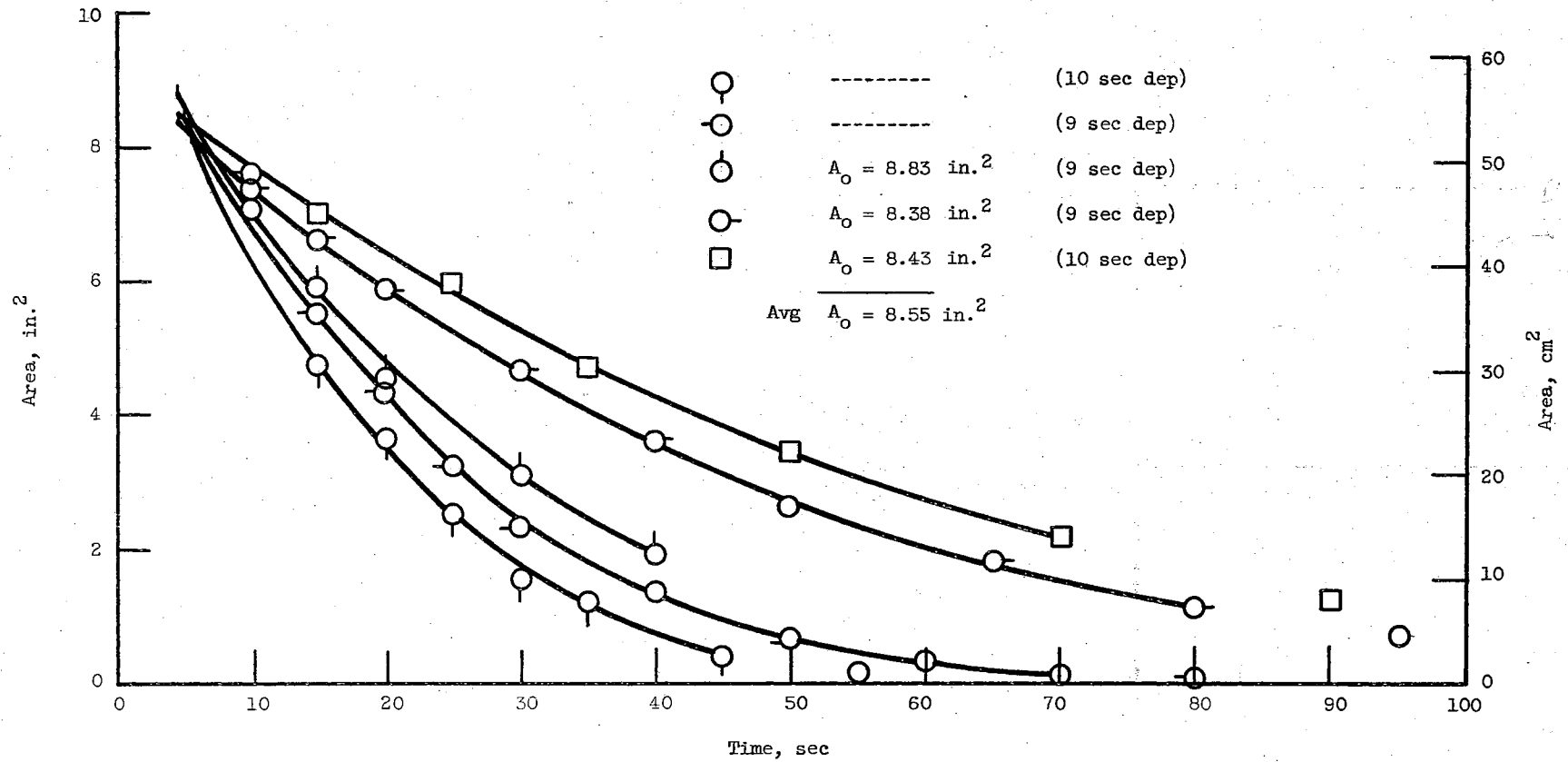


Figure 21. Plan Area of Drop Versus Time -  $A_0 = 8.55 \text{ in.}^2$

vapor area is at its maximum diameter (and thereby distends the drop) or whether no vapor breakthrough is occurring. For liquid masses two milliliters and larger, there are a sufficient number of breakthrough areas occurring so that there is no net distortion of the liquid outline over a period of time (other than that lost to vaporization). For the 0.357- and 0.990-milliliter masses, however, it is more likely that a quasi-steady-state condition would not exist as evidenced by Figure 47. Figure 47 shows a mass of approximately one milliliter in which the number of breakthrough areas range from zero to three.

The experimental area-volume relationship is shown in Figure 22, where comparison is made with a theoretically derived curve. The theoretical curve is calculated from the straight line approximations to the universal drop thickness curve as shown in Figure 6. The expressions for the three regions are (15):

- (a) Small drop domain,  $V^* < 0.8$

$$A = 1.5 \left( \frac{3\sqrt{\pi}}{4} \right)^{2/3} V^{2/3} \quad (28)$$

- (b) Intermediate drop domain,  $0.8 < V^* < 155$

$$A = 1.25 \left( \frac{\rho_l g}{\sigma g_c} \right)^{1/4} V^{5/6} \quad (29)$$

- (c) Extended drop domain,  $V^* > 155$

$$A = 0.54 V \left( \frac{\rho_l g}{\sigma g_c} \right)^{1/2} \quad (30)$$

In the small drop domain, it should be mentioned that the area given by Equation (28) is not the projected (plan) area, but is the average of the projected and surface area of the lower half of a sphere, which is assumed to be the effective heat transfer area. Both Equations (29) and (30) are expressions for the projected area of a drop.

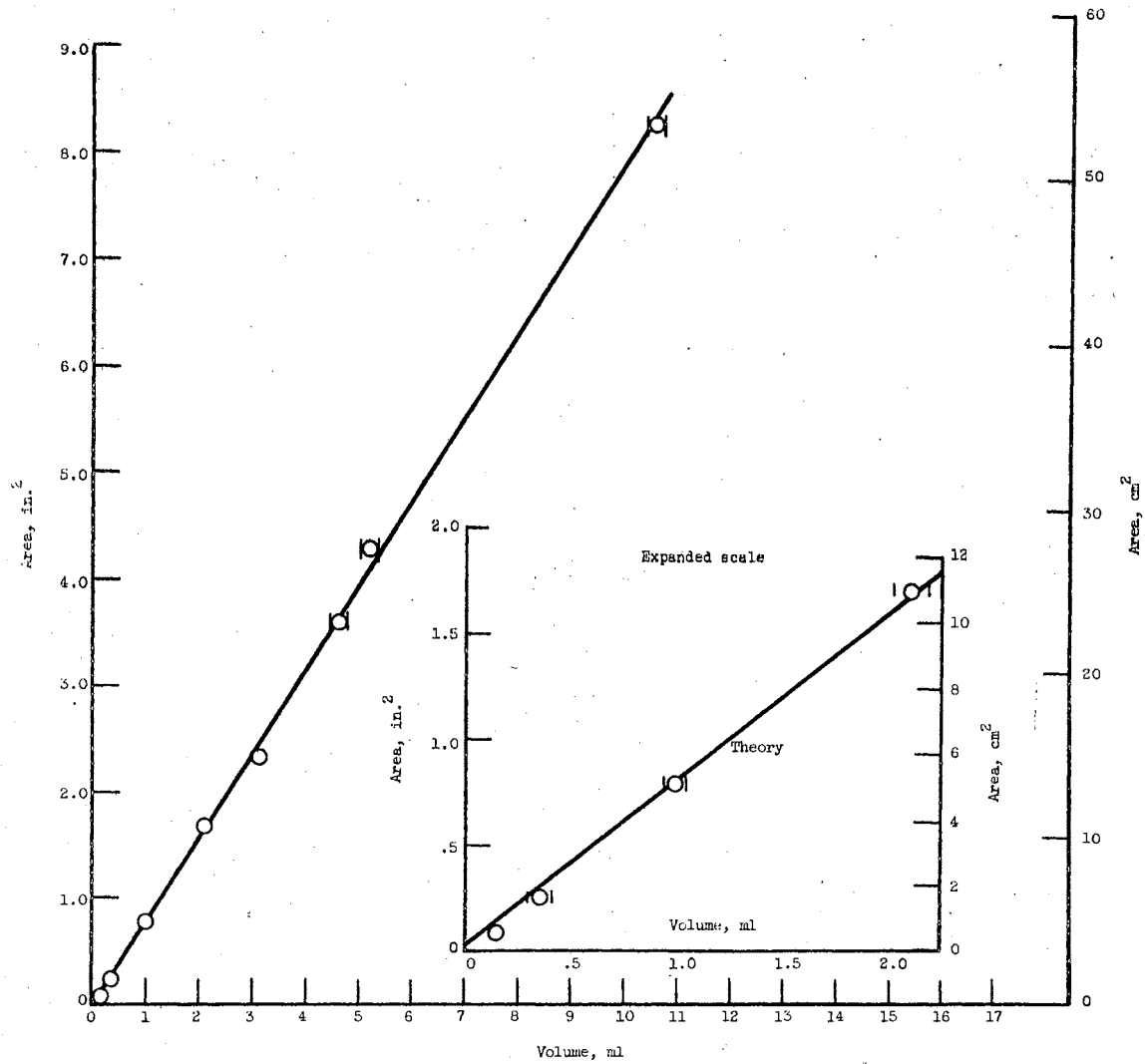


Figure 22. Comparison of Theoretical and Experimental Values of Drop Plan Area as a Function of Drop Volume

The smallest initial drop size here, 0.161 milliliter, corresponds to a  $V^*$  value of 146, which is close to the extended drop region. Hence, the deviation of the theoretical and experimental curves seen in the expanded scale portion of Figure 22 is not due to the difference between the projected area of a sphere and its effective heat transfer area, since drops as small as 0.03 milliliter volume are in the intermediate drop size range, where liquid masses have a flat-disc shape.

The agreement between the experimental measurements and theoretical curves of Figure 22 is generally good, although at the smaller drop sizes, the percentage deviation becomes large. It appears that the vapor breakthrough in the extended masses neither distends nor contracts a liquid mass of equal volume having no vapor breakthrough. Since parts of the plate surface are clearly visible through the vapor breakthrough areas, however, one may conclude that the average thickness of the liquid regions must be increased by the vapor breakthrough. This increase in thickness of the liquid regions will form the basis of a modification to existing expressions for heat transfer coefficients and vaporization times that will later be made.

#### Total Vaporization Times

The total vaporization times of various sizes of liquid nitrogen drops as a function of  $\Delta T$  are shown in Figure 23. In most cases, each open symbol represents the average of ten separate measurements. In a few cases 95 per cent confidence limits are indicated. In other cases, the limits are sufficiently small to be included within the symbol. The entire set of data is presented in Appendix B. A summary of this data is included in Table I.

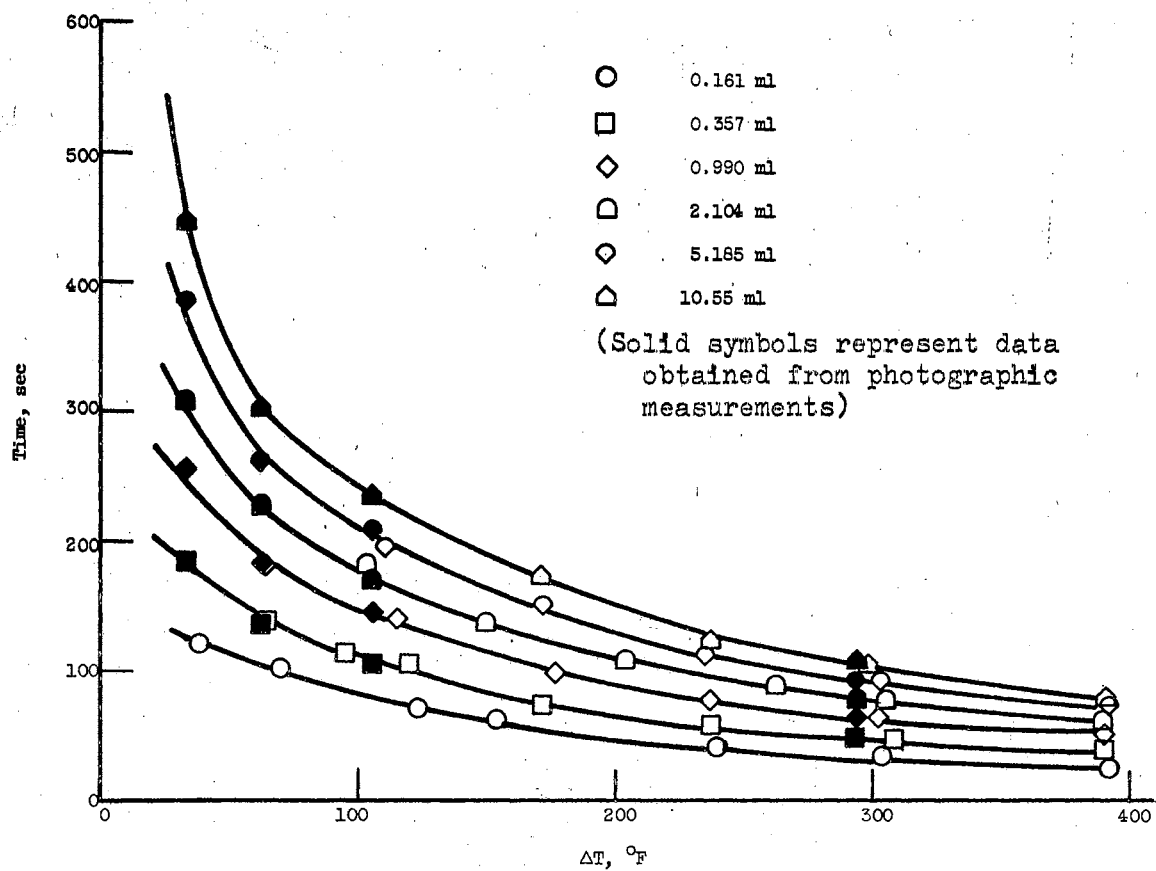


Figure 23. Total Vaporization Time of Drops of Various Initial Volumes as a Function of  $\Delta T$

TABLE I

## SUMMARY OF MEASURED TOTAL VAPORIZATION TIMES

(\*\*Denotes  $\tau$  value constructed from photographic measurements)

Depositor No. 3 (0.357 ml)				Depositor No. 4 (0.990 ml)			
$T_{avg}$	$\Delta T$ (°F)	$\tau_{avg}$ (sec)	$2\sigma_{\tau}$ (sec)	$T_{avg}$	$\Delta T$ (°F)	$\tau_{avg}$ (sec)	$2\sigma_{\tau}$ (sec)
69	390	40.8	0.8	69	390	52.1	1.6
- 12	308	48.4	2.6	18	302	65.5	1.4
- 84	237	60.1	1.5	83	237	79.4	1.1
-148	172	75.1	2.6	-144	177	98.7	3.5
-201	119	106.7	3.2	-205	115	141.2	2.8
-226	95	114.3	2.4	-257	63	179	3.6
-257	63	139	4.2	-288	32	245	-
-290	30	180	-				
Depositor No. 5 (0.161 ml)				2-ml Beaker (2.104 ml)			
$T_{avg}$	$\Delta T$ (°F)	$\tau_{avg}$ (sec)	$2\sigma_{\tau}$ (sec)	$T_{avg}$	$\Delta T$ (°F)	$\tau_{avg}$ (sec)	$2\sigma_{\tau}$ (sec)
72	392	26.7	3.3	69	389	62.9	2.8
- 17	303	35.5	2.2	- 16	305	77.9	1.1
- 81	239	42.9	2.5	- 58	262	88.6	0.4
-167	153	63.0	2.6	-117	203	110.4	1.4
-198	123	73.4	3.2	-171	149	138.6	2.5
-251	69	102.9	1.2	-217	103	182.5	6.7
-282	38	122.5	6.6	-292	28	310	-
5-ml Beaker (5.185 ml)				10-ml Beaker (10.548 ml)			
$T_{avg}$	$\Delta T$ (°F)	$\tau_{avg}$ (sec)	$2\sigma_{\tau}$ (sec)	$T_{avg}$	$\Delta T$ (°F)	$\tau_{avg}$ (sec)	$2\sigma_{\tau}$ (sec)
71	392	75.0	2.7	70	390	80.4	2.5
- 18	303	93.0	3.3	- 23	298	107.9	1.6
- 85	235	111.8	3.1	- 83	237	125.4	2.7
-149	172	152.1	4.0	-150	171	174.8	4.4
-210	110	196.7	6.8	-288	32	440	-
-284	36	370	-	-294	26	480	-
-294	26	418	-				

The solid symbols of Figure 23 were obtained indirectly by photographic means. As data were gathered at increasingly smaller  $\Delta T$  values, it was found that the large masses of nitrogen eventually included small, white frost particles within the interior. Due to the long vaporization times at low  $\Delta T$ 's the liquid nitrogen evidently condensed the traces of water vapor in the atmosphere. As the drops became smaller, the frost particles tended to come together, at which time their weight was sufficient to force the bottom of the drop to touch the plate surface. Consequently, the drop vaporized quite rapidly due to the onset of nucleate or transition boiling. Of course, the total vaporization times thus obtained were meaningless since only part of the drop lifetime was spent in the film boiling regime.

Fortunately, the smallest drops (0.161 milliliter) had a sufficiently low lifetime and small surface area that such a transition did not occur, even for the lowest  $\Delta T$  values. Hence, the 0.161-milliliter vaporization times were judged to be reliable. For larger drop sizes, reasonable values could occasionally be obtained, interspersed with values that were much too low. Low values could easily be anticipated since any transition to nucleate or transition boiling was evident. Since it was also observed that contact induced by frost particles did not occur until the drop size had become smaller than 0.161 milliliter, the possibility of obtaining total vaporization times for the drops of large initial size presented itself.

The technique employed to obtain total vaporization times for larger masses was, first, to deposit a ten-milliliter mass and take single frame exposures every five seconds throughout its lifetime. After obtaining and plotting the area against time data from these

photographs, the time at which an area of  $0.0759 \text{ in.}^2$  was reached was noted. Since the total vaporization time curve was already known for a mass size having  $0.0759 \text{ in.}^2$  area (0.161 milliliter) by direct measurements, as seen in Figure 24, the total lifetime was obtained by adding the lifetime of the 0.161 milliliter mass onto the time required for vaporization from a ten milliliter mass to a 0.161 milliliter mass. This procedure assumes that the vaporization rates of the various sized masses may be superimposed in those regions where equality of areas exist. It should be observed that the question of whether a mass having an area of  $0.0759 \text{ in.}^2$  corresponds to a 0.161 milliliter mass, as indicated experimentally, or another value indicated by the theoretical curve of Figure 22, is immaterial. This is so because the lowest curve of Figure 23 is most accurately that for a mass having an initial surface area of  $0.0759 \text{ in.}^2$ , and only secondarily, for a 0.161 milliliter volume mass.

Curves from which  $\tau$  values were obtained at  $\Delta T = 33^\circ$ ,  $105^\circ$ , and  $293^\circ \text{ F}$  are shown in Figures 24 through 28.

To verify the accuracy and validity of this technique, photographs were also taken at a  $\Delta T$  of  $293^\circ \text{ F}$ , where  $\tau$  values were obtainable by direct measurements. It is seen from Figure 25 that quite good agreement is obtained. At lower  $\Delta T$ 's of about  $65^\circ$  and  $110^\circ \text{ F}$ , the direct and indirect data points also exhibit good agreement.

#### Comparison With Theory

Theoretical total vaporization times are derived in Reference 15 for the entire spectrum of drop sizes by integration of Equation (26), after having obtained expressions for  $h(V)$  and  $A(V)$ . For the three



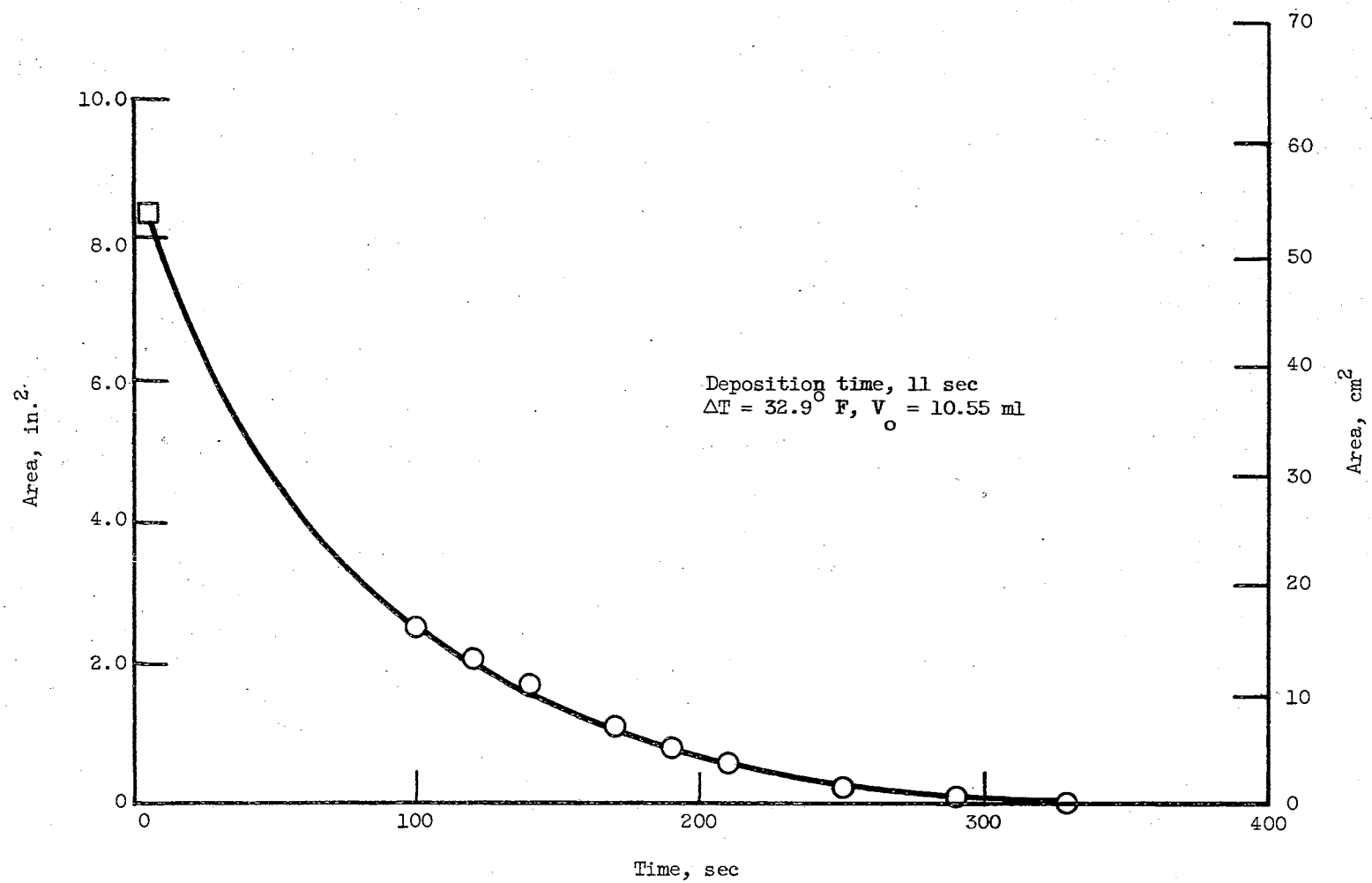


Figure 24. Plan Area of Drop Throughout Drop Lifetime -  
 $\Delta T = 32.9^\circ \text{ F}$

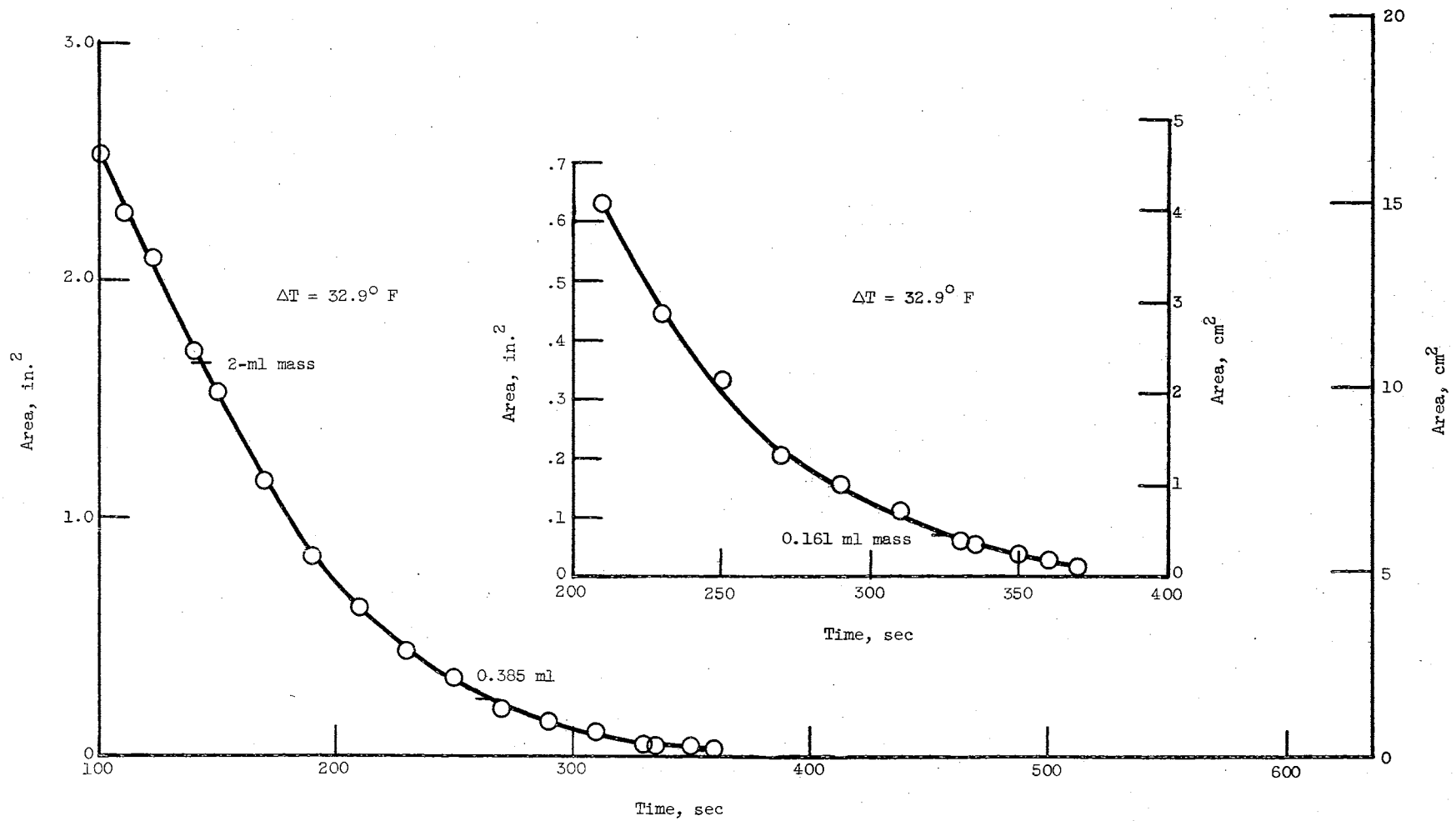


Figure 25. Plan Area of Drop Throughout Drop Lifetime -  
 $\Delta T = 32.9^\circ \text{F}$

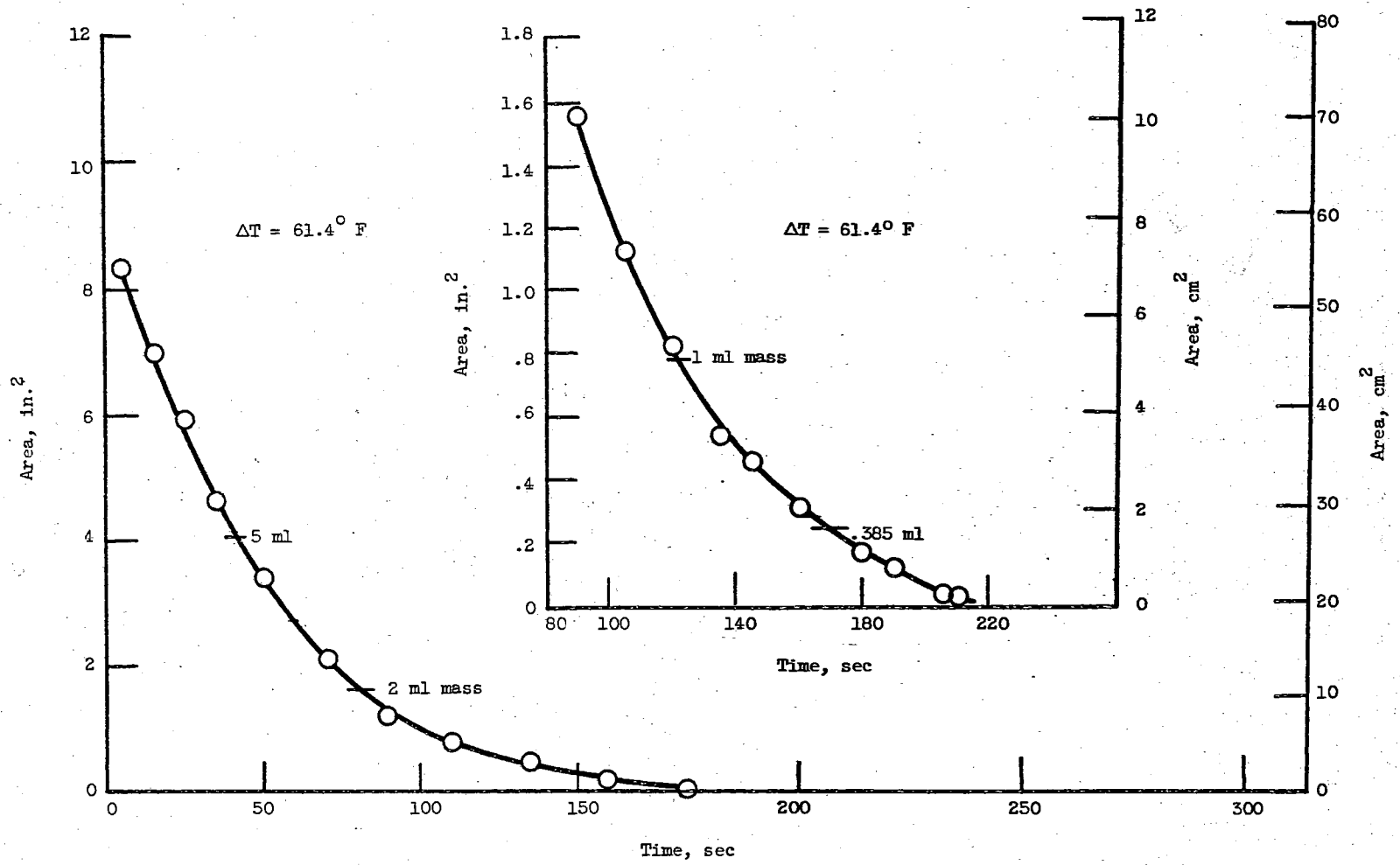


Figure 26. Plan Area of Drop Throughout Drop Lifetime -  $\Delta T = 61.4^\circ \text{F}$

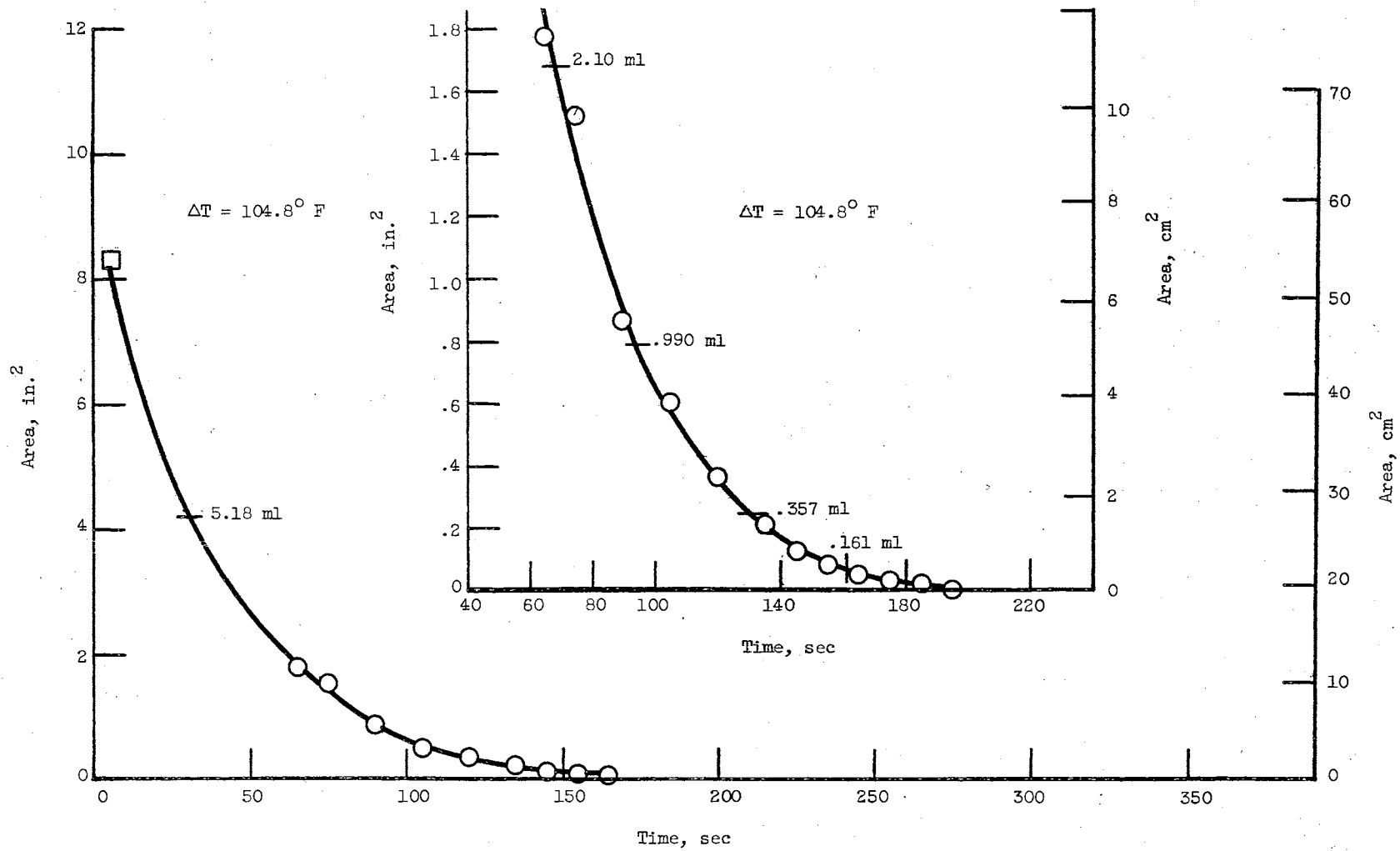


Figure 27. Plan Area of Drop Throughout Drop Lifetime -  $\Delta T = 104.8^\circ \text{ F}$

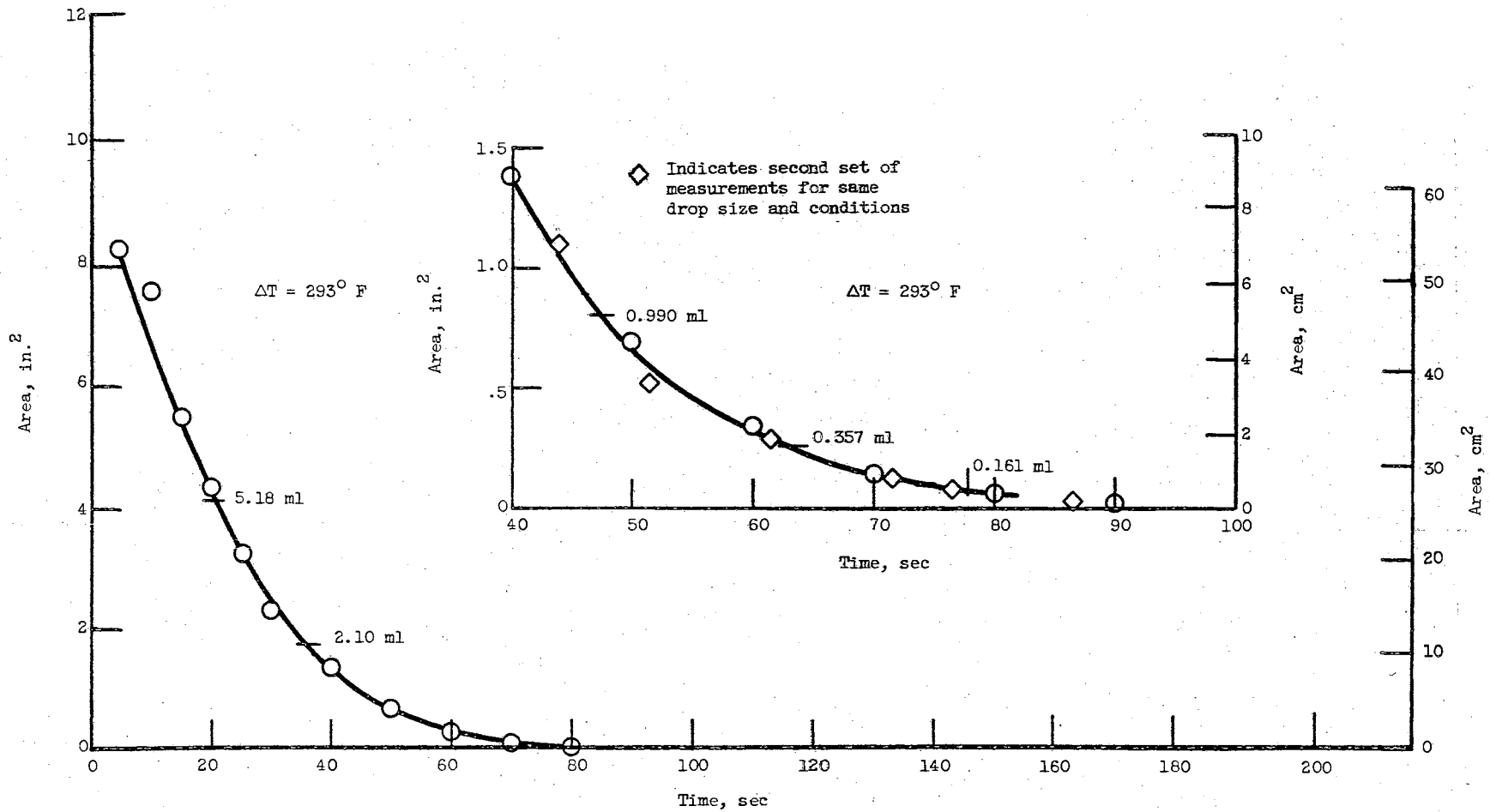


Figure 28. Plan Area of Drop Throughout Drop Lifetime -  $\Delta T = 293^\circ \text{ F}$

drop size regions,

Small drops:

$$t = 1.21 \left( \frac{\rho_l^3 \mu_v \lambda^4}{k_v^3 g \lambda^* \rho_v \Delta T^3} \right)^{1/4} v_o^{5/12} \quad (31)$$

Intermediate drops:

$$t = 2.23 \left( \frac{\lambda^4 \rho_l^{5/2} g_c^{1/2} \sigma^{1/2} \mu_v}{k_v^3 \lambda^* g^{3/2} \rho_v \Delta T^3} \right)^{1/4} v_o^{1/3} \quad (32)$$

Extended drops:

$$t = 4.52 \left( \frac{\lambda^4 \rho_l^2 \sigma g_c \mu}{k_v^3 \lambda^* g^2 \rho_v \Delta T^3} \right)^{1/4} v_o^{1/4} \quad (33)$$

Equations (31) through (33), as written, do not contain correction factors for radiation heat transfer. Before one could expect agreement between the experimental  $\tau$  measurements and the values predicted by Equations (31), (32), and (33), one must either correct the experimentally measured values or include the correction factors within the equations. For the moment, these correction factors will be bypassed and comparisons will be made which are still illustrative. In a later section, the correction factors and their consequences will be discussed at length. Since cryogenic fluids are much colder than their room temperature surroundings, another important heat source contributing to drop evaporation is that occurring by convection from the room temperature nitrogen atmosphere to the top surface of the drop.

Equations (31) to (33) were adopted to computer solution and solved for the six mass-sizes used here at various  $\Delta T$  values. Two of the curves so generated are shown in Figure 29. The vapor properties were evaluated at the film temperature. A subroutine was used in which the

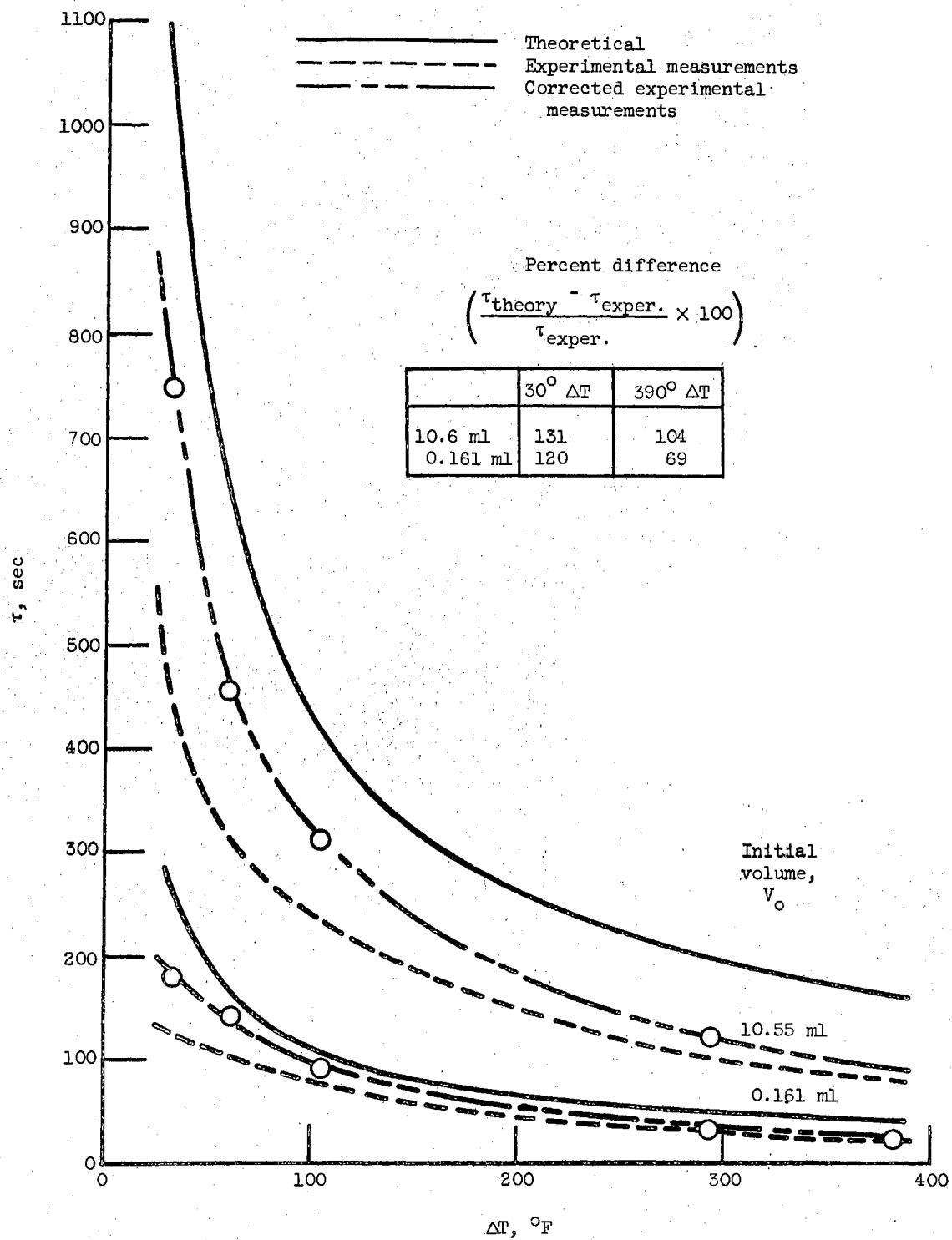


Figure 29. Corrected Total Vaporization Time Versus  $\Delta T$

property values were read in at several temperatures over the range studied ( $139.2^{\circ}$  R to  $540^{\circ}$  R). At any particular film temperature, the subroutine evaluated the properties by linear interpolation between the nearest two values read into the program. Since as many as 200 points of a property value may be read in over the given temperature range, the linear interpolation process may be made as accurate as is necessary. The property values used are tabulated in Appendix C, while the complete computer program is given in Appendix D.

Examining Figure 29, it is evident that, in general, the theoretical curves are higher than the experimental ones, and very much higher at low  $\Delta T$  values. For the ten milliliter mass at  $\Delta T = 25^{\circ}$  F, the theoretical value is about 130 per cent higher, while at  $\Delta T = 390^{\circ}$  F, the theoretical value is 105 per cent higher. The experimental values are uncorrected for radiation and free convection, however, and so these differences are of little significance at this point. The following section will deal with these corrections.

#### Corrected Total Vaporization Times

The paths of heat flow to a vaporizing liquid drop using the Baumeister model (12, 13, 14, and 15) are: (1) conduction across the vapor gap between the heated plate surface and the lower surface of the liquid drop, and (2) radiation from the plate surface to the lower surface of the drop. Equations (31) to (33) have been presented herein without the radiation correction factor derived in Reference 15.

If one is to compare the present experimental results with the theoretical results of Reference 15, all additional heat and mass transfer paths occurring in the actual case must be subtracted or



compensated for so as to reduce the case to one having only a single heat flow path, that is, conduction across the vapor film, as described previously.

In the actual case, the vaporizing drop is surrounded by a comparatively hot nitrogen atmosphere and by an enclosure at room temperature. Hence, besides radiation from the plate to the bottom surface of the drop, radiation from the surroundings to the top surface of the drop must also be considered. In addition, heat transfer may occur by convection of the gaseous nitrogen atmosphere to the top surface of the drop. If the theory predicting total vaporization times is correct, then these additional heat flow paths will tend to vaporize the drop more quickly than predicted, since only a single heat flow path is considered in the theory. Thus, these additional heat inputs must be subtracted so that corrected vaporization times could be calculated.

#### Procedure for Obtaining Corrected Total Vaporization Times

Single frame exposures at five-second intervals were taken of ten-milliliter masses at several  $\Delta T$  values throughout their lifetime. At low  $\Delta T$  values, it was necessary to "splice" ten-milliliter mass lifetimes to those of 0.161-milliliter lifetimes. From these photographs, measurements of the projected areas of drops were obtained and plotted against time as shown in Figure 24, for example. A smooth curve was drawn through the data points. Values of area and time were then taken from the curve to be used in a computer program calculating instantaneous heat transfer coefficients.

Previous measurements, shown in Figure 22, showed that the relationship between projected area and volume of a drop agreed well with

Baumeister's (15) approximate expressions except for the smaller mass sizes. Due to the likelihood that a small part of nitrogen vaporized from the already small drops while in the depositor, Baumeister's approximate area-volume relations were used to calculate the liquid volume associated with a given projected area.

From the area-time curves as sketched in Figures 24-28, the following quantities are defined:

$$t_{avg} = \frac{t(i) + t(i-1)}{2} ; i = 2, m \quad (34)$$

$$A_{avg} = \frac{A(i) + A(i-1)}{2} \quad (35)$$

$$\Delta t = t(i) - t(i-1) \quad (36)$$

$$D_{avg} = \sqrt{\frac{4}{\pi} A_{avg}} \quad (37)$$

The heat transferred to the drop by free convection was estimated by the following expression (42), which is applicable for a cooled plate facing upward in natural convection:

$$\frac{hL}{k} = 0.27 (Gr_L Pr)^{1/4} \quad (38)$$

Equation (38) is recommended for use in the range  $3(10^5) < Gr < 3(10^{10})$ , and can be applied to a circular disk if  $L$  is replaced by  $0.9 D$ . Using the above expression, the free convection heat transfer coefficient is calculated for each time increment as

$$h_{fc} = 0.3 \frac{k}{D_{avg}} (Gr Pr)^{1/4} \quad (39)$$

where the Grashof number is also based on  $0.9 D$ .

Knowing the free convection coefficient for a time increment, the free convective heat transfer for that time increment is simply

$$Q_{fc} = h_{fc} A_{avg} \Delta T \Delta t \quad . \quad (40)$$

For the radiation heat transfer to the drop, two separate contributions were calculated. The first was the contribution from the room temperature environment to the top surface of the drop. The second was the radiant energy from the plate surface to the lower surface of the drop. Configuration factors were taken as unity in both cases. In view of typically high emissivity values for liquids (0.96 for water), a value of unity was also chosen for liquid nitrogen so that the maximum radiative contribution could be computed. Radiation from the nitrogen drop to the surroundings was neglected since at the low saturation temperature the radiant energy is only 0.4 per cent of that coming from 540° F surroundings. The contributions are:

$$Q_{rup} \approx \sigma A_{avg} T_{amb}^4 \frac{\text{BTU}}{\text{SEC}} \quad (41)$$

$$Q_{rdn} \approx \sigma A_{avg} T_w^4 \frac{\text{BTU}}{\text{SEC}}$$

from which

$$Q_r = (Q_{rup} + Q_{rdn}) \Delta t \quad \text{BTU} \quad . \quad (42)$$

Concerning the value of  $T_{amb}$ , measurements of nitrogen atmosphere temperature during all of the experimental runs indicated that the following expression for  $T_{amb}$  could be conveniently used in the computer program:  $T_{amb} = 475 + \frac{\Delta T}{7.4} \text{ } ^\circ \text{R.}$

In the actual vaporization of a drop, the total heat transfer to the drop is calculated from

$$Q_{comb} = \lambda \rho_1 (V_{i-1} - V_i) \quad \text{BTU} \quad . \quad (43)$$

Since a period of time  $\Delta T$  was required to vaporize the mass of nitrogen,

$\rho_i (V_{i-1} - V_i)$ , a larger time period would have been required had radiation and free convection to the liquid mass not been operative.

The modified time interval is then

$$t_{rc} = \frac{Q_{comb}}{(Q_{comb} - Q_{fc} - Q_r)} \Delta t. \quad (44)$$

These calculations are performed for each time interval. The corrected total vaporization time, in which radiation and free convective heat additions have been accounted for, is obtained by summing the successive values of  $t_{rc}$ .

A means of checking the results of the previous calculation was desirable. Hence, the same type of calculations were carried out, but were based upon integrated mean values over the drop lifetime. In calculating  $h_{fc}$ , a diameter corresponding to the integrated mean area was used. That is, for

$$A_{int} = \frac{\sum_{i=2}^{i=m} A_{avg,i} \Delta t}{\tau}, \quad (45)$$

$$D_{int} = \sqrt{\frac{4}{\pi} A_{int}}.$$

Likewise, the Grashof number was based on the same diameter, and radiation exchange based upon  $A_{int}$ . Values for total vaporization times calculated in this manner are generally a little lower than those obtained by the incremental calculation. The computer results are summarized in Table II.

It is evident from Figure 29, that even with the corrections for radiation and free convection, the experimental results are substantially lower at low  $\Delta T$ 's than those predicted by theory. One is

TABLE II  
 SUMMARY OF MEASURED TOTAL VAPORIZATION TIMES  
 CORRECTED FOR RADIATION AND FREE CONVECTION

0.357 ml			
$\Delta T$ , °F	Measured $\tau$ , Sec.	Incrementally Corrected $\tau$ , Sec.	Corrected $\tau$ , Avg. Intec. Area Sec.
383	41.5	46.0	46.1
293	49.7	55.8	55.2
105	116	148	145
62	151	205	197
33			
0.161 ml			
383		28.7	Interpolated values from 0.357 ml calculations
293		34.9	
105		95.1	
62		146	
33	126	185	
10.55 ml			
383	83.0	93.6	94.2
293	108	125	125
105	236	314	301
62	301	458	407
33	494	751	748

consequently led to question the free convection estimate, which is strictly applicable to a cooled plate, rather than a liquid mass whose surface is rippled and distorted by vapor breakthrough. It might be speculated that the free convection has been underestimated because of the induced agitation of the boundary layer. However, one can also speculate that vapor breakthrough helps to maintain a superheated vapor covering over the mass, reducing the energy transport to the upper surface to a near zero value. Kutateladze (35) mentions this possibility for the case of a spheroid. Latest experimental evidence appears to refute this possibility, however. Baumeister and Hendricks (43) have conducted preliminary experiments in which the vapor flowing from beneath the drop is made visible. A considerable radial velocity is exhibited, while the axial velocity component (normal to the plate surface) does not appear to be appreciable.

#### Dimensionless Total Vaporization Times

Experimental results will be expressed here in dimensionless form and compared with Baumeister's generalized dimensionless correlation of  $t^*$  against  $V^*$ . Figure 7 is reproduced directly from Reference 15 and shows an impressive array of data for various fluids over a large size range plotted against the  $t^*$  versus  $V^*$  correlation.

For future reference it should be observed that the theoretically derived curve of Figure 7 actually consists of three separate segments, corresponding to drop sizes in the small, intermediate and extended ranges. The three segments arise because of the straight-line approximations to the universal drop thickness curve shown in Figure 5, which are used in evaluating the drop heat transfer areas expressed in

Equations (28), (29), and (30). The dimensionless vaporization time expressions for the three regions are:

Small Drop Region

$$t^* = 1.21 V^{*5/12} \quad (46)$$

Intermediate Drop Region

$$t^* = 2.23 V^{*1/3} - 0.97 \quad (47)$$

Extended Drop Region

$$t^* = 4.52 V^* - 4.96 \quad (48)$$

It has already been seen in the previous section that the experimental and theoretical total vaporization times (dimensional) of nitrogen drops are not in very good agreement. The same lack of agreement is to be expected in a dimensionless plot, but such a plot will prove enlightening in other aspects.

The points plotted in Figure 30 are those calculated from the uncorrected total vaporization time measurements. The unflagged symbols represent vaporization times taken from the best curves drawn through the data points of Figure 23 for the six mass sizes studied herein.

The flagged symbols represent data taken from photographic measurements of area against time. More specifically, a series of closeup photographs of the smallest drop size at a given  $\Delta T$  yielded an area-time curve over the drop lifetime. Such curves were obtained at several  $\Delta T$ 's. The lifetime of any smaller sized drop was then obtainable from the appropriate curve. The smallest drop sizes for which lifetimes could be obtained with reasonable accuracy are still seen to be in the intermediate drop range, where  $0.8 < V^* < 155$ . The uncorrected data are seen to agree well with the correlation in the range of  $V^*$  from

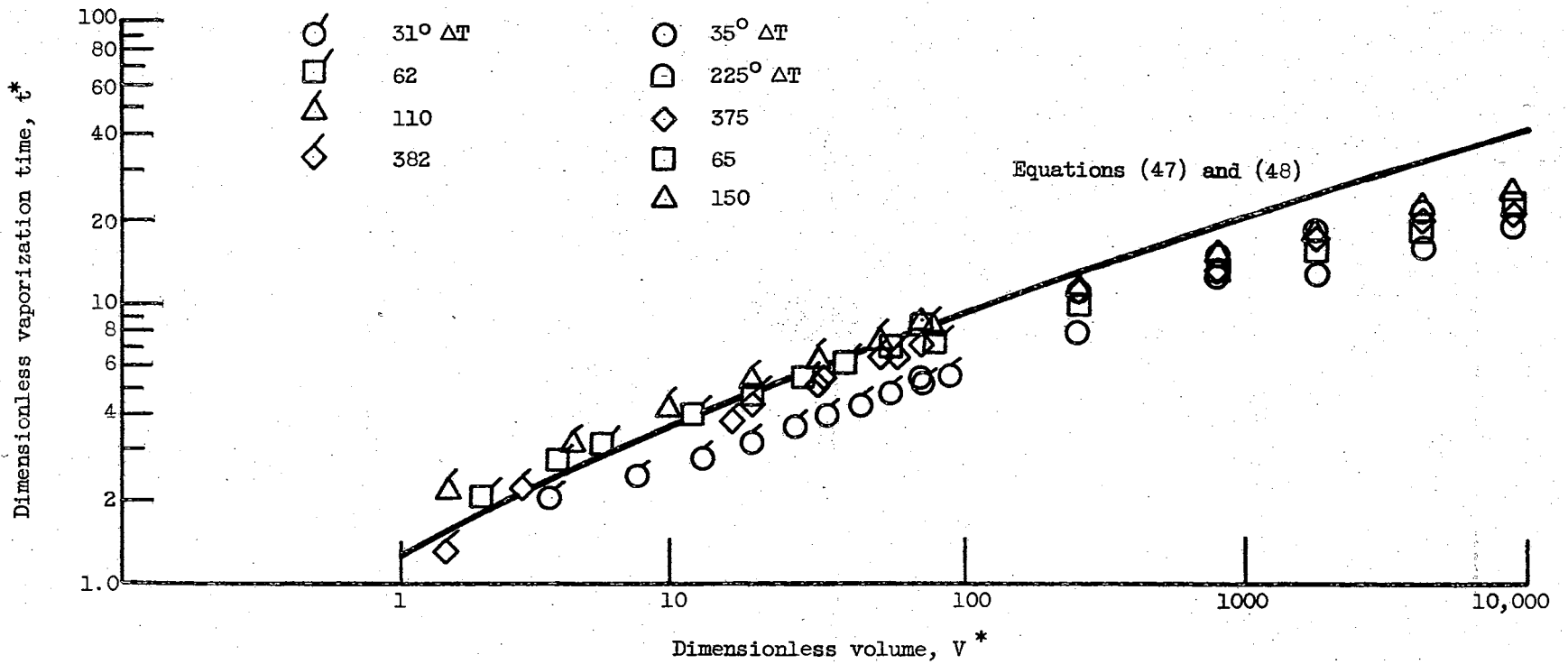


Figure 30. Dimensionless Vaporization Time Versus Dimensionless Volume (Uncorrected for Radiation or "Free Convection")



one to one hundred, except for the data at the lowest  $\Delta T$ ,  $31^\circ$  F. For higher  $V^*$ , divergence from the theoretical curve is evident. Perhaps the agreement for the intermediate size range without any "correction" is an indication that a superheated vapor layer does indeed cover the smaller masses, making free convection heat addition negligible.

When the corrected total vaporization times are non-dimensionalized and plotted against  $V^*$  the graph of Figure 31 is obtained. Corrections were not applied to drop sizes smaller than  $V^* = 85$  primarily because the Grashof number calculated for these small masses is less than  $10^5$ , which is the lower limit of applicability of the free convection correlation. Again, as would be expected from the dimensional comparison already made, the  $t^*$  data appears to depart somewhat from the theoretical curve. If one had only the information shown by the logarithmic plot, one might be tempted to explain this departure as being due to a combination of experimental measurement errors. The reasonableness of this explanation may be determined by calculating the changes in variables necessary to bring the data into agreement with the theoretical curve.

For the largest mass size  $V^* = 8855$ . Maximum and minimum experimental values of  $t^*$  are 30.0 and 24.0. The error in volume measurement necessary to shift the data points horizontally to the theoretical curve is

$$\frac{V^*_{\text{act}}}{V^*_{\text{theor}}} = \frac{8855}{3400} = 2.6 \quad (\text{Minimum})$$

$$\frac{V^*_{\text{act}}}{V^*_{\text{theor}}} = \frac{8855}{1650} = 5.4 \quad (\text{Maximum}) .$$

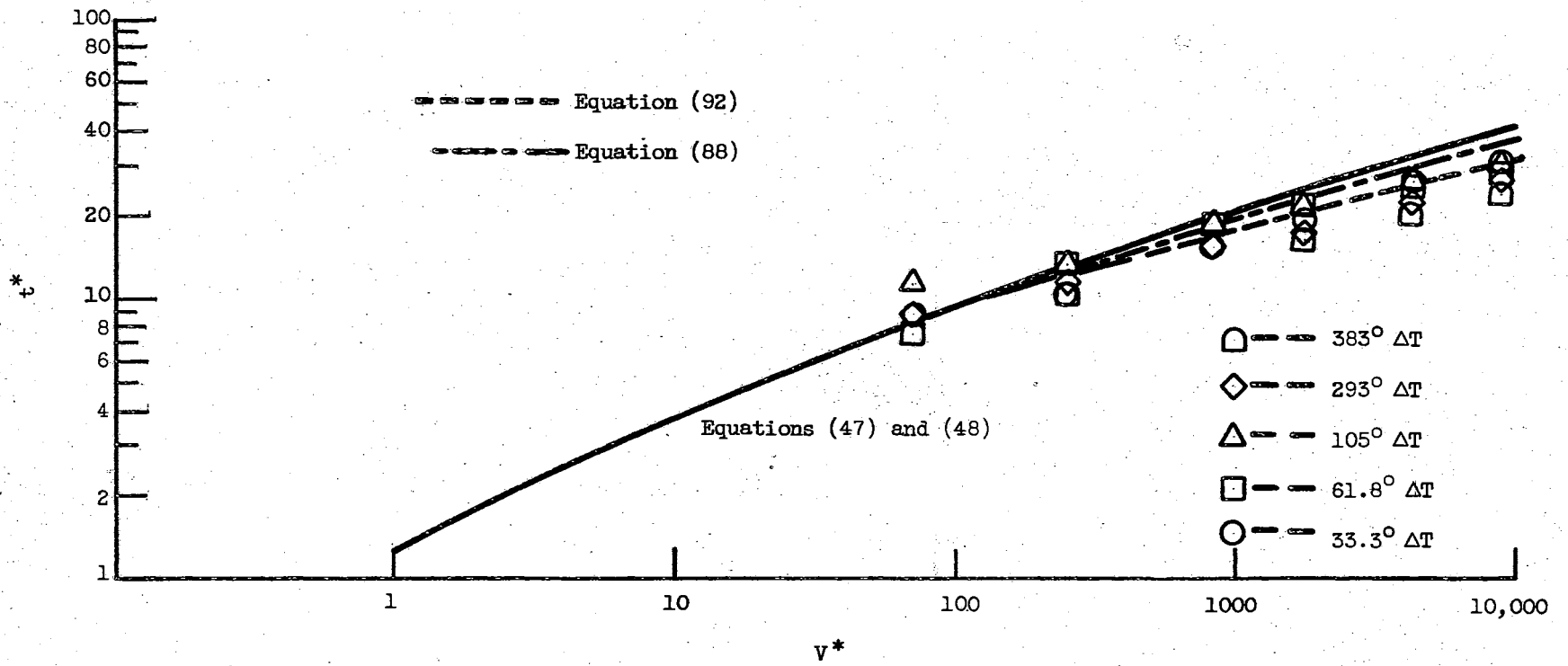


Figure 31. Dimensionless Vaporization Time Versus Dimensionless Volume (Data Corrected for Radiation and "Free Convection")

Physically, this means that if the mass were only  $10.55/2.6 = 4.06$  milliliter, agreement would have occurred. This would involve a minimum error in volume measurement of  $((10.6 - 4.1)/4.1) \times 100 \approx 160$  per cent.

If one considers the error in total vaporization time necessary to produce agreement,

$$\frac{t_{\text{theor}}^*}{t_{\text{act}}^*} = \frac{39.0}{30.0} = 1.3 \quad (\text{Minimum})$$

$$\frac{t_{\text{theor}}^*}{t_{\text{act}}^*} = \frac{39.0}{24.0} = 1.625 \quad (\text{Maximum})$$

corresponding to errors of 23 and 38.5 per cent. In terms of seconds, this would correspond to errors of 225 seconds (for a total vaporization time of 750 seconds) at  $\Delta T = 32^\circ \text{ F}$ , and 26 seconds (for a total vaporization time of 41.6 seconds) at  $\Delta T = 380^\circ \text{ F}$ .

If one considers erroneous measurement of the plate surface temperature, one may calculate  $t^*$  values for several different wall temperatures until a value of  $t^*$  is obtained that agrees with the theoretically predicted value. For the data obtained at a measured wall temperature of  $432.5^\circ \text{ R}$ , agreement would result if the temperature were  $665^\circ \text{ R}$ , a difference of  $233^\circ \text{ R}$ . Similarly, for the data at wall temperatures of  $244^\circ$  and  $201^\circ \text{ R}$ , errors of  $45^\circ$  and  $32^\circ \text{ R}$ , respectively, are required. Finally, at the lowest wall temperature,  $171^\circ \text{ R}$ , an error of only  $9^\circ \text{ R}$  is required to bring agreement. Although such a temperature error is conceivable in this instance, the previous cases indicate that the discrepancy between measurements and the theory ( $t^*$ ,  $V^*$  data) are probably not attributable to errors in measurement of plate temperatures.

Comparing these errors with the estimated errors, the volume

measurement of the 10.55 milliliter mass involves an error of  $\pm 1.1$  per cent. Measurement of the total vaporization time is estimated to involve a maximum error of  $\pm 8$  per cent (99 per cent confidence level for depositor number five at  $\Delta T = 38^\circ \text{ F}$ ), while the surface temperature measurement is estimated to be accurate to within a few degrees ( $5^\circ \text{ F}$ ). It seems obvious then, that the discrepancy is not attributable to experimental error. It appears more likely that the mechanisms acting to vaporize the extended drops have been inadequately and/or inaccurately described, either in the correction factors applied herein or in the theory upon which the universal correlation is based.

One additional factor which may influence drop lifetime is the intermittent contacts of the liquid with the solid surface, which have been reported to occur (by Bradfield, (44)) even in the region of stable film boiling. The solid surface of Reference 44 was reported to have a surface roughness of 70 micro-inch rms, with occasional mesa-like roughness of the order of 0.001 inch above the mean roughness high, compared with 10 micro-inch rms on the aluminum surface used here. Perhaps one can only be certain of the role of possible intermittent liquid contacts by conducting the same type of tests as those of Bradfield, which involved applying a potential gradient of 50,000 volts per inch across the vapor gap to determine electrically when contact with the plate occurred. However, it is believed that an indication of the lack of excessive surface roughness, and the absence of liquid-solid contact, is given by results of Leidenfrost temperature tests which are discussed fully in the following section. Briefly, evidence seemed to indicate that part of the metastable Leidenfrost line (see Figure 1) had been traversed. This would not have been possible with a rough surface,

that is, a surface with protrusions sufficiently pronounced to result in intermittent contact with the liquid. In addition, the Leidenfrost temperatures determined in the present tests are very low compared with results previously reported (26 and 45), also indicating a smooth test surface.

#### Leidenfrost Temperature

In most previous studies, the Leidenfrost temperature was determined by noting the  $\Delta T$  at which the total vaporization time was a maximum. In the present study, it was not possible to establish experimentally a maximum in the total vaporization time curves because of the inability to maintain larger drops in the film boiling region throughout their lifetimes. Conceivably, this could be done using the photographic technique previously described but this would be very tedious.

The Leidenfrost temperature was obtained in the present study by slowly increasing or decreasing the plate temperature while a liquid mass was being vaporized. If the mass were initially in the film boiling region at a  $\Delta T$  of about  $30^{\circ}$  F, the plate was slowly cooled. At some point in the cooling process the drop would go into the nucleate boiling region. The temperature at which this occurred was recorded. Drops were also deposited at plate temperatures such that nucleate boiling was initially observed. The plate temperature was slowly increased and the temperature at which the drop made the transition to film boiling was recorded. These results are shown in Table III.

In general, the transition temperatures were a few degrees higher in going from the nucleate-to-film-boiling region. This occurrence is reasonable if one accepts the conclusion of Reference 2 which maintains

TABLE III  
 PLATE TEMPERATURE AT TRANSITION FROM NUCLEATE TO  
 FILM BOILING

Decreasing Plate Temperature				
Depositor	Transition Temperature			Cooling Rate of Plate
No.	MV.	°F	°F( $\Delta T$ )	°F/Min.
5	-5.345	-306.4	14.0	-
3	-5.330	-304.8	15.6	2.8
4	-5.315	-303.2	17.2	3.2
10-ml Beaker	-5.370	-309.0	11.4	10.4

Increasing Plate Temperature				
				Warming Rate of Plate
5	-5.250	-296.6	23.8	6.7
3	-5.225	-294.0	26.4	9.2
4	-5.265	-298.1	22.3	12.4
10-ml Beaker	-5.310	-302.7	17.7	11.7

Maximum Transition Temperature,  $-294^{\circ}\text{F}$  or  $26.4^{\circ}\text{F } \Delta T$

Minimum Transition Temperature,  $-309^{\circ}\text{F}$  or  $11.4^{\circ}\text{F } \Delta T$

(Plate temperature indicated by thermocouple No. 2)

the existence of a metastable Leidenfrost line (Figure 1, B' - D'). It seems more reasonable to accept the nucleate-to-film transition temperature in lieu of the possibility of traversing the metastable Leidenfrost line in the film-to-nucleate direction.

In the foregoing procedures the plate undergoes a ramp-type temperature transient. Hence, the plate surface temperature will differ from the indicated temperature of the center thermocouple, which is 1/16 inch below the surface. It is estimated that the difference is less than 0.1° F. For the particular conditions of this study (most importantly, a surface roughness of 10  $\mu$ in. rms for the boiling surface), the Leidenfrost  $\Delta T$  lies somewhere between 11° and 26° F. Most likely, the Leidenfrost temperature is closer to the upper limit and will be taken here as 24° F  $\Delta T$ , or  $T_w = -297^\circ$  F, which was obtained with the smallest drop size and slowest warming rate. This compares with other studies (26 and 35) of pool film boiling where minimum heat fluxes are predicted to occur at  $\Delta T$ 's of 85.9° and 63° F, respectively.

Berenson (26) has derived the following expression predicting the  $\Delta T$  minimum

$$(\Delta T)_{\min} = 0.127 \frac{\rho_v \lambda}{k_v} \left[ \frac{g(\rho_l - \rho_v)}{(\rho_l + \rho_v)} \right]^{2/3} \left[ \frac{g_c \sigma}{g(\rho_l - \rho_v)} \right]^{1/2} \left[ \frac{\mu_v}{g_c(\rho_l - \rho_v)} \right]^{1/3} \quad (49)$$

where the vapor properties are evaluated at the film temperature. This equation is solved by a trial and error procedure, and for liquid nitrogen, it is found that  $(\Delta T)_{\min} = 85.7^\circ$  F, which is considerably different from the experimentally measured value in this study.

## Heat Transfer Coefficients

Instantaneous heat transfer coefficients throughout drop lifetimes were calculated at several  $\Delta T$  values using photographic measurements to determine changes in liquid mass with time. Equation (26) is used for these calculations and is repeated here for convenience.

$$h(V) A(V) \Delta T = \lambda \rho_l \frac{dV}{dt} = Q_{\text{comb}} \quad (26)$$

As described in "Corrected Total Vaporization Times" the projected area measurements were translated into terms of volume by Equations (28), (29), and (30). Before calculating  $h$  values, corrections were made for radiative and free convective heat additions, as also previously described. Three sets of heat transfer coefficients,  $h_{\text{comb}}$ ,  $h_{\text{c r}}$ , and  $h_{\text{c r fc}}$ , were calculated. These heat transfer coefficients are defined as follows:

$$h_{\text{c}} = \frac{Q_{\text{comb}}}{A_{\text{avg}} (\Delta T) \Delta T} \quad \frac{\text{BTU}}{\text{Hr-ft}^2\text{-}^\circ\text{F}} \quad (50)$$

$$h_{\text{c r}} = \frac{Q_{\text{comb}} - Q_{\text{rad}}}{A_{\text{avg}} (\Delta T) \Delta T} \quad \frac{\text{BTU}}{\text{Hr-ft}^2\text{-}^\circ\text{F}} \quad (51)$$

$$h_{\text{c r fc}} = \frac{Q_{\text{comb}} - Q_{\text{rad}} - Q_{\text{fc}}}{A_{\text{avg}} (\Delta T) \Delta T} \quad \frac{\text{BTU}}{\text{Hr-ft}^2\text{-}^\circ\text{F}} \quad (52)$$

Figures 53 through 62 in Appendix E illustrate the variation in  $h$  with drop area. The theoretical curves are based upon Equation (19),

$$h = 0.68 \left( \frac{k_v^3 \lambda^* g \rho_l \rho_v}{\Delta T \mu_v L_e} \right)^{1/4} \quad (19)$$

When  $L_e$  is evaluated from the three regions of the universal drop shape curve (Figure 5, as in Reference 15), the following three expressions



are obtained:

Small Drop Domain:

$$h = 1.1 \left( \frac{k_v^3 \lambda^* g \rho_l \rho_v}{\Delta T \mu_v V^{1/3}} \right)^{1/4} \quad (53)$$

Intermediate Drop Domain:

$$h = 1.075 \left( \frac{k_v^3 \lambda^* g^{1/2} \rho_l^{1/2} \rho_v \sigma^{1/2} g_c^{1/2}}{\Delta T \mu_v V^{2/3}} \right)^{1/4} \quad (54)$$

Extended Drop Domain:

$$h = 1.64 \left( \frac{k_v^3 \lambda^* \rho_v \sigma g_c}{\Delta T \mu_v V} \right)^{1/4} \quad (55)$$

For vaporization of the larger drops (0.2 to 10 ml) the  $h$  values are significantly higher than the predicted values. Corrections for free convection are seen to be minor for high wall temperature (or high temperature differences), but become of much greater significance at the lowest wall temperature. In all cases, the experimental  $h$  values are higher than the theoretical values. This is in logical agreement with previous results which indicated lower vaporization times than predicted by theory.

For the smaller drops ( $< 0.2$  ml) the uncorrected  $h$  values are in fairly good agreement with the theoretical values except for  $\Delta T = 32^\circ \text{F}$ . In that case, the free-convective correction results in much better agreement with the theoretical curve. Referring to Figure 31, this would bring the  $32^\circ \text{F}$   $\Delta T$  data points into closer agreement with the dimensionless universal curve of  $t^*$  against  $V^*$ . As noted previously, for drops less than about 0.2 milliliter, the uncorrected  $t^*$  against  $V^*$  data agree reasonably well with the theoretical curve. The results of this section indicate that for drops smaller than 0.2 milliliter, the

free convection correction factor can be ignored at higher  $\Delta T$ 's, while at low  $\Delta T$ 's, it is not only of significance, but is apparently also of the correct magnitude to bring about reasonably good agreement with the theoretical predictions.

In Appendix F graphs illustrating the variation of heat transfer coefficients during vaporization of large and small drops are shown, i.e.,  $h$  is plotted as a function of time.

It is conventional to plot heat transfer coefficients as a function of  $\Delta T$ . This has been done in Figure 42, which is obtained by cross plotting values taken from the smooth curves drawn through Figures 32 through 41. Also shown are the theoretical curves predicted by Hamill and Baumeister (45) and Baumeister (15). The pool film boiling coefficient is calculated from the equation

$$h = 0.410 \left[ \frac{k_v^3 \lambda^* \rho_v g (\rho_l - \rho_v)}{\mu_v (T_w - T_s) \ell^*} \right]^{1/4} \quad (56)$$

This is very similar to Berenson's expression (26)

$$h = 0.425 \left[ \frac{k_v^3 \lambda^{**} \rho g (\rho_l - \rho_v)}{\mu_v (T_w - T_s) \ell^*} \right]^{1/4} \quad (57)$$

where  $\lambda^{**}$  is given by

$$\lambda^{**} = \lambda \left( 1 + 0.5 \frac{C_p \Delta T}{\lambda} \right) \quad (58)$$

As seen from Figure 42, there is reasonable agreement between the theoretical and experimentally obtained coefficients for the small drop sizes ( $< 0.1$  ml), which are in the intermediate size range in Baumeister's dimensionless volume convention. For the larger drop sizes, as seen previously, the agreement is not very good. It should be remarked that the heat transfer coefficient data plotted in Figure 42 are rather

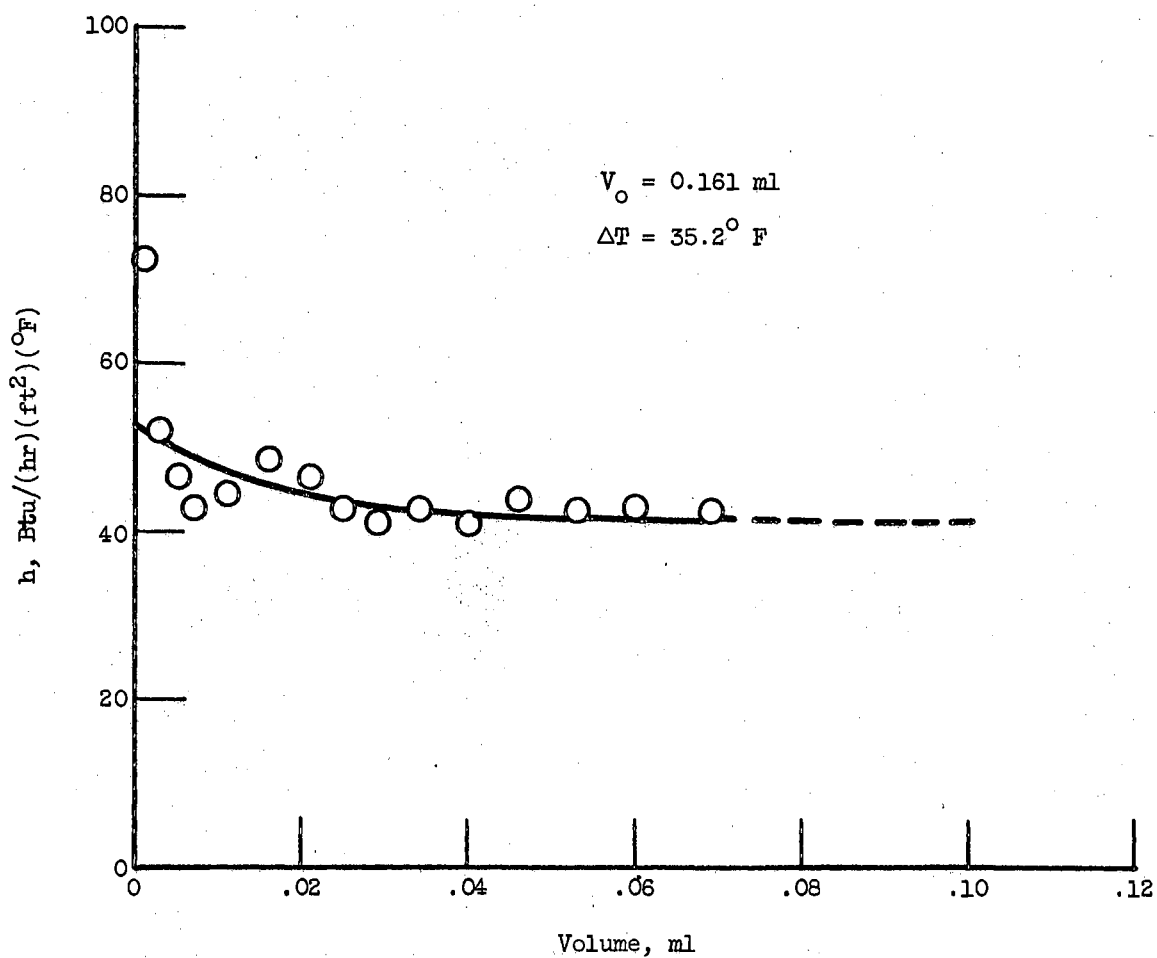


Figure 32. Heat Transfer Coefficient (Corrected) During Drop Vaporization as a Function of Drop Volume -  $\Delta T = 35.2^\circ \text{ F}$

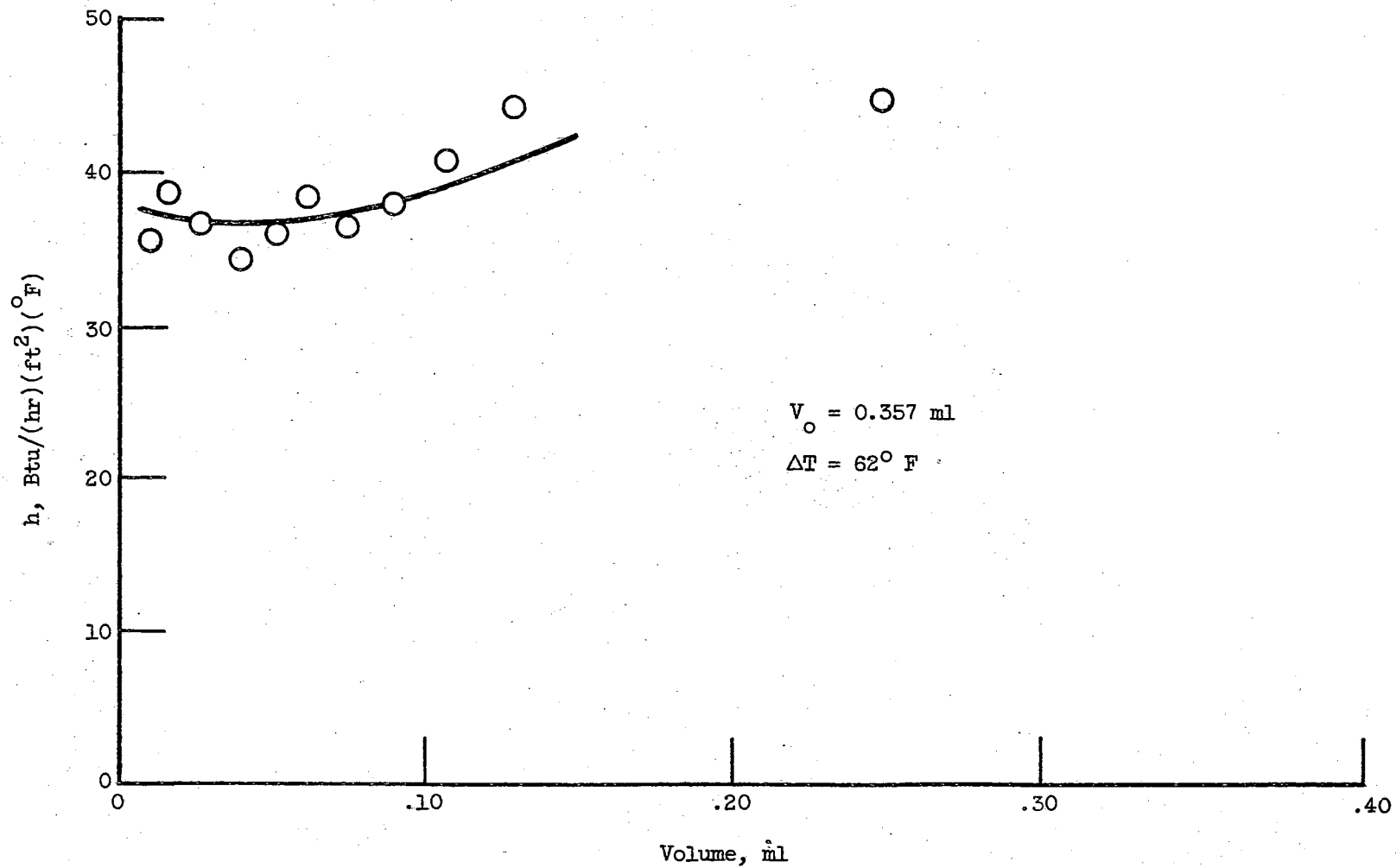


Figure 33. Heat Transfer Coefficient (Corrected) During Drop Vaporization as a Function of Drop Volume -  $\Delta T = 62^\circ \text{ F}$

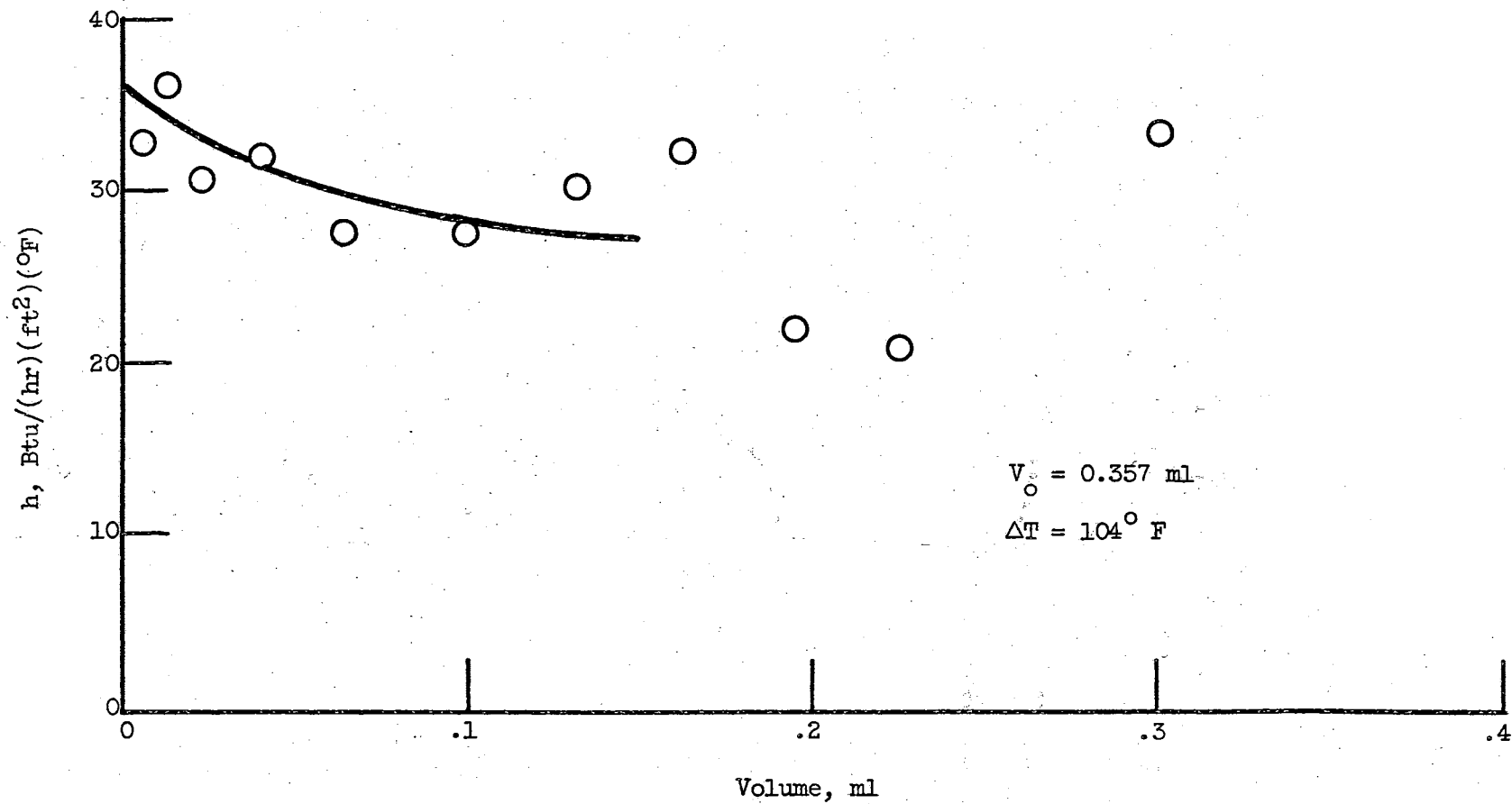


Figure 34. Heat Transfer Coefficient (Corrected) During Drop Vaporization as a Function of Drop Volume -  $\Delta T = 104^\circ \text{ F}$

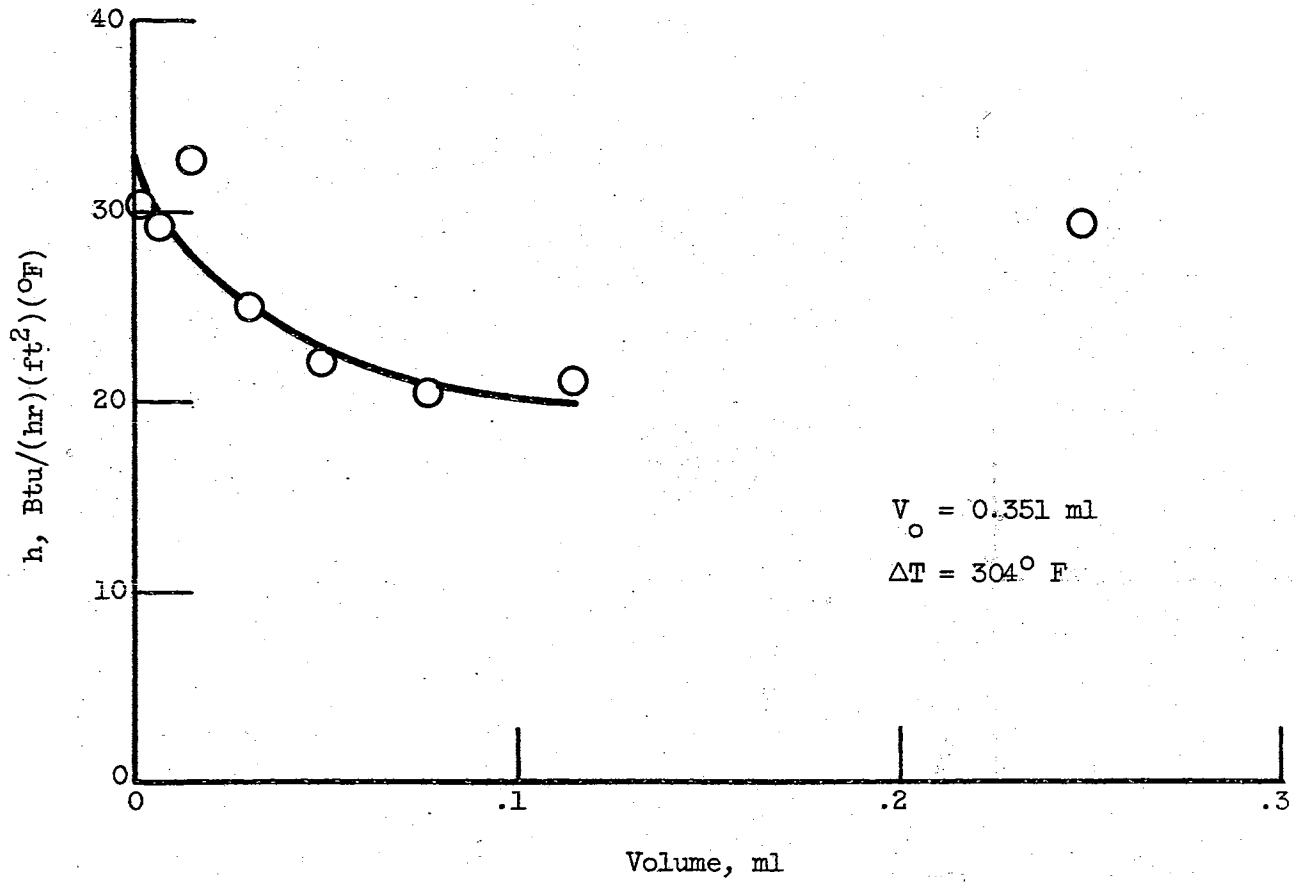


Figure 35. Heat Transfer Coefficient (Corrected) During Drop Vaporization as a Function of Drop Volume -  $\Delta T = 304^\circ \text{ F}$

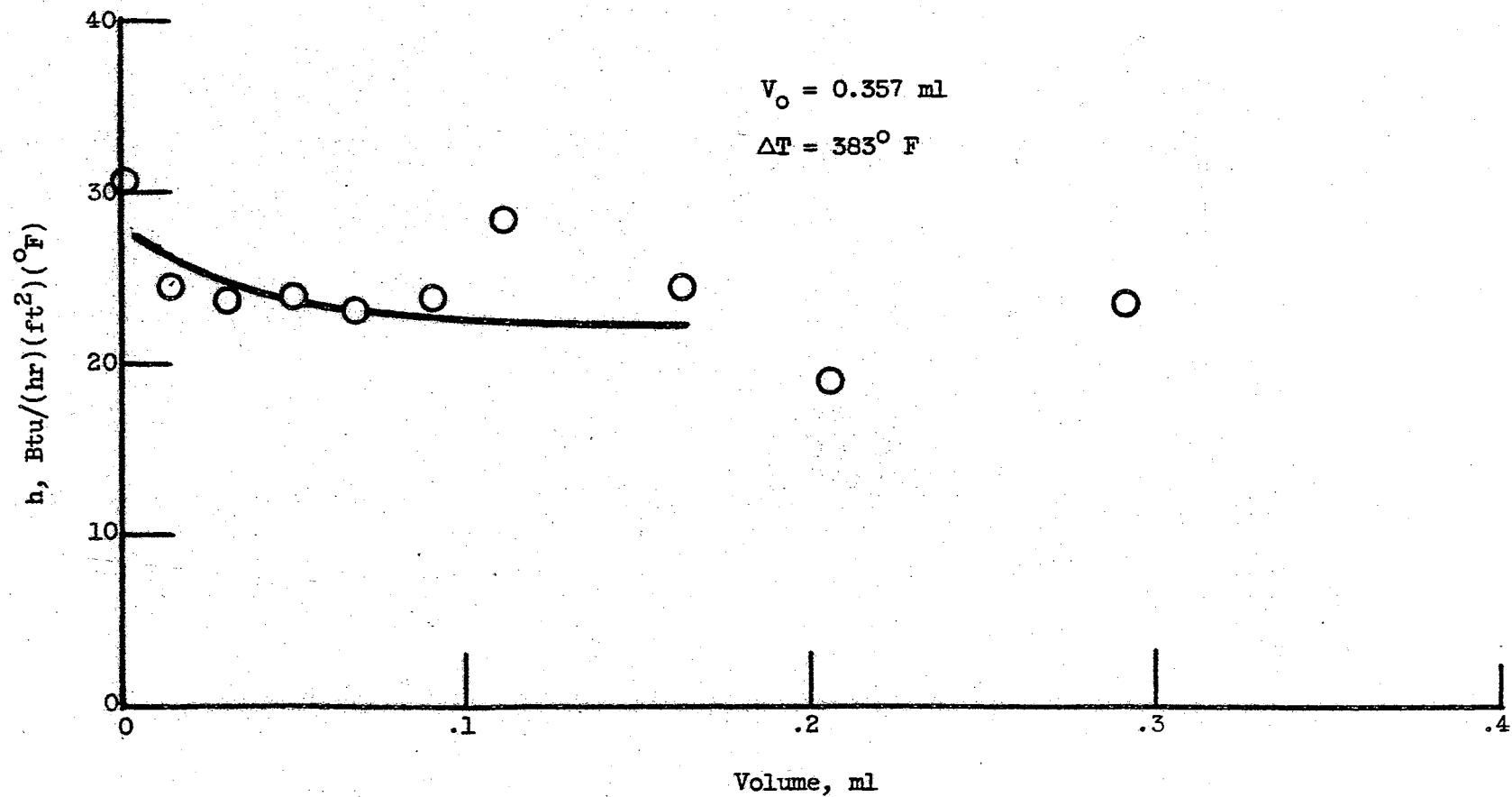


Figure 36. Heat Transfer Coefficient (Corrected) During Drop Vaporization as a Function of Drop Volume -  $\Delta T = 383^\circ \text{ F}$

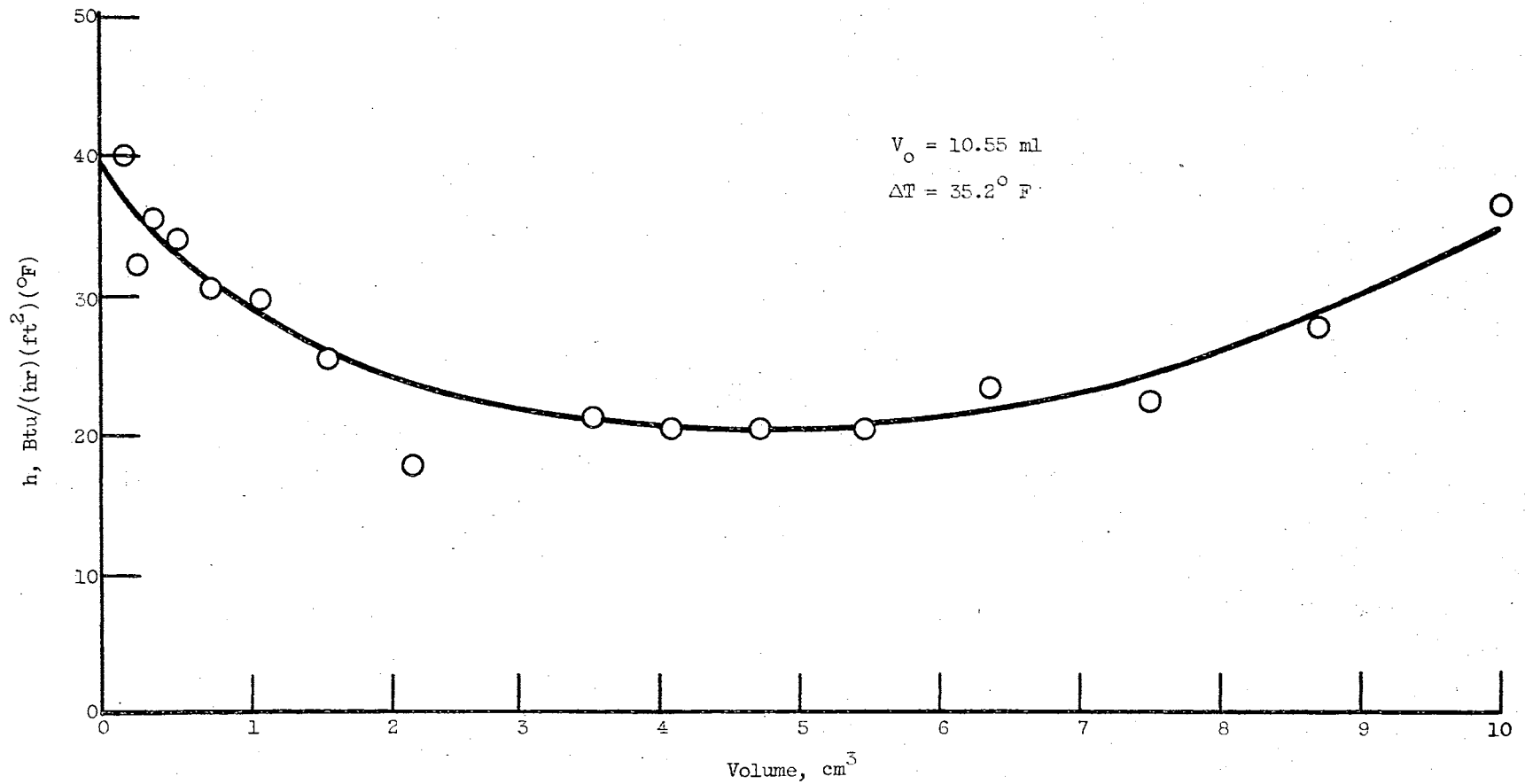


Figure 37. Heat Transfer Coefficient (Corrected) During Drop Vaporization as a Function of Drop Volume -  $\Delta T = 35.2^\circ \text{ F}$



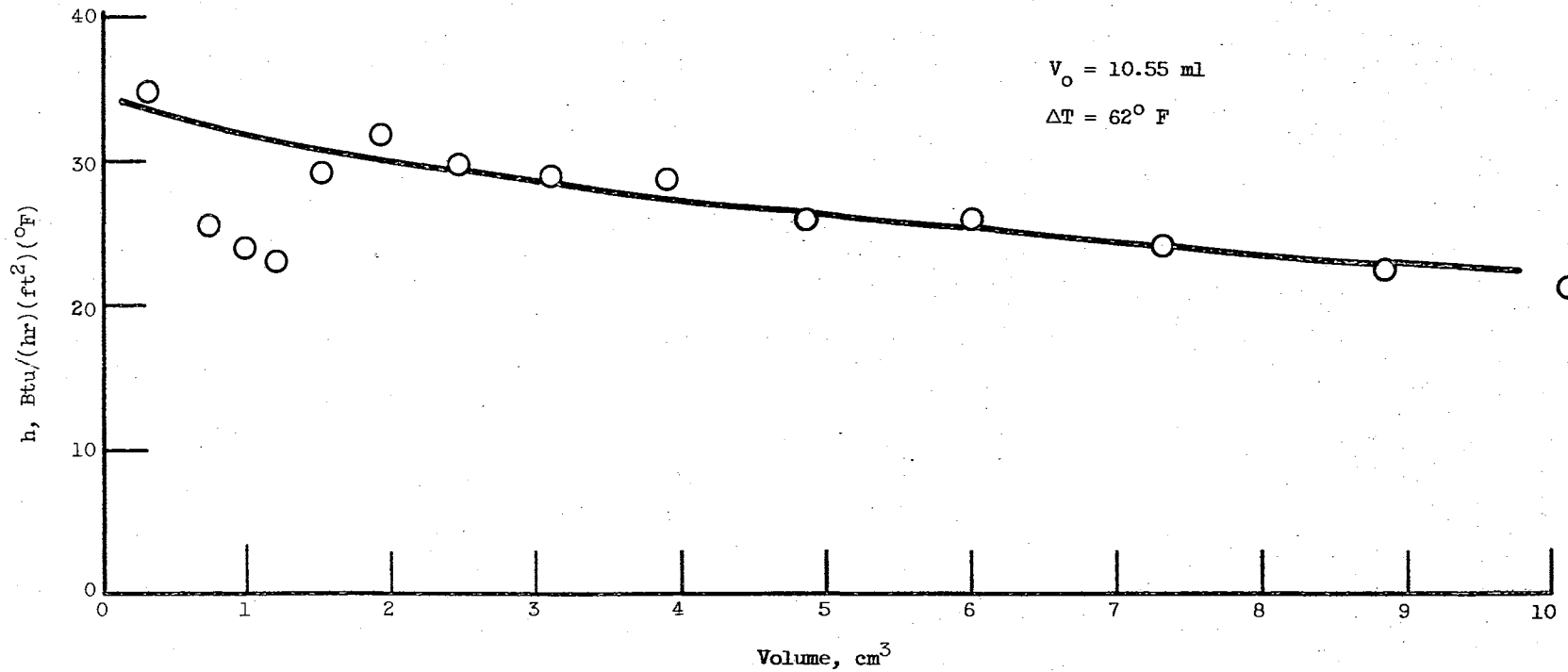


Figure 38. Heat Transfer Coefficient (Corrected) During Drop Vaporization as a Function of Drop Volume -  $\Delta T = 62^\circ \text{ F}$

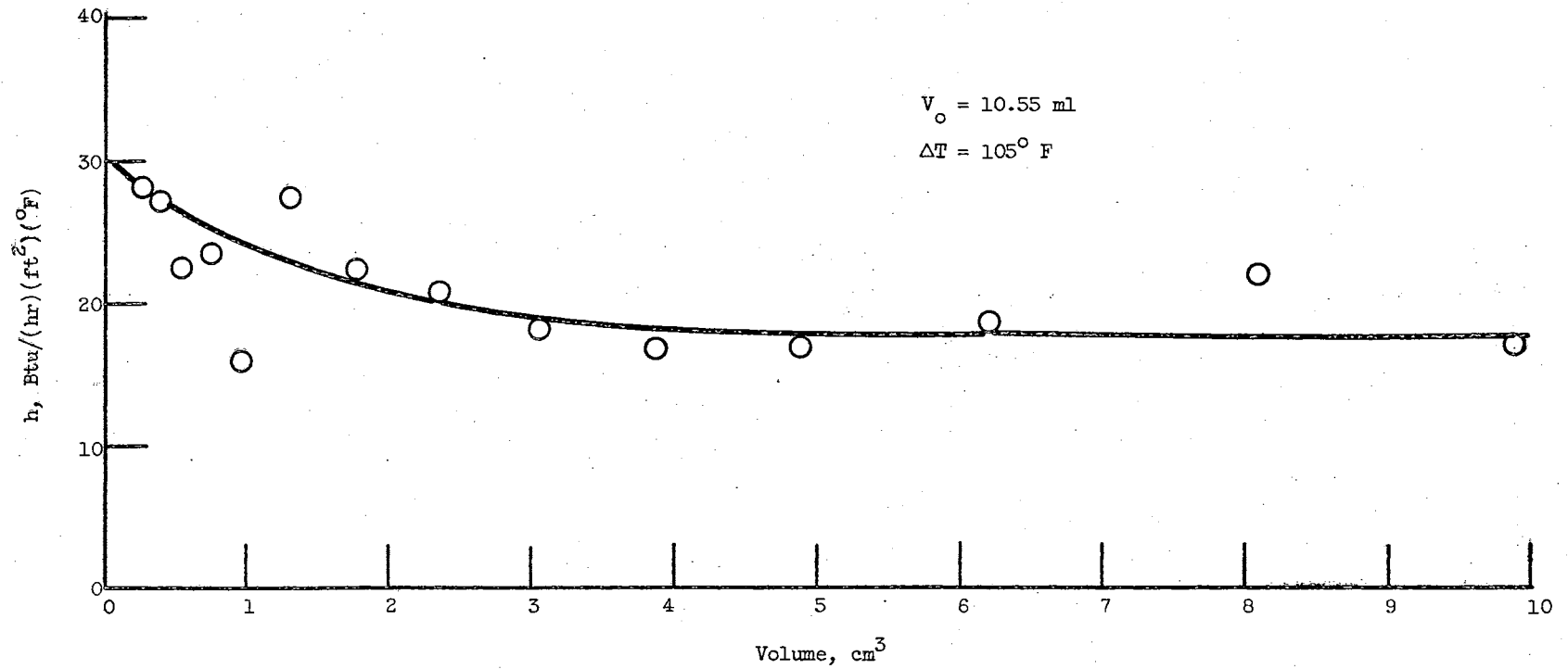


Figure 39. Heat Transfer Coefficient (Corrected) During Drop Vaporization as a Function of Drop Volume -  $\Delta T = 105^\circ \text{ F}$

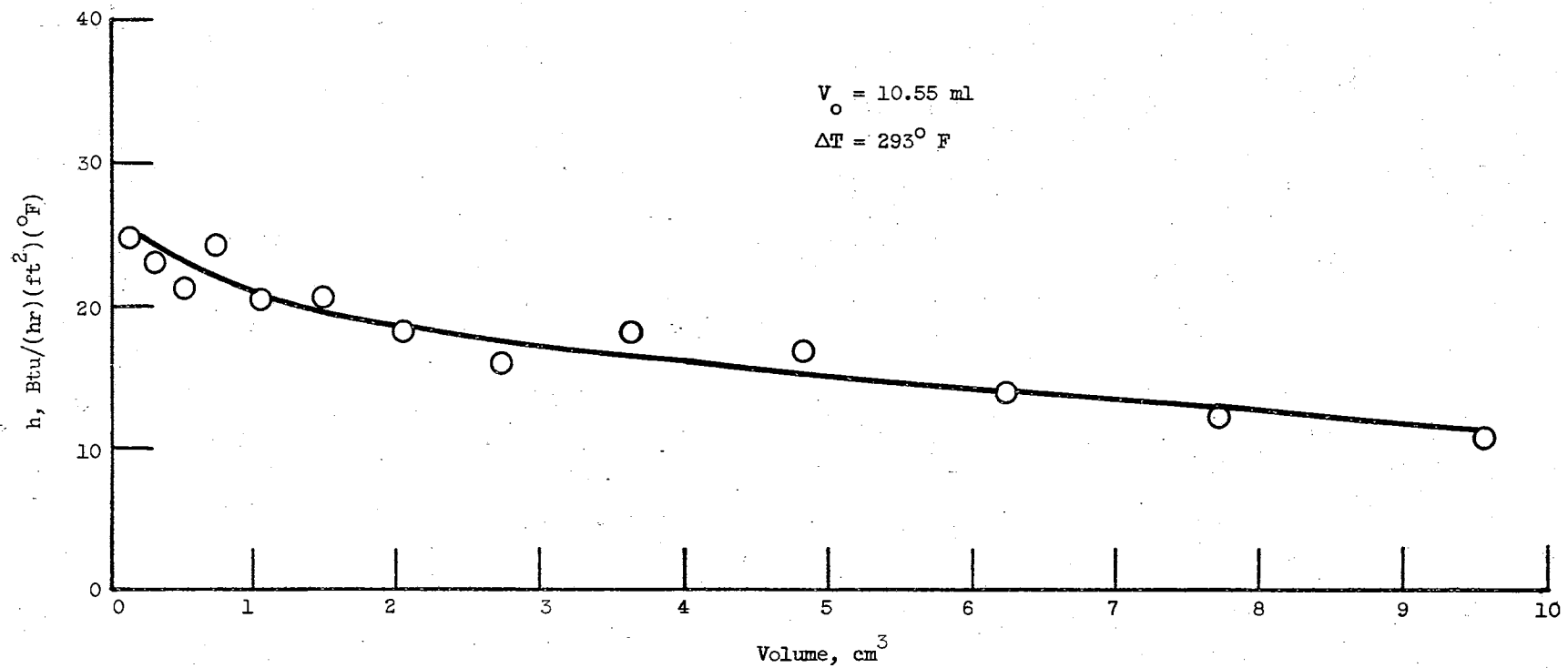


Figure 40. Heat Transfer Coefficient (Corrected) During Drop Vaporization as a Function of Drop Volume -  $\Delta T = 293^\circ \text{ F}$

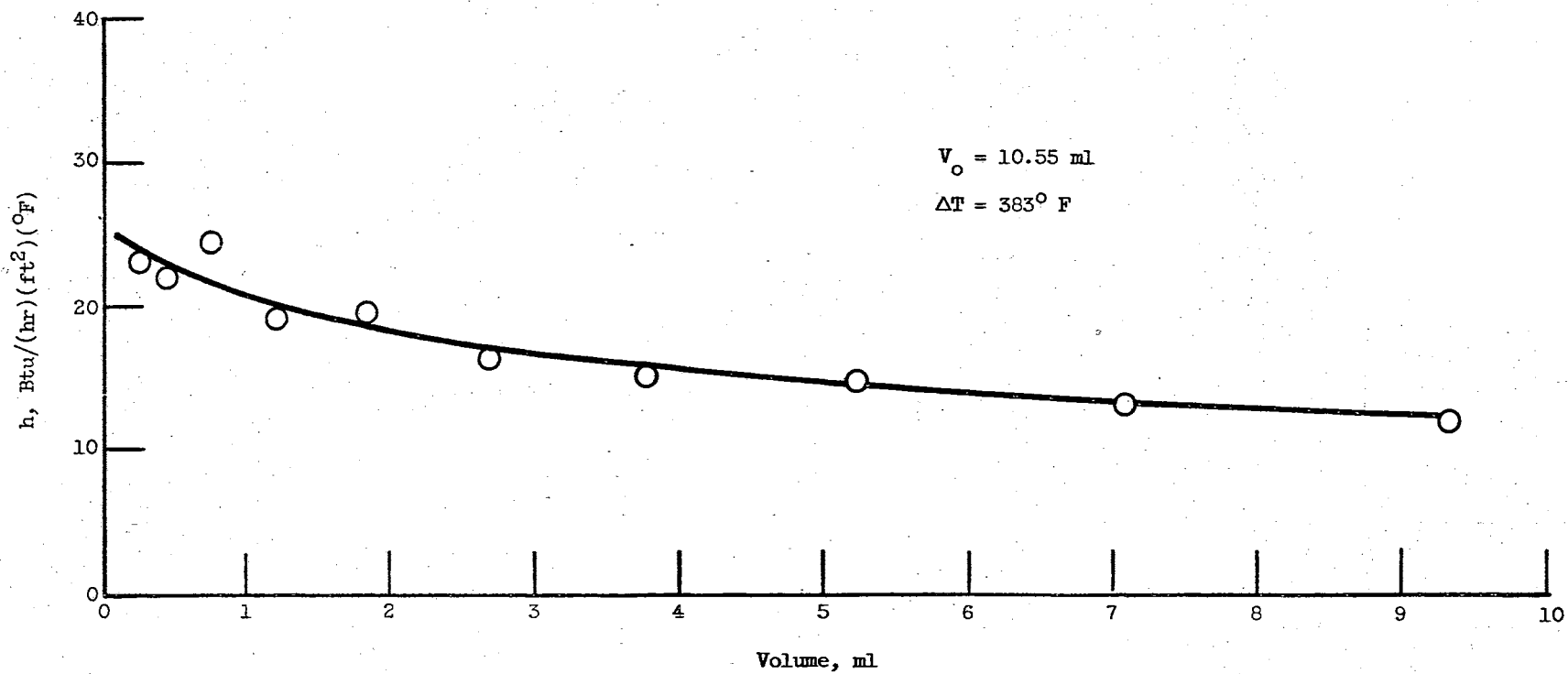


Figure 41. Heat Transfer Coefficient (Corrected) During Drop Vaporization as a Function of Drop Volume -  $\Delta T = 383^\circ \text{ F}$

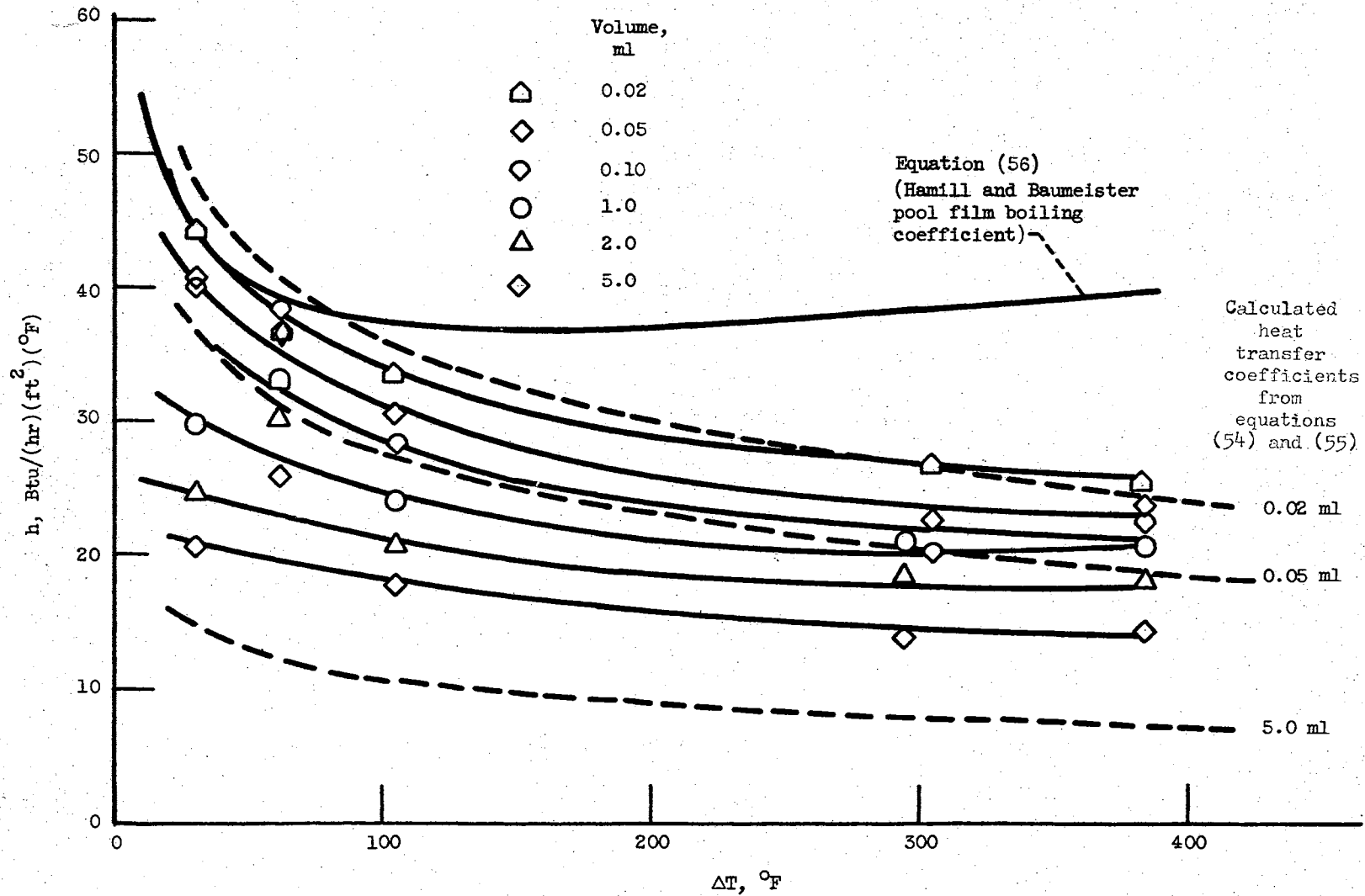


Figure 42. Corrected Heat Transfer Coefficient Versus  $\Delta T$  for Various Drop Volumes

difficult to obtain with accuracy. Consequently, while the experimental curves are certainly of qualitative interest, their quantitative value is difficult to estimate.

#### Vapor Breakthrough Dynamics

Interfacial instability phenomena have been found applicable to pool film boiling (22, 23, 25, 27, and 28). The most recent study (45) derives a heat transfer coefficient intimately related to quantities such as the optimum cell diameter (wavelength) and the optimum vapor dome (bubble) diameter. Hence, it is logical to determine whether heat transfer in the film boiling of discrete extended bubbly masses is also governed by such instability phenomena.

According to Reference 15, bubble breakthrough seems to have a relatively minor effect on heat transfer, as concluded from the apparent agreement of experimental data with the universal correlation of Figure 7. It is speculated that vapor breakthrough does not alter the heat transfer area, the presence of holes merely increasing the perimeter of the bubbly mass. The net result appears to be that the total flux of heat input to the bubbly drop is nearly equal to that calculated by assuming no bubble breakthrough. This would, of course, be a fortunate occurrence, since the universal correlation of  $t^*$  against  $V^*$  of Reference 15 contains no provision for effects of bubble breakthrough. The following data have been gathered in order to provide, perhaps, additional information that may be pertinent to the transfer of heat to extended liquid masses.

Measurements were made of cell size (distance between bubble centers), vapor dome diameter and vapor dome frequency. Measurements

were made for mass sizes from ten milliliters down to about 0.24 milliliter, where no vapor breakthrough occurred, for  $\Delta T$ 's from  $32^\circ$  to  $390^\circ$  F. Qualitative results were also obtained which illustrated the irregular shapes of masses experiencing bubble breakthroughs.

To illustrate the qualitative results, Figure 43 is a tracing from a photograph which shows the outline of a drop experiencing a vapor breakthrough and its reflection. The photograph was taken with the plate at room temperature, and outside the Isolatorlab to permit such a closeup view. The undisturbed drop thickness is about 0.24 inch while the vapor dome reaches a thickness of about 0.40 inch. Figure 44 shows three sets of simultaneous top and side views of the bubbling masses, all of which illustrate the distorted thickness caused by the vapor breakthrough. Figure 45 shows a sequence of five sequential views,  $1/64$  second apart, showing the growth of a vapor dome. The distortion in thickness is again obvious.

Figure 56 illustrates two typical frequency-diameter histories of vapor breakthrough in a 0.36-milliliter mass at a wall temperature of about  $70^\circ$  F. The liquid mass is not shown -- only the vapor breakthrough regions are illustrated. The dashed lines indicate a raising of the drop surface, while the solid lines show the edge of the liquid through which the breakthrough is occurring. The lifetimes indicated on the figure,  $8/64$  and  $9/64$  second, are typical, and did not seem to vary much with  $\Delta T$  or size of the liquid mass.

Figure 47, which shows approximately a 1-milliliter mass, illustrates the randomness of the breakthrough process. The mass shown in part (a) is seen to have no vapor breakthroughs, although a vapor dome is beginning to rise. Part (b) shows one breakthrough and one

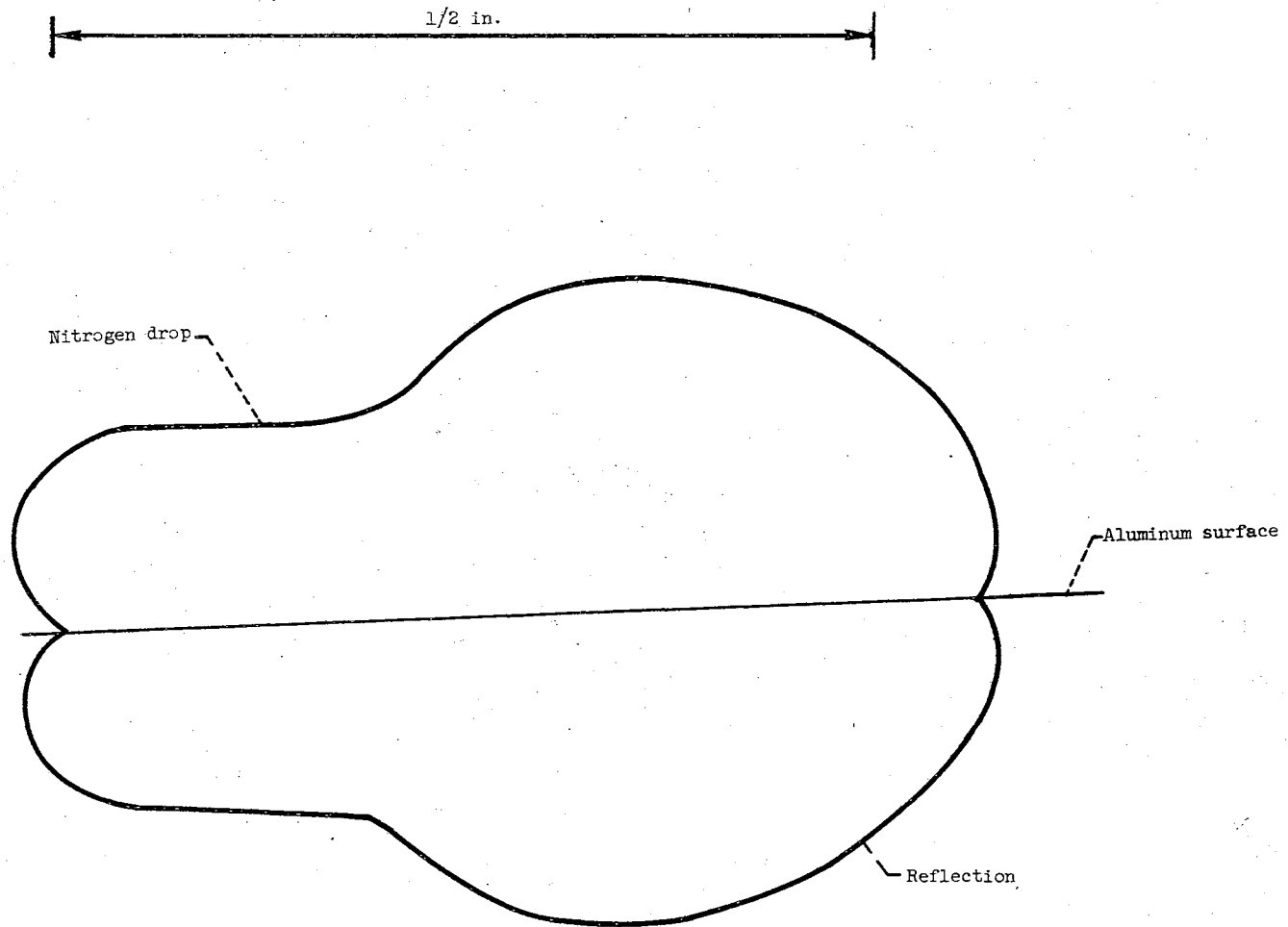


Figure 43. Tracing of Side View of Drop Experiencing Vapor Breakthrough



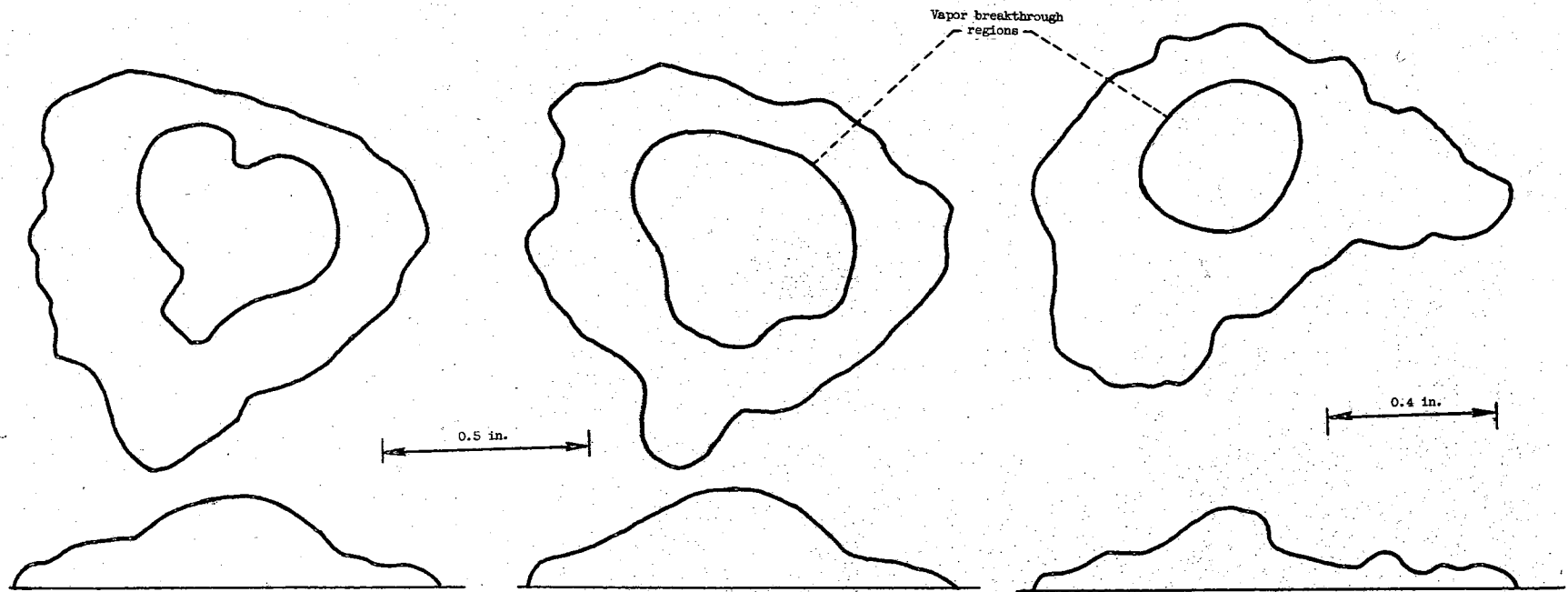


Figure 44. Simultaneous Top and Side View of Drops Experiencing Vapor Breakthrough

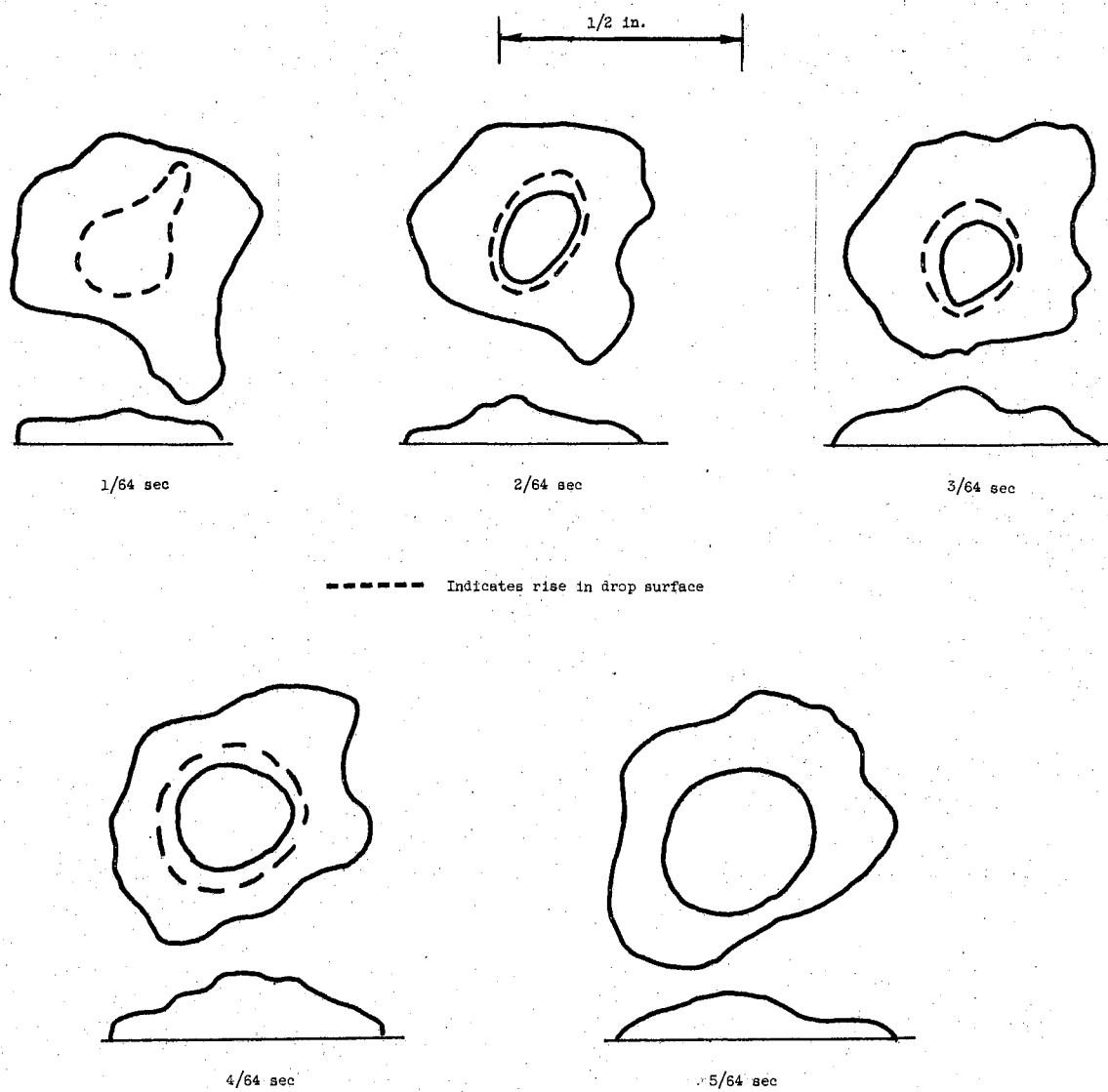


Figure 45. Sequential Top and Side Views of A Drop Experiencing Vapor Breakthrough

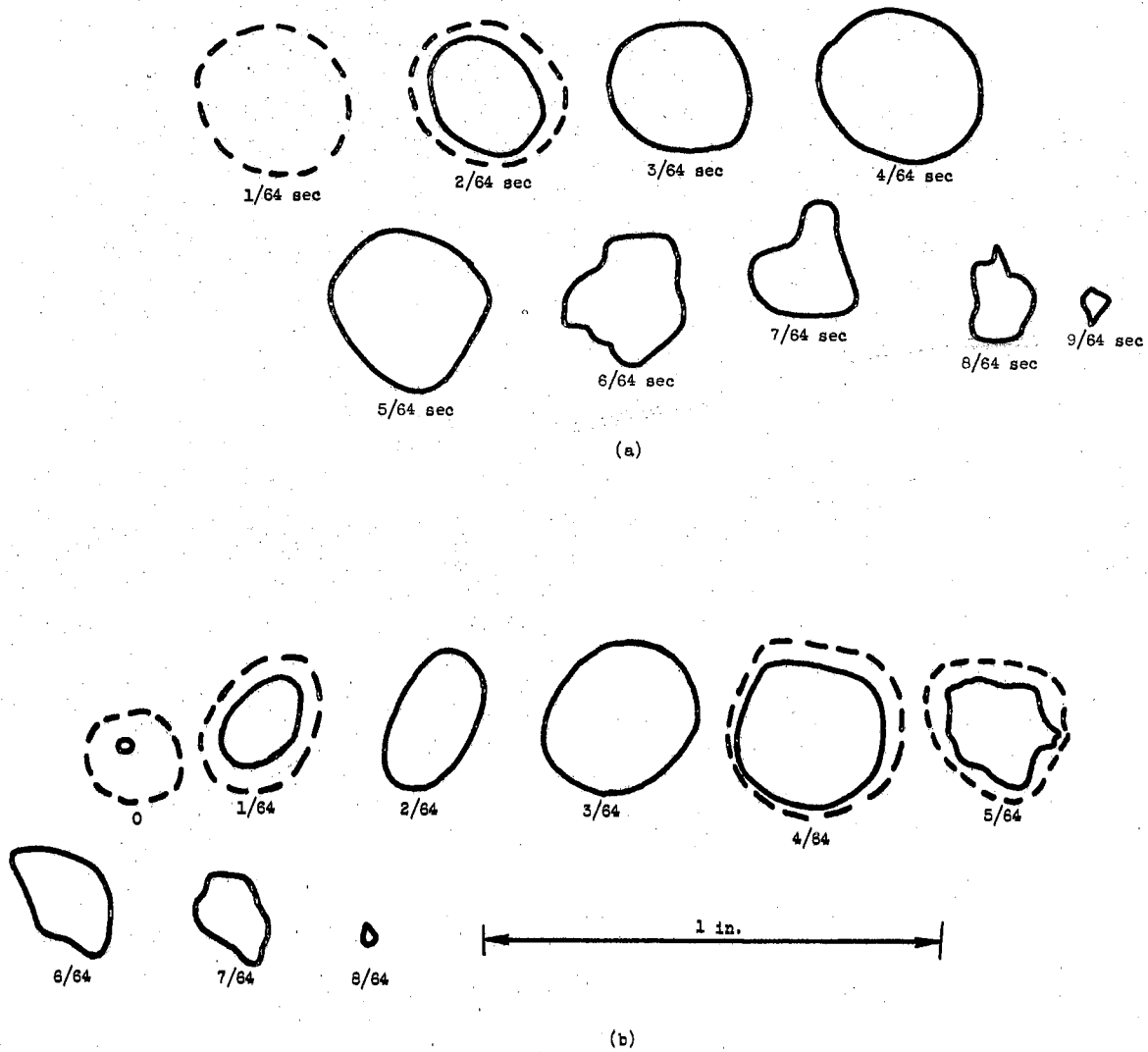


Figure 46. Area-Time History of Vapor Breakthrough Region in Two Drops

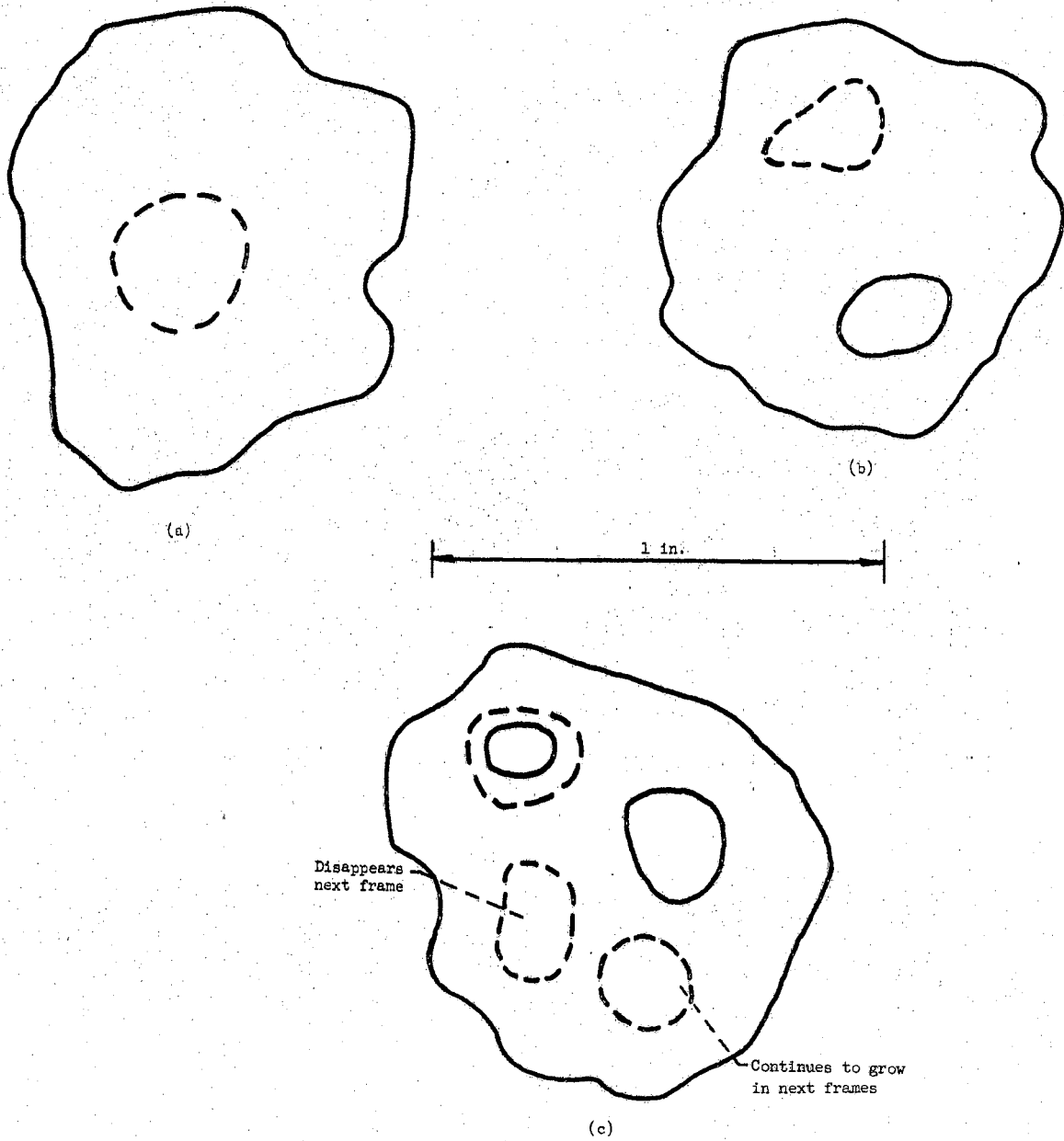


Figure 47. Vapor Breakthrough Regions at Several Times During Vaporization of  $\approx 0.9$  ml Drop

in the early growth (or later collapse) stage. Part (c) shows two breakthroughs and one imminent breakthrough; this photograph illustrates that the 1-milliliter mass apparently has the capacity for sustaining as many as four vapor breakthrough regions. The average center-to-center spacing of the vapor regions in part (c) is 0.357 inch. This compares with the critical wavelength of 0.263 inch, calculated from Equation (1) and the most dangerous wavelength of 0.456 inch, calculated from Equation (2).

Measurements of the maximum diameter of vapor domes for three  $\Delta T$  values were made. The results are summarized in Figure 48 and Table IV. The complete set of data is given in Appendix G. The areas were measured using a planimeter, as previously described, and the diameters were then calculated from these measurements. Figure 48 compares the measured values with those predicted by Equation (71), which indicates the diameter to be virtually independent of  $\Delta T$ . The data of Figure 48 not only indicate a slight decrease of diameter with decreasing  $\Delta T$ , but the diameters are significantly larger than that predicted by Equation (71).

Distances between vapor dome centers (cell spacings) were also measured at several  $\Delta T$  values for 10-milliliter mass sizes and are summarized in Table V. The average center-to-center cell spacings are also plotted in Figure 49 as a function of  $\Delta T$ . The complete set of data is given in Appendix H. An increase in cell size with decreasing  $\Delta T$  seems to be indicated, although again the precise variation is uncertain because of the large uncertainty intervals.

Finally, measurements of the vapor fraction of various sizes of liquid masses are shown in Appendix I. The vapor fraction is defined as the sum of the areas where vapor breakthrough is occurring, divided

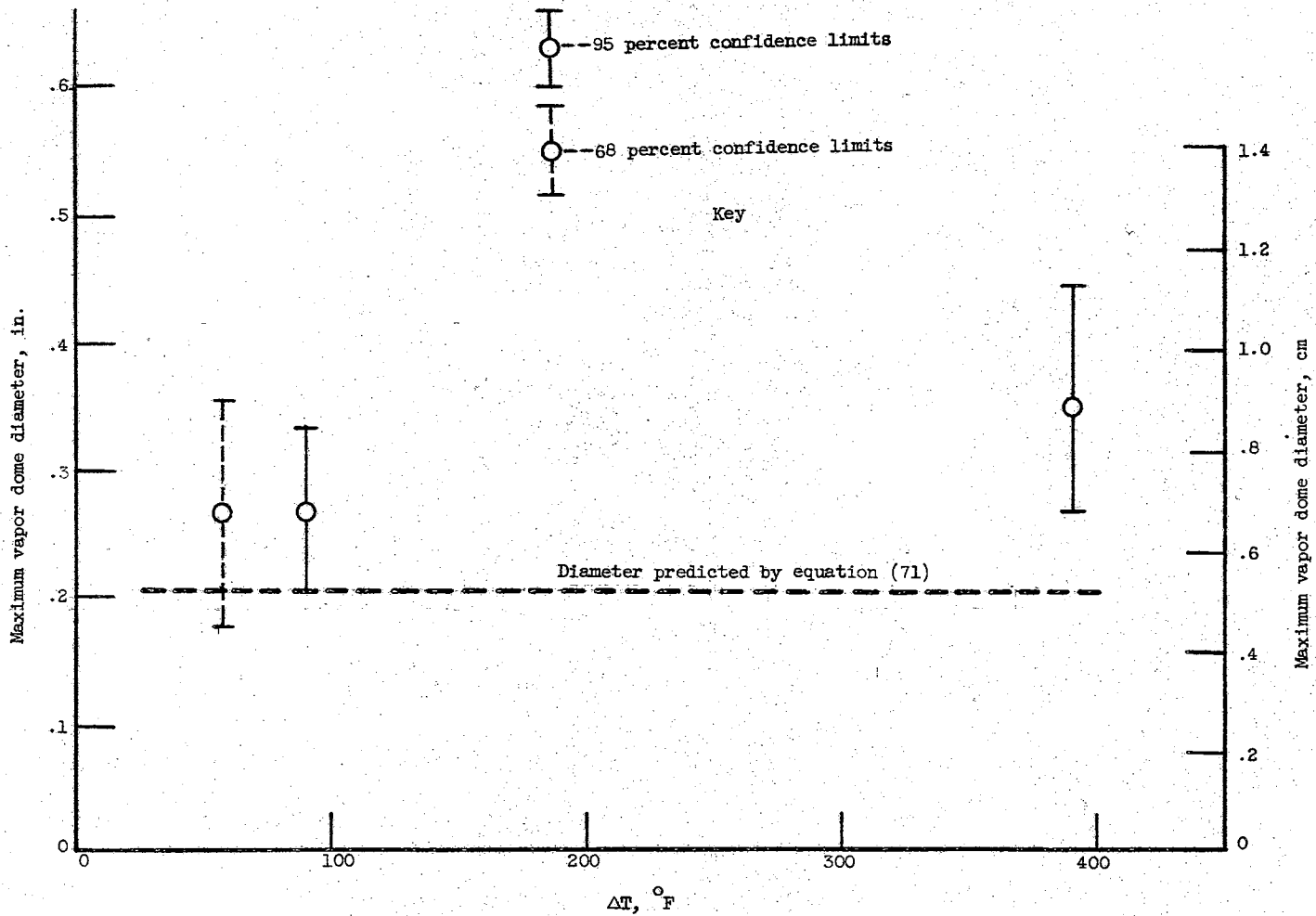


Figure 48. Comparison of Theoretical and Experimental Values of Maximum Vapor Dome Diameters as a Function of  $\Delta T$

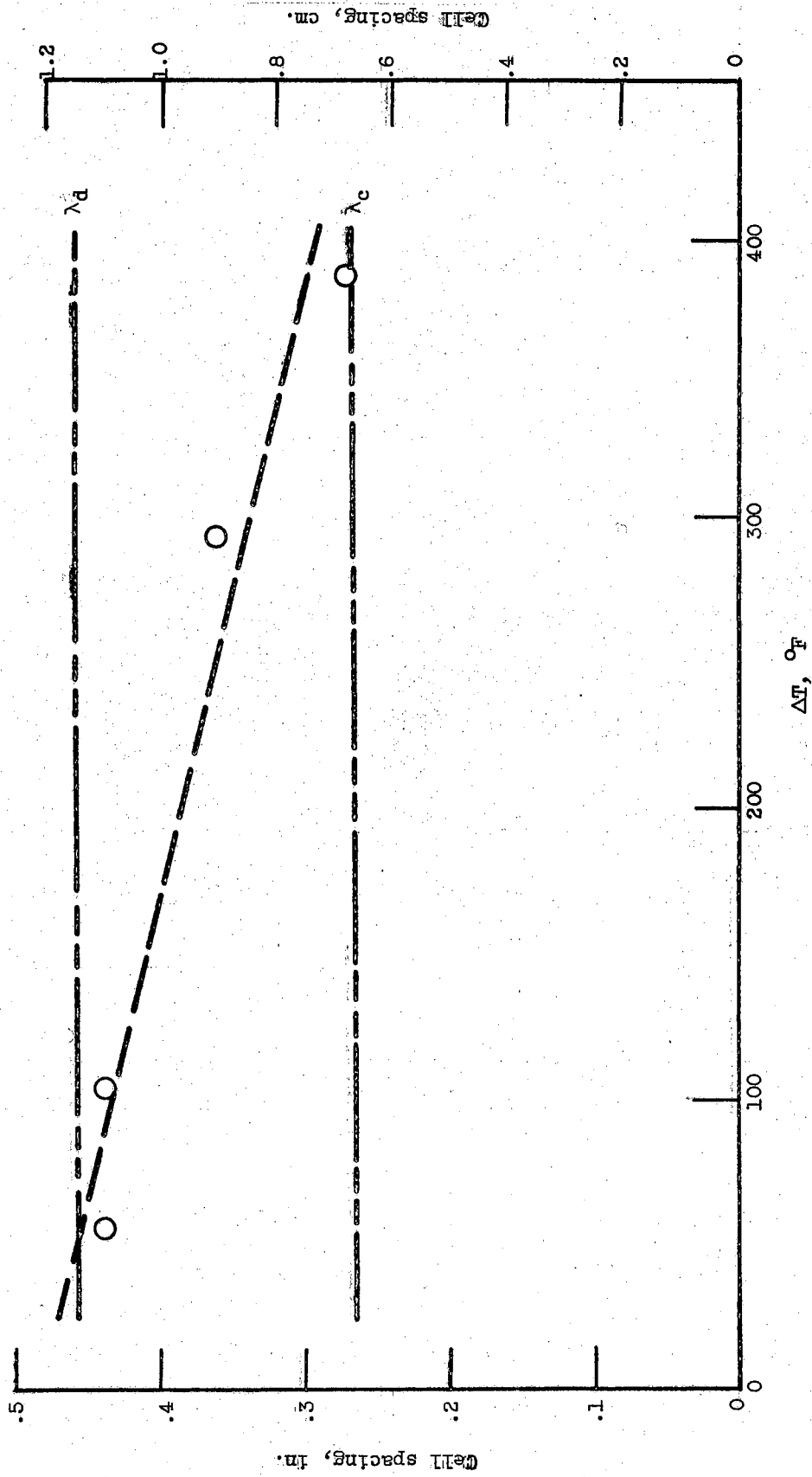


Figure 49. Comparison of Theoretical and Experimental Cell Spacing as A Function of  $\Delta T$

TABLE IV  
 MAXIMUM VAPOR DOME AREAS (MEASURED)  
 AND CORRESPONDING DIAMETERS  
 (CALCULATED)

$\Delta T$ °F	$A_{\max}$ in. <sup>2</sup>	$D_{\max}$ in.
57	.0565	.267
90	.0708	.268
383	.0984	.352

TABLE V  
 CELL SPACING (CENTER-TO-CENTER)

$\Delta T$ °F	Cell Spacing in.
57	0.44
105	0.44
294	0.37
379	0.27



by the total area within the liquid mass periphery. A rough average of the vapor fraction  $A_v/A$  is 0.20.

## CHAPTER VII

### ANALYSIS

The photographic results of this investigation indicate that vapor breakthrough produces distortions in the thickness of a liquid mass (Figures 43, 44, and 45). Also, the area-volume relationship predicted for the case of no bubble breakthrough seems to be in very good agreement with data taken for the actual case of numerous bubble breakthroughs (Figure 22). In addition, photographs leave no doubt that when vapor breakthrough occurs, a fairly regular circular area is created in the liquid mass, through which the plate surface is clearly visible. Hence, if a vapor mass with breakthrough occupies the same area as a mass with no breakthrough, the average thickness of the liquid regions for the former case will be greater than the average thickness of a mass with no vapor breakthrough. The foregoing observations will be utilized in modifying the average drop thickness,  $t$ , introduced in Baumeister's universal heat transfer correlations, which contains no provision for the consequences of vapor breakthrough. It is believed that inclusion of vapor breakthrough effects will offer at least a partial explanation of the discrepancies between experiment and theory previously noted (Figures 29, 31, and 53 through 62).

In the Baumeister cylindrical disc model we have the following relationships:

$$V = At \quad (59)$$

$$A = \pi r_0^2 \quad (60)$$

from which

$$r_o^4 = \frac{V^2}{\pi^2 t^2} \quad (61)$$

At a point in the analysis of Reference 12, the expression  $r_o^4/V$  occurs.

The quantity is then termed a characteristic length, defined by

$$L_e = \frac{r_o^4}{V} = \frac{V}{\pi^2 t^2} \quad (62)$$

For the actual case of vapor breakthrough (refer to Figure 50),  $A$  is less than  $A_o$ . Consequently,

but

$$V \neq At$$

$$V = A't' \quad (63)$$

The area  $A'$  is defined by

$$A' = A - n A_{vd} \quad (64)$$

and the average thickness of the drop (which consists only of the liquid region) is now

$$t' = \frac{A}{A'} t = \frac{At}{(A - n A_{vd})} \quad (65)$$

The expression for  $t$  in the extended drop region is given by Reference 15:

$$t = 1.85 \left( \frac{\sigma g_c}{\rho_t g} \right)^{1/2} \quad (66)$$

Accounting for vapor breakthrough,

$$t' = \frac{1.85 A}{A - n A_{vd}} \left( \frac{\sigma g_c}{\rho_t g} \right)^{1/2} \quad (67)$$

Likewise, from Equation (62),

$$L_e' = \frac{V}{\pi^2 t'^2} = \frac{(A - n A_{vd})^2}{A^2} \frac{V}{\pi^2 t^2} = \left( \frac{A - n A_{vd}}{A} \right)^2 L_e \quad (68)$$

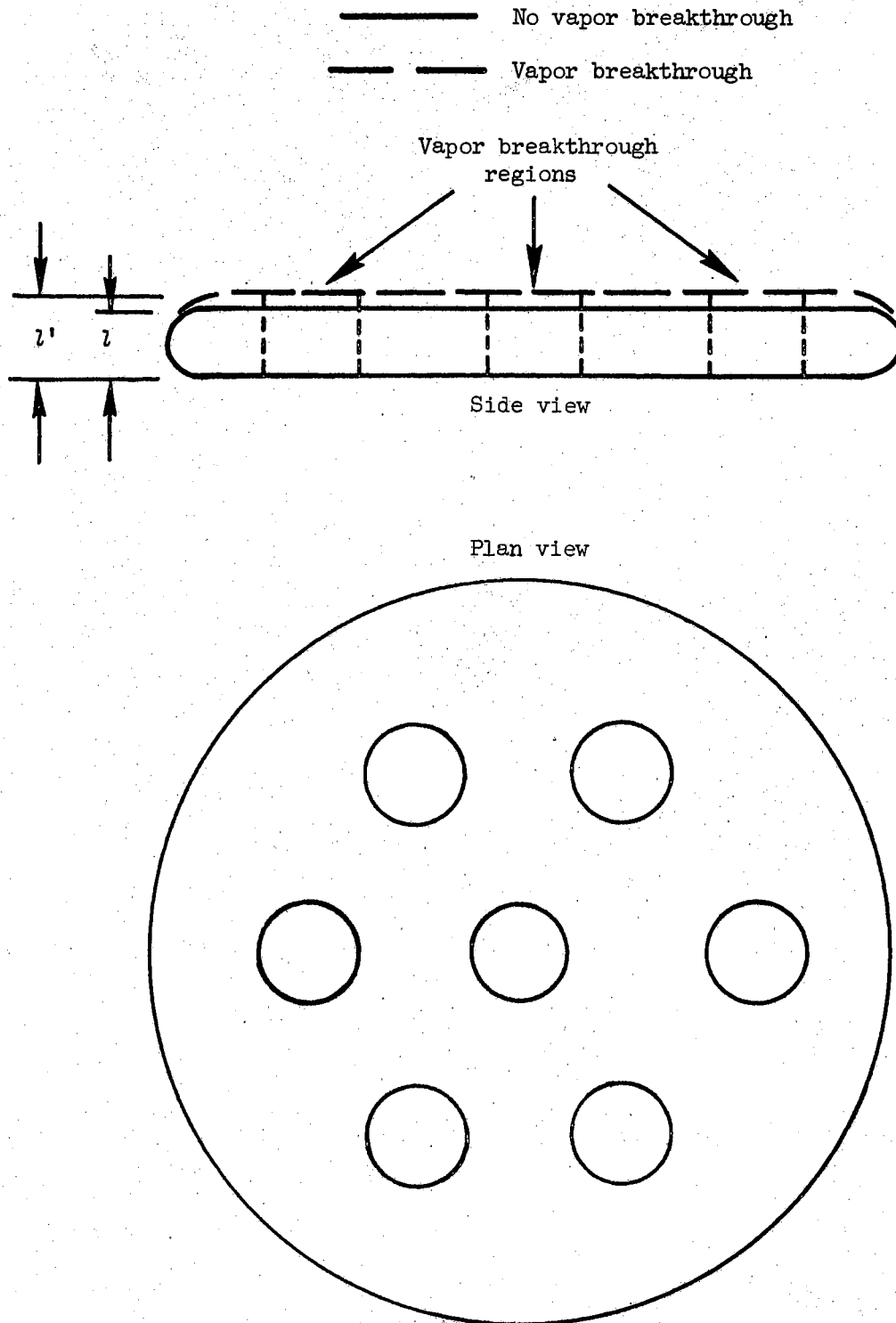


Figure 50. Schematic Model of Extended Liquid Drop Experiencing Several Vapor Breakthroughs

The generalized heat transfer coefficient (Equation (19)), becomes

$$h = 0.68 \left( \frac{k_v^3 \lambda^* g \rho_t \rho_v}{\Delta T \mu_v L_e} \right)^{1/4} \quad (69)$$

For the extended drop region, the heat transfer coefficient (see Equation (44)) becomes

$$h' = \frac{1.075 A^{1/2}}{(A - n A_{vd})^{1/2}} \left( \frac{k_v^3 \lambda^* g^{1/2} \rho_t^{1/2} \rho_v \sigma^{1/2} g_c^{1/2}}{\Delta T \mu_v V^{2/3}} \right)^{1/4} = \frac{hA^{1/2}}{(A - n A_{vd})^{1/2}} \quad (70)$$

A modified heat transfer coefficient will, of course, influence the vaporization rate and the total vaporization time. The total vaporization time is obtained by direct integration of Equation (26), except that both A and h will be replaced by their modified values (Equations (64) and (70)). Before the resulting expression may be integrated, however, some functional dependence of the total vapor area upon volume must be established, where the total vapor area is  $A_{vap} = n A_{vd}$ .

To establish this functional relationship assume first that the vapor dome diameter is the optimum vapor dome diameter derived in Reference 46, namely

$$D = 4.90 \left[ \frac{g_c \sigma}{g(\rho_t - \rho_v)} \right]^{1/2} \quad (71)$$

for pool film boiling. This expression compares well with an empirical expression obtained by Berenson (26) for n-pentane and carbon tetrachloride, in which the prefactor constant in Equation (71) is replaced by 4.7. The area of a vapor dome is thus

$$A_{vd} = \frac{\pi D^2}{4} = 13.84 \left[ \frac{g_c \sigma}{g(\rho_t - \rho_v)} \right] \quad (72)$$

Convenient expressions for the vapor dome spacing are the critical wavelength (Equation (1)) and the most dangerous wavelength (Equation (2)). Previous results of Patel (28) indicated actual values between these two but closer to the most dangerous wavelength. Hence, a spacing equal to the most dangerous wavelength will be assumed here. The number of vapor domes  $n$  in a particular drop will be estimated by

$$j = \frac{A(V)}{\lambda_d^2} \quad (73)$$

Actually, for  $0 < j < 1.0$ ,  $n$  will be zero, that is, the drop is of insufficient size to permit a breakthrough. For  $1.0 < j < 2.0$ ,  $n$  will be unity, etc. However, as an approximation and for simplicity  $n$  will be assumed equal to  $j$  and will thus be a continuous function of drop volume, rather than a step function.

The total vapor area in a given volume of liquid undergoing film boiling is thus

$$A_v = n A_{vd} = \frac{A(V)}{\lambda_d^2} \frac{(18.84) g_c \sigma}{g(\rho_l - \rho_v)} \quad (74)$$

Substituting the most dangerous wavelength value, Equation (2), and evaluating the liquid nitrogen properties at one atmosphere

$$A_v = 0.1592 A(V) \quad (75)$$

For other fluids having a much higher surface tension, the constant in Equation (75) will be correspondingly lower, that is, for high surface tension fluids less vapor breakthrough will occur and the total vapor area will be less, on the average, than that for liquid nitrogen. The expression for  $j$ ,  $A(V)/\lambda_d^2$ , is useful as an index to the amount of water breakthrough that will occur.

Since vapor breakthrough is expected to occur first in the extended

drop region, Equation (30) may be used to evaluate  $A(V)$ . Using Equation (2) to evaluate  $\lambda_d$ , from Equation (73),

$$j = \frac{A(V)}{\lambda_d} = 0.00457 V \left( \frac{\rho_l g}{\sigma g_c} \right)^{3/2} \quad (76)$$

Evaluating  $j$  for various liquids,

Nitrogen:

$$j = 3.83 V \quad (77)$$

Ethyl Alcohol:

$$j = 1.292 V \quad (78)$$

Carbon Tetrachloride:

$$j = 1.222 V \quad (79)$$

Benzene:

$$j = 1.065 V \quad (80)$$

Water:

$$j = 0.290 V \quad (81)$$

where  $V$  is given in milliliters. These relations are shown graphically in Figure 51. It is interesting to observe that for liquid nitrogen  $j$  exceeds unity for  $V > 0.26$  milliliter. This agrees well with the experimental observations that breakthrough did not occur for  $V < 0.24$ . By contrast, the  $j$  index indicates that vapor breakthrough cannot occur in water volumes less than about 3.4 milliliters. Compared with ethyl alcohol and carbon tetrachloride, about three times as many breakthroughs are indicated in liquid nitrogen drops of equal volume.

Results reported by Patel (28) for approximately ten-milliliter masses show one to two vapor breakthrough areas for water, nine or ten for carbon tetrachloride, and five or six for benzene. These results are in essential agreement with the predictions of Equations (79), (80),

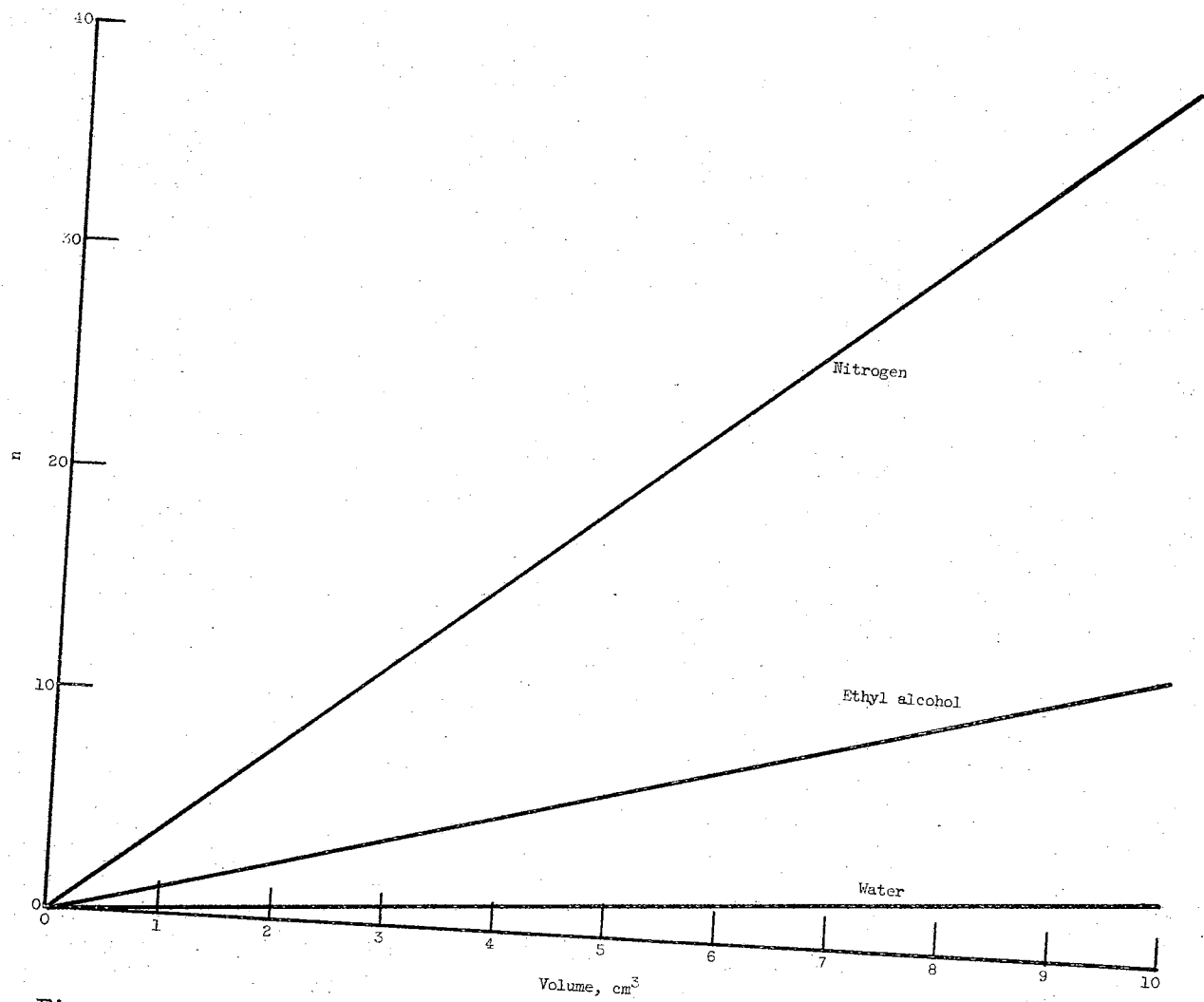


Figure 51. Prediction of Number of Vapor Breakthroughs In a Given Volume of Liquid



and (81), although the observed values are all a little lower than the predicted values.

While the  $j$  value is a measure of the number of vapor cells capable of being sustained by a fluid mass, practical considerations make it difficult to describe the vapor area at any particular time. The first difficulty is that boiling is a stochastic phenomenon, so that average quantities must be dealt with, rather than discrete quantities. For example, in a large, extended fluid mass, vapor domes may grow at slightly different rates, achieve different final diameters, and have their birth times distributed continuously over a period of one vapor-dome lifetime. Such phenomena are particularly difficult to describe at small drop volumes. For example, in a volume capable of supporting two cells, the vapor domes are not likely to grow and disappear simultaneously, giving rise to two new vapor domes. Evidence of this was seen in Figure 47, where at one instant, no vapor breakthroughs were present, while at another time, it seemed likely that as many as four breakthroughs could be sustained.

Even if the dome growth were regular and uniform, an average vapor area over a single growth-collapse cycle must be determined. Finally, dome spacings between  $\lambda_c$  and  $\lambda_d$  are possible, with the average spacing apparently being somewhat less than  $\lambda_d$ . Hence, to describe the true relationship between vapor area and liquid volume would require considerable study and quantitative information that is beyond the scope of this investigation. For the present purposes, a quasi-steady state distribution of vapor areas will be assumed to exist such that the vapor dome diameters are at their maximum value. In effect, this assumes that when a vapor dome begins decreasing in size, the adjacent vapor domes

located  $\lambda/2$  distance away will begin their growth; at any time then the vapor area within the distance  $\lambda$  is roughly constant.

To determine the effect of vapor breakthrough on total vaporization time, Equations (70), (64), and (30) are substituted in Equation (26) to obtain

$$\lambda \rho_i \frac{dV}{dt} = \frac{1.64 \sqrt{A(V)}}{[A(V) - 0.1592 A(V)]^{1/2}} \left( \frac{k_v^3 \lambda^* g_c \rho_v \sigma}{\mu_v V} \right) \left[ 0.54 V \left( \frac{\sigma g_c}{\rho_i g} \right)^{-1/2} \right] \Delta T. \quad (82)$$

Simplifying and rearranging Equation (82), one obtains

$$0.95 \left( \frac{\lambda^4 \rho_i^2 \mu_v \sigma g_c}{3 \lambda^* \rho_v g^2} \right)^{1/4} \frac{dV}{V^{3/4}} = dt. \quad (83)$$

Using Equations (23) and (27) to express in terms of  $V^*$  and  $t^*$ ,

$$0.95 \frac{dV^*}{V^{*3/4}} = dt^* \quad (84)$$

$$\int_{V^* = 155}^{V^*} \frac{dV^*}{V^{*3/4}} = \int_{t'^*}^{t^*} dt^* \quad (85)$$

The lower limits of integration are at the beginning of the extended drop region, where vapor breakthrough first occurs. The remainder of the drop lifetime is unaffected by breakthrough and the previously derived expressions (Equations (46) and (47)), relating  $t^*$  and  $V^*$  remain unaffected. Integrating,

$$4.4 V^{*1/4} - 14.61 = t^* - t'^* \quad (86)$$

The expression for drop lifetime in the intermediate drop region is

$$t^* = 2.23 V^{*1/3} - 0.97 \quad (47)$$

at  $V^* = 155$ ,

$$t'^* = 2.23 (155)^{1/3} - 0.97 = 11.00 \quad (87)$$

and substituting into Equation (86),

$$t^* = 4.14 V^{*1/4} - 3.61 \quad (88)$$

This compares with the expression derived for no vapor breakthrough,

$$t^* = 4.52 V^{*1/4} - 4.96 \quad (48)$$

The dashed line of Figure 31 shows the curve predicted by Equation (88). Although the modified curve agrees with the trend of the data quantitative agreement is still lacking. In view of the approximations used to derive Equation (88), it is interesting to note the change in the  $t^*$  expression produced by assuming a vapor cell spacing of  $\lambda_c$  instead of  $\lambda_d$ . It is seen from Equation (73) that the vapor area is a fairly strong function of the spacing, that is,  $A \propto (1/\lambda^2)$ . Since  $\lambda_d = \sqrt{3} \lambda_c$ , the vapor area would become

$$A_v = 0.4776 A(V) \quad (90)$$

With such a change, one would obtain

$$3.26 V^{*1/4} - 11.49 = t^* - t'^* \quad (91)$$

and

$$t^* = 3.26 V^{*1/4} - 0.51 \quad (92)$$

At  $V^* = 10,000$ ,  $t^* = 32.1$  which would bring the modified curve directly through the data of Figure 31.

The results of this section show that the trend of data may be attributable to vapor breakthrough promoting overall heat transfer to the extended liquid drop. Physically, the effect of vapor breakthrough is to decrease the liquid area within a given perimeter, thereby

increasing the average thickness in the liquid regions. This is manifested mathematically as a decrease in the geometry factor,  $L_e$ , which has the effect of increasing the heat transfer coefficient and decreasing the total vaporization time. Quantitative predictions are limited, however, by the lack of data from which one can determine the average vapor fraction of an extended liquid mass.

## CHAPTER VII

### DISCUSSION

The results described in the sections dealing with total vaporization times, dimensionless total vaporization times, and heat transfer coefficients are all intimately related. They are different manifestations of the prime result of these experiments -- that the nitrogen drops vaporize more quickly than predicted by theory.

Because of difficulties and unique problems involved in working with cryogenic fluids, however, this central result must be examined and weighed closely before one concludes that the theory has been shown to be inadequate. With ordinary fluids sufficient experimental uncertainties are encountered which make interpretation of results difficult at times. With cryogenic fluids, additional uncertainties arise and existing ones are generally magnified. Hence, a measure of caution must be employed in comparing the experimental results with existing theory.

As an example of a difficulty that arises only because of the cryogenic nature of the liquid, one need only go so far as the free convection correction factor used to estimate the heating produced by the comparatively hot ambient atmosphere. The correction factor is only an approximation, since it is strictly applicable only for a cooled solid plate facing upward and for  $10^5 < G_r < 10^{10}$ . For drop sizes smaller than about 0.030 milliliters, the Grashof number is less than  $10^5$  and hence the correlation, strictly speaking, is not applicable.

Since, in most cases, most of the drop lifetime was spent in the size range greater than 0.030 milliliters this does not result in serious error but does introduce additional uncertainty.

Also, in regard to the free convection coefficient, the heat transferred to the liquid in this manner results in mass evaporation from the top surface of the drop. Hence, a mass flux from the top surface interferes with the process of free convection. In addition, as has been pointed out previously, bubble breakthrough phenomena certainly must influence heat transfer processes to the drop, but of course, are not accounted for in any free convection correlation.

Related to mass evaporation from the top surface of the drop, it should also be pointed out that the Baumeister analyses of drop evaporation assume that all heat transferred from the plate to the lower surface of the drop results in mass evaporation at the lower surface, that is, mass transfer at the upper surface is assumed negligible. Perhaps, this assumption is not valid for the case of liquid nitrogen, and in addition to improved heat transfer resulting from bubble breakthrough, as proposed herein, mass evaporation from the top surface should also be examined. As noted in Reference 3, one of the least understood aspects of the Leidenfrost phenomenon is mass evaporation (or lack of it) from the upper surface of a vaporizing liquid mass. Detailed investigation establishing the presence and effect of mass transfer from the upper surface is certainly required.

Regarding the hypothesis set forth herein regarding a net improvement in heat transfer to extended masses arising from numerous vapor breakthroughs, additional comments are warranted. Justification for the preceding hypothesis may be generated from heuristic reasoning, before

analyzing the experimental results. Previous studies have shown the similarity of extended pool boiling phenomena with the film boiling of discrete masses as in the Leidenfrost phenomenon. Specifically, the results of Reference 28 indicate that bubble growth in extended liquid masses is governed by a Taylor type instability, as has been established with pool film boiling (22, 26, and 27). In the analysis of Hamill and Baumeister (45), a heat transfer coefficient for pool film boiling is derived which is dependent upon the size and spacing of vapor domes. An increased vapor dome area is seen to result in a decreased heat transfer coefficient. Hence, it appears reasonable that the heat transfer coefficient for the film boiling of discrete masses undergoing vapor breakthrough should also be influenced to some extent by vapor breakthrough dynamics.

The possible influence of vapor breakthrough has been mentioned in Reference 15. However, because of the apparent agreement of experimental results with the universal  $V^*$  and  $t^*$  correlation, it was concluded that vapor breakthrough produced effects that were compensating; hence, no net effect on heat transfer was evident. One is then faced with the question of how vapor breakthrough phenomena can be used to explain the significantly improved heat transfer to extended nitrogen masses, while other fluids are reported to be uninfluenced by such phenomena. Perhaps this may be explained (at least partially) with the aid of Figure 51. This figure shows that for a ten-milliliter mass, liquid nitrogen will have 38 breakthroughs, which is about three times as many as for ethyl alcohol. For water, only two breakthroughs will occur. For liquid nitrogen masses having 12 breakthroughs, as with the ethyl alcohol masses, only three milliliters of fluid is required. This corresponds

to a dimensionless volume of roughly 2500, and from Figure 31, the departure of the data from the theoretical curve in this region is not so appreciable that it could not, at first glance, be attributed to experimental error.

Hence, it appears that no effects of bubble breakthrough were noted previously because the liquids were of sufficiently high surface tension and small size that too few breakthroughs existed to produce any noticeable effects. Use of a low surface tension fluid such as liquid nitrogen has thus made it possible to study for the first time breakthrough phenomena on a scale considerably larger than any previous studies.



## CHAPTER IX

### CONCLUSIONS

The principal conclusions derived from the present study are as follows:

1. Measurements of total vaporization times of liquid nitrogen masses require correction factors to account for radiation and "free convection" heat addition to the vaporizing drops, particularly at low  $\Delta T$  values where drop lifetimes are large.
2. Free convection and radiation correction factors to drop lifetime based on an integrated mean drop area produce modified lifetimes in fairly close agreement with results obtained by applying these factors over small time increments (10 sec) throughout drop lifetime.
3. For liquid nitrogen drop sizes smaller than 0.161 milliliter vaporization times are in agreement with Baumeister's dimensionless vaporization time prediction (except for the lowest  $\Delta T$ ).
4. For drop sizes greater than 0.161 milliliter measured vaporization times are significantly smaller than those predicted. After vaporization times have been corrected, discrepancies are still evident for mass sizes greater than one milliliter.
5. The preceding discrepancies in measured and predicted total vaporization times are not a result of experimental errors.

6. The preceding total vaporization time discrepancies are at least partially due to improved heat transfer to the drop arising from numerous vapor breakthroughs in large liquid masses.
7. The Leidenfrost point for liquid nitrogen at one atmosphere occurs at a  $\Delta T$  of about  $25^{\circ}$  F, and differs considerably from predicted values of  $86^{\circ}$  and  $63^{\circ}$  F.
8. Vapor dome diameters decrease slightly with decreasing  $\Delta T$ . The smallest measured values of maximum vapor dome diameters are larger than that predicted from hydrodynamic instability theory.
9. Vapor dome spacing lies between the critical and most dangerous wavelengths, decreasing from a value near  $\lambda_d$  at low  $\Delta T$ 's to a value near  $\lambda_c$  at  $\Delta T$ 's of about  $390^{\circ}$  F.
10. Heat transfer to extended liquid drops is apparently improved by the mechanism of vapor breakthrough.
11. Modifications of the universal  $t^*$  against  $V^*$  correlations based on improved heat transfer due to vapor breakthrough result in qualitative agreement with the experimental results. Quantitative agreement is dependent upon detailed investigations of vapor breakthrough dynamics.

## CHAPTER X

### RECOMMENDATIONS

In view of the "free convection" heating of cryogenic fluids by a room temperature atmosphere, some uncertainty exists in the corrected total vaporization times by virtue of uncertainty in the applicability of a free convection heat transfer coefficient. To establish that the shorter vaporization times for large masses are indeed a result of improved heat transfer due to vapor breakthrough, it is recommended that studies be made of ordinary fluids (e.g., water, ethyl alcohol) of sufficient size that appreciable numbers of vapor breakthroughs occur. Since a free convection correction would not be required in these cases, the influence of vapor breakthrough could be more readily established.

Concerning the effect of vapor breakthrough on heat transfer, the modified theory developed herein is based upon quantities such as maximum vapor dome diameter, cell spacing and time-averaged vapor fraction of an extended liquid mass. Experimental measurements indicate a variation in maximum diameter with  $\Delta T$ , whereas the modified theory assumes a constant value (which is smaller than all measured values). Also, while a cell size equal to  $\lambda_d$  is assumed in the theory, experimental measurements indicate a value varying from  $\lambda_c$  to  $\lambda_d$  over the  $\Delta T$  range investigated. Because of such discrepancies, it is recommended that thorough and extensive studies of vapor breakthrough dynamics be conducted in order to describe the statistics of these quantities.

Finally, it is recommended that studies of mass transfer from the top surface of vaporizing drops be made. Although in the present investigation, molecular mass diffusion does not occur by reason of the lack of a driving potential (100-per cent atmospheric nitrogen environment), it is conceivable that not all vaporization caused by heat addition to the drop occurs at the lower surface of the drop. The need for such a study is prompted not specifically by the present study, but rather by virtually all past studies. The recent experiments of Wachters (37) have served to emphasize this need.

## REFERENCES

1. Leidenfrost, J. G. "De Aquae Communis Nonnullis Qualitatibus Tractatus." Duisburg on Rhine (1756). This treatise has been translated into English by Carolyn Wares and the pertinent portion published in Int. Jour. of Heat and Mass Transfer, 9 (November, 1966), pp. 1153-1156.
2. Baumeister, K. J., R. C. Hendricks, and T. O. Hamill. Metastable Leidenfrost States. NASA TN D-3226, April, 1966.
3. Bell, K. J. "The Leidenfrost Phenomenon: A Survey." Submitted for publication in AIChE CEP Symposium Series (1967).
4. Pleteneva, N. A., and P. A. Rebinder. "Subjection to Laws in the Evaporation of Drops of Liquids in the Spheroidal State." (Russian) Jour. Phys. Chem., 20, No. 9, (1946), pp. 961-972.
5. Pleteneva, N. A., and P. A. Rebinder. "Effect of Surface-Active Substances on Evaporation of Water Drops in the Spheroidal State." (Russian) Jour. Phys. Chem., 20, No. 9 (1946), pp. 973-979.
6. Borishansky, V. M., and S. S. Kutateladze. "Certain Facts Concerning Evaporation of Liquid in the Spheroidal State." (Russian) J. Tech. Phys., 17, No. 8 (1947), pp. 891-902.
7. Borishansky, V. M. "Heat Transfer to a Liquid Freely Flowing Over a Surface Heated to a Temperature Above the Boiling Point." AEC Trans. Series, AEC-TR-3405 (1953).
8. Gottfried, B. S. "The Evaporation of Small Drops on a Flat Plate in the Film Boiling Regime." (Ph.D. Thesis, Case Institute of Technology, May, 1962.)
9. Lee, C. J. The Leidenfrost Phenomenon for Small Droplets. (Ph.D. Thesis, Oklahoma State University, Stillwater, Oklahoma, 1965).
10. Gottfried, B. S., C. J. Lee, and K. J. Bell. "The Leidenfrost Phenomenon: Film Boiling of Liquid Droplets on a Flat Plate." Int. Jour. Heat Mass Transfer, 9 (November, 1966), pp. 1167-1188.
11. Patel, B. M., and K. J. Bell. "The Leidenfrost Phenomenon for Extended Liquid Masses." CEP Symp. Series 62, No. 64. "Heat Transfer, Los Angeles." (1966), pp. 62-71.

12. Baumeister, K. J. "Heat Transfer to Water Droplets on a Flat Plate in the Film Boiling Regime." (Ph.D. Thesis, University of Florida, Gainesville, Fla., 1964.)
13. Baumeister, K. J. Film Boiling Heat Transfer to Water Drops on a Flat Plate. NASA TMX-52103, 1965.
14. Baumeister, K. J. Creeping Flow Solution of the Leidenfrost Phenomenon. NASA TN D-3133 (1965).
15. Baumeister, K. J. "A Generalized Correlation of Vaporization Times of Drops in Film Boiling on a Flat Plate." Vol. VI, Proc. Third Int. Heat Transfer Conference. AIChE, Chicago, Ill., (1966).
16. Godleski, E. S. "The Leidenfrost Phenomenon for Binary Liquid Solutions." (Ph.D. Thesis, Oklahoma State University, 1967).
17. Godleski, E. S., and K. J. Bell. "The Leidenfrost Phenomenon for Binary Liquid Solutions." Proc. Third Int. Heat Trans. Conf., IV (August, 1966), pp. 51-58.
18. Taylor, G. I. "The Instability of Liquid Surfaces When Accelerated in a Direction Perpendicular to Their Plane, I." Proceedings, Royal Society of London, Vol. 201, Series A (1950), p. 192.
19. Bellman, R., and R. H. Pennington. "Effects of Surface Tension and Viscosity on Taylor Instability." Quarterly of Applied Mathematics, Vol. 12 (1954), p. 151.
20. Lamb, H. Hydrodynamics. New York: Dover Publications, 1945, p. 455.
21. Milne-Thompson, L. M. Theoretical Hydrodynamics. New York: The Macmillan Company, 1950, p. 371.
22. Zuber, N. "On the Stability of Boiling Heat Transfer." Trans. ASME, Vol. 80 (April, 1958), pp. 711-715.
23. Chang, Y. P. "Wave Theory of Heat Transfer in Film Boiling." Jour. Heat Transfer, Vol. 81, Series C (Feb., 1959), pp. 1-12.
24. Bromley, L. A. "Heat Transfer in Stable Film Boiling." Chem. Eng. Progr., Vol. 46 (May, 1950), pp. 221-227.
25. Zuber, N. "Hydrodynamic Aspects of Boiling Heat Transfer." (Ph.D. Thesis, Department of Engineering, University of California, Los Angeles, 1959.)
26. Berenson, P. J. "Film Boiling Heat Transfer From a Horizontal Surface." Jour. Heat Transfer, Vol. 83, Series C (August, 1961), pp. 351-358.

27. Hosler, E. R., and J. W. Westwater. "Film Boiling on a Horizontal Plate." ARS Journal, 32 (1962), p. 553.
28. Patel, B. M. "The Leidenfrost Phenomenon for Extended Liquid Masses." (Ph.D. Thesis, Oklahoma State University, 1965.)
29. Brentari, E. C., P. J. Giarratano, and R. V. Smith. Boiling Heat Transfer for Oxygen, Nitrogen, Hydrogen, and Helium. NBS Technical Note 317, Sept., 1965.
30. Richards, R. J., W. G. Stewart, and R. B. Jacobs. A Survey of the Literature on Heat Transfer From Solid Surfaces to Cryogenic Fluids. NBS Technical Note 122, October, 1961.
31. Flynn, T. M., J. W. Draper, and J. J. Roos. "The Nucleate and Film Boiling Curve of Liquid Nitrogen at 1 Atmosphere." Adv. in Cryo. Engr. 7 (1962), pp. 539-545.
32. Frederking, T. H. K., and D. J. Daniels. "The Relation Between Bubble Diameter and Frequency of Removal From a Sphere During Film Boiling." ASME Jnl. of Heat Transfer, 87 (February, 1966).
33. Frederking, T. H. K., Y. C. Wu, and B. W. Clement. "Effects of Interfacial Instability on Film Boiling of Saturated Liquid Helium I Above a Horizontal Surface." AIChE Journal (March, 1966), pp. 238-44.
34. Froessling, N. Gerlands Beitr. Geophys., Vol. 52, 1938, p. 170.
35. Kutateladze, S. S. Fundamentals of Heat Transfer. New York: Academic Press, Inc., 1963.
36. Wade, S. H. "Evaporation of Liquids in Currents of Air." Transactions of Chemical Engineering Society, Vol. 20 (1942).
37. Wachters, L. H. J., H. Bonne, and H. J. van Nouhuis. "The Heat Transfer From a Hot Horizontal Plate to Sessile Water Drops in the Spheroidal State." Chemical Engineering Science, Vol. 21 (1966), pp. 923-926, Pergamon Press Ltd., Oxford, England.
38. Batten, R. D. "Surface Temperature Transients in the Film Boiling Regime. (M.S. thesis, School of Chemical Engineering, Oklahoma State University, May 1966.)
39. Kannuliuk, W. G., and P. G. Law. J. Sci. Instrum., 23 (July 1946), pp. 154-155.
40. NBS Circular 561. Reference Tables for Thermocouples. U.S. Dept. of Commerce, 1955.
41. NBS Circular 564. Tables of Thermal Properties of Gases. U.S. Dept. of Commerce, Nov. 1, 1955.

42. Kreith, F. Principles of Heat Transfer. Scranton, Penna.: International Textbook Company, 1966.
43. Baumeister, K. J. Personal Communication, Aug. 24, 1967.
44. Bradfield, W. S. "Liquid-Solid Contact in Stable Film Boiling." IEC Fund. Quart. V, 2 (May 1966), pp. 200-204.
45. Grober, H., S. Erk, and U. Grigull. Fundamentals of Heat Transfer. New York: McGraw-Hill Book Co., 1961.
46. Hamill, T. D., and K. J. Baumeister. Film Boiling Heat Transfer From a Horizontal Surface as an Optimal Boundary Value Process. NASA TM X-52183, 1966.



APPENDIX A

CALIBRATION OF DEPOSITORS

Depositor No. 3  
Liquid Mass,  
gm

.2743  
.2844  
.3066  
.2791  
.2769  
.2678  
.2909  
.2919  
.2942  
.2772  
Sum 2.8433

Avg. = .2843

$\sigma = 0.0241$

Vol =  $0.385 \pm .065$

% Error =  $\pm 16.9$

Cor. Vol =  $0.357 \pm .060$

Depositor No. 5  
Liquid Mass,  
gm

0.1170  
.1260  
.1254  
.1278  
.1332  
.1225  
.1376  
.1261  
.1230  
.1395  
Sum 1.2788

Avg. = 0.1279

$\sigma = 0.00704$

Vol =  $0.1736 \pm 0.0201 \text{ cm}^3$

% Error =  $\pm 11.6$

Cor. Vol =  $0.161 \pm .019$

Depositor No. 4  
Liquid Mass,  
gm

0.7683  
.7639  
.8054  
.7806  
.7995  
.7944  
.8005  
.7765  
.7692  
.8064  
Sum 7.8647

Avg. = .7865

$\sigma = .0169$

Vol =  $1.067 \pm .046 \text{ cm}^3$

% Error =  $\pm 4.32$

Cor. Vol =  $0.990 \pm .043$

2-ml Beaker  
Liquid Mass,  
gm

2.0826  
2.1295  
2.1328  
2.0618  
2.0696  
2.1738  
2.1044  
2.1791  
2.0860  
2.0609  
Sum 21.0805

Avg. = 2.108

$\sigma = 0.0440$

Vol =  $2.1080 \pm 0.0880 \text{ cm}^3$

% Error = 4.17

Cor. Vol =  $2.1040 \pm 0.0878 \text{ cm}^3$

5-ml Beaker Liquid Mass, gm	10-ml Beaker Liquid Mass, gm
5.2846	10.6269
5.1146	10.6156
5.1806	10.4592
5.2895	10.7264
5.0977	10.4546
5.1644	10.5795
5.2711	10.3949
5.1581	10.4731
5.1459	10.5929
<u>5.2336</u>	<u>10.7399</u>
Sum 51.9401	Sum 105.664
Avg. = 5.1940	Avg. = 10.5664
$\sigma = 0.0709$	$\sigma = 0.1177$
Vol = 5.1940 $\pm$ 0.1418	Vol = 10.566 $\pm$ 0.118
% Error = 2.73	% Error = 1.12
Cor. Vol = 5.1852 $\pm$ 0.1416	Cor. Vol = 10.548 $\pm$ 0.118
3.1-ml Beaker Liquid Mass, gm	4.6-ml Beaker Liquid Mass, gm
3.143	4.573
3.184	4.715
3.098	4.647
3.103	4.752
<u>3.112</u>	<u>4.694</u>
Sum 15.640	Sum 23.3810
Avg. = 3.128	Avg. = 4.604
$\sigma = 0.0358$	$\sigma = 0.0690$
Vol = 3.128 $\pm$ .072 cm <sup>3</sup>	Vol = 4.604 $\pm$ 0.138 cm <sup>3</sup>
% Error = 2.30	% Error = 3.0%
Cor. Vol = 3.123 $\pm$ .072	Cor. Vol = 4.596 $\pm$ .138

APPENDIX B

TOTAL VAPORIZATION TIME MEASUREMENTS

Depositor No. 3

(0.357 ml)

Avg. $T_w = 69.2^\circ \text{ F}$ $\Delta T = 389.6^\circ \text{ F}$	Avg. $T_w = -12.1^\circ \text{ F}$ $\Delta T = 308.3^\circ \text{ F}$	Avg. $T_w = -83.6^\circ \text{ F}$ $\Delta T = 236.8^\circ \text{ F}$
<u><math>\tau</math>, sec</u>	<u><math>\tau</math>, sec</u>	<u><math>\tau</math>, sec</u>
40.5	48.0	61.5
41.2	49.9	60.2
41.2	47.5	59.6
40.5	48.6	59.3
41.2	47.5	59.5
41.0	48.0	60.1
40.4	46.0	61.3
41.2	50.0	60.0
40.1	49.2	60.3
41.1	49.8	59.6
Avg. $\tau = 40.8 \pm 0.8 \text{ sec}$	Avg. $\tau = 48.4 \pm 2.6 \text{ sec}$	Avg. $\tau = 60.1 \pm 1.5 \text{ sec}$

Avg. $T_w = -148.1^\circ \text{ F}$ $\Delta T = 172.3^\circ \text{ F}$	Avg. $T_w = -201.4^\circ \text{ F}$ $\Delta T = 119.0^\circ \text{ F}$	Avg. $T_w = -225.8^\circ \text{ F}$ $\Delta T = 94.6^\circ \text{ F}$
<u><math>t</math>, sec</u>	<u><math>\tau</math>, sec</u>	<u><math>\tau</math>, sec</u>
76.9	104.8	114.5
77.4	106.4	115.3
75.2	105.6	114.8
75.8	108.7	112.6
75.3	106.0	
74.5	108.6	
74.0		
74.4		
73.8		
73.4		
Avg. $\tau = 75.1 \pm 2.6 \text{ sec}$	Avg. $\tau = 106.7 \pm 3.2 \text{ sec}$	Avg. $\tau = 114.3 \pm 2.4 \text{ sec}$

Depositor No. 4

(0.990 ml)

Avg. $T_w = 69.4^\circ \text{ F}$ $\Delta T = 389.8$	Avg. $T_w = -17.6^\circ \text{ F}$ $\Delta T = 302^\circ \text{ F}$	Avg. $T_w = -83.0^\circ \text{ F}$ $\Delta T = 237.4^\circ \text{ F}$
<u><math>\tau</math>, sec</u>	<u><math>\tau</math>, sec</u>	<u><math>\tau</math>, sec</u>
51.9	65.5	79.1
52.8	65.2	79.5
50.3	65.7	78.7
53.2	66.7	80.2
52.4	64.9	79.2
51.7	64.8	80.0
51.6		
52.4		
52.6		
51.8		
Avg. $\tau = 52.1 \pm 1.6$	Avg. $\tau = 65.5 \pm 1.4$	Avg. $\tau = 79.4 \pm 1.1$

Avg. $T_w = -143.7^\circ \text{ F}$ $\Delta T = 176.7^\circ \text{ F}$	Avg. $T_w = -205.1^\circ \text{ F}$ $\Delta T = 115.3^\circ \text{ F}$	Avg. $T_w = -257^\circ \text{ F}$ $\Delta T = 63^\circ \text{ F}$
<u><math>\tau</math>, sec</u>	<u><math>\tau</math>, sec</u>	<u><math>\tau</math>, sec</u>
96.6	140.7	179
96.9	142.0	
96.6	139.5	
99.5	140.9	
99.6	143.5	
101.5	140.3	
99.9		
97.2		
99.0		
100.1		
Avg. $\tau = 98.7 \pm 3.5$	Avg. $\tau = 141.2 \pm 2.8$	(Only one measurement available. Others consistently low due to onset of frost-induced nucleation)

Depositor No. 5

(0.161 ml)

Avg.  $T_w = 71.6^\circ \text{ F}$   
 $\Delta T = 392.0^\circ \text{ F}$

 $\tau$ , sec

26.5  
 23.6  
 25.1  
 29.0  
 28.4  
 27.4  
 26.5  
 28.3  
 26.0  
 26.3

Avg.  $\tau = 26.7 \pm 3.3$ 

Avg.  $T_w = -17.3^\circ \text{ F}$   
 $\Delta T = 303^\circ \text{ F}$

 $\tau$ , sec

37.2  
 33.4  
 35.3  
 35.0  
 36.0  
 34.8  
 36.2  
 35.4  
 36.5

Avg.  $\tau = 35.5 \pm 2.2$ 

Avg.  $T_w = -81.3^\circ \text{ F}$   
 $\Delta T = 239.1^\circ \text{ F}$

 $\tau$ , sec

40.4  
 43.6  
 43.6  
 43.3  
 43.3  
 43.3

Avg.  $\tau = 42.9 \pm 2.5$ 

Avg.  $T_w = -167.0^\circ \text{ F}$   
 $\Delta T = 153.4^\circ \text{ F}$

 $\tau$ , sec

60.5  
 63.6  
 62.2  
 63.5  
 64.4  
 63.1  
 63.7

Avg.  $\tau = 63.0 \pm 2.6$ 

Avg.  $T_w = -197.8^\circ \text{ F}$   
 $\Delta T = 122.6^\circ \text{ F}$

 $\tau$ , sec

72.0  
 73.9  
 74.3  
 70.9  
 74.4  
 75.1

Avg.  $\tau = 73.4 \pm 3.2$ 

Avg.  $T_w = -217.2^\circ \text{ F}$   
 $\Delta T = 103.2^\circ \text{ F}$

 $\tau$ , sec

78.0  
 75.1  
 75.9

Avg.  $\tau = 76.3 \pm 3.0$ 

Avg.  $T_w = -281.8^\circ \text{ F}$   
 $\Delta T = 38.4^\circ \text{ F}$

 $\tau$ , sec

123.5  
 122.2  
 127.7  
 118.3  
 123.5  
 119.6

Avg.  $\tau = 122.5 \pm 6.6$ 

Avg.  $T_w = -251.1^\circ \text{ F}$   
 $\Delta T = 69.4^\circ \text{ F}$

 $\tau$ , sec

103.5  
 102.5  
 102.5  
 103.6  
 102.5

Avg.  $\tau = 102.9 \pm 1.2$

## 2-ml Beaker

(2.104 ml.)

Avg. Deposition Time = 6 sec.

Avg.  $T_w = 68.7^\circ \text{F}$   
 $\Delta T = 389.1^\circ \text{F}$

Avg.  $T_w = -15.3^\circ \text{F}$   
 $\Delta T = 305.1^\circ \text{F}$

Avg.  $T_w = -58.8^\circ \text{F}$   
 $\Delta T = 261.6^\circ \text{F}$

 $\tau$ , sec

63.8  
 67.0  
 66.4  
 63.9  
 66.0  
 66.8  
 67.4  
 67.5  
 64.4  
 65.5

 $\tau$ , sec

81.6  
 80.2  
 81.3  
 80.9  
 80.7

 $\tau$ , sec

91.7  
 91.3  
 91.5  
 92.0  
 91.8

Avg.  $\tau = 65.9 \pm 2.8$  secAvg.  $\tau = 80.9 \pm 1.1$  secAvg.  $\tau = 91.6 \pm 0.4$  sec $\tau_{\text{corr}} = 62.9 \pm 2.8$  sec $\tau_{\text{corr}} = 77.9 \pm 1.1$  sec $\tau_{\text{corr}} = 88.6 \pm 0.4$  sec

Avg.  $T_w = -116.6^\circ \text{F}$   
 $\Delta T = 203.8^\circ \text{F}$

Avg.  $T_w = -171.4^\circ \text{F}$   
 $\Delta T = 149.0^\circ \text{F}$

Avg.  $T_w = -217.2^\circ \text{F}$   
 $\Delta T = 103.2^\circ \text{F}$

 $\tau$ , sec

113.5  
 112.4  
 114.0  
 113.7  
 112.7

 $\tau$ , sec

141.7  
 140.6  
 140.1  
 142.3  
 143.2

 $\tau$ , sec

181.7  
 186.2  
 181.7  
 187.2  
 186.6  
 191.0  
 183.8

Avg.  $\tau = 113.3 \pm 1.4$  secAvg.  $\tau = 141.6 \pm 2.5$  secAvg.  $\tau = 185.5 \pm 6.7$  sec $\tau_{\text{corr}} = 110.3 \pm 1.4$  sec $\tau_{\text{corr}} = 138.6 \pm 2.5$  sec $\tau_{\text{corr}} = 182.5 \pm 6.7$  sec



5-ml Beaker

(5.185 ml)

Avg. Deposition Time = 9 sec.

Avg.  $T_w = 71.3^\circ \text{ F}$   
 $\Delta T = 391.7^\circ \text{ F}$

Avg.  $T_w = -17.8^\circ \text{ F}$   
 $\Delta T = 302.6^\circ \text{ F}$

Avg.  $T_w = -85.4^\circ \text{ F}$   
 $\Delta T = 235.0^\circ \text{ F}$

 $\tau$ , sec

77.3  
 80.8  
 76.1  
 79.4  
 79.4  
 78.9  
 81.0  
 81.0  
 80.1  
 79.9  
 80.3  
 79.3

 $\tau$ , sec

94.0  
 98.0  
 95.4  
 99.0  
 98.8  
 98.3  
 97.8  
 97.0  
 97.7  
 99.0

 $\tau$ , sec

113.4  
 116.8  
 118.9  
 116.3  
 118.0  
 116.2  
 115.3  
 115.2  
 117.0  
 116.0

Avg.  $\tau = 79.5 \pm 2.7 \text{ sec}$ Avg.  $\tau = 97.5 \pm 3.3 \text{ sec}$ Avg.  $\tau = 116.3 \pm 3.1 \text{ sec}$  $\tau_{\text{corr}} = 75.0 \pm 2.7 \text{ sec}$  $\tau_{\text{corr}} = 93.0 \pm 3.3 \text{ sec}$  $\tau_{\text{corr}} = 111.8 \pm 3.1 \text{ sec}$ 

Avg.  $T_w = -148.9^\circ \text{ F}$   
 $\Delta T = 171.5^\circ \text{ F}$

Avg.  $T_w = -210.3^\circ \text{ F}$   
 $\Delta T = 110.1^\circ \text{ F}$

 $\tau$ , sec

155.1  
 156.3  
 157.5  
 158.0  
 156.8

 $\tau$ , sec

198.5  
 198.9  
 197.5  
 201.9  
 207.4  
 203.1

Avg.  $\tau = 156.6 \pm 4.0 \text{ sec}$ Avg.  $\tau = 201.2 \pm 6.8 \text{ sec}$  $\tau_{\text{corr}} = 152.1 \pm 4.0 \text{ sec}$  $\tau_{\text{corr}} = 196.7 \pm 6.8 \text{ sec}$

10-ml Beaker

(10.548 ml)

Avg. Deposition Time = 11 sec

Avg.  $T_w = 69.6^\circ \text{F}$  $\Delta T = 390.0^\circ \text{F}$ Avg.  $T_w = -22.9^\circ \text{F}$  $\Delta T = 297.5^\circ \text{F}$  $\tau$ , sec

84.4

85.2

86.1

88.8

85.9

85.5

85.9

85.2

85.1

87.0

 $\tau$ , sec

111.6

114.3

113.2

113.3

113.8

113.8

113.3

113.9

Avg.  $\tau = 85.9 \pm 2.5$  sec $\tau_{\text{corr}} = 80.4 \pm 2.5$  secAvg.  $\tau = 113.4 \pm 1.6$  sec $\tau_{\text{corr}} = 107.9 \pm 1.6$  secAvg.  $T_w = -83.2^\circ \text{F}$  $\Delta T = 237.2^\circ \text{F}$ Avg.  $T_w = -149.7^\circ \text{F}$  $\Delta T = 170.7^\circ \text{F}$  $\tau$ , sec

129.2

129.8

130.3

133.3

129.9

131.3

131.5

131.8

 $\tau$ , sec

176.6

181.8

183.0

179.6

181.1

179.9

Avg.  $\tau = 130.9 \pm 2.7$  sec $\tau_{\text{corr}} = 125.4 \pm 2.7$  secAvg.  $\tau = 180.3 \pm 4.4$  sec $\tau_{\text{corr}} = 174.8 \pm 4.4$  sec

APPENDIX C

PROPERTY VALUES EMPLOYED IN COMPUTER CALCULATIONS

(Property Values Obtained From Ref. 41)

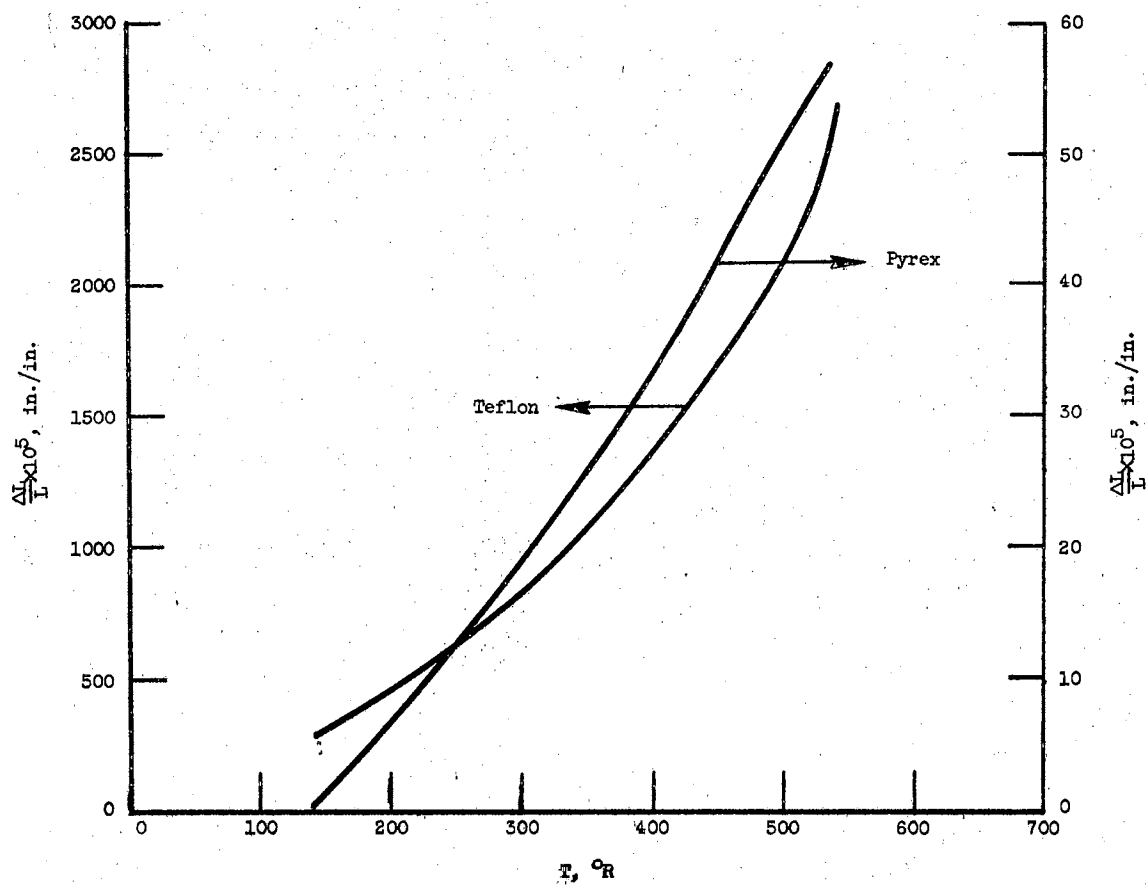


Figure 52. Thermal Expansion Coefficient for Teflon and Pyrex

Temp., °R	Specific Heat, $C_p$ BTU/lb°R	Temp., °R	Vapor Density $\rho_v$ Lb/ft <sup>3</sup>	Temp., °R	Thermal Conduc- tivity, k, BTU/hr-ft-°F
140	.2610	139.2	.28077	140	.00420
180	.2561	160	.23350	180	.00506
216	.2518	180	.21725	198	.00598
252	.2505	198	.19649	216	.00651
270	.2501	216	.17962	234	.007028
288	.2498	234	.16542	252	.007532
324	.2494	270	.14290	288	.008568
342	.2492	288	.13383	306	.009072
360	.2491	306	.12586	324	.009576
432	.2488	342	.11248	342	.010066
468	.2987	360	.10680	360	.010542
504	.2487	378	.10168	378	.011046
		414	.09278	396	.011522
		432	.08890	432	.012488
		450	.08552	450	.012936
		486	.07898	468	.013398
		504	.07615	504	.014294
		522	.07352	522	.014714
		558	.06876	540	.015134
Temp., °R	Viscosity, $\lambda$ lb/hr-ft				
140	0.0132				
180	0.01661				
270	0.02441				
360	0.03133				
450	0.03756				
540	0.04319				

APPENDIX D

COMPUTER PROGRAM

```

C   COMPUTATION OF CORRECTED HT. TR. COEFFICIENTS AND TOTAL VAPORIZATION TIMES
C   INSTANTANEOUS AND TOTAL HEAT TRANSFER FROM VAPORIZATION RATE CURVES, -4.85
C   LIQUID VOLUME CORRESPONDING TO GIVEN AREA CALCULATED BY BAUMEISTERS EQNS.
      DIMENSION AREAG(80), TIME(80), VOLA(80)
      DIMENSION VIS(20), TVIS(20), CP(30), TCP(30)
      DIMENSION CONDV(50), TCONDV(50), RHOV(50), TRHOV(50)
20  FORMAT (I3, 6F10.6/8F10.6/(8F10.6))
21  FORMAT (6F10.5)
22  FORMAT (5E15.6)
23  FORMAT (8F10.6)
24  FORMAT (5E15.6/)
25  FORMAT (2F10.3)
11  READ (5,21) GC, GRAV, RHOL, SIGMA, ALAM, TSAT
      READ (5,23) (AREAG(I), TIME(I), I=1,16)
12  READ (5,20) ICP, (CP(I), TCP(I), I=1,ICP)
13  READ (5,20) IRHOV, (RHOV(I), TRHOV(I), I=1,IRHOV)
14  READ (5,20) IVIS, (VIS(I), TVIS(I), I=1,IVIS)
15  READ (5,20) ICONDV, (CONDV(I), TCONDV(I), I=1,ICONDV)
      TWALL = 201.
      TAMB = 475. + (1.0/7.4)*(TWALL-TSAT)
      DELT=TAMB-TSAT
      TFRCON=(TSAT+TAMB)/(2.0)
      CALL VALUE (TCP, CP, ICP, TFRCON, CPA)
      CALL VALUE (TVIS, VIS, IVIS, TFRCON, VISA)

```

```

CALL VALUE (TCONDV, CONDV, ICONDV, TFRCON, CONDVA)
CALL VALUE (TRHOV, RHOV, IRHOV, TFRCON, RHOVA)
PR= ((CPA)*(VISA))/(CONDVA)
AREAG(1) = 0.240
VOLA(1) = 0.357*(.3531E-04)
TIME(1)=0.0
TOTTIM = 151.
SIGMAR = 0.173E-08
TIMCC=0.0
TIMRC=0.0
TIMRCN = 0.0
TIM=0.0
SUM=0.0
SUMCOM=0.0
SMAREA=0.0
SUMCC = 0.0
SUMFC = 0.0
TIMRAD=0.0
SUMRAD=0.0
10 DO 30 I=2,16
   IF (AREAG(I).LT.0.001817) GO TO 40
   IF (AREAG(I).GT.0.144) GO TO 41
   VOLA(I)=(((AREAG(I)/144.)/1.25)**1.2)*(((SIGMA*GC/(RHOL*GRAV))**.3)
   GO TO 1
40 VOLA(I) = (0.83*AREAG(I)/144.)**1.5
   GO TO 1
41 VOLA(I) = ((AREAG(I)/144.)*1.85)*(((SIGMA*GC/(RHOL*GRAV))**.5)
1 DELTIM = TIME(I)-TIME(I-1)

```



```

AVTIME= (TIME(I)+ TIME(I-1))/2.
AVAREA=(AREAG(I) + AREAG(I-1))/2.
AREATM = AVAREA*DELTIM
SMAREA = SMAREA + AREATM
AVGDIA=(SQRT((4./3.14)*(AVAREA)))
GR=((RHOVA)**2.)*((GRAV)*(0.1296E+08))*(1./(TFRCON))*((TAMB-TSAT)/
1((VISA)**2.))*(((.9)*(AVGDIA/12.))**3.)
HFRCNI=(0.3)*((CONDVA)/((AVGDIA)/(12.)))*(((GR)*(PR))**(1./4.))
QFRCON=HFRCNI*(AVAREA/144.)*DELT*(DELTIM/3600.)
SUM = SUM + QFRCON
QDOTFC=QFRCON/DELTIM
SUMFC= SUMFC + QDOTFC
QCOMB = ALAM*RHOL*(VOLA(I-1)-VOLA(I))
SUMCOM= SUMCOM + QCOMB
HCOMBI=QCOMB/((AVAREA/144.)*(TWALL-TSAT)*(DELTIM/3600.))
QDOTCC=QCOMB/DELTIM
SUMCC = SUMCC + QDOTCC
A=QCOMB-QFRCON
B=QDOTCC-QDOTFC
TIM = TIM + ALAM*RHOL*(VOLA(I-1)-VOLA(I))/B
HINST=A/((AVAREA/144.)*(TWALL-TSAT)*(DELTIM/3600.))
QRADUP = SIGMAR*AVAREA/144.*(TAMB**4.)/3600.
QRADDN = SIGMAR*AVAREA/144.*(TWALL**4.)/3600.
QDOTRD=QRADUP+QRADDN
QRAD=QDOTRD*DELTIM
SUMRAD=SUMRAD+QRAD
C=QDOTCC-QDOTFC-QDOTRD
D = QCOMB - QFRCON - QRAD

```

```

E = QCOMB - GRAD
HMCCR = D/A*HINST
HCR = E/A*HINST
TIMRAD = TIMRAD + ALAM*RHOL*(VOLA(I-1)-VOLA(I))/C
TIMRCN = TIMRCN + ALAM*RHOL*(VOLA(I-1)-VOLA(I))/E*DELTIM
TIMCC=TIMCC+ALAM*RHOL*(VOLA(I-1)-VOLA(I))/(QCOMB-QFRCON)*DELTIM
TIMRC=TIMRC+ALAM*RHOL*(VOLA(I-1)-VOLA(I))/(QCOMB-QFRCON-GRAD)*DELT
1IM
VOL = VOLA(I)/(1.3531E-04)
WRITE (6,21) TIME(I), TIMRCN
WRITE (6,21) AVAREA, AVGDIA, VOL, TIMCC, TIMRC
WRITE (6,22) AVTIME, DELTIM, TIM, TIMRAD
WRITE (6,22) QCOMB, QFRCON, GRAD, QDOTCC
WRITE (6,22) A, B, C, D, E
WRITE (6,22) SUMCOM, SUM, SUMRAD, HCR
WRITE (7,25) VOL, HMCCR
30 WRITE (6,24) GR, HFCRNI, HCOMBI, HINST, HMCCR
3 DO 31 I=1,1,1
  QGROSS = ALAM*RHOL*VOLA(I)
  AVINTA=SMAREA/TOTTIM
  DINTAV=(SQRT((4./3.14)*(AVINTA)))
  GR=((RHOVA)**2.)*((GRAV)*(1.296E+08))*(1./(TFRCON))*((TAMB-TSAT)/
1((VISA)**2.))*(((.9)*(DINTAV/12.))**3.)
  HFCRNI=0.3*((CONDVA)/((DINTAV)/12.))*(((GR)*(PR))**1./4.)
  QFRCON=HFCRNI*(AVINTA/144.)*DELT*(TOTTIM/3600.)
  TAUC=QGROSS/(QGROSS-QFRCON)*TOTTIM
  GRADDN = SIGMAR*AVINTA/144.*(TWALL**4.)/3600.*TOTTIM
  GRADUP = SIGMAR*AVINTA/144.*(TAMB**4.)/3600.*TOTTIM

```

```

QRAD=QRADUP+QRADDN
TAUR=QGROSS/(QGROSS-QFRCON-QRAD)*TOTTIM
TAURAD = QGROSS/(QGROSS-QRAD)*TOTTIM
HCCAVG=QGROSS/((AVINTA/144.)*(TWALL-TSAT)*TAUC)*3600.
HNETAV=HCCAVG*TAUC/TAUR
HCMR = HCCAVG*TAUC/TAURAD
HCONDA=HCCAVG*TAUC/TOTTIM
VOL = VOLA(1)/(0.3531E-04)
WRITE (7,25) VOL, HNETAV
WRITE (6,22) HCONDA, HCCAVG, HNETAV, HCMR
WRITE (6,21) TOTTIM, TAUC, TAUR, TAURAD
WRITE (6,22) QGROSS, QFRCON, QRAD
31 WRITE (6,22) GR, AVINTA, DINTAV
STOP
END
3IBFTC VALUE
SUBROUTINE VALUE(X,G,IG,XA,GA)
DIMENSION G(1),X(1)
1 FORMAT(1X,41HINPUT VALUE OUTSIDE RANGE OF KNOWN VALUES/1X,12HINPUT
2 VALUE=,E15.8,5X,10HLOW VALUE=,E15.8,5X,12HUPPER VALUE=,E15.8)
XX1=XA-X(1)
IF(XX1.NE.0.0)GO TO 100
GA=G(1)
GO TO 102
100 DO 105 K=2,IG
XX2=XA-X(K)
IF(XX2*XX1)106,106,105
106 I=K

```

```
      IF (XX2.EQ.0.0.OR.XX1.EQ.0.0)GO TO 104  
      GO TO 103  
105  XX1=XX2  
      WRITE(6,1) XA,X(1),X(IG)  
      STOP  
104  GA=G(I)  
      GO TO 102  
103  SLPE=(G(I)-G(I-1))/(X(I)-X(I-1))  
      GINSPT=G(I)-SLPE*X(I)  
      GA=SLPE*XA+GINSPT  
102  RETURN  
      END
```

APPENDIX E

HEAT TRANSFER COEFFICIENTS AS A FUNCTION  
OF DROP PROJECTED AREA

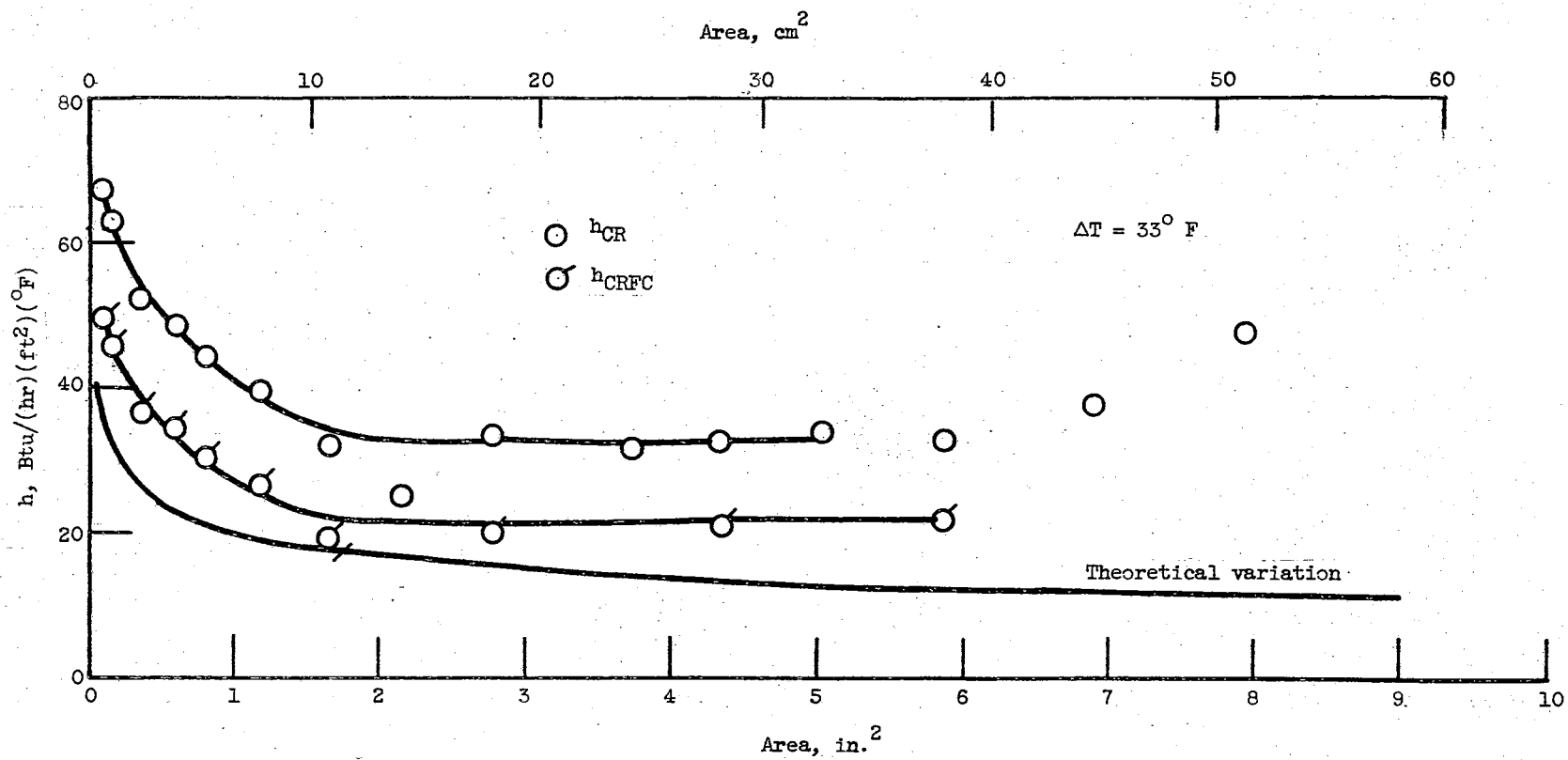


Figure 53. Comparison of Experimental and Theoretical Heat Transfer Coefficients as a Function of Drop Projected Area -  $\Delta T = 33^\circ \text{F}$

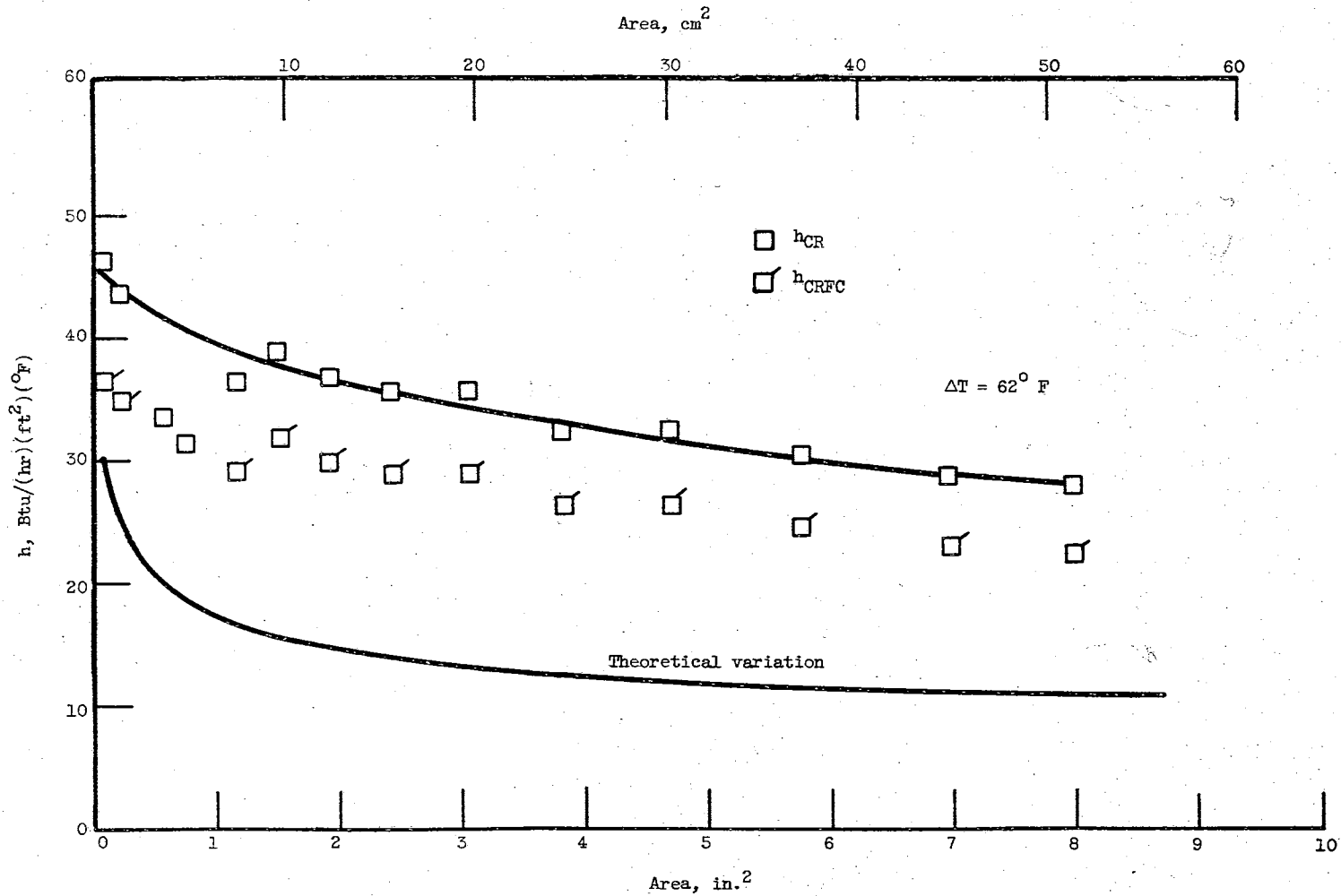


Figure 54. Comparison of Experimental and Theoretical Heat Transfer Coefficients as a Function of Drop Projected Area -  $\Delta T = 62^\circ \text{ F}$

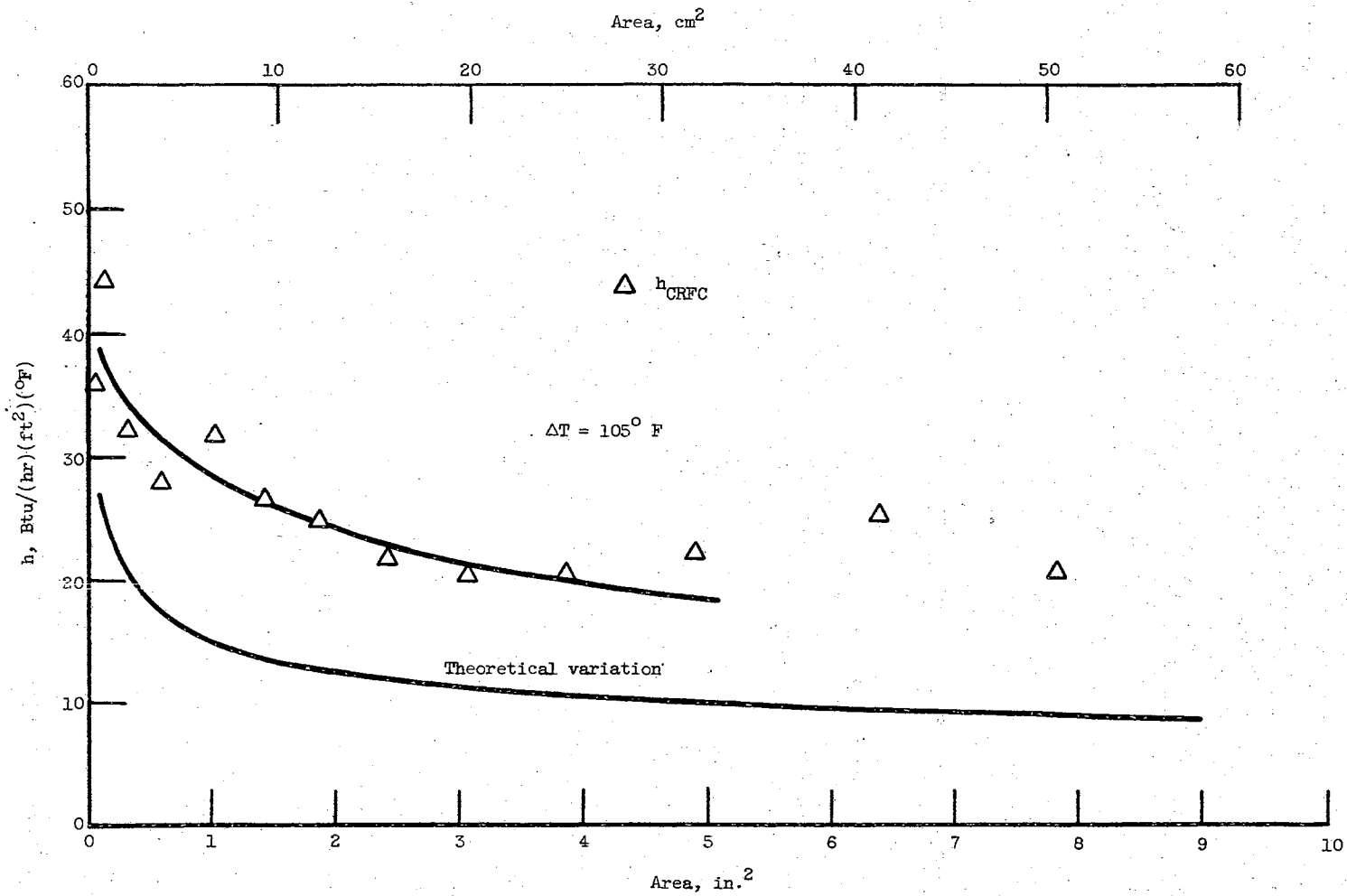


Figure 55. Comparison of Experimental and Theoretical Heat Transfer Coefficients as a Function of Drop Projected Area -  $\Delta T = 105^\circ \text{F}$



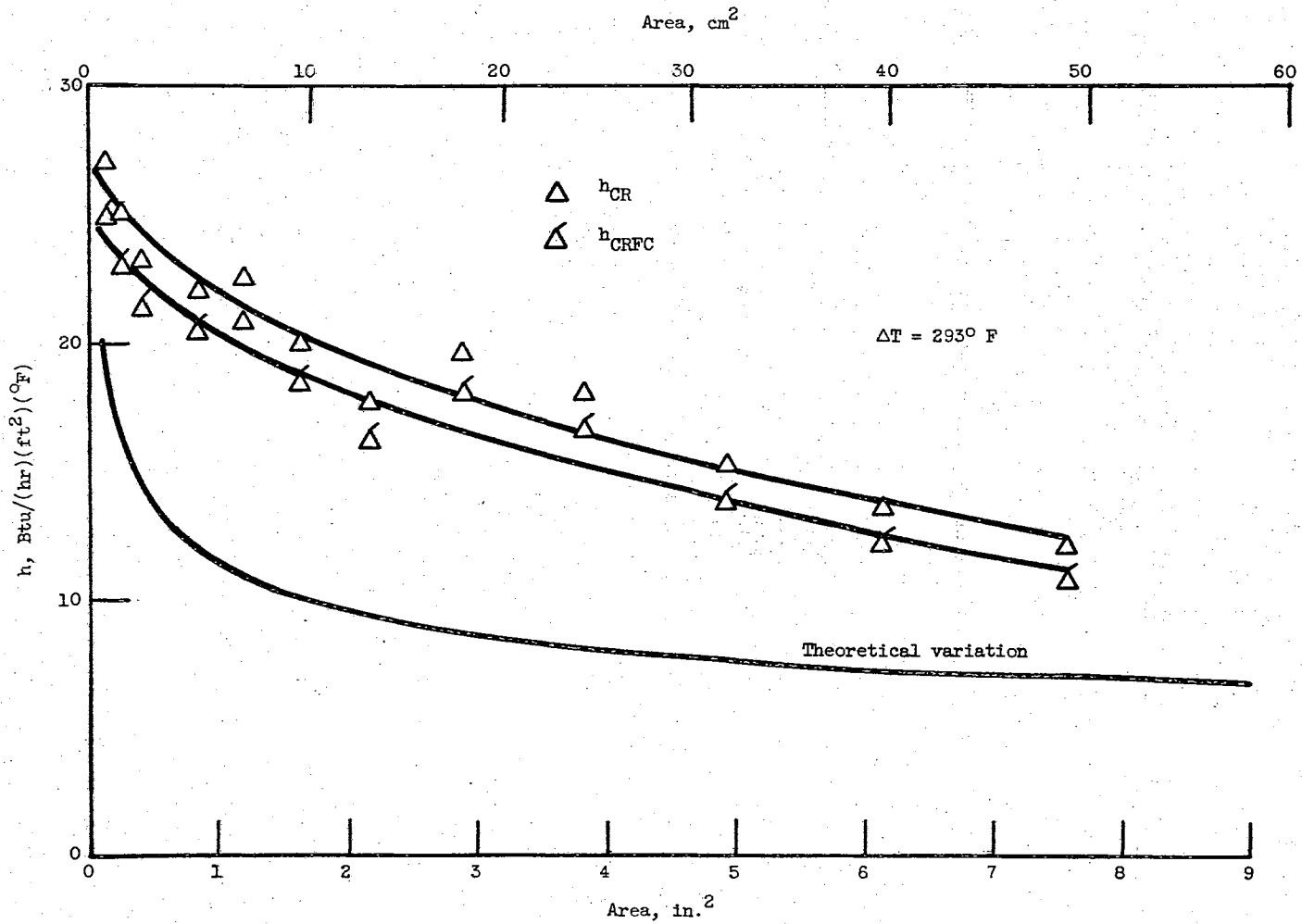


Figure 56. Comparison of Experimental and Theoretical Heat Transfer Coefficients as a Function of Drop Projected Area -  $\Delta T = 293^\circ \text{F}$

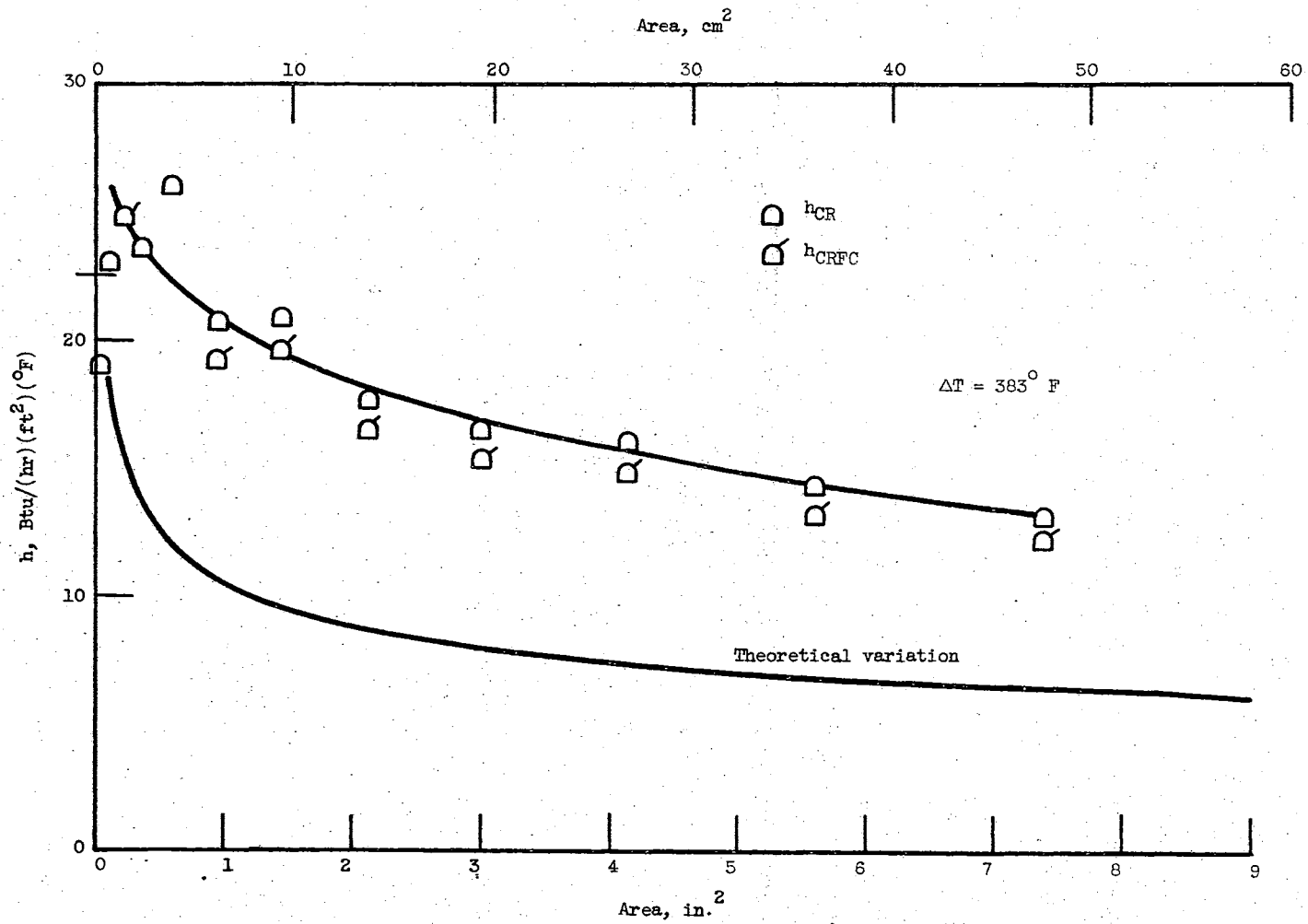


Figure 57. Comparison of Experimental and Theoretical Heat Transfer Coefficients as a Function of Drop Projected Area -  $\Delta T = 383^\circ\text{F}$

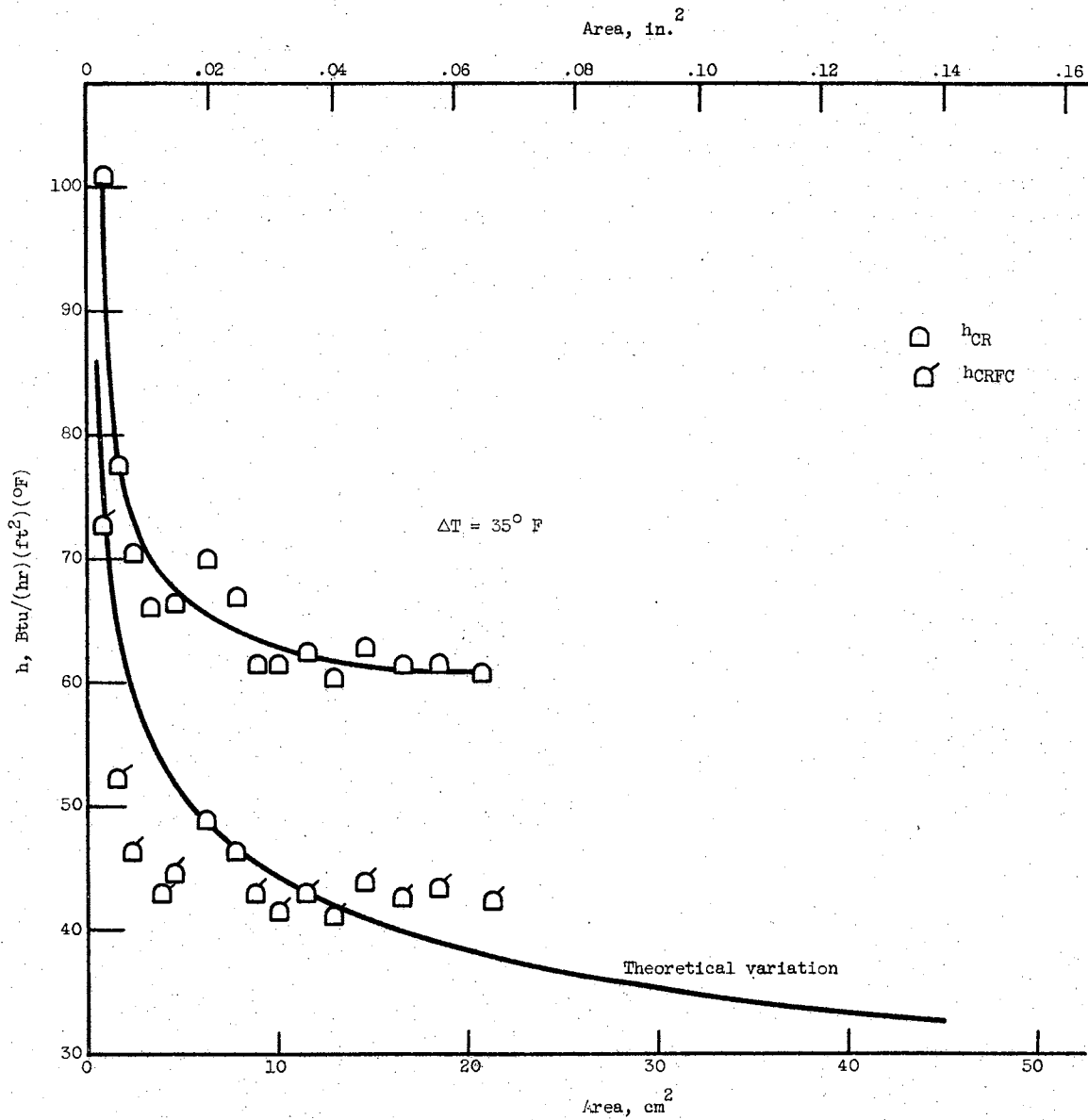


Figure 58. Comparison of Experimental and Theoretical Heat-Transfer Coefficients as a Function of Drop Projected Area -  $\Delta T = 35^\circ\text{F}$

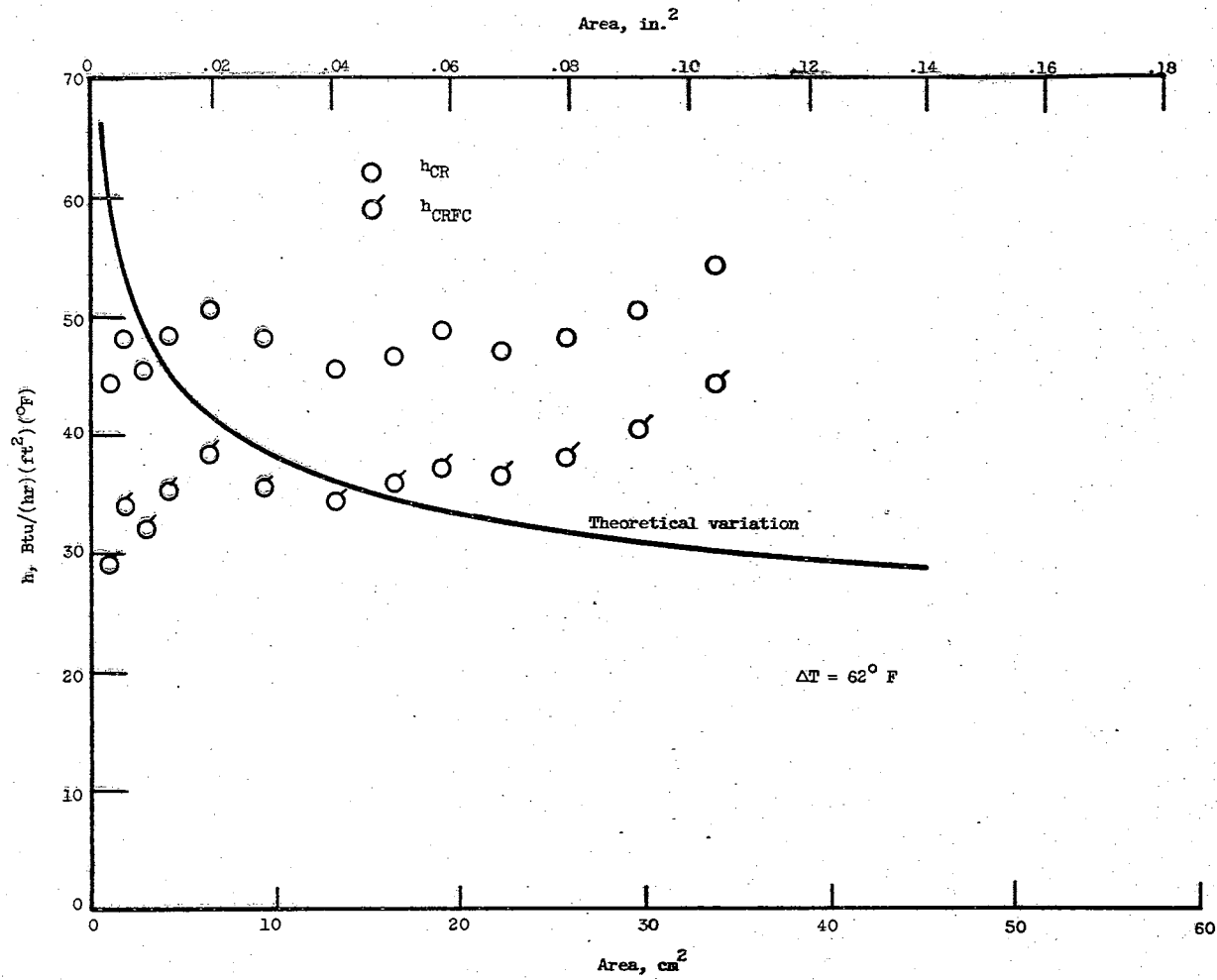


Figure 59. Comparison of Experimental and Theoretical Heat Transfer Coefficients as a Function of Drop Projected Area -  $\Delta T = 62^\circ \text{ F}$

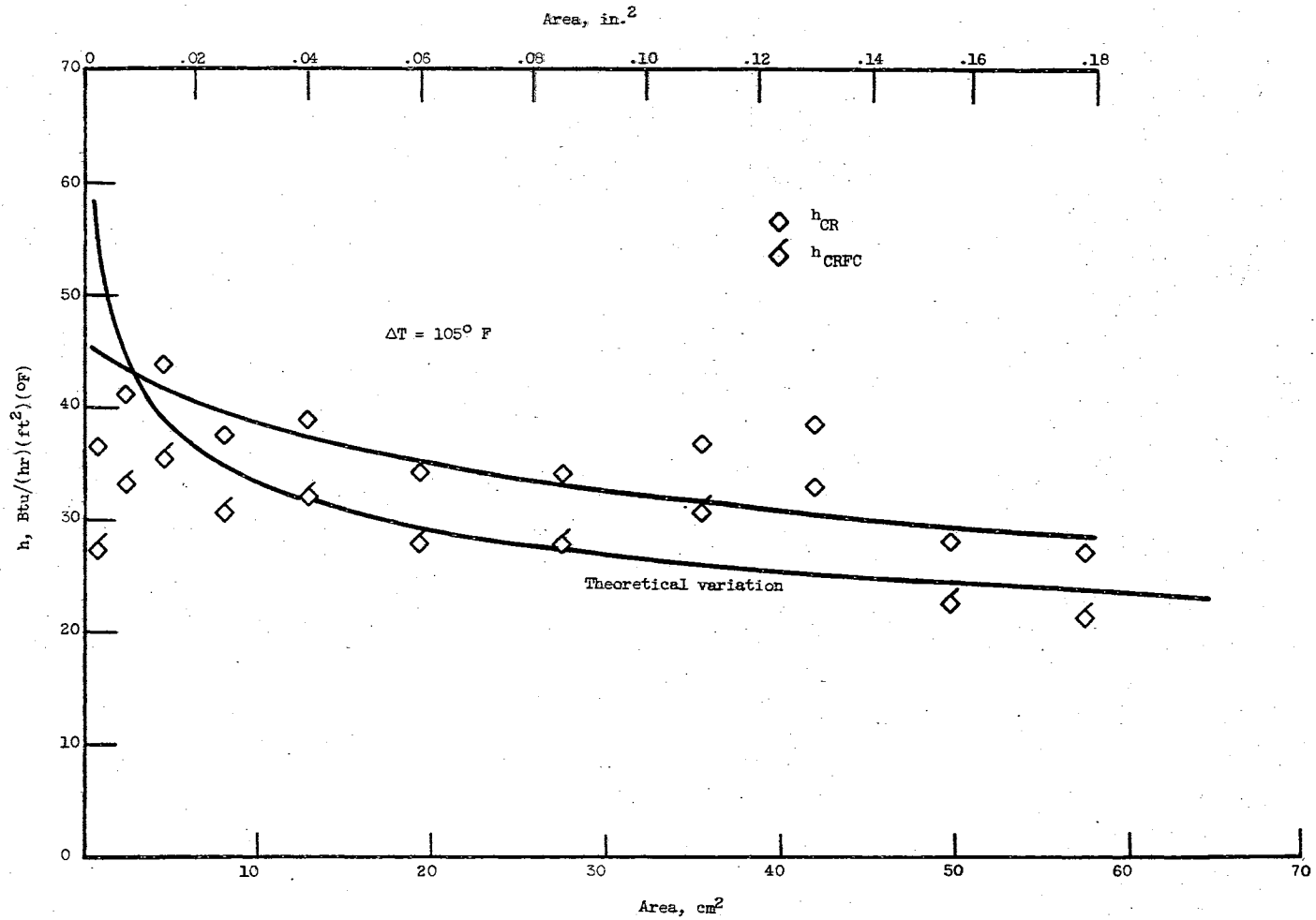


Figure 60. Comparison of Experimental and Theoretical Heat Transfer Coefficients as a Function of Drop Projected Area -  $\Delta T = 105^\circ \text{F}$

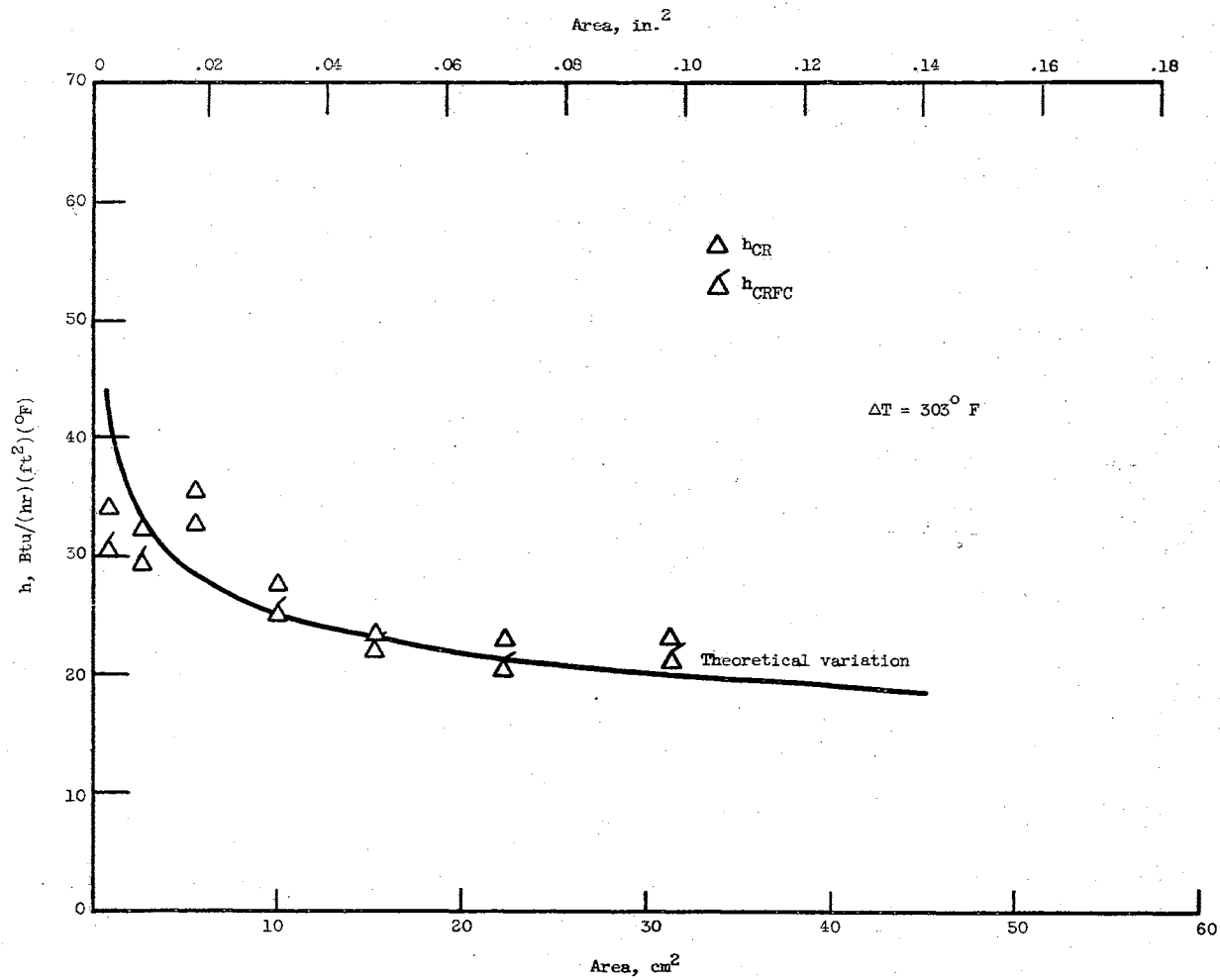


Figure 61. Comparison of Experimental and Theoretical Heat Transfer Coefficients as a Function of Drop Projected Area -  $\Delta T = 303^\circ \text{ F}$

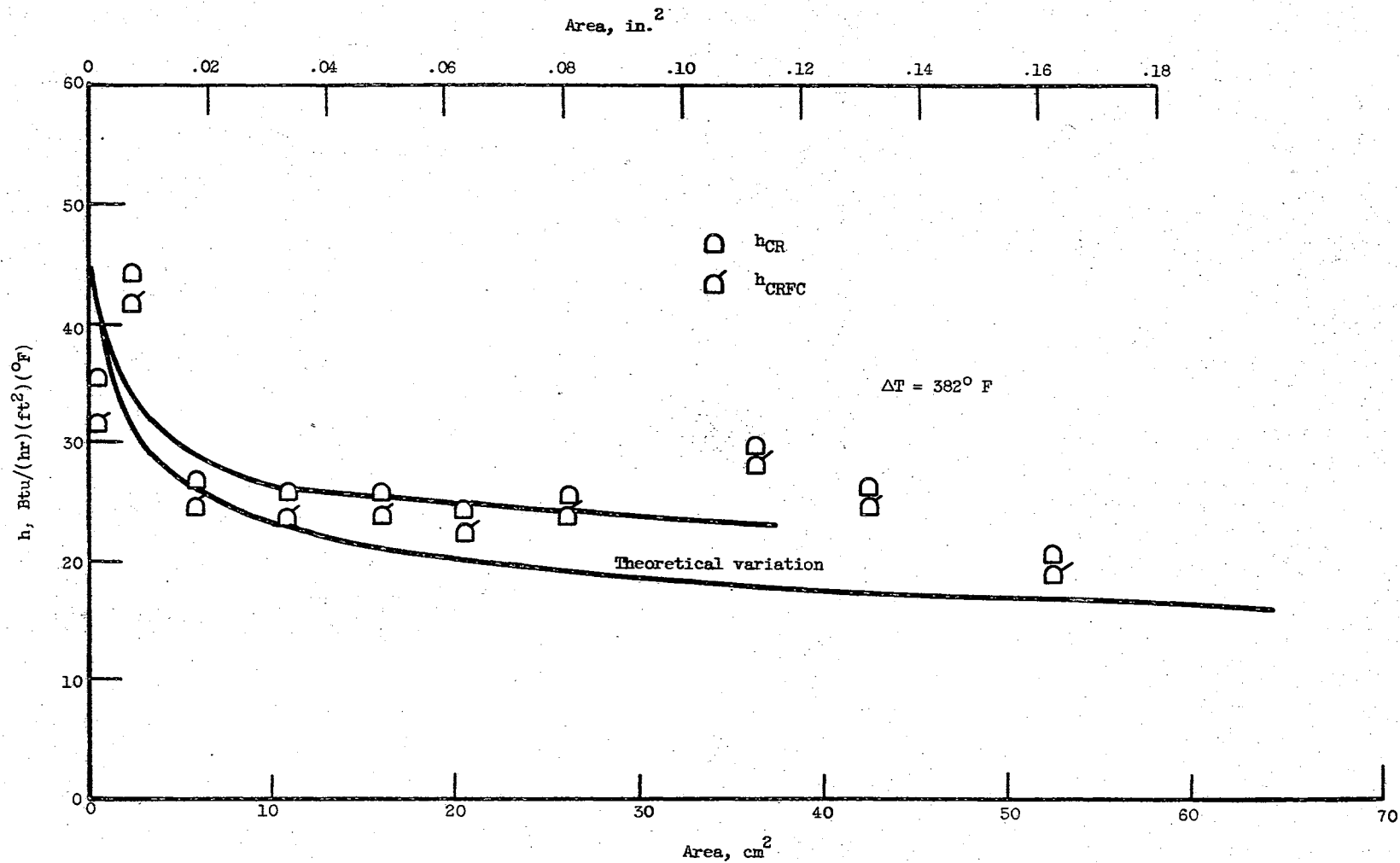


Figure 62. Comparison of Experimental and Theoretical Heat Transfer Coefficients as a Function of Drop Projected Area -  $\Delta T = 382^\circ \text{ F}$

APPENDIX F

INSTANTANEOUS HEAT TRANSFER COEFFICIENTS

DURING DROP LIFETIME



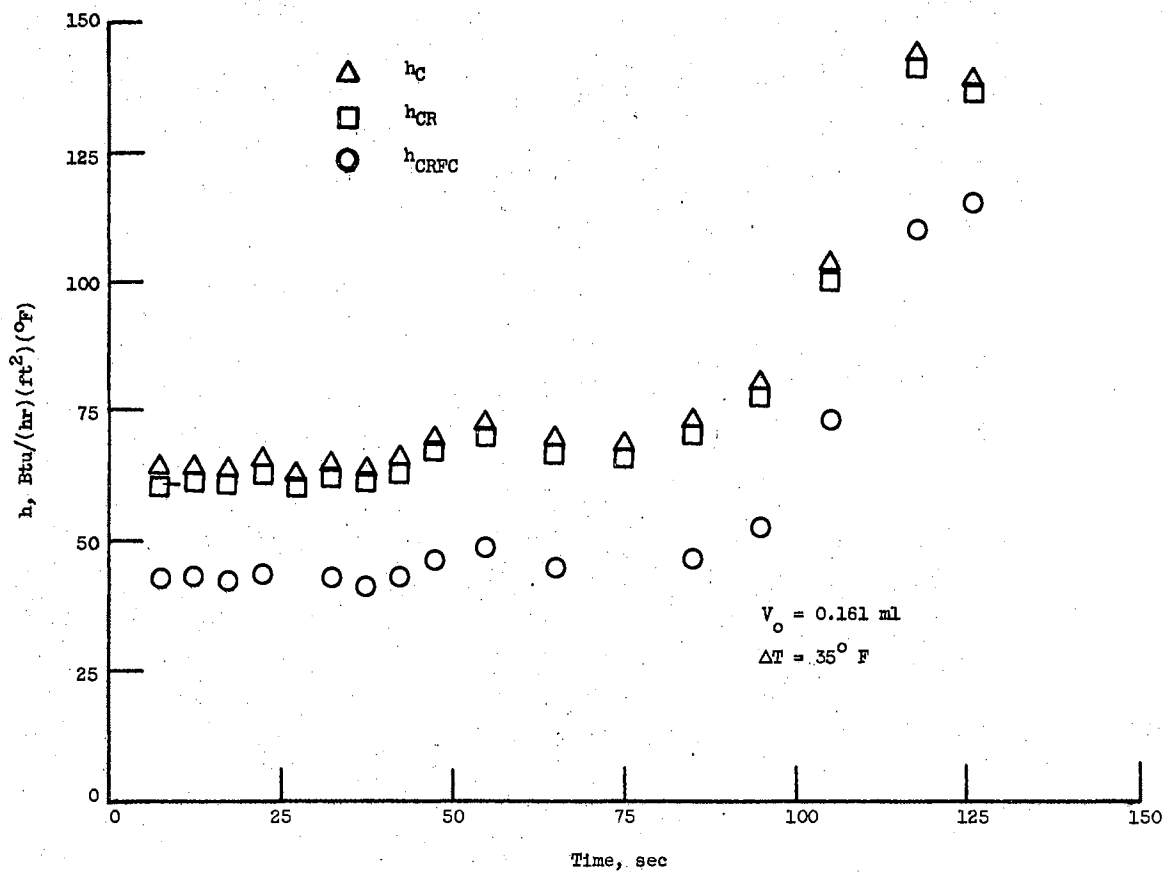


Figure 63. Variation of Heat Transfer Coefficient to Drop During Drop Lifetime -  $\Delta T = 35^\circ \text{ F}$

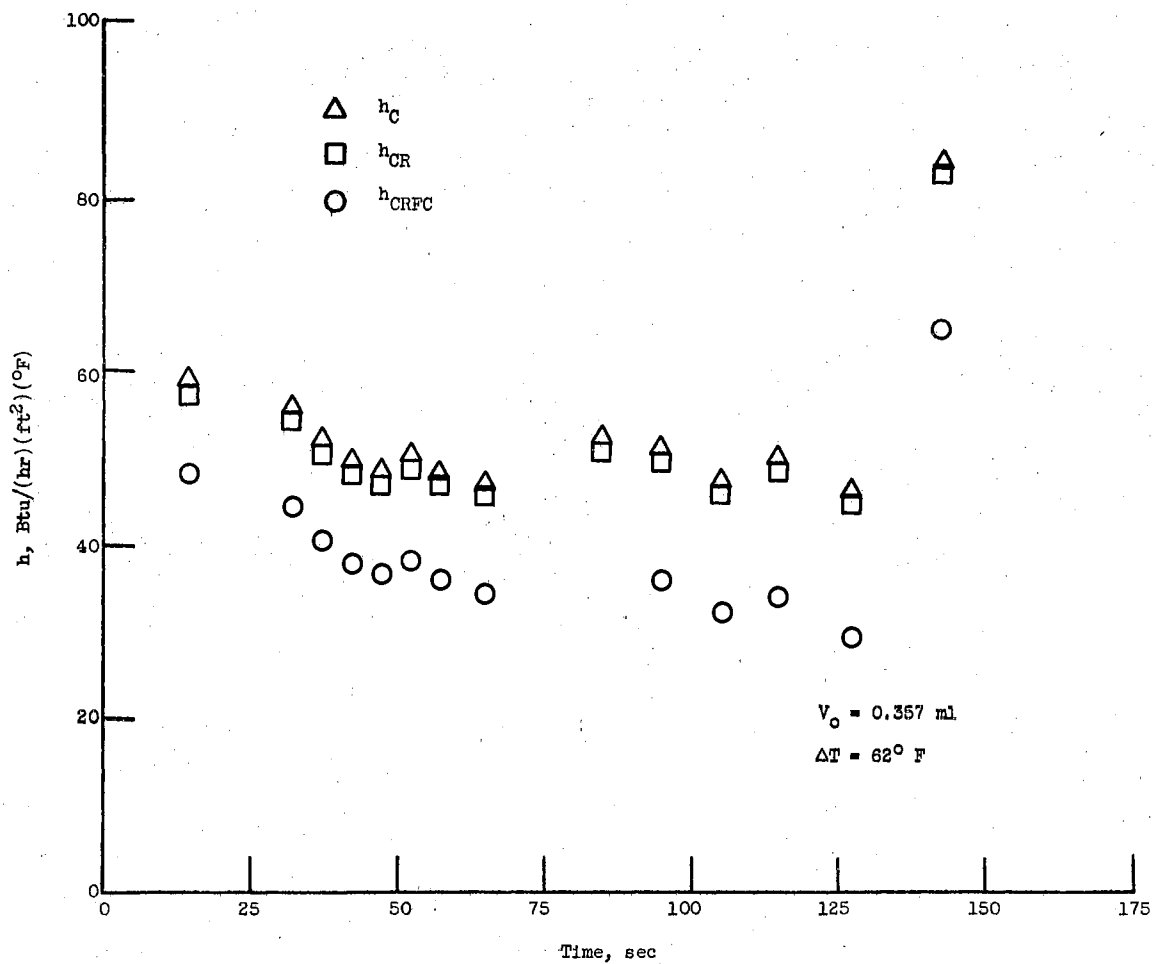


Figure 64. Variation of Heat Transfer Coefficient to Drop During Drop Lifetime -  $\Delta T = 62^\circ \text{ F}$

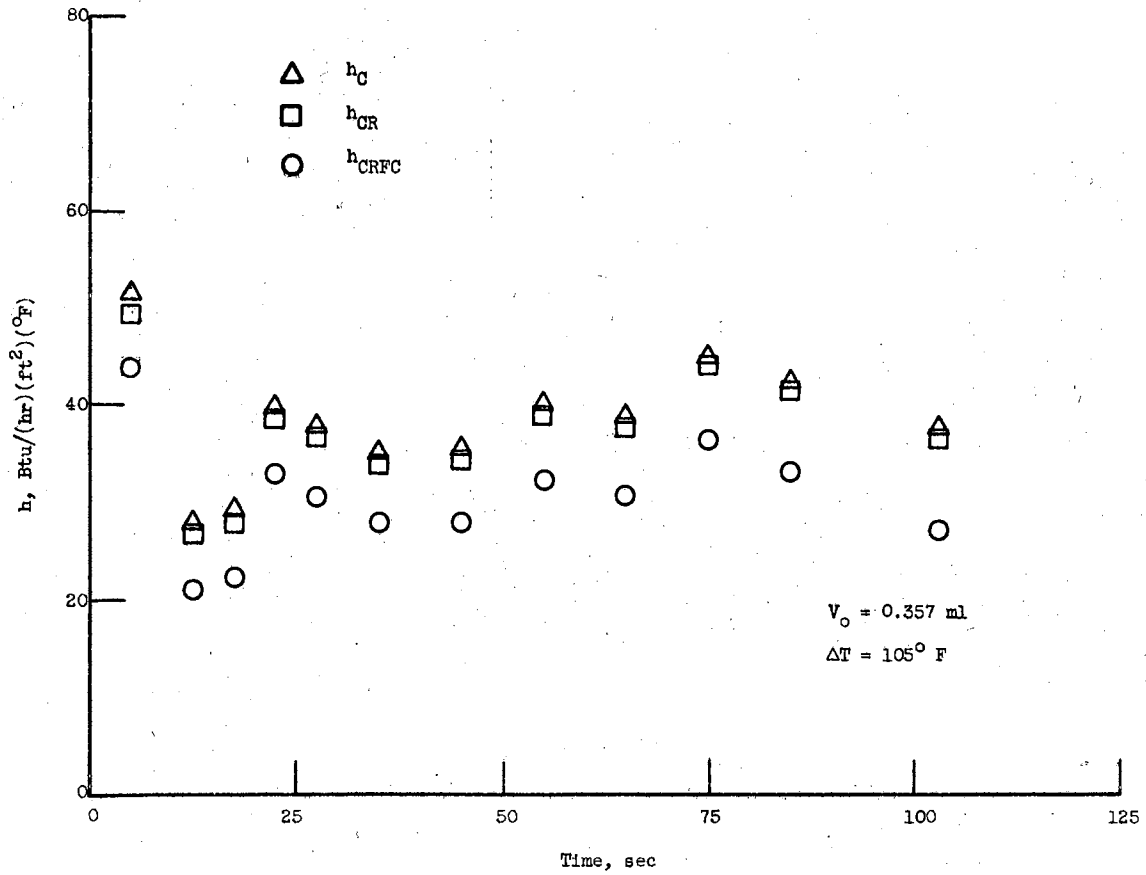


Figure 65. Variation of Heat Transfer Coefficient to Drop During Drop Lifetime -  $\Delta T = 105^\circ \text{ F}$

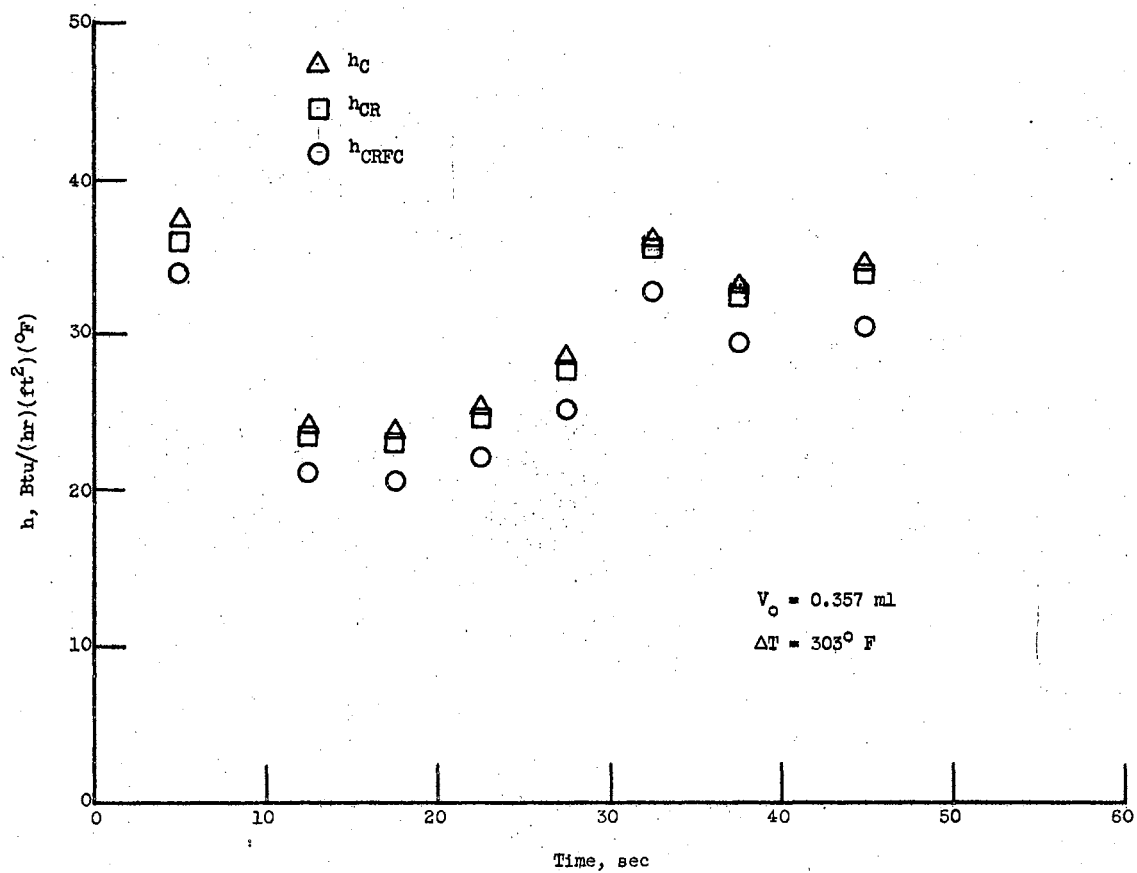


Figure 66. Variation of Heat Transfer Coefficient to Drop During Drop Lifetime -  $\Delta T = 303^\circ \text{ F}$

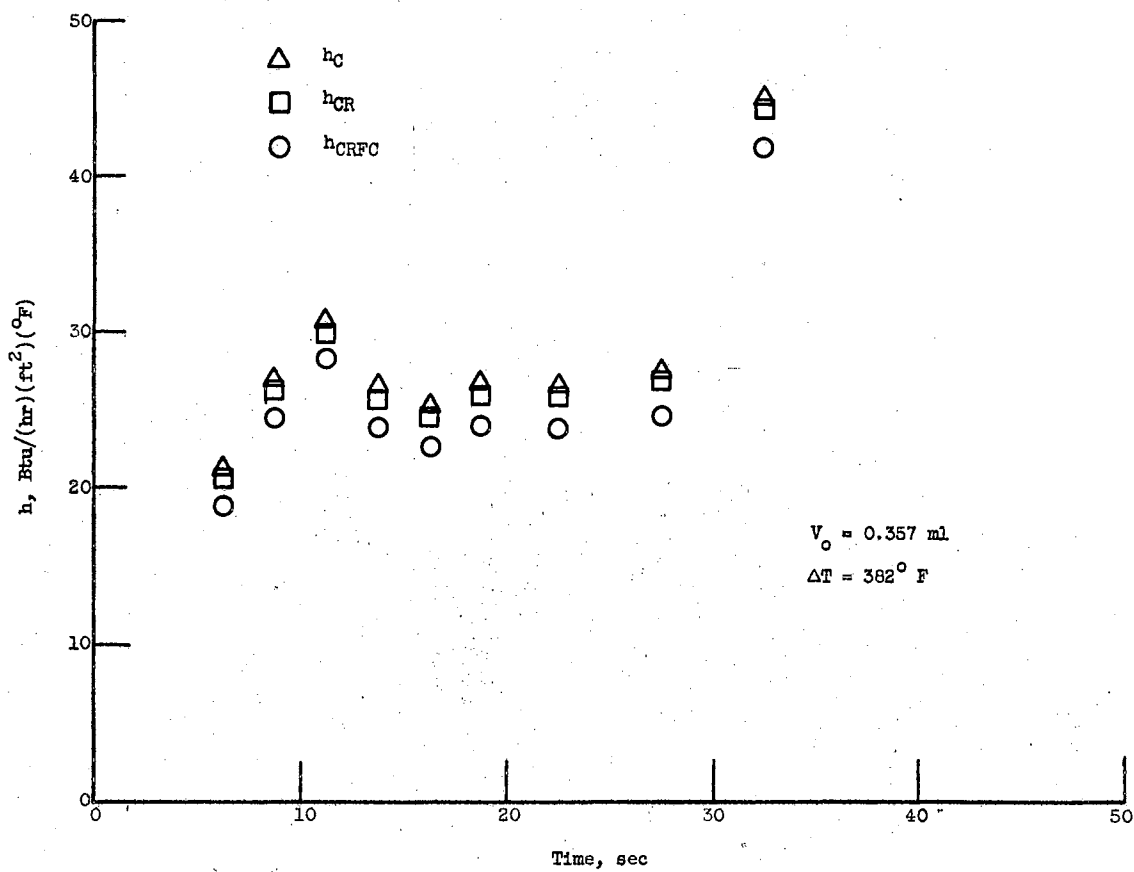


Figure 67. Variation of Heat Transfer Coefficient to Drop During Drop Lifetime -  $\Delta T = 382^\circ \text{ F}$ .

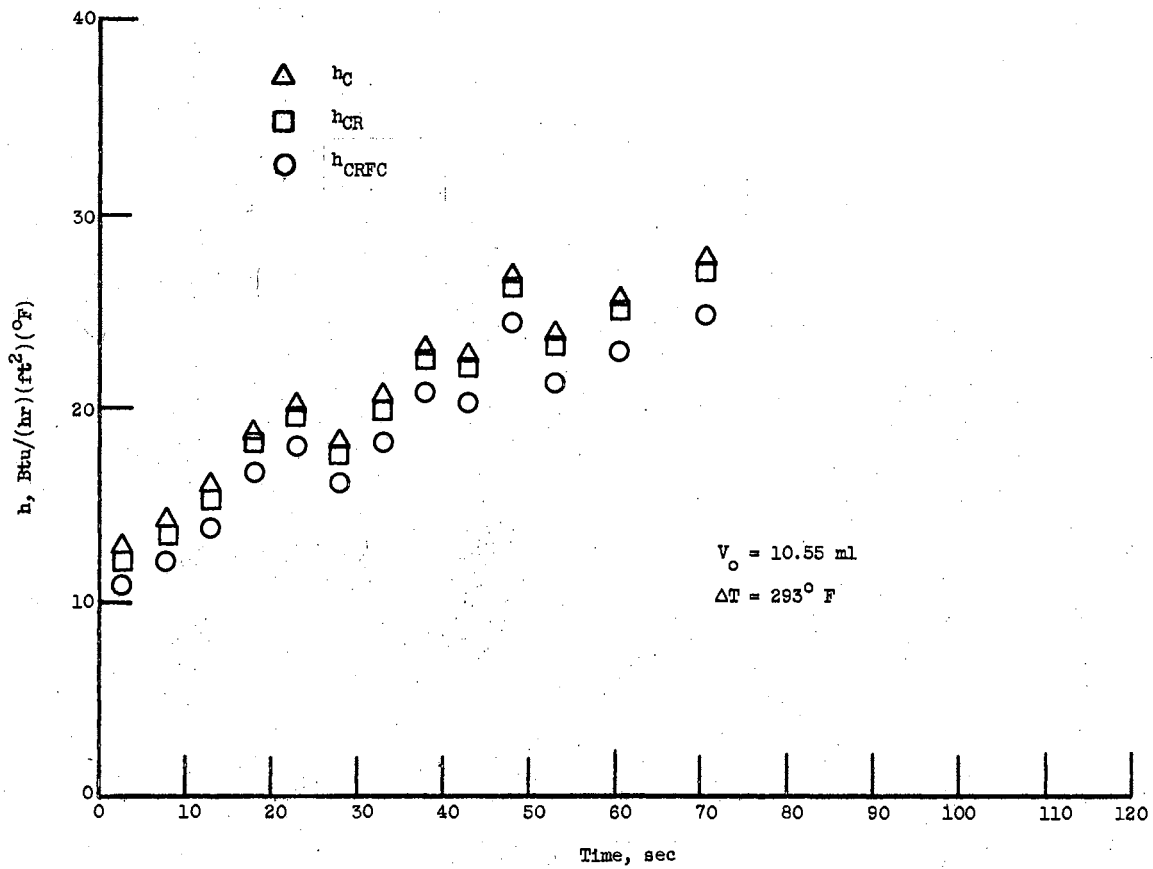


Figure 68. Variation of Heat Transfer Coefficient to Drop During Drop Lifetime -  $\Delta T = 293^\circ \text{ F}$

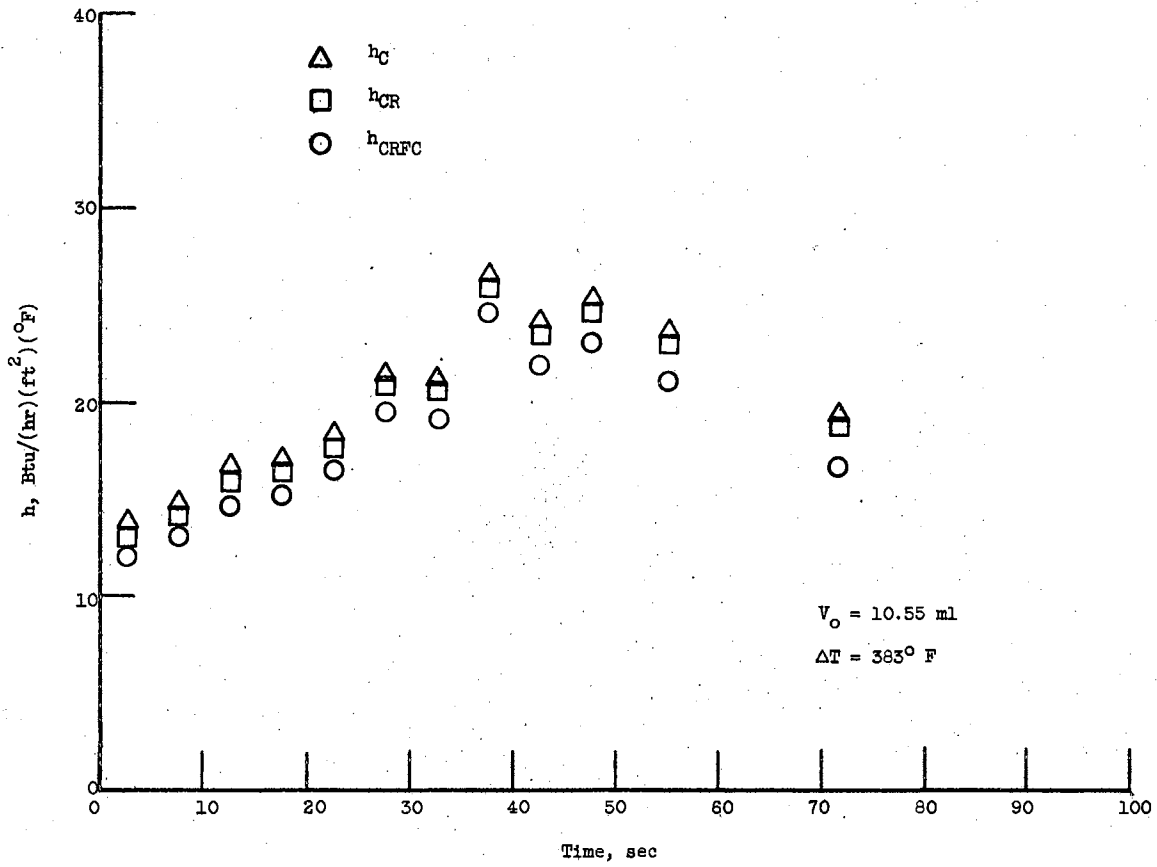


Figure 69. Variation of Heat Transfer Coefficient to Drop During Drop Lifetime -  $\Delta T = 383^\circ \text{ F}$

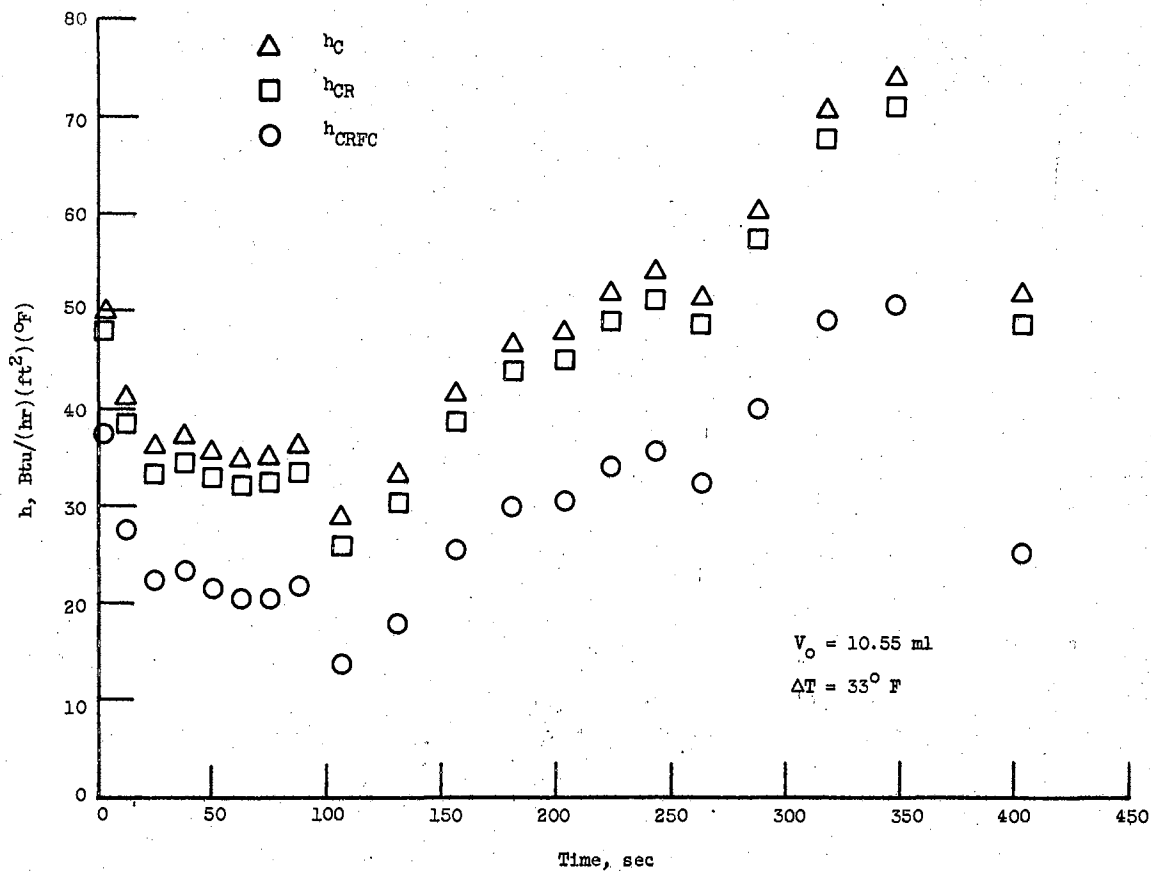


Figure 70. Variation of Heat Transfer Coefficient to Drop During Drop Lifetime -  $\Delta T = 33^\circ \text{ F}$



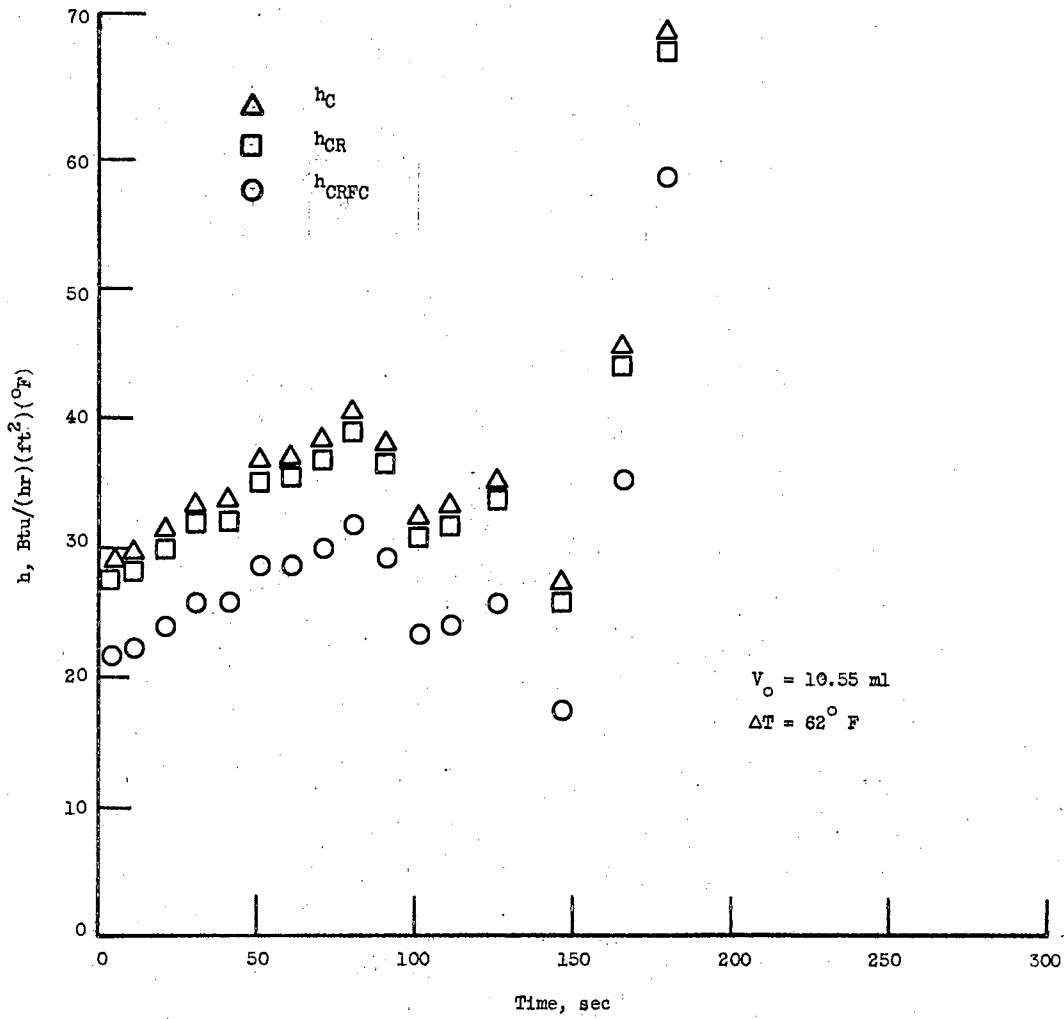


Figure 71. Variation of Heat Transfer Coefficient to Drop During Drop Lifetime -  $\Delta T = 62^\circ \text{ F}$

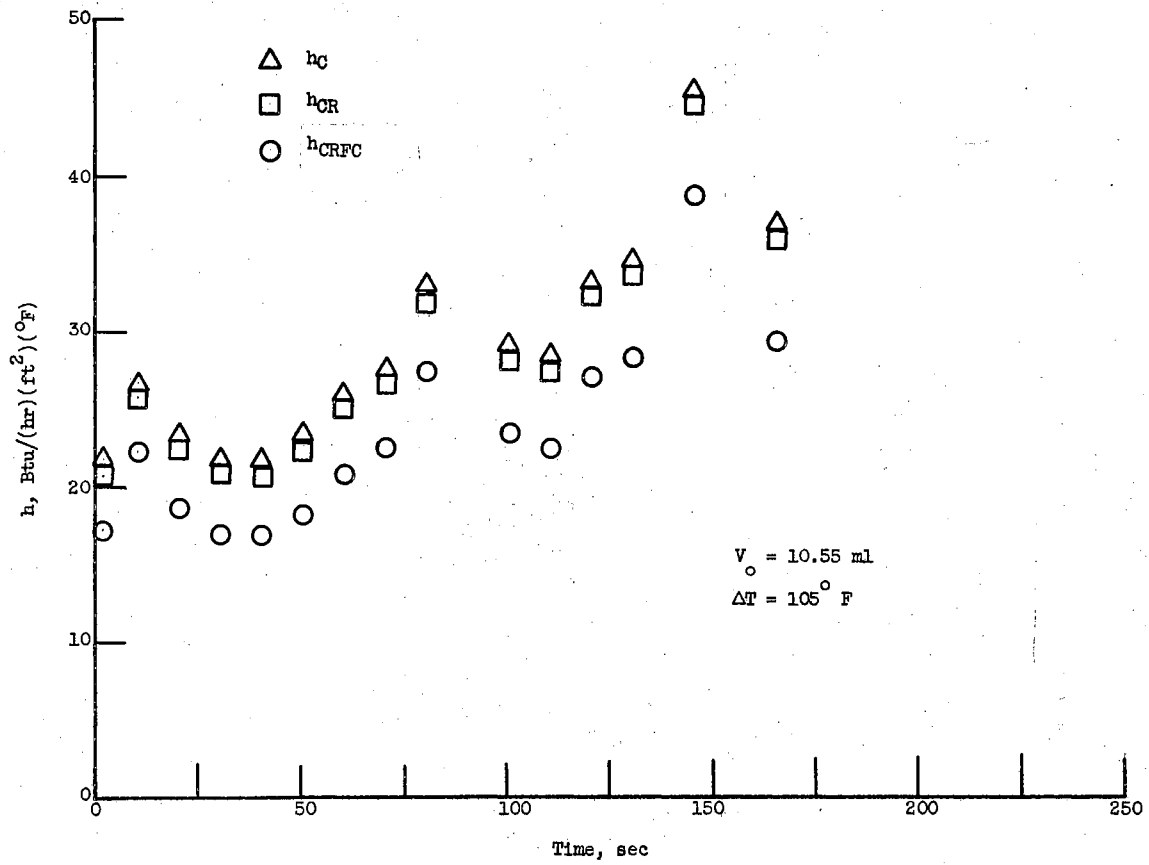


Figure 72. Variation of Heat Transfer Coefficient to Drop During Drop Lifetime -  $\Delta T = 105^\circ \text{ F}$

APPENDIX G

MAXIMUM VAPOR DOME AREAS (MEASURED) AND  
CORRESPONDING MAXIMUM DIAMETERS  
(CALCULATED)

T = 57° F		T = 90° F		T = 383° F			
A, in <sup>2</sup>	D, in	A, in <sup>2</sup>	D, in	A, in <sup>2</sup>	D, in	A, in <sup>2</sup>	D, in
.0434	.235	.0527	.259	.0916	.342	.0722	.303
.0648	.287	.0433	.235	.0860	.331	.0774	.314
.0540	.262	.0459	.242	.0822	.324	.0697	.298
.0685	.295	.0523	.258	.0885	.336	.0877	.334
.0512	.255	.0946	.347	.0895	.338	.1055	.367
.0582	.272	.0662	.291	.0822	.324	.1468	.433
.0542	.263	.0604	.277	.0885	.336	.1267	.402
.0565	.268	.0426	.233	.1213	.393	.1292	.406
=====	=====	.0549	.265	.1210	.393	.0707	.300
		.0482	.248	.1327	.411	=====	=====
		.0536	.261	=====	=====		
		.0708	.300				
		=====	=====				
Avg = 0.0564	Avg = 0.267	Avg = 0.0571	Avg = 0.268			Avg = 0.0984	Avg = 0.352
= 0.0077	= 0.091	= 0.0151	= 0.032			= 0.0238	= 0.042

APPENDIX H

CELL SPACING



APPENDIX I

MEASUREMENTS OF VAPOR FRACTION

Approximate Drop Size, ml	$\frac{A}{V}$ $\frac{A}{A}$	$\Delta T,$ $^{\circ}F$
.3	.215	52
.3	.190	383
.3	.195	90
.3	.180	383
.3	.185	90
.7	.170	383
.7	.165	383
.9	.210-.220	383
.9	.195-.350	383
.9	.205-.265	383
.9	.175-.190	383
.9	.165	383
10	.175	379

Avg. = 0.195



VITA

Edward George Keshock  
Candidate for the Degree of  
Doctor of Philosophy

Thesis: LEIDENFROST FILM BOILING OF INTERMEDIATE AND EXTENDED BUBBLY  
MASSES OF LIQUID NITROGEN

Major Field: Mechanical Engineering

Biographical:

Personal Data: Born in Campbell, Ohio, March 2, 1935, the son of Michael and Sophia Keshock. Married to Mary Jo McKulka, Uniontown, Pennsylvania, November, 1959. Two children, Kathleen, October, 1960, and Michael, May, 1963.

Education: Attended McCartney grade school, Campbell, Ohio, and graduated from Memorial High School, 1952, in Campbell, Ohio. Received the Bachelor of Mechanical Engineering degree from the University of Detroit in June, 1958; received the Master of Science degree with a major in Mechanical Engineering at Oklahoma State University in May, 1966; completed requirements for the Doctor of Philosophy degree in May, 1968.

Professional Experience: Employed as a trainee engineer with the U. S. Steel Corporation and the Engineering Research Division of Ford Motor Co., Dearborn, Michigan during co-op assignments while completing degree requirements at the University of Detroit, 1965-68. Employed as a research engineer in the Nuclear Reactor Division, Lewis Research Center, National Aeronautics and Space Administration, 1958-64. Currently employed as an Assistant Professor of Mechanical Engineering at Cleveland State University, Cleveland, Ohio.